Many-objective Optimisation Based on Decomposition Strategies

Enhancing, Contrasting and Visualising Pareto Front Approximations of Evolutionary Algorithms

Kai Eivind Wu

Department of Automatic Control and Systems Engineering

University of Sheffield

This dissertation is submitted for the partial fulfilment of the degree of

Doctor of Philosophy

August 2021

Executive Summary

Many-objective optimisation analysis is frequently carried out today on problems of ever-increasing complexity. Metaheuristic evolutionary algorithms represent effective and practical tools in solving such issues. The current PhD thesis describes four contributions to the field of study.

A new method for the creation of reference points and an indexing system of reference vectors are proposed, generating more evenly distributed reference points than the popular uniform design method.

A new quality metric/indicator for diversity evaluation on MaOP approximations is proposed. The numerical studies show that the new indicator varies more systematically with the diversity change of PF approximations compared to how frequently applied existing diversity indicators behave.

A new visualisation method for revealing high dimensional MaOP approximations is proposed. The new method satisfies all the desired requirements of a visualisation method in a balanced manner.

A real-life application case study is performed on an additive manufacturing problem: optimisation analysis on process parameters of a selective laser melting manufacturing process. The three proposed methods and related algorithms are utilised to enhance, contrast, and visualise the Pareto Front approximations. The outcome shows that the proposed methods are readily used to enhance the quality of the Pareto front and the Pareto optimal process parameters of the manufacturing operation.

Acknowledgements

I would like to express my deep gratitude and appreciation to my supervisor, Professor George Panoutsos, for his support, guidance, and encouragement throughout my PhD study. I would also like to thank my parents for their understanding, motivation, and dedication to my research. A sincere thank goes to HiETA Technologies Ltd for providing the comprehensive experimental test data, which forms the foundation of Chapter 6 of the thesis. A special thank goes to Dr Adrian Rubio-Solis for analysing and modelling the Selective Laser Melting test data. I am also grateful to my fellow PhD students and colleagues at the University of Sheffield in general and in the Department of Automatic Control and Systems Engineering, particularly for their inspiration and help resolve various issues, both professionally and administratively as well as socially.

Statement of Originality

I hereby declare that the contents of this dissertation are original and are of my own work except as explicitly noted in the text and have not been submitted in whole or in part for consideration for any other degree or at any other university. In addition, Chapter 6 covers a joint study I have had with Dr Adrian Rubio-Solis and my supervisor, Prof. George Panoutsos, who cooperatively performed the modelling work. At the same time, HiETA Technologies Ltd provided the data from comprehensive experiments on the edge and bulk crack length density formed in Selective Laser Melting manufacturing of three different products.

List of Publications

The work presented in this thesis have been partially published in IEEE CEC conference proceedings:

1) K. E. Wu and G. Panoutsos, "A New Method for Generating and Indexing Reference Points in Many-objective Optimisation," 2020 IEEE Congress on Evolutionary Computation (CEC), Glasgow, UK, 2020, pp. 1-8.

2) K. E. Wu and G. Panoutsos, "A new Diversity Performance Indicator for Many-objective Optimisation Problems," 2021 IEEE Congress on Evolutionary Computation (CEC), Krakow, Poland, 2021, pp. 144-152.

3) K. E. Wu and G. Panoutsos, "A Visualisation Method for Pareto Front Approximations in Many-objective Optimisation," 2021 IEEE Congress on Evolutionary Computation (CEC), Krakow, Poland, 2021, pp. 1929-1937. (The paper attained The Best Student Paper, Runner up Award).

Table of Contents

List of Figures

List of Tables

Chapter 1 Introduction

1.1 General Remarks

Optimisation analysis is continuously performed everywhere, on occasions, so long as different alternatives can be chosen. When we move from A to B, we usually want to get to position B in the shortest time and the shortest walk distance possible. But the goal of reaching position B could be hindered or influenced by physical barriers in between, like fences, buildings, etc. The time spent and length to be covered are our objective functions which are functions of the walking route we choose [1]. Here, all possible walking paths are described as the decision variables, while those hinders are constraints of the problem, forcing us to choose certain route combinations.

Summarised, optimisation is a process of finding the best inputs (Decision Variables), out of their feasible domain, to the outcome function (Objective Functions) to obtain the optimal output from the outcome function. The process of searching input values that lead to a maximum of an objective function is called maximisation. On the contrary, it is called minimisation when it leads to a minimum. An optimisation process is often changeable to minimisation and vice versa [1]. Therefore, research focuses on either of the two, often concentrating on minimisation problems.

The optimisation methodologies can be deployed in mechanical design and production, manufacturing, electrical engineering, civil engineering, process control, economics and finance, etc. Significant savings can be obtained through the analyses of such operations.

1.1 General Remarks

It is often the case that optimisation of more than one objective must be carried out simultaneously. When used in design work, critical design parameters for reliability and economy are optimised so that the system's availability is maximised while the costs are minimised. Most commonly, the system’s reliability and the cost of realisation are two conflicting objectives. Compromises or trade-offs of the conflicting factors need to be found. In aerospace engineering problems, the strength and weight of components are often two conflicting factors. The clue is to maximise the former and at the same time to minimise the latter. In business life, profit, output, performance, and efficiency are desired to be maximised, while resources, time, and money to be spent are always limited and are minimised.

The optimisation of only one objective function is called Single Objective optimisation (SOO). When two or more objective functions are optimised simultaneously, the process is called multi-objective optimisation problems (MOP) or many-objective optimisation problems (MaOP) if the objectives exceed three. In such cases, a single solution leading to the optimum of all objective functions is non-existent if the objectives are conflicting, which means that none of the objective functions can be improved in value without worsening one or more of the other objective functions [1]–[3]. Instead, trade-off solutions must be found [1]. Such Trade-offs are called Pareto Optimal Solutions or Non-dominated Pareto Optimal. Such solutions form an (m-1) dimensional surface in an objective function space called Pareto Front (PF). PF reveals different Pareto optimal solutions representing other possibilities for a Decision Maker (DM) in decision making in operation. Without other choices made by a human DM, all Pareto optimal solutions are incomparable since they represent different operational options, all under optimised states [1].

Scientists and researchers have been working with the optimisation theory for a very long time. The French mathematicians Fermat and Lagrange worked to find optima of functions as early as the 14th and 15th centuries. Newton and Gauss invented the finding of optimum by iteration [1]. Before the age of electronic computers, optimisation analysis was done analytically. Rapid development within optimisation theory and practice have taken place after computers have been widely accepted into use. Most of the methods in the early stages are, although numerically based, deterministic. Heuristic and metaheuristic solution techniques emerged around the mid-20th century and rapidly developed. The prefix “meta” means “change” while “heuristic” means to find the solutions by trial and fail through using constantly improved solutions. The methods are iterative, stochastic, and formulated so that the optima are searched and reached self-guided by algorithms. Heuristic methods used for solving optimisation problems may search for solutions more quickly than other classical methods do and cases where classic methods cannot find any satisfactory solution due to the problems' size and complication. But heuristic methods cannot mathematically guarantee that optimised results can be attained. Researchers today tend to call all stochastic techniques metaheuristic ones.

Two objective and three-objective problems are often considered a group of problems of their own because solutions on PF may be readily visualised by traditional figures and charts and thus easier to be found and evaluate. Also, effective and efficient solution techniques exist. When the number of objectives increases, new challenges emerge that are often inadequately dealt with using existing MOP methodologies (computational efficiency, visualisation, optimisation effectiveness etc.). For example, researchers argue that the most exciting MaOPs can have up to 15 objectives [2]. Moreover, it is incredibly

difficult or almost impossible to develop a single method that can solve all kinds of optimisation problems due to the diverse nature of challenges. Wolpert, D. H. and W. G., Macready formulate the famous No Free Lunch Theorem for optimisation [4], which roughly says that "no algorithm performs well on all possible functions, but only on a subset that arises from the constraints of real-world problems". New solution methodologies must be constantly invented to deal with ever-increasing real-life challenges. One of the major groups of solution techniques of MOPs utilises **Reference vectors-based algorithms** [5]. The MOP is divided into a set of sub-problems using a set of aggregation functions or references vectors or points to guide the search towards the true PF, and these sub-problems are solved simultaneously.

1.2 Aims and Objectives

The work presented in this thesis focuses on studying the issues of many-objective optimisation problems based on metaheuristic solution techniques solved by decomposition-based algorithms. The motivation arises from the fact that while metaheuristic decomposition-based methods are prevalent and effective in a variety of cases [2], [6], [7], moving to a higher number of objectives (MaOP) still poses several challenges; these are briefly summarised as follows [3]:

Evaluating the convergence and diversity and selecting the next generation of candidate solutions targeting having the best combination of convergence and diversity possible is computationally expensive and challenging when using existing methodologies.

Maintaining the solutions' diversity is difficult in high dimensional objective space. It requires that the reference points utilised to guide the decomposition-based search for PF must be placed so that the solutions are distributed most possibly equal-distantly on the true PF.

Difficulty in representing the PF: many discrete Pareto Optimal approximations represent the PF surface. The needed number increases almost exponentially with the number of objectives, requiring a large population size in Evolutionary Algorithms. It slows down and eventually jeopardise the solution process and make it challenging for a decision-maker in his/her decision making based on final solution sets.

Difficulty in visualising the solution sets: approximated PF landscape of many-objective optimisation problems (MaOP) consists of vectors in high dimensional objective space. It is nontrivial to reveal these quantities mainly because the number of axes in such a visualisation exceeds three. A large amount of data is needed to be displayed simultaneously on the other.

1.2 Aims and Objectives

The thesis focuses on finding new methodologies to solve the first, second, and fourth challenges outlined above.

The scope of this PhD research work is twofold:

- To develop new computational and mathematical methods for enhancing the performance of MaOP methodologies and underpinning algorithms that lead to qualitative and quantitative improvements, focusing on the more effective creation of reference vectors, performance indicators and high dimensional Pareto Front visualisation methods.
- To utilise the new methodologies towards demonstrating the utility and creating new knowledge in real-life applications in the advanced manufacturing industry.

Specific research objectives are:

- Develop new and more efficient reference point generation methods for better diversified PF solutions used for Decomposition-based MaOP solution methodology.
- Create more applicative diversity indicators for the evaluation of high dimensional PF approximations.
- Develop an appropriate visualisation method for displaying features of high dimensional PF approximations.
- Apply the new methods and algorithms to optimisation analysis of Laser Selective Manufacturing processes.

1.3 Main Findings

Several interesting findings have been obtained through this PhD work, and the main achievements are:

Introduction of a generalisation of Das and Dennis method to create more equidistant reference points, which can be implemented into any existing decomposition-based evolutionary algorithms for MaOPs for improving the diversity of Pareto Front approximations. The work was published in 2020 IEEE Congress on Evolutionary Computation (CEC)

A new performance indicator is launched for diversity to assess the performance of PF approximations for high dimensional MaOPs. The work has been published in the 2021 IEEE Congress on Evolutionary Computation (CEC).

A new visualisation method is proposed to depict PF and its approximation sets in high dimensional space, where high dimensional vectors are mapped onto a 2-D space plot. The work was published in the 2021 IEEE Congress on Evolutionary Computation (CEC). The paper was nominated as the best student paper and attained Runner Up score among the nominated ones.

The proposed methodologies are implemented in a real-life additive manufacturing case study -- Optimisation of Process Parameters in Selective Laser Melting (SLM) operation. New insights and knowledge were revealed for the manufacturing process as part of the optimisation application. The work is prepared for publication as a journal paper in an international journal in the field of study.

1.4 Impact of the Work on the Scientific Community and the Society

The current study's achievements contribute significantly to the theory of MaOP and positively affect the practical usage of MaOP methodology in real-life studies.

First, a new method for creating reference points is proposed for reference point-based Many objective Optimisation Problems. Reference points in objective space are widely used in MaOP algorithms in assisting the searching process towards optimality. Das and Dennis's current standard practice of generating reference points on a unit simplex plane often leads to uneven distribution on the actual Pareto Front (PF). The generated reference points are projected onto it. The new reference points are more evenly generated on an m dimensional B-norm surface created adaptively by tracking the true PF. The method is thus named as B-norm based PF tracking method (Bn-PFt). An indexing system of reference points is also proposed to ease the work of algorithmic development. Systematic numerical studies performed on B-norm surfaces of various B values show that the proposed Bn-PFt method's reference points are more evenly distributed on the PF surfaces than those projected onto the same surfaces generated using Das and Dennis.

Second, approximation sets of MaOP need to be evaluated for performance regarding their convergence and diversity properties. Developing consistent performance indicators for accessing quality approximations from many-objective optimisation algorithms is still challenging, particularly as the number of objectives increases. We introduce a new pure unary diversity indicator, Inverse Ratio of Net Avertence angle (IRNA). IRNA is formulated using reference vectors by minimising the included angles between approximated solution set and reference vectors. It is achieved by rotating the system of

reference vectors in all dimensions with an optimised spatial angle. Any eventual systematic bias in included angles is removed, and the highest possible diversity score of a solution set is obtained. Candidates of an approximation set are first identified for diversity evaluation, and the chosen ones are then used for convergence assessment. Based on numerical results from testing synthetic solutions on a unit simplex plane and benchmark functions up to 10 objectives, the proposed performance indicator IRNA is more sensitive to capturing diversity changes than other state-of-the-art performance indicators as the number of objectives increases. Thus, it is deemed particularly suitable for many-objective optimisation problems.

Third, a new visualisation method is introduced for a graphical depiction of PF and its approximation sets in high dimensional space, where high dimensional vectors are mapped onto 2D space. Visualisation of Pareto Front (PF) approximations of many-objective optimisation problems (MaOP) is critical in understanding and solving a MaOP. Research is ongoing on developing effective visualisation methods with desired properties, such as simultaneously revealing dominance relation, PF shape and distribution, etc. State-of-the-art visualisation methods in the literature only retain some of the required properties. A new visualisation method is proposed in this paper, which possesses all the visualisation method's preferred properties. The new method (ProD) is based on displaying the projection of solution vectors against their distances to a reference vector, and a vector would link Ideal point and Nadia point. MaF benchmark problems are used to demonstrate the effectiveness of ProD. Results show that ProD exhibits a more balanced performance than the state-of-the-art in capturing desired visualisation properties. In particular, good performance is observed in portraying dominance relations, PF shape and distribution.

1.4 Impact of the Work on the Scientific Community and the Society

Further, part of the newly developed theories in the current work and its derived algorithms are applied in solving a real case manufacturing problem of MOP in Selective Laser Melting (SLM). The results from the analysis are useable for the finding of optimal process parameters of the operation. New insights and knowledge were revealed for the manufacturing process as part of the optimisation application.

1.5 The Organisation of the PhD Thesis

Chapter 1. The thesis starts with a brief introduction on computational optimisation topics in general and on evolutionary SOP, MOP and MaOP in particular, and their usage and importance in today's research field. Some significant challenges in the field of research are concisely explained. The aims and objectives and the main findings of the thesis work are also highlighted. The significance of the present study on the impact on the scientific community and society is briefly described.

Chapter 2 highlights the topics and challenges of data-driven optimisation where knowledge in data science and machine learning applied in evolutionary optimisation are highlighted. Further, it covers a more detailed summary and state of the art description on knowledge of evolutionary computational methods for single-, multi- and many-objective optimisation problems and related topics, such as performance metrics, benchmark problems and visualisation of high dimensional PFs for purposes in the testing of new algorithmic developments. These are utilised to evaluate the quality of obtained PF approximation sets. Also covered are real-world applications using meta-heuristic optimisation methodology, showing the subject's importance and significance.

Chapters 3-5 present the main results from this author's research work under the supervisor's guidance. **Chapter 3** explains a new and generalised method for creating equally spaced reference points for decomposition-based Many objective Optimisation Problems. A convenient indexing system of reference points is also proposed to ease programming work. **Chapter 4** introduces a new performance metric for pure diversity, contributing to assessing the performance of high dimensional PF approximations. **Chapter 5** is dedicated to proposing a new visualisation method for PF's graphical

depiction and its approximation sets in high dimensional space. High dimensional vectors are mapped onto 2D space.

Chapter 6 demonstrates utilising the newly developed theories and methodologies to analyse a real-life manufacturing problem: optimisation on reducing cracks of various types formed on products manufactured using Selective Laser Melting (SLM) technique.

Chapter 7 gives the main conclusions of the thesis and a brief description of the future work.

Chapter 2 Data-driven Evolutionary Optimisation

Chapter Outline

Data-driven evolutionary optimization is widely used in our daily lives to improve the efficiencies of operations people perform and enhance human activities' achievements. The objective functions and constraints are often formulated with surrogate models (also called meta-models) based on carefully performed experiments or numerical simulations. The optimisation problems are regularly solved exercising evolutionary and swarm algorithms; both are nature-inspired. The first one emulates natural evolution, while the other mimics the swarm behaviours of social animals.

This chapter gives an overview of data-driven evolutionary optimisation and a literature study on major achievements and remaining challenges of revolutionary and swarm optimisation, focusing on decomposition-based MaOP solution techniques. These algorithms are regularly implemented to solve complicated optimisation problems. Tools of data-driven evolutionary optimization are utilised, especially in problems where no analytical mathematical functions are available for the objectives or constraints. The topic is multi-disciplinary, consisting of evolutionary computation, machine learning and deep learning, and data science. Moreover, issues related to benchmark testing applied for the development and verification of new algorithms and performance indicators or metrics for measuring the quality of Pareto front approximations are presented. Some most frequently used statistical test

methods are also discussed. In addition, some commonly employed visualisation methodologies are presented. Further, an overview of the metaheuristic optimisation case studies in advanced design, engineering, and manufacturing are presented. In the end, a summary of the chapter and the conclusions are made.

2.1 Introduction

Optimisation of objective functions with respect to their independent variables, often called decision variables, is widely performed to improve operations' efficiencies and enhance the achievements of human activities. The objective functions and constraints can be formulated using physical laws governing the process, or numerical simulations, such as finite element method (FEM) and computational fluid dynamics (CDF) methods or surrogate models (also called meta-models) based on carefully performed experiments or numerical simulations. Evolutionary and swarm algorithms are frequently used to solve complicated problems of optimisation. The field of research is often called data-driven evolutionary optimization. The tools are utilised primarily in problems with no analytical mathematical functions for the objectives or constraints. The topic is multi-disciplinary, consisting of evolutionary computation, machine learning and deep learning, and data science.

This chapter gives an overview of data-driven evolutionary optimisation and a literature study on significant achievements and remaining challenges of metaheuristic optimisation, focusing on decomposition-based MaOP solution techniques.

2.1.1 Main process flow of data-driven evolutionary optimization

Jing et al. [8] have illustrated the main process flow of data-driven evolutionary optimization. See Fig. 2.1.

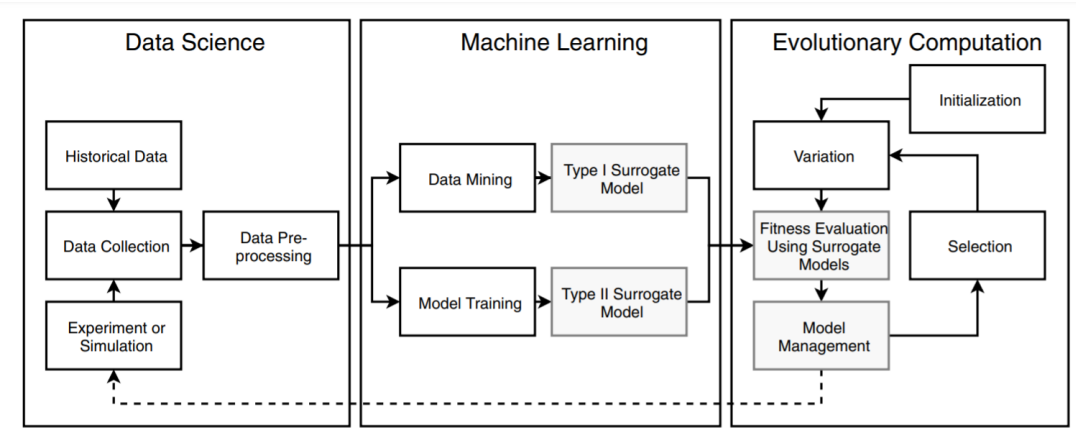

Figure 2.1 - Process of data-driven evolutionary optimization [8].

The data quality in the form of a big or small amount of collected data, data's heterogeneity, noise, embedded errors, incompleteness, distribution, etc., may influence the quality of the modelling result. Knowledge of data science is adopted to pre-process the data to become more suited for modelling objectives and constraint functions. Further, tools from machine learning are exercised in modelling work, while evolutionary computation techniques are used to solve the optimization problem.

2.1.2 Definition of optimization problems

Optimisation problems can be formulated as:

$$\text{Optimise } \{f_i(\boldsymbol{x})\},\ i = 1, 2, \dots, m \qquad \text{Eq. 2.1}$$

with respect to $x_j,\ j = 1, 2, \dots, n$

subject to:

$$h_k(x) = 0, \qquad k = 1, 2, \dots, K \qquad \text{Eq. 2.2}$$

$$g_l(x) \leq 0, \qquad l = 1, 2, \dots, L \qquad \text{Eq. 2.3}$$

where:

- $\boldsymbol{x} = [x_1, x_2, \dots, x_n]^T$: is the decision variable vector, which can be continuous, discrete, or mixed in n-dimensional decision space.
- $f_i(\boldsymbol{x})$: objective function i and is nonlinear in general.
- $h_k(\boldsymbol{x})$: equality constraints function k and is nonlinear in general.

- $g_l(\boldsymbol{x})$: inequality constraints function l and is nonlinear in general.
- m: number of objective functions of the problem to be optimised.
- K: number of equality constraints.
- L: number of inequality constraints.

A single-objective optimisation problem (SOP) is a problem if only one objective function is optimised. A multi-objective optimisation problem (MOP) is formed when the number of objective functions is less or equals 3, and a many-objective optimisation problem (MaOP) is shaped when the number of objective functions is more than 3 ($m \geq 4$). In MOP and MaOP, a solution that leads to the optimum of all objective functions does not exist if the optimisation system is nontrivial. A trade-off solution must be found [9].

The problem is unconstrained if there is neither equality nor inequality constraints and is an equality-constrained optimisation problem if there are only equality constraints. The problem is a nonlinearly constrained optimisation problem if either the objective functions or some of the constraint functions are nonlinear, or both. Similarly, the problem is a linear constrained optimisation problem if both objective and constraint functions are linear. Further, it is a combinatorial optimization problem when optimality is found from a finite set of objects, where the set of feasible solutions is discrete. Likewise, it is a discrete optimisation problem if all decision variables can only take discrete values. If all decision variables can only take binary values, it is a binary optimisation problem. Moreover, the problem is a convex optimisation if the objective functions are of a convex type [10] and is an optimal control problem when some of the objective functions contain integrals. At the same time, some of the equality constraints are formulated in differential equations [10].

A minimisation problem of $f_i(\boldsymbol{x})$ can be written as a maximisation problem of -$f_i(\boldsymbol{x})$ or 1/$f_i(\boldsymbol{x})$.

Unlike SOP, many more solutions exist in MOP, called Pareto optimal set (PS). The objective function values in the objective space are called the Pareto front (PF). Different Pareto optimal solutions represent other possibilities or options in decision making in operation. Without other choices made by a human decision-maker (DM), all Pareto optimal solutions are equally good since they indicate different operational targets [3], [11]. A decision space is also called a search space. A vector of objective functions relates one-to-one or one-to-many to decision vectors in decision space. The inverse mapping from the search space to the fitness space/objective space creates the fitness landscape. Pareto optimality is reached when all objective vectors $\boldsymbol{F}$ on PF dominate all other vectors $\boldsymbol{A}$ outside PF if and only if $\boldsymbol{F}$ is at least as good as $\boldsymbol{A}$ in all objectives and better in at least one. A non-dominated objective vector is Pareto optimal, which has the property that improving the value of any objective function results in worsening the value of at least one other objective. Dominance relationship between 2 output values of a system of objective functions $f(\boldsymbol{x}_1)$ and $f(\boldsymbol{x}_2)$ can be expressed as: [9]

$$\boldsymbol{f}(\boldsymbol{x}_1) = [f_1(\boldsymbol{x}_1), f_2(\boldsymbol{x}_1), \dots, f_m(\boldsymbol{x}_1)]^T$$

and

$$\boldsymbol{f}(\boldsymbol{x}_2) = [f_1(\boldsymbol{x}_2), f_2(\boldsymbol{x}_2), \dots, f_m(\boldsymbol{x}_2)]^T \quad \text{Eq. 2.4}$$

where $\boldsymbol{x}_1$ and $\boldsymbol{x}_2$ are two decision variable vectors. For a minimisation process, $\boldsymbol{f}(\boldsymbol{x}_2)$ is said to be dominated by $\boldsymbol{f}(\boldsymbol{x}_1)$ if $\boldsymbol{f}(\boldsymbol{x}_1) \leq \boldsymbol{f}(\boldsymbol{x}_2)$, for all $f_i(\boldsymbol{x}_1)$, where $i = 1, 2, \dots, i \neq j, \dots, m$, and at least for one of the objectives functions in $\boldsymbol{f}(\boldsymbol{x})$, $f_j(\boldsymbol{x})$, there $f_j(\boldsymbol{x}_1) < f_j(\boldsymbol{x}_2)$. If any other objective function vectors do not dominate $\boldsymbol{f}(\boldsymbol{x}_1)$, $\boldsymbol{f}(\boldsymbol{x}_1)$ is called a non-dominated solution of objective functions or a global Pareto optimal solution.

Other general relationships between two vectors $\boldsymbol{a}$ and $\boldsymbol{b}$ are defined as:

1) Equivalence: $\boldsymbol{a}$ is equivalent to $\boldsymbol{b}$ when the corresponding objectives in $\boldsymbol{a}$ and $\boldsymbol{b}$ are equal.
2) Coverage: $\boldsymbol{a}$ covers $\boldsymbol{b}$ If $\boldsymbol{a}$ either dominates $\boldsymbol{b}$ or $\boldsymbol{a}$ is equivalent to **b**.
3) Incomparability: $\boldsymbol{a}$ and $\boldsymbol{b}$ are incomparable if both are neither equivalent nor mutually dominate one another.
4) Non-dominated set of vectors: a set of vectors is a non-dominated set if all vectors in the set are mutually non-dominating.

The process of searching for a non-dominated solution or Pareto optimal set out of many possible solutions is called Pareto-based ranking or Pareto Filtering [3], [11]. PF usually has a dimension (m-1). Occasionally, PF has a lower dimension than (m-1), and in such a case, it is referred to as degenerate Pareto front.

A PF is, in general, approximated in discrete points, which have the closeness to the Pareto front and the coverage in the objective space. The searched approximated Pareto front provides the decision-makers with the quality of their decision-making performance for a criterion at the expense of one or other criteria. A high quality approximated Pareto front has the characteristics of [14]:

1) The distance between the Pareto front and the approximation is minimised.
2) The solutions in the approximated Pareto front are uniformly distributed, which can be mathematically expressed as

$$Uniformity\ (X) = Var_{s \in X}\big(dissimilarity(s, X - s)\big)$$

in which X is the solution set, s is an element of the solution set and $dissimilarity(s, X - s)$ measures the variance of s compared to other solutions in the set X.

3) The extent of the approximated front is maximized, which can be described mathematically as

$$Extent\ (X) = \sum_{s \in X} dissimilarity(s, X - s)$$

The last two combined characteristics are often termed the diversity of PF approximation.

2.1.3 The organisation of the chapter

The rest of the chapter is organized as follows. **Section 2.2** presents an overview of Data-Driven Evolutionary Optimisation and its main challenges. **Section 2.3** highlights features and main algorithms in Evolutionary and Swarm optimisation. **Section 2.4** covers issues related to Benchmark testing applied for development and verification on new algorithms. **Section 2.5** is devoted to discussing performance indicators or metrics for measuring the quality of Pareto Front approximations. **Section 2.6** discusses some most frequently used statistical test methods. **Section 2.7** presents some commonly used visualisation methodologies. **Section 2.8** provides an overview of the metaheuristic optimisation methodology used in advanced design, engineering, and manufacturing. **Section 2.9** provides a summary of the chapter and conclusions.

2.2 Overview of Data Science and Machine Learning applied in Data-driven Optimisation

Data science is an interdisciplinary subject that targets knowledge extraction from noisy and unstructured data. The obtained insights are applied in various applications, such as modelling for machine learning inference. Machine learning methodologies may be used to construct and verify surrogate models by utilising the cleansed, aggregated and manipulated data after treatments based on data science methodologies.

2.2.1 Data Science in Data-driven Optimisation

Data science consists of five major parts of data treatment: capture, maintenance, processing, analysis and communication.

1) Capture: data acquisition, data entry, signal reception, data extraction. It handles the issues such as where the data are received, e.g., from neatly performed experiments, computational expensive numerical simulations, historical data, etc. It also deals with data import and formatting design, how data signals are received, and how the targeted or core data are recorded when received.
2) Maintenance: data warehousing, data cleansing, data staging, data processing, data architecture design. It deals with how data are stored, cleared for discrepancies, how data are immediately stored for data processing, how data should be purposefully prepared for their usage, and the design of standards according to specific policies, rules, and models.
3) Processing: data mining, clustering/classification, modelling, and summarization. It covers tasks of extracting and discovering patterns in large data sets, grouping similar data instances together and labelling

data, creating a data model for system use and presenting the summary of data for ease of informative perception.

4) Analysis: exploratory/confirmatory, predictive analysis, regression, qualitative analysis. Exploratory data analysis consists of methods to explore the big data set that leads to conclusions. Confirmatory data analysis utilises statistical tools such as significance, inference, and confidence to evaluate the findings. Predictive analysis extracts information from data and finds trends and behaviour patterns. Regression analysis estimates the relationships between a dependent variable and independent variables. Qualitative data analysis targets identifying, examining, and interpreting characteristics in textual data.
5) Communication: data reporting, data visualization, business intelligence, decision-making. Data reporting deals with collecting and formatting raw data and applying them to assess the performance of operations. The data visualisation reveals data properties in a chart, diagram, picture, etc. The working area of Business intelligence and decision-making is to process data to form the basis for business decision-making by employing proper software.

Some of the main subjects in data science, which are relevant to this thesis work, are described further in specific detail.

Features or decision variable data are either quantitative or qualitative. Quantitative data have numerical quantity and can be continuous or discrete, e.g., probability density, number of tests, etc. In contrast, qualitative data have qualitative categories of a fixed number, e.g. {M, F} for gender, which is also called categorical features or factors [13].

Data acquisition from performed experiments requires knowledge in the design of experiments (DOE) which adopt knowledge of applied statistics for

planning, conducting, analysing, and interpreting test results. Data obtained from correctly performed experiments form the basis for establishing surrogate models. A key element in the experiment design is making a sampling plan for design variables. Data are often expensive to be generated by physical experiments, and there is always a limit for how much data can be made available for data collection. The choice among data points in decision space based on the uniformity principle is ensured by maximising the minimum distances among design or sampling points or minimising correlation measures among the sample data [14]. Standard methods are developed based on these principles. The most representative of the approaches are factorial design [15], Latin Hypercube sampling (LHS, e. g., [14]), and orthogonal arrays (OA, e. g., [16]), and hybrids of the fundamental methodologies, e.g., OA-based LHS [17] and other optimal LHS schemes [15]. LHS is a sampling-based stratified approach where the range of decision variables is divided into several strata, and a sampling point is identified on each stratum randomly. The sampling with the best uniformity and spreading should be used.

Summary statistics of a data set are purposely calculated when data are obtained. These can be the sample mean, p-sample quantile ($0 < p < 1$), sample median, sample range, sample variance or the sample standard deviation, empirical probability density function and cumulative distribution function. p-sample quantile is a percentage p of the sample data which is less than or equal to a given value. The sample median is the sample 0.5-quantile or 50 sample percentile.

Data sets are studied through visualisation. Bar plots, box plots, histograms, and scatter plots are frequently used. A bar plot is often used to visualise categorical features. A boxplot shows a data set with its minimum, maximum, and the first (25% percentile), second (50% percentile), and third quartiles (25%

percentile). It may identify outliers in the data set [13]. A histogram reveals the distribution of a quantitative feature. The data set range is divided into several bins, and the counts of the values falling in each bin are shown as functions of the feature. The data set's variability is observed, its central tendency, i.e., how the data are gathered around, and its location, spread, and shape.

2.2.2 Machine Learning in Data-driven Optimisation

Machine learning (or data mining) techniques make predictions through modelling data. Interpretation of a model and assessment of its uncertainty is achieved by adopting statistical learning methodologies. Three major tasks are carried out. First, construct approximate mathematical models for data based on previous experiences. Second, select the best possible model by fitting or calibrating a function to observed data. Third, quantify the uncertainty in the model using probability theory and statistical inference.

Major algorithms in machine learning are supervised learning, unsupervised learning, reinforcement learning, and their combined variants. Models are learned or trained in supervised learning using training data sets, such as regression and classification operations. In u*nsupervised learning,* patterns in data sets are identified, and the data sets are neither classified nor labelled, such as dimension reduction and data clustering manoeuvres. In r*einforcement learning,* models are trained to make a sequence of decisions based on rewarding desired behaviours and punishing undesired ones, such as control of robotics of various kinds.

2.2.2.1 *Some primary data preparation techniques*

Commonly used basic techniques in machine learning are clustering, dimension reduction, regression and classification.

Clustering is used to split data into groups based on similarity principles of connectivity, distance, distribution or density. Subspace clustering or bi-

clustering is used to find the data structure high dimensional space. K-means Clustering partitions the data into K groups, where K < the total number of data and is a user-defined parameter. The data need to be normal-distributed in terms of the Euclidean distance in each cluster. Hierarchical clustering establishes a hierarchy of clusters by merging and splitting sub-clusters according to their similarity. It can use any form of similarity to do the clustering. No user-defined number of clusters is necessary. But it suffers high computational complexity ($O(N^3)$, N is the number of data) and requires ($O(N^2)$) memory. Two major versions exist, agglomerative hierarchical clustering and divisive hierarchical clustering. The first is a bottom-up approach, starting with each data point as a cluster and then merging similar clusters pairwise. The second approach is top-down, beginning with all data in one cluster and recursively splitting the clusters hierarchy by hierarchy.

Dimension reduction reduces the number of problem features by removing those redundant or less influential ones. It contributes to noise reduction, feature selection or extraction, modelling, data visualization, and data analysis. The primary technique is principal component analysis (PCA). It can be either done by a linear transform the n-dimensional data to a lower-dimensional coordinate system by maximizing the variance of the data [8] or by singular value decomposition. Classical PCA methods suffer the limitation that only effects of linear correlation between independent variables are accessed. Thus, nonlinear PCA methodologies are invented, such as principal curve, manifolds kernel PCA and neural networks based PCA.

Regression is the general term for establishing a functional relationship between a dependent variable as output (objective function) and the input of independent variables (decision variables). Several alternative models can be created. The best selection among the models is based on the bias-variance

trade-off in model evaluations. Higher-order models usually give smaller sample bias created using training data but may show more significant variances based on test data sets. The choice can be accessed and made using statistical methods, such as cross-validation, Akaike's information criterion, Bayesian information criterion, minimum description length, etc. The law of parsimony or Occam's razor says that the simplest model that can describe the data is the best.

Classification groups new observations to given known categories, which can be considered a supervised form of clustering. Extra challenges emerge when the data are class-imbalanced, i.e., some classes have much more data than others. The number of examples in the training dataset for each class label is heavily imbalanced. It can be mitigated by over-sampling the minority class and under-sampling the majority class.

2.2.2.2 *Some major machine learning models*

Some popular and frequently used data-driven surrogate models are polynomial regression (PR), multi-layer perceptron (MLP), radial-basis-function neural networks (RBFNN), support vector machines (SVMs), Gaussian process regression model (GPR), decision trees (DT), fuzzy rule systems (FRS), and ensembles.

Polynomial Response Surface (PRS) models a dependent variable as nth degree polynomial of independent variables [15]. Training data determine coefficients of various terms in the polynomial. The computational complexity increases with the increasing order and the amount of training data required.

The multi-layer perceptron (MLP) [18] uses feedforward neural networks. An MLP has an input layer, one or several hidden layers, activation functions and output layers. The outputs are expressed as a linear combination (weightings) of function values of activation function, which again are expressed as a linear

combination of function values of the previous hidden layer, and so on until it is done with the input layer. The activation function is a nonlinear function to tackle the model's nonlinearity. Examples of these functions are the sigmoid, tanh, softmax, rectified linear unit (ReLU), and variants. A linear activation function results in a higher learning speed than a nonlinear one.

Radial-basis-function neural networks (RBFNN) [19] also use artificial neural networks but typically have three layers (input, hidden, and output layers). RBFNN uses radial basis functions as activation functions, which are local functions, such as Gaussian function, reflected sigmoid, and multiquadric functions, strongly dependent on the distance between the places in the decision space where function values are estimated and the chosen centres of radial basis functions. Two alternative methods are used to train an RBFNN. One is to find parameters in the chosen RBF function and weights using supervised learning on training data. The other is to determine RBF function parameters by using the cluster centres and their spread through clustering the training data first. Afterwards, the weights are trained using the training data and the least square method.

Support vector machines (SVMs) are primarily used as machine learning models for classifications [20] and surrogate models. Data of n-dimensions are classified by an n-1 hyperplane which divides data with the most significant margin. SVM can be extended to classify inseparable data using loss functions like hinge loss, logistic loss, and exponential loss. It can also classify nonlinear data clusters by adopting kernel functions [21].

Gaussian process regression model (GP) [22], also called the kriging model, is an interpolation method that considers the statistical relationships (correlations) between the data. The effects of distance and direction between sample points to the predictions at a given point are considered through spatial

correlations, contributing to the prediction variation. A mathematical function is fitted to all points within a specified radius to determine the prediction at a location. Kriging is particularly useful when the data are spatially correlated and have a directional bias, and it can both predict the functional relationship and measure the uncertainty of the approximations [22].

Decision trees (DT) [23] consist of three nodes: root, decision, and leaf nodes. Root or higher up leaf nodes and decision nodes divide data into several classes. The decision-making process or classification or regression tasks are visualised and made. Specific criteria regulate the depth of a decision tree.

Fuzzy rule systems (FRS) [24] use fuzzy sets to mimic expert knowledge. A fuzzy set describes the “truth” of a statement in terms of a degree from 0 to 1 specified by a membership function. Multiple fuzzy sets can be combined to form fuzzy subsets, each defined by a fuzzy membership function. The parameters of membership functions can be determined using training data. One significant advantage of fuzzy systems is their good interpretability, and they can be used for regression and classification.

Ensembles [25] combine several accurate and diverse base models to predict function value so that both bias and variance are simultaneously minimised. A decision-making procedure determines the final model selection.

2.2.2.3 *Sensitivity Analysis*

Sensitivity analysis is used to determine the contribution of a decision variable to the total change of objective function value. It gives answers as the relative importance of decision variables of the problem. A decision variable may be kept to a constant value if its variation contributes limitedly to the overall change of an objective function (e.g., less than 5% of the total). Such an analysis may also provide a priority list of decision variables if input variables' uncertainty is reduced concerning Maximum Uncertainty Reduction. It can also

be used to find out interactions among parameters or decision variables in the model. Moreover, it provides valuable insights for generating new samples by identifying the main region of interest in decision space.

Several methods are established with differences in whether an approach is local or global, qualitative or quantitative, parametric or non-parametric and model-based or not. Typical examples mentioned are the Morris method [26] and the Sobol's method [27].

2.2.2.4 *Verification Methods for Surrogate Models*

Modelling errors [28] are analysed based on either metrics relying on testing methods or metrics relying on sampling methods. The former group contains main methods such as Jackknife error, Bootstrap error, Cross-validation, Predictive Estimation of Model Fidelity (PEMF) error, etc. The performance of the metrics depends on the type of surrogate model used and the functional relationship the surrogate model simulates. The latter includes Coefficient of Determination, Mean Square Error (MSE), Root Mean Square Error (RMSE), Maximum Absolute Error (MaxAE), Relative Maximum Absolute Error (RMAE), Mean Absolute Error (MeanAE), Relative Average Absolute Error (RAAE), etc. The efficacy of these metrics relies on the number and the quality of test data adopted in the calculations.

2.2.2.5 *Surrogate Model Management*

Surrogate model management is related to enhance the modelling accuracy and the solution efficiency. Surrogate model management in data-driven evolutionary optimisation is categorized into offline and online methods, depending on whether new data are attained and utilised in the ongoing optimisation process.

It is of an offline type when no extra data are sampled and added to the optimisation process. The accuracy of surrogate models in such a case is hard

to be validated. The key issue is how to as far as possible improve the quality and enlarge the amount of data, and efficiently use the limited data to build robust and accurate surrogate models. Several major techniques are available [8]: **data pre-processing** by local regression smoothing method for noisy data; **data mining** where synthetic data are generated; **semi-supervised learning** in which implicit information is also used in the modelling work; **model selection** where the most efficient surrogate models are chosen based on validation error analysis; **ensemble learning** where a number of different models are combined in a model ensemble; **multi-form optimisation** in which the problem is formulated using multi-fidelity models with unequal computational costs in fitness evaluations; **transfer learning** in which common knowledge from similar problems are utilised to save computational costs.

A data-driven evolutionary optimisation is of an online type when new data are added into the search during the optimisation process so that the global and local accuracy of surrogate models are improved, and the optimization performance is enhanced in that false optimum is detected and removed by recursively checking the validity of solutions either through performing numerical simulations or physical experiments. Methods for online surrogate management are grouped into **population based**, **generation based**, and **individual based ones** [8]. In a population based method, multiple populations generated based on disparate models of different fidelity co-evolve at the same time. The population of low fidelity carries out a preliminary search, and the optimality obtained is checked and verified using the population of high fidelity, i.e., of expensive models. In a generation based method, the surrogates are enhanced generation-wise, for instance, by training and optimising the surrogates using the attained data and the converged solutions are evaluated using a model of high fidelity. The surrogates are then updated, and a new

round of search is performed based on the updated surrogates. In an individual based method, individual data are chosen, and their quality is evaluated using models of high fidelity, which is done to reduce randomness and speed up the evolution. The representative techniques are **pre-selection**, **random strategy**, **best strategy**, **clustering method** and **uncertainty based strategy** [8]. In pre-selection, a larger population than targeted is first created in the optimisation process and the best targeted number of solutions are sifted out. In random strategy, a specified number of individuals from the offspring population is randomly selected and evaluated using the model of high fidelity. In best strategy, the best N' individuals from N offspring are evaluated using the high fidelity fitness function. In a clustering method, the number of individuals to be evaluated using the expensive real fitness function is reduced by grouping the population into a number of clusters and only the individuals closest to each cluster centre is evaluated using the real fitness function. In an uncertainty based strategy, individuals that are far from the existing training samples are selected for model updating to enhance the model quality and to promote the exploration type of search.

2.3 Evolutionary and Swarm Optimization

2.3.1 Evolutionary and Swarm optimization versus classical optimisation methods

Classical optimisation methods may be categorised into gradient-based methods, such as Newton's method, Quasi-Newton Method, and gradient-free methods, such as Line Search, Pattern Search [10], [19], [29]. Gradient-based methods are often preferred when the objective function is differentiable since the optimal search direction can be found precisely. Derivative-free search methods find their usage when derivatives of the objective function are difficult to determine. The main advantage of the classical methods is the quick convergence to optimum and thus the limited consumption of computational power. But the solution may quickly get stuck in a local optimum and may converge slowly due to a low or a negative gradient. In addition, complicated black-box optimisation problems are nontrivial to be solved by classical methods.

Evolutionary and Swarm optimisation methodologies are also gradient-free methods. The optimisation is searched stochastically by functional evaluations and by applying random modifications on best candidate solutions obtained so far, and new best candidates are found based on environmental selection. New rounds of iteration continue until the optimality is hopefully found after a certain number of iterations. However, no guarantee is given to find the global optimum of the problem. Compared to classical methods, evolutionary and swarm optimisation algorithms can deal with complex optimisation problems that are otherwise difficult to solve optimally. Also, they may efficiently avoid being trapped in local optima while searching for the global optimum. The major weakness of the methods is that they often have high computational complexity.

2.3.2 Evolutionary and swarm algorithms

Metaheuristic optimisation algorithms are roughly divided into two major groups. One is developed based on the principles that emulate natural evolution for new creatures: mutation, crossover and environmental selection, which result in evolutionary algorithms. The other mimics swarm behaviours of social animals such as bird flocks and ant colonies, which lead to swarm algorithms.

All evolutionary algorithms utilise a set of randomly initialized starting points for search. The best candidate solutions are evaluated and selected using the fitness function and other criteria, resulting in the parent population. Crossover and mutation operations are performed on the parent population to generate a new offspring population. The best candidates are again chosen as the new parent population for the next round of iterations, and the process is repeated until a termination condition is reached. It differs between non-elitist and elitist environmental selection. The former selection is based on the offspring only, while the latter is based on parent and offspring populations together.

The swarm optimization algorithms use different swarm behaviours or solution principles. For instance, the optimality can be searched by guiding a population of candidate solutions called particles, moving around in the search space and working cooperatively in search for optimality; the intensity of pheromones of natural ants is utilised as the preference of optimised solutions in the ant colony algorithm, where the level of pheromone intensity increases with the number of ants who visit the specific route (solution).

A balance in exploration and exploitation should be baked into a metaheuristic optimisation algorithm and its parameter settings to avoid locking the solution to a local optimum. At the same time, a reasonable rate of convergence to the global optimum is secured. The exploration is the

terminology for searching over a broader region for optimum, while exploitation is for a local search to optimum [30]–[32].

Representative evolutionary algorithms are genetic algorithms (GA), evolution strategies (ES), genetic programming (GP), differential evolution (DE), memetic algorithms (MA), estimation of distribution algorithms (EDA). In contrast, swarm algorithms are ant colony optimization (ACO), particle swarm optimization (PSO), etc.

Genetic algorithms (GA) [33] mimic natural evolution: genetic mutations on the individual decision variables, a crossover between decision variables, and environmental selection on the population based on the fitness evaluation [33]. A candidate solution is a phenotype with a set of properties; each called a chromosome or a genotype. The genomes can be randomly recombined (crossover) and mutated to form new phenotypes or candidate solutions, subject to new selection based on their fitness evaluation. A new parent population is thus formed, ready for the next round of iteration [34]–[36]. Although GA is a popular metaheuristic algorithm, it suffers high computational power consumption due to its repeated fitness function evaluation for complex problems and exponentially increased mutation operations when the number of decision variables is large.

Evolution strategies (ES) [37] have some similarities with GA but differ in several aspects. For instance, ES uses a normally distributed random vector to mutate genomes, and the mutation strength (the standard deviation of the normal distribution) can be determined by self-adaptation. Moreover, the correlations of mutation strengths for decision variables are expressed by a self-adapted covariance matrix or updated using covariance matrix adaptation (CMA-ES) [38]–[40]. Another difference is that environmental selection of ES is

made based on the fitness rankings while it is performed randomly in a pool of parent candidates in GA [37].

Genetic programming (GP) [41] is also an evolutionary algorithm similar to GA. Still, it differs in using other presentations of objective functions or the search space, such as a decision tree structure, resulting in different initialization and variation operators. Crossover and mutation are performed using sub-trees from parents forming a new tree as offspring. The fitness evaluations can be done in many ways, and the alternatives available are more than the case in GA.

Ant colony optimization (ACO) [42] utilises the preference of optimised solutions by natural ants based on the intensity of pheromones. N artificial ants (N candidate solutions) are engaged to find the best route for access to food, and the problem is to find the shortest path. When an ant passes a specific path, it lays down pheromones. The search initialised using an equal number of ants in each route alternative and an equal amount of pheromones that fades out as the iterations continue. Over time, the route covered with the most significant amount of pheromones is the optimal one.

Differential evolution (DE) [32]–[37] searches for global optimum also by iteratively performing operations such as mutation, crossover, and environmental selection. The mutation on decision variables is done by perturbation using the difference vector of two or more randomly chosen solutions in the current population multiplied by a user-defined ratio factor F, which results in a donor vector for each individual in the population. The solution vector of the population best is often used. The crossover is performed using either binomial or exponential methods, creating a trial vector. The j^{th} component of offspring is taken either from its parent or the donor vectors according to the crossover rate (Cr), a user-defined parameter. Fitness

evaluations make the environmental selection of both the parent and the trial vectors. DEs have been further improved using different crossover and mutation operations [43], by adapting the main parameters to different iteration stages [44], [46]–[48] and by combining with other solution techniques to form a hybrid optimisation method [49]–[51]. DE is flexible in use. Its main limitation is that its parameters are sensitive to the nonlinearity of the objective function [43].

Particle swarm optimization (PSO) [52] searches for optimality by guiding a population of candidate solutions called particles, moving around in the search space. The start-up positions of particles are generated randomly. Starting from the current location with the individuals' current velocity, the particles move towards their individual best position and the population's common best position. After each iteration, the individual and the population best are updated [29]–[31]. The swarms can be formed as one or sub-groups, called topology considerations [53]. The efficiency of PSO is very much dependent on the choice of its parameter [31].

Memetic algorithms (MA) [54] is a hybrid search method. The evolutionary algorithm is embedded with local greedy search algorithms, performed before the offspring are evaluated for environmental selection to reduce the likelihood of premature convergence. Such a local search method can be taken from gradient-based methods. MA benefits from the explorative search ability of evolutionary algorithms while profits the exploitative power of a greedy local search.

Estimation of distribution algorithms (EDA) [55], also called probabilistic model-building genetic algorithms (PMBGAs), are population-based search algorithms. Compared to other similar methods, EDAs, instead of applying

genetic operators, create offspring using explicit probabilistic models built and sampled based on promising parent solutions.

2.3.3 Evolutionary Multi-objective Optimization

Multiple solutions of MOPs usually exist and form a solution set, known as Pareto optimal solution set. The corresponding objective function values in the objective space shape the Pareto front. The Pareto front and the Pareto optimal solutions are expressed in discrete solution points, i.e., representative data subsets. The quality of the solutions is measured in convergence and diversity, i.e., how well the solutions are converged to optimality and the uniformity and the extent of the coverage over the whole Pareto front.

Another issue is handling objective functions of different scales in multi-objective optimisation problems. Many alternatives have been tried to normalise the objective functions to avoid having objective functions in mostly different scales in the analysis. The most commonly used method of normalisation [9]: the objective functions are normalised by the differences in optimal function values in the Nadir and Ideal (or Utopia) points. The Ideal point is an auxiliary point with the least values of each objective function as coordinates. In contrast, Nadir point, on the contrary, consists of coordinates of the largest of each objective. The variational part of objective functions then varies between 0 and 1.

The coordinate values at Nadir Point [9]:

$$Z_i^{Nad} = \max_{f(\boldsymbol{x}) \epsilon Pareto\ Front} f_i(\boldsymbol{x}) \quad \text{Eq. 2.4}$$

The coordinate values at Utopia Point:

$$Z_i^{*} = \min_{f(\boldsymbol{x}) \epsilon Pareto\ Front} f_i(\boldsymbol{x}) \quad \text{Eq. 2.5}$$

In practice, the attaining of exact Nadir point and Ideal point for problems of more than two objectives is nontrivial because it requires knowledge of the

whole Pareto-optimal surface and the acquisition of extreme Pareto optimal solutions, which are both problematic and computationally costly to be realized. The paradox is that obtaining the whole Pareto-optimal surface using most existing MOP algorithms demands some prior information about the location of Nadir point.

Normalised objective functions:

$$f_{i,normalized} = \frac{(f_i - Z_i^*)}{Z_i^{Nad} - Z_i^*}, where\ i = 1, 2, \dots, m \qquad \text{Eq. 2.6}$$

Analysis of multi-objective optimisation of objective functions of different scales might be done by transformation according to Eq. 2.4 to Eq. 2.6.

The methods of solving MOP can be roughly divided into three main categories: A priori, Posterior and Interactive methods [9], [10], [57].

A priori methods: extra preference information about the system to optimise is provided before the solution process starts. Some scalarization methods belong to this group, which are discussed in some detail in a later section.

A posteriori methods: solution of whole Pareto Front is obtained without preference information on solution requirements. Most of the evolutionary algorithms belong to this category of techniques.

Interactive methods: decision-makers act interactively by continually providing preference opinions and information to analysers during the solution process.

MOPs cannot be solved directly by classical optimization algorithms such as gradient-based methods. Instead, the problems need to be converted into one or several single-objective optimization problems. It can be done by weighted aggregation methods or ε-constraint method.

The weighted aggregation methods can, in more general form, be commonly expressed as [9]:

$$F(\boldsymbol{x}) = \left(\sum_{i=1}^{m} w_i[f_i(\boldsymbol{x}) - z_i^*]^p\right)^{1/p} \quad \text{Eq. 2.7}$$

in which p ∈ (0,∞), $\boldsymbol{z}^*$ is the ideal point, composed of the minimum values of each objective, w_i is the weight for the i^{th} objective function and 0 ≤ w_i≤ 1, $\sum_1^m w_i = 1$, and m is the number of objective functions.

ε-constraint method is expressed as:

$$minf_j(\boldsymbol{x}), \quad s.t.\ f_i(\boldsymbol{x}) \leq \varepsilon_i, i \neq j \quad \text{Eq. 2.8}$$

where ε_i is a user-chosen constraint value for the i^{th} objective function, and the j^{th} function is to be minimised. By altering ε_i, various Pareto optimal solutions can be attained.

Both methods suffer from the fact that it is nontrivial to determine the parameter of a weight vector or constraints. Moreover, the optimisation must be repeated each time a given weight vector or set of constraints is provided, leading to low computational efficiency.

Mitigating the above challenges can be done using Decomposition Approaches, Dominance Based Approaches and Performance Indicator-Based Approaches.

Decomposition Approaches utilise specific scalarising functions to transform the MOP into single-objective optimisation subproblems, which are solved simultaneously in a single run [58]. The choice of parent candidates here is based on aggregated fitness value of solutions. These approaches have low computational complexity, enjoy the advantage of an explicit neighbourhood relationship, and possess natural diversity maintenance. The methods are the main subject of this thesis and are further discussed in section 2.3.5.

Dominance Based Approaches [59] utilise the dominance relationship and crowding distance to select the better ones among different solutions. The individuals in the population are sorted into several non-dominated fronts or

layers according to their dominance ranks. The crowding distance of a solution is calculated on the same front or layer-wise according to its two neighbours to enhance the solution's diversity. The environmental selection is made based on the size of the crowding distance. The extreme solutions of each front are assigned a large crowding distance always to be selected. The elitist non-dominated sorting genetic algorithm (NSGA-II) [60] is the most frequently used algorithm of this kind. The offspring and parent populations are combined, sorted, and the crowding distance is determined for all the individuals. Ranking in descending order according to the crowding distance, the better half of the combined population are selected as the parent population of the next generation.

Performance Indicator-Based Approaches [31], [32], [43], [44], [61] apply specific performance indicators that measure the convergence and diversity properties of candidate solutions and determine the fitness of solutions by judging their influence on the performance indicators and selecting parent candidates for generations of new candidates for the subsequent round iterations. A representative algorithm is the indicator-based evolutionary algorithm (IBEA) [61]. IBEA exploits a binary performance indicator (see section 2.8 for its definition) to compare solutions pairwise and then assigns a fitness value to each individual for environmental selection. Other indicator based algorithms can be mentioned: the S-metric selection based evolutionary multi-objective algorithm (SMS-EMOA) [62] and the fast hypervolume based evolutionary algorithm (HypE) [63]. Performance Indicator-Based Approaches have an advantage over the dominance-based method, where the diversity aspect is considered by performance indicator and thus is absent in the algorithmic formulation.

2.3.4 Evolutionary Many-Objective Evolutionary Optimization

New challenges emerge as the number of objectives increases to beyond three. The environmental selection pressure falls radically as the number of objectives increases when using non-dominance based MOEAs. The increasing portion of solutions becomes non-dominated so that the selection operation gradually turns out to be impossible to continue, and the convergence process ceases completely. Further, the computational complexity for indicators, such as hypervolume indicator, escalates drastically as the number of objectives increases, causing the use of indicators as selection criteria unpractical. Moreover, the search efficiency of Decomposition-based approaches is also severely worsened for partial, discontinuous or discrete problems and degenerated Pareto fronts because a large portion of pre-defined uniformly distributed reference vectors remains unexploited. At the same time, they still consume computational power to be created and explored. Another difficulty in handling many-objective optimisation problems is “the curse of dimensionality”. The number of data that sufficiently represent the Pareto front increases nearly exponentially as the number of objectives raises. Moreover, the Pareto front for most optimization problems is irregular. It is nontrivial to evaluate the diversity of PF from many-objective optimisation problems.

Several measures have been suggested to mitigate the challenges, such as reducing the number of objectives, modifying Pareto dominance, introducing additional criteria, etc. Additional criteria can be introduced in dominance enhancement-based algorithms to strengthen the dominance relationship in selecting new parent solutions among generated candidate solutions, thus increasing selection pressure towards convergence. User preferences are suggested to be used as a quality metric for PF of MaOP solutions and as guidance for the search process. When user preferences are not available, PF's knee points and knee regions can be searched [64].

Several classification works have been done to categorise types of MaOP algorithms [12]. One alternative is to group the methods into eight different classes [12]:

1) Relaxed dominance-based approach: The relaxed dominance-based approaches enhance the selection pressure in non-dominated sorting operation [8], [9]. The methods' common feature is that new candidates are selected by jumping over some non-dominated solutions in the vicinity of the previous iteration to enhance the selection pressure towards convergence.
2) Diversity-based approach [65]: the environmental selection is strengthened by maintaining the diversity to mitigate dominance resistance due to the high number of objectives in the optimisation problem.
3) Decomposition-based approach [65]: the MaOP is transformed into a set of single-objective optimisation subproblems, which are solved simultaneously. Here, the convergence and diversity are balanced for regular PF shapes, but sufficient diversified solutions are challenging for irregular PFs.
4) Reference set-based approach: A reference set of points or vectors is utilised and adapted to guide the search toward solutions of good diversity. Non-dominate Sorting Genetic Algorithm III (NSGA-III) [2] and Reference Vector-guided Evolutionary Algorithm (RVEA) [7] are typical algorithms of this kind. The significant challenges with this approach are the obstacles in creating and adapting the reference points and evaluating the solutions in a high dimensional objective space.
5) Preference-based approach [66]–[69]: instead of PF search in the entire objective space, decision makers' preferences are used in the search,

which is also called the region of interest (ROI). Determining the user preference is a tedious task in practice and needs repeated feedback from the decision-makers.

6) Dimensionality reduction approach [70]: redundant or less influential objectives are eliminated in the optimisation process. The methods usually increase the computational cost, reduce search efficiencies and escalate complexity in decision-making.
7) Indicator-based approach [78-80]: use indicator values of a temporary solution set to select better candidates for the next round of iterations. A decent indicator value results in a solution set close to PF. The fast hyper-volume approximation method [71] is a representative algorithm of this kind. Other examples are the shift-based density estimation indicator MaOP [78], stochastic-ranking-based multi-indicator algorithm [79]. The methods are often computationally expensive and provide solutions that are weaker in diversity than those from reference set-based approaches.
8) Hybridization method [72]: combine the methodologies from different algorithm classes to guide the search towards optimality.

Representative evolutionary many-objective optimization algorithms are Non-dominate sorting genetic algorithm III (NSGA-III), reference vector-based evolutionary algorithm (RVEA), knee-driven evolutionary algorithm (KnEA), two-archive evolutionary algorithm (Two_Arch), preference-based algorithms, grid-based evolutionary algorithm (GrEA), corner sort algorithm.

Non-dominate sorting genetic algorithm III (NSGA-III) [2] uses the same framework of the evolutionary cycle of NSGA-II: initialisation, crossover and mutation to create an offspring population from the current population. However, it differs from NSGA II in the environmental selection, where a set of widely and uniformly distributed reference points in the objective space is

utilised in the selection process to maintain diversity among solutions. The candidate solutions associated with each of these reference points are selected to attain a set of diverse and well-distributed nondominated solutions as a new parent population. NSGA-III often has a slower convergence speed than the indicator-based method IBEA and grid-based method GrEA but gives PF approximations of better diversity. See discussions in Chapters 5 and 6.

Reference vector guided evolution algorithm (RVEA) [7] exploits a system of reference vectors in the objective space to specify the preferred directions of locations of the solutions in contrast to other decomposition-based algorithms in which a scalarizing function is adopted to tuning MOP or MaOP into a set of SOP problems. The uniformly distributed reference vectors are first generated on a unit hyperplane using the canonical simplex-lattice design method [73]. Further, RVEA uses the angle between a reference vector and the vector of the candidate solution as a diversity indicator, which is more scalable to optimisation problems of a high number of objectives. The population is partitioned into N (population size) subspaces divided by the reference vectors. A metric called as Angle-Penalized Distance of candidates found so far is used to perform the Environmental Selection for offspring, which is proportional to the norm of the translated vector of candidate solution and the amount of penalty function that increases with the number of iterations and the acute angle between the vector of candidate solution and the reference vector. The translated vector is the difference vector between the candidate solution and the minimal objective values calculated from the combined population in that subspace. Moreover, adaptation mechanisms for adjusting the reference vectors can be conveniently implemented to improve the diversity of solutions of irregulated PFs [74].

Knee-driven evolutionary algorithm (KnEA) [75] takes a second criterion for environmental selection to replace the dominance-based one. Based on a similar framework of genetic algorithms such as NSGA II, the environmental selection in KnEA is made on candidates of current knee points, which are the solutions that are farther away from the hyperplane constructed by the boundary solutions of the current population.

The two-archive algorithm uses two archives to store temporarily sorted candidate solutions separately, one is convergence based, and the other is diversity based [76]. Interactions between and inside CA and DA play essential roles in environmental selection. The method is further developed to an improved version Two_Arch2 [77], in which the selection methodologies in CA and DA are changed. CA applies the $I_{\varepsilon+}$ indicator [77], and DA utilises the Pareto dominance, calculated in $L_{1/m}$ norm-based distance as the similarity measure, where m is the number of objective functions. It combines the strength of indicator- and Pareto-based MOEAs. The mutation operation occurs only in CA, and the crossover operation is applied between candidates in CA and DA.

Preference-based MaOPs use DM's preference to narrow down the critical search area of PF to reduce the number of solutions to a manageable level. PICEA-g [78] is the most frequently used algorithm of this type.

In a grid-based evolutionary algorithm (GrEA), the objective space is divided into hypercubes, and the selection of candidates for the next generation (iteration) undergoes according to grid dominance. The selection pressure towards convergent and diversified solutions is increased. Grid-based evolutionary algorithm (GrEA) [79] can be mentioned as a representative algorithm of this kind.

Corner sort algorithm [80] utilises the corner solutions, which are always non-dominated and easy to find by only comparing one objective, to carry out the non-dominated sorting operation with the advantage that a large number of objective comparisons under the dominance sorting is omitted with saved computational time.

2.3.5 Decomposition-Based Strategies for Many-objective Evolutionary Optimisation

The decomposition-based MOP methods are extendable to solve MaOPs [81]–[83]. The performance of decomposition-based MaOP methods relies heavily on scalarising functions [84] and the generation of a proper set of reference vectors [85], where each subproblem is formed using a different reference vector which may also change over the iterations. The points of intersections between the true PF and the reference vectors should be located equidistantly. It is often challenging for the methods to attain solutions with good diversity because of the high dimensionality of MaOPs, although the convergence and the diversity of solutions are well balanced during the solution process.

The scalarization functions of Eq. 2.8 provides a general form of scalarization functions. The linear weighted aggregation function rises if p = 1 and $\boldsymbol{z}^*$= [z_1^*, $z_2^*, \dots, z_m^*$] is set to the origin. Although simplicity is conserved, the linear model can only give Pareto optimal solutions on the convex part of the Pareto front. When used on the concave part, only extremal solutions can be approximated independently on how the weight vector is altered.

The Chebyshev scalarizing function is attained when $p \to \infty$,

$$F(\boldsymbol{x}) = max_i[w_i|f_i(\boldsymbol{x}) - z_i^*|] \qquad \text{Eq. 2.9}$$

As Eq.2.8 indicates, when p → ∞, all terms in Eq. 2.8 diminish compared with the maximal one: $w_i[f_i(\boldsymbol{x}) - z_i^*]^p$. It leads to Eq. 2.10.

Another frequently utilised scalarization method is Penalty Boundary Intersection (PBI) [58]:

$$min_{\boldsymbol{x}\in\Omega}\ g^{pbi}(\boldsymbol{x}|\boldsymbol{w},\boldsymbol{z}^*) = d_1 + \theta \times d_2 \qquad \text{Eq. 2.10}$$

$$s.t.\ d_1 = \frac{\boldsymbol{w}^T[\boldsymbol{F}(\boldsymbol{x})-\boldsymbol{z}^*]}{\|\boldsymbol{w}\|_2},\ d_2 = \|\boldsymbol{F}(\boldsymbol{x}) - \boldsymbol{z}^* - d_1 \times \boldsymbol{w}\|_2 \qquad \text{Eq. 2.11}$$

in which θ is a penalty parameter to be tuned.a

Other scalarization functions exist, such as Weighted Exponential Sum, Weighted Product, Quadratic Mean, Exponential Mean and more are explained in [86]–[88]. More recently, the Multiplicative Scalarizing Function (MSF) and Penalty based SF (PSF) are suggested in [89].

The weighted sum method (WSM) is efficient computationally compared to other methods. However, it cannot solve problems with non-convex shapes because only solutions of the extremal ones are found in such cases. A Decomposition Evolutionary Multi-Objective based on Local Weight Sum algorithm (MOEA/D-LWS) proposed in [90] may overcome the shortcoming. In [81], the decomposition-based MaOP algorithm uses two adjustments on the direction vectors (MaOEA/D-2ADV) to ensure convergence and diversity.

The standard decomposition-based methods often adopt Das and Dennis method to create uniformly distributed reference vectors on the simplex plane. The reference vectors generated are insufficient when used to solve optimisation problems of irregular PFs because a set of evenly distributed reference vectors are applied, which cannot cover the PFs uniformly in a satisfactory manner. In such cases, the adaptation of reference vectors or reference points and clustering methods can be taken into use [91]. Hua et al. [92] suggest a hierarchical clustering algorithm to group the non-dominated solutions, upon which the environmental selection is carried out. Multiple reference vector sets can be used to find Pareto optimal solutions of a degenerate Pareto front [93]. Liu et al. [94] propose an adaptive reference

vector-based algorithm inspired by the idea of an improved growing neural gas network.

2.3.6 Handling of Constraints

Constraints are additional conditions of an optimisation problem that the feasible solution must satisfy. In general, two main types constraints exist [9], [95], [96]: equality constraints and inequality constraints. Also, it differs between hard constraints and soft constraints. Hard constraints are those which must be satisfied by the feasible set of candidate solutions. Soft constraints are those that are preferred but not required to be satisfied.

In general, three cases of constraints are handled individually: [9]

- An inequality constraint is of a binding type when an equality constraint coincides with the inequality constraint at its boundary at the optimal point. The word “binding” means that the optimal point cannot be moved along the equality constraint.
- An inequality constraint is a non-binding type when an equality constraint is located inside the feasible areas described by the inequality constraint at the optimal point. For a non-binding inequality constraint, the optimisation problem can be solved by ignoring the inequality constraints.
- A candidate solution is infeasible when the answer violates the constraint of the problem.

Handling constraints is a significant task in finding solutions to the optimisation problem. Four main approaches are frequently used for SOP:

- Method of Lagrange multipliers: can be used for finding the optimum of a function subject to equality constraints [9], [10], [97].
- Karush–Kuhn–Tucker (KKT) conditions: can be used to formulate optimisation problems with inequality constraints, which can be solved numerically [10], [11].

- Penalty functions: Both equality and inequality constraints can be dealt with by using penalty functions. For a minimisation process, the areas in the solution space bounded by constraints set too much higher function values, such as infinity. A solution in these areas is never attractive and is never chosen. For a maximisation process, on the contrary, the function values are set to zeros in those areas [10], [95], [97].
- Decision variable substitution: an equality constraint can also be considered an equation that must be satisfied under the optimisation process. It can be done by expressing a decision variable by the other input variables and taking away the variable from the optimisation process [9], [10].

Moreover, constraints in constrained multi-objective optimisation problems (CMOP) are mainly dealt with by simultaneously balancing convergence, diversity, and feasibility. These three factors are fundamental issues for CMOPs. The feasibility of the solution is described by the constraint violation function ($CV = 0$) value is zero, which is expressed as:

$$CV(\boldsymbol{x}) = \sum_{j=1}^{J} c_j(\boldsymbol{x}) + \sum_{k=1}^{K} c_k(\boldsymbol{x}) \quad \text{Eq. 2.12}$$

in which $c_j(\boldsymbol{x})$ and $c_k(\boldsymbol{x})$ are the degree of constraint violations of j^{th} inequality constraint $g_j(\boldsymbol{x})$ and k^{th} equality constraints of $h_k(\boldsymbol{x})$, respectively, and are formulated as:

$$c_j(x) = max\{g_j(\boldsymbol{x}), 0\}, j = 1, 2, \dots, J \quad \text{Eq. 2.13}$$

$$c_k(x) = max\{h_j(\boldsymbol{x}) - \epsilon, 0\}, k = 1, 2, \dots, K \quad \text{Eq. 2.14}$$

in which ϵ is a sufficiently small tolerance term and is often sat as $\epsilon = 10^{-6}$. J and K are the total inequality and equality constraints, respectively.

Many constraint handling techniques are based on the principle that the searching population are first pushed into the feasible region. Then iteration towards true PF in convergence and diversity starts accordingly. Such a strategy's weakness is that the solution might be captured in local optima or feasible local regions [98]. Li et al. [98] have categorised the existing constraint handling techniques into three groups. The first one is based on the principle that feasible solutions dominate non-feasible ones. Infeasible solutions have been ignored entirely in some formulations; this approach is called a naïve constraint handling method [99].

Deb et al. [100] introduced a constrained dominance relation for constrained multi-objective optimisation (CMOP), which is formulated as:

Approximation $\boldsymbol{F}^{(1)}$ constraint-dominates approximation $\boldsymbol{F}^{(2)}$ if:

1) $\boldsymbol{F}^{(1)}$ is feasible while $\boldsymbol{F}^{(2)}$ is not.
2) Both of them are infeasible, while $CV(\boldsymbol{F}^{(1)}) < CV(\boldsymbol{F}^{(2)})$, where $CV(\boldsymbol{F})$ is the constraint violation function.
3) Both are feasible and $\boldsymbol{F}^{(1)} \prec \boldsymbol{F}^{(2)}$.

Here, infeasible solutions are made use of in further iteration processes. Feasible solutions can evolve toward optimality, while infeasible solutions can iterate toward feasibility.

Montes and Coello [101] summarise and group the constraint handling techniques for MOP into 7 categories: feasibility rules, stochastic ranking, ε-constrained method, novel penalty functions, novel special operators, multi-objective concepts and ensemble of constraint-handling techniques.

2.3.7 Evaluation of Uncertainties and Robust Optimisation

Uncertainties in the optimisation problem are evaluated through the problem formulation is subject to variations related to the input vector, objective function, constraints, and how these uncertainties influence the finding of the Pareto optimal set. Decision-makers in practice prefer to search for the robust Pareto optimal set, which is less sensitive to uncertainties in variables. The issue can be tackled by finding the most robust PF instead of the global Pareto-optimal one [102].

Uncertainties of additive noise are often grouped into three categories [103]. The first one is related to perturbations imposed on decision variables depart from Pareto optimality. The second one is associated with noise in the fitness evaluations, which generates errors on PF. The third one is connected to changes in model parameters due to shifting environmental and operational conditions, which causes vagueness in objective function evaluations. The Multi-or Many-objective Optimization Problem under the above three categories of uncertainties can be formulated by adding perturbations to the respective terms [103]:

$$\text{Optimise } \{f_i(\boldsymbol{x}', \boldsymbol{c}')\},\ i = 1, 2, \dots, m \qquad \text{Eq. 2.15}$$

with $f_{1:m}(\boldsymbol{x}', \mathbf{c}') = \bar{f}_{1:m}(\boldsymbol{x}', \mathbf{c}') + e_{1:m}$

with respect to $x_j' \in \Omega,\ j = 1, 2, \dots, n$

subject to:

$$h_k(\boldsymbol{x}') = 0, \qquad k = 1, 2, \dots, K \qquad \text{Eq. 2.16}$$

$$g_l(\boldsymbol{x}') \leq 0, \qquad l = 1, 2, \dots, L \qquad \text{Eq. 2.17}$$

where:

- $\boldsymbol{x}' = [x_1 + \delta_1,\ x_2 + \delta_2, \dots,\ x_n + \delta_n]^T$ is the decision variable vector under perturbation vector $\boldsymbol{\delta} = [\delta_1,\ \delta_2, \dots,\ \delta_n]^T$.

- $\mathbf{c}' = \left[c_1 + \nu_1,\ c_2 + \nu_2, \dots,\ c_J + \nu_J\right]^T$, where $\boldsymbol{c} = \left[c_1,\ c_2, \dots,\ c_J\right]^T$ and $\boldsymbol{\nu} = \left[\nu_1, \nu_2, \dots,\ \nu_J\right]^T$ are the parameter vector $\boldsymbol{c}$ and their perturbation vector $\boldsymbol{\nu}$ in the objective functions. J is the total number of model parameters.
- $\boldsymbol{e} = [e_1,\ e_2, \dots,\ e_m]^T$ is the noise vector on objective functions.
- $\bar{f}_{1:m}(\boldsymbol{x}', \mathbf{c}')$ are the averaged fitness evaluations.

Additional uncertainty is linked to multiplicative noise, where the objective function is perturbed by multiplying a noise term:

$$f_i(\boldsymbol{x}', \boldsymbol{c}') = f_i(\boldsymbol{x}', \boldsymbol{c}')(1 + \varepsilon_i), \qquad i = 1, 2, \dots, m \qquad \text{Eq. 2.18}$$

where $\boldsymbol{\varepsilon}$ is the vector of random noise.

In [104], the fourth class of uncertainty is proposed, called feasibility uncertainties, which comes from errors in satisfying the constraints of decision variables.

Uncertainties have been treated as the interval optimization problem, where intervals in PF are quantified. The result is reflected in the variations in the decision variables and model parameters, which display a solution's insensitivity to variable perturbations. A robust Pareto optimal solution is insensitive to perturbations on decision variables and the model parameters [103].

Robust Solutions can also be searched based on the Robust counterpart approach, Expectation-Based Search and Variance-Based Search [103], all utilising response function values when subject to perturbations caused by decision variables and model parameters. In such an analysis, the degree of optimality is inevitably weakened, which means that a robust optimization searches for the best trade-off between optimality and robustness [103].

The Robust counterpart approach is made by optimising:

$$F(\boldsymbol{x}, \boldsymbol{\varepsilon_x}, \boldsymbol{a}, \boldsymbol{\varepsilon_a}) = sup_{\boldsymbol{\xi} \in R(\boldsymbol{x}, \boldsymbol{\varepsilon_x}), \boldsymbol{\eta} \in A(\boldsymbol{a}, \boldsymbol{\varepsilon_a})} f(\boldsymbol{\xi}, \boldsymbol{\eta}) \qquad \text{Eq. 2.19}$$

in which sup means, in this case, the largest. $R(\boldsymbol{x}, \boldsymbol{\varepsilon})$ is a neighbourhood of $\boldsymbol{x}$ of size $\boldsymbol{\varepsilon_x}$, i.e., $\boldsymbol{\xi} = \boldsymbol{x} \pm \boldsymbol{\varepsilon_x}$. $A(\boldsymbol{a}, \boldsymbol{\varepsilon_a})$ is a neighbourhood of $\boldsymbol{a}$ of size $\boldsymbol{\varepsilon_a}$, $\boldsymbol{\eta} = \boldsymbol{a} \pm \boldsymbol{\varepsilon_a}$.

In expectation-based search, the expected objective function due to perturbations is optimised:

$$\mu(\boldsymbol{x}) = \int f(\boldsymbol{x} + \boldsymbol{\delta}, \boldsymbol{a} + \boldsymbol{\nu}) p(\boldsymbol{\delta}, \boldsymbol{\nu}) d\boldsymbol{\delta} d\boldsymbol{\nu} \qquad \text{Eq. 2.20}$$

in which $p(\boldsymbol{\delta}, \boldsymbol{\nu})$ is the joint probability density function of perturbation of decision variable $\boldsymbol{x}$ and model parameter $\boldsymbol{a}$. Using a population-based search algorithm, Eq. 2.20 can be approximated as:

$$\bar{f}(\boldsymbol{x}) = \frac{1}{N} \sum_{i=1}^{N} f(\boldsymbol{x} + \boldsymbol{\delta}, \boldsymbol{a} + \boldsymbol{\nu}) \qquad \text{Eq. 2.21}$$

in which N is the sample size, $\delta_i \sim \mathcal{N}(0, \sigma_{\delta_i}^2)$, $\nu_i \sim \mathcal{N}(0, \sigma_{\nu_i}^2)$, $i = 1, \ldots, N$, are Gaussian noises.

In dispersion based robustness search, the variance of the objective function due to perturbations is optimised:

$$Var(\boldsymbol{x}) = \int (f(\boldsymbol{x} + \boldsymbol{\delta}, \boldsymbol{a} + \boldsymbol{\nu}) - f(\boldsymbol{x}, \boldsymbol{a}))^2 \, p(\boldsymbol{\delta}, \boldsymbol{\nu}) d\boldsymbol{\delta} d\boldsymbol{\nu} \qquad \text{Eq. 2.22}$$

and using a population-based search algorithm, Eq. 2.22 can be approximated as:

$$S(\boldsymbol{x}) = \frac{1}{N} \sum_{i=1}^{N} (f(\boldsymbol{x} + \boldsymbol{\delta}, \boldsymbol{a} + \boldsymbol{\nu}) - f(\boldsymbol{x}, \boldsymbol{a}))^2 \qquad \text{Eq. 2.23}$$

Optimality and Robustness are two objectives that are usually in conflict, and a trade-off between the objectives and the degree of robustness must be searched [105]. It can be done through multi-objective optimisation by combining Eq. 2.21 or 2.23 with the normal objective functions of the optimisation problem.

2.4 Benchmark Testing

Benchmark problems are a large set of easily implemented, artificially constructed, multi-objective test problems. They are easy to describe, understand and visualise, easy and fast to implement, and optima are often known in advance. Benchmark testing is vital for developing new and better EAs by understanding evolutionary algorithms' strengths and weaknesses.

2.4.1 Essential Properties of Benchmark Functions

Huband et al. [106] provide a comprehensive review of the topic of benchmarking. In the contest of this work, benchmarks for MOP and MaOP are focused. The major properties of such benchmark functions are summarised as below:

Scalability: A problem is scalable in terms of decision variables when for any problem of n_0 variables, it can be created for n_1 variables and $n_1 > n_0$. A similar definition is valid for problems of scalable objective functions.

Fitness landscape: The relationship between the Pareto optimal set and the Pareto optimal front can be one-to-one or many-to-one. Many-to-one is more challenging to an algorithm because it has to choose among multiple sets of decision variable vectors that result in the same objective vector.

Flat regions: are a subset of decision variable vectors that map a single point in objective space. In such areas, changes of decision variables lead to no alteration in the objective values. No helpful gradient information is available for further searching, and the problem is thus harder to be solved.

Unimodality/Multimodality: An objective function with only a single optimum has unimodality. In contrast, it contains multimodality when it has multiple local optima. The later optimisation problem is multimodal and is more difficult to solve as it can be stuck in local optima.

A deceptive objective function is an objective function with a true optimum and a deceptive optimum, and the search space favours the search towards the deceptive optimum.

The bias of the fitness landscape: evenly distributed samples of decision variables lead to unevenly distributed PF. Problems with solid bias may require analysis in both objective and decision spaces.

Separable/non-separable decision variable to objective function: when no effect of interaction between decision variable x_i and others on the global optimum of an objective function, x_i is said to be separable on the objective function. Otherwise, it is non-separable. When every objective of a problem is separable, it is a separable problem. Otherwise, it is a non-separable problem. Separable objectives can be solved more easily by estimating each decision variable independently. The final PF optimal set can be found as a cross-product of the optimal sets for each individually optimised decision variable. A particular case of separable objective functions is that objective functions are separable to a distance variable that only influences the convergence process. A position variable only affects the diversity of PF approximations. Decision variables that cannot be characterised as distance or position variables are mixed.

Extremal/medial decision variable: when a Pareto optimal set consists of a single value at the edge of its domain, the decision variable is an extreme one. If, on the contrary, it is located scattered in the central area of the domain, it is called a medial one. Extremal/medial decision variables influence the speed of convergence towards true PF.

Convex/concave/linear PF: A PF is convex when it covers its convex hull and is concave when it covers its concave hull and is linear when it is both

concave and convex. A mixed PF has parts of convex, concave, and linear shape.

The degenerate front is a PF front of dimension two lower than the problem's objective space dimension. Degenerate PFs are more challenging to find for algorithms searching for even spread of solutions across the Pareto optimal front.

Discontinuous PF: a disconnected PF, which often requires more iterations and is solved less efficiently using decomposition-based solution principles.

2.4.2 Major Benchmark Suites

A common weakness with the existing benchmarks is that they often share common characteristics and are formulated with decision variables of either position or distance types, i.e., none with mixed ones [106].

Deb, K. [107] suggests a two objective test problem toolkit for constructing two objective benchmark problems by combining three primary functions: position, distance, and shape. The benchmarks are used to test an algorithm’s ability to diversify along with PF, converge to the true PF, and determine PF's shape, respectively. It should be noted that some choice of the shape functions may affect the optimisation problem of having mixed parameters. When the chosen functions are multimodal, disconnected, or biased, an optimisation problem of mixed decision variables can be formed [106].

Zitzler et al. [108] propose a ZDT test suite, all of which can almost be created using Deb’s toolkit. The ZDT problems include multimodal problem PF of many-to-one problems (ZDT6), disconnected PF problems (ZDT3), multifrontal problem (ZDT4). The ZDT test suite's advantages are two-fold: PFs are well defined, and test results from different sources are available, making easy comparisons. But it only has problems with two objectives, no flat regions in decision space, no degenerate PF, and no problem is non-separable.

Deb et al. [109] recommend a DTLZ test suite by which the nine benchmarks are formed scalable to any number of objectives adopted in investigations MaOPs. Tests on MaOP algorithms can be performed concerning the effects of decision variable dependencies, multimodality, discontinuity, mixed convexity/concavity, degenerate, mixed parameters, and constraints. The characteristics absent are fitness landscapes with flat regions, deceptive optima, and non-separable problems [106].

Van Veldhuizen [110] introduces seven multi-objective test problems, MOP1–MOP7, based on the literature's available information. These benchmarks are less methodically constructed and are more challenging to solve. Effects of non-separability and multimodality, discontinuity, mixed parameters, degeneration have been considered. But most of the benchmarks have only two or three parameters and unscalable decision variables or objective functions of non-separable problems [106].

Huband et al. [106] suggest the WFG Toolkit, which can be used to construct nine scalable, multi-objective test problems (WFG1–WFG9). A benchmark problem is defined by a vector of parameters related to a targeted problem in objective space. The vector is established using a series of transition vectors from a vector of decision variables. Starting with several shape functions that determine the fitness space's geometry, each transition vector manipulates and regulates the benchmark function characteristics via a series of composable transformations. The WFG Toolkit provides a variety of predefined shape and transformation functions.

Cheng et al. [111] introduce a test suite of 15 benchmark functions, MaF1-MaF15, for evolutionary many-objective optimisation. The purposes of this introduction have been to eliminate shortcomings of existing test suites and to introduce more realistic benchmark cases as problems in real-world

applications. They claim that PFs of most DTLZ and WFG functions have a standard form and are similar to simplex shape, none with a convex pattern, which favour decomposition-based algorithms. Moreover, PF of degenerate type in higher dimensions (higher than 4) is absent. The MaF benchmark problems cover PF properties of being multimodal, disconnected, degenerate, non-separable, and an irregularly shaped complex Pareto set or with a large number of decision variables.

MaF benchmark problems have been adopted as test functions in CEC'2018 Competition on Many-Objective Optimisation [112].

2.5 Performance Indicators/Metrics for Testing of MaOP Algorithms

2.5.1 General Remarks

The qualitative and quantitative quality of an algorithm can be evaluated based on testing on Benchmark functions developed up to date and various performance metrics invented for evaluations. Many researchers have formulated the requirements for benchmark testing on new MOO solution methodologies and specific test metrics. [109], [113]–[121]

The main criteria for comparisons of different MOO algorithms are their abilities: [113]

1) to find the best-converged estimates to the right Pareto front (i.e., convergence).
2) to find the most diverse solutions to right Pareto front (i.e., diversity),
3) to calculate with the highest speed of convergence (i.e., computational efficiency),
4) to have mostly repeatable results from several runs (i.e., search robustness).

The comparisons on the performance of the algorithms of existing MOP solution techniques are complex and complicated. It is especially the case if the algorithm differs fundamentally in solution principles to its comparing algorithms. It is hard to find suitable standard metrics to be used in the comparison. Secondly, EMOs are stochastic, and the contrast must be based on statistical principles. Thirdly, MOP problems are diverse and complex, and no single solution technique is equally valid for all issues [116]. Some ideas are transformed into metrics for comparison, often used to measure MOP solution techniques' performance with the challenges in mind.

A MOP algorithm's performance is usually measured by determining how close the calculated Pareto front is to the actual optimal Pareto Front [116].

A MOP algorithm's efficiency: can partially be measured regarding the total number of objective function evaluations required to find the Pareto optimal. This needed number of objective function evaluations should be kept to a minimum since MOO solution techniques of EA are more dependent on functional assessment than traditional optimisation methods. Functional evaluations take the most significant computer power [116].

Robustness of a MOP algorithm: reflects the algorithm's ability to give similar results regarding mean value and variance from several runs. EA algorithms are stochastic, which means that the starting conditions are generated randomly, and comparable runs give different results and consume changed computational time. The robustness can be indicated by the width of the “band” around the Pareto front created by several algorithms runs, and the narrower a band suggests a more robust algorithm [116].

Parameters under comparison of different algorithms:

1) The number of independent runs: the number of times the algorithms are run independently. The robustness of the algorithm is tested through the variation of the results.
2) Population sizes for each run: number of candidates in a population. The population sizes influence the number of solutions used in the further search. Increasing population size generally reduces the efficiency and robustness of optimisation calculation [116].
3) It is equivalent to the maximum number of nondominated objective vectors and should be kept equal for all algorithms tested against each other [119].

4) A maximum number of function evaluations: the number of times a calculation of the objective functions during the solution process shall be kept equal under comparisons of algorithms being tested [119].
5) Parameter settings: parameters used in the algorithms being compared shall be tuned to their optimal values [116].

Black-box problems: [119] objective functions are considered black-boxes, i.e. putting values of decision variables into the black-boxes, objective function values come out as outputs, and the analytic forms of these problems cannot be utilised in the analysis.

Pareto compliance: [119] the metric used for MOO comparison should be compliant with the Pareto front location, i.e., the improved metric value indicates a more accurate approximation of Pareto Front.

In this work, the classical and most commonly used test functions of two and three objective functions and various decision variables are tested to validate the suggested method SOFO.

2.5.2 Taxonomy of Performance Metrics

Performance metrics are used to evaluate MaOP algorithms' performance and help decision-makers judge optimisation algorithms' efficiency. Performance indicators lead to information loss by summarising information to assess candidate solutions [122]. Nevertheless, the aim of PIs on an approximation set is to capture the core information searched robustly and accurately [122]; this is particularly important to be achieved for MaOP problems, for example, to maintain accuracy as the number of objectives increase.

While the definition of convergence of a solution set is well understood within MaOP research [19], the definition of good uniformity for a solution set is less clear. Inspired by the definition of biodiversity, Wang et al. [123] suggest

a definition of good uniformity that states that a solution set should have the same dissimilarity with their neighbours. A superior diversity should provide decision-makers with the maximum amount of information.

Zitzler et al. [124] have formulated a set of fundamental requirements on performance indicators. Ideally, a performance indicator should be both compatible ($A < B$ leads to statement C is true) and complete (if C is true, then $A < B$), which are often two challenging requirements to be satisfied simultaneously in the development of PIs. It must be compatible in practical use if it is meaningful in comparing two approximation sets.

Performance indicators can be classified as unary, binary and k-nary [125]. Unary PIs are those with which the evaluation function takes only one approximation set, which is assessed by assigning a score [126]. The majority of performance indicators are of unary types, such as Hypervolume indicator (HV) [127], Inverted Generational Distance indicator (IGD) [128], and newly developed PI of Coverage over Pareto Front (CPF) [129].

Several unary PIs may be combined to evaluate several qualities of approximations [127]. But challenges may exist related to determining the sequence of their usage or finding proper utility functions for their combined application [126].

Binary performance indicators are also developed to simultaneously take two approximation sets, A and B, in their evaluation. Typical examples of binary PIs: epsilon (ε) family [125], Two set coverage (C) [130], R-metric [131].

Further on, k-nary quality indicators have also been studied, in which k independent approximation sets are adopted in the evaluation function of a performance indicator [123]. It is a great challenge to establish proper utility functions in formulations of k-nary PIs, and their usage is so far limited.

Performance indicators in MaOP have also been roughly grouped into three categories: those which essentially evaluate convergence [126], those mainly assessing diversity [132], and those measuring both convergence and diversity [133].

Numerous performance indicators have been designed for the assessment of MaOP solution sets. Earlier comprehensive surveys on quality indicators and their properties can be found in the literature [123], [134].

The idea of using reference vectors to create a diversity score for contrasting two competing solution sets has been implemented successfully in the past [124], [129], [134].

Mostaghim and Teich [133] introduced SDM as the percentage of non-dominated solutions distributed along with a standard set of reference lines in objective space. The higher the SDM of an approximation set, the better the diversity of the solutions. Although possible, the method has not been extended to MaOP analysis.

Using reference vectors, Cai et al. [124] define a diversity indicator (DIR) by identifying the systematic deviations of candidate solutions' locations in terms of the mean values and variances called coverage vector. It stores the number of reference vectors linked to each candidate solution. But the formulation may not be adequate to deal with situations in which small clusters of candidate solutions exist. Equally, a high diversity score may result in each solution covering only one reference vector as a case of perfectly distributed solutions. Still, the former distribution is not uniform compared to the latter one. It is illustrated in Fig. 1 in a two objective optimisation case.

2.5.3 Some Frequently Used Performance Metrics

2.5.3.1 *Error Ratio*

Error Ratio (ER): [110] is the percentage of dominated solutions in a population of size N:

$$ER = \frac{\sum_{i=1}^{N} e_i}{N} \quad \text{Eq. 2.24}$$

In which

- N: the population size.
- e_i = 0 if i^{th} candidate solution is a Non-dominated solution.
- e_i = 1 if i^{th} candidate solution is a Dominated solution.

Error Ratio reflects the success rate of candidates in the population, so the lower the value of ER, the better the MOO algorithm.

2.5.3.2 *Generational Distance (GD)*

Generational Distance (GD): [110] is the Euclidean distance between the nearest of an algorithm calculated Pareto optimal point and the actual Pareto optimal point.

$$GD = \frac{\sqrt{\sum_{i=1}^{M}(min\ (d_i))^2}}{M} \quad \text{Eq. 2.25}$$

in which:

- M: is the number of Pareto optimal points calculated by the algorithm
- $min\ (d_i)$: is the shortest distance between algorithm simulated Pareto optimal point i to the corresponding nearest true Pareto optimal point

GD indicates the accuracy of the calculation of the MOP algorithm. If GD ≈ 0 means that the algorithm finds the right Pareto Front. The weakness is that GD is not Pareto compliant, which means that a smaller GD value does not always indicate a more accurate approximated Pareto Front.

Another modified metric is created to overcome the weakness of the Non-Pareto Compliance of GD metric.

2.5.3.3 *Inverted Generational Distance (IGD)*

Inverted Generational Distance (IGD) [128] is used to evaluate the performance of an algorithm. IGD is given as:

$$IGD(Q, P^*) = \frac{1}{|P^*|}\sqrt{\sum_{x \in P^*} (\min_{y \in A} d(x, y))^2} \quad \text{Eq. 2.26}$$

in which:

- Q : are nondominated objective vectors (points on objective space) calculated by the algorithm. Q is normalised.
- P^*: are uniformly distributed actual objective vectors over the Pareto Front of the MOP problem.
- $d(x, y)$: is the Euclidean distance between x (calculated Pareto optimal point) and y (true Pareto optimal point) in the normalised objective space.
- Q and P^* are first normalised component-wise using the respective maximum and minimum components of objective values among P^*.

IGD is an indicator of how close a calculated Pareto optimal front is to the true one. The smaller the value of IGD is, the more accurate the solutions are. IGD is Pareto compliant.

The mean and standard deviation can be obtained from the test on a single test function, i.e., average value μ and standard deviation σ of IGD of several similar runs of the MOO algorithm.

2.5.3.4 *Spacing Metric (SP)*

Spacing metric (SP) [135] indicates the spread of and spacing between Pareto front approximations calculated by an algorithm.

$$SP = \sqrt{\frac{1}{M-1}\sum_{i=1}^{m} (\overline{dnn} - dnn_i)^2} \quad \text{Eq. 2.27}$$

where:

$$dnn_i = \min_{\forall j \in [1,\dots,M], j \neq i} \left(\sum_{k=1}^{m} \left| f_i^k - f_j^k \right| \right) \quad \text{Eq. 2.28}$$

- M: number of points in Non-dominated solutions.
- m: number of objective functions.
- $\overline{dnn} = \frac{1}{M} \sum_{i=1}^{M} dnn_i$, i.e., the average value of dnn_i.
- $(f_i^1, f_i^2, \dots, f_i^m)$: are components of objective function value of calculated Pareto optimal point i.

SP reflects the distribution of calculated Pareto front approximations, and SP goes towards 0 means that the solutions are nearly equidistant. SP's weakness is that it cannot be used as a metric for MOP problems of higher dimensions since consecutive solutions in higher dimensions do not exist.

2.5.3.5 *Diversity Performance Metric*

A Diversity Performance Metric: [134] averaged accumulated difference of successive distances of the calculated Pareto points and a corresponding average distance of right Pareto points.

$$\Delta = \sum_{i=1}^{M-1} \frac{\left| d_i - \bar{d} \right|}{M - 1} \quad \text{Eq. 2.29}$$

in which:

- M: the total number of Pareto Points in the solution.
- d_i: successive distance of the calculated Pareto points i.
- $\bar{d}$: average successive distance of actual Pareto points.

An algorithm with a smaller Δ value is preferred.

2.5.3.6 *Mean Standard Score (MSS)*

The mean standard score (MSS) [134]: the average and standard deviation of the IGD values obtained from testing on many test functions, and each is done several times with similar runs of the MOP algorithm. MSS is given as:

$$MSS = \frac{1}{K}\sum_{i=1}^{K}\frac{\sum_{j=1}^{L}(I_{ij} - \mu_i)}{\sigma_i} \quad \text{Eq. 2.30}$$

in which:

- K is the number of test problems the MOO algorithm is tested on.
- L is the number of test runs on each test problem.
- I_{ij} is the IGD value obtained by the MOO algorithm in a run j for i^{th} test problem, i =*1*, …, K.
- μ_i is the average value of the i^{th} test problem, i =*1*, …, K.
- σ_i is the standard deviation of the i^{th} test problem, i =*1*, …, K.

The mean standard score (MSS) of the obtained IGD values for a group of test problems can rank MOP algorithms. It can be considered a comprehensive criterion to evaluate the overall performance of a MOP algorithm.

2.5.3.7 *Set Coverage Metric*

The Set Coverage Metric: [134] the ratio of some calculated Pareto optimal Q solutions dominated by true Pareto optimal P^* and number of P^* solutions. The metric may be used in the comparison of MOP problems in higher dimensions than 2D.

2.5.3.8 *Chi-Square-like Deviation Metric*

The Chi-Square-like Deviation Metric [134]: the number of calculated Pareto optimal Q points within a hypervolume formed around each correct Pareto point P^* solution and a user-defined neighbourhood distance σ, are counted. The number is compared with the number corresponding to a $P's$ uniform distribution and the deviation is calculated.

2.5.3.9 *ε-Performance Metric*

The ε-Performance Metric: [134] is a measure of diversity by registering the proportion of how many estimated Pareto points which located inside a user-specified ε hypercube ($\varepsilon = [\varepsilon_1, \varepsilon_2, \ldots, \varepsilon_m]$, in which m is the number of objective

functions) around reference Pareto points. See Figure 2.2. If a calculated Pareto point falls inside such a hypercube, the score is increased by one. Otherwise, the score is not changed. Only the nearest calculated point regarding the Euclidean distance to the reference point is counted. If there are other points in the same hypercube, they can be analysed in neighbouring hypercubes. The metric is given by the ratio of the final score and the number of reference Pareto points used. The metric provides a measure of both convergence and diversity, and it may vary between 0 and 1, with the value 1 indicating full convergence. The metric can be used for problems of any number of dimensions in objective space.

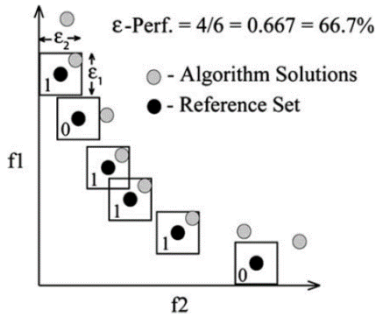

Figure 2.2 - Calculation of the ϵ-performance metric. [134]

2.5.3.10 *Hyper-Volume Metric*

The Hyper-Volume Metric: [127] calculates the volume of the objective space formed by a calculated set. A larger metric value is preferred. A detailed discussion of the metric is given in Chapter 4.

2.5.3.11 *Shannon's Entropy*

Shannon's Entropy H(S): [134] is also a metric for calculating Pareto Front's diversity. It is defined as:

$$H(s) = -\sum_{i=1}^{N} p_i ln\,(p_i) \qquad \text{Eq. 2.31}$$

in which:

- N: number of calculated Pareto points.

- p_i: density of i^{th} calculated Pareto point.

$$p_i = \frac{density(\overrightarrow{q_i})}{\sum_{j=1}^{N} density(\overrightarrow{q_j})} \quad \text{Eq. 2.32}$$

where:

- q_i and q_j are calculated Pareto Point i and j, respectively.
- Density $(\overrightarrow{q_i})$= $\sum_{j=1}^{N}$ influence $(\overrightarrow{q_j}, \overrightarrow{q_i})$, and
- Influence $\left(\overrightarrow{q_j}, \overrightarrow{q_i}\right) = \frac{1}{|\overrightarrow{q_i} - \overrightarrow{q_j}|^2}$, i.e., the influence of q_j on q_i is proportional to the inverse of distance squared.

If all solutions are equally spaced, i.e., diversity is at its maximum, influence of q_j on q_i is the same for all points, and all p_i is equal, and each equals $1/N$. The Shannon's Entropy H(S) becomes $ln(N)$, the maximum value it can take. On the other hand, when all solutions are gathered together, i.e., diversity is 0, the influence of q_j on q_i is infinity, and all p_i goes towards 0 if N is large. Shannon's Entropy H(S) goes towards 0, the minimum value it can take.

2.5.3.12 *Algorithm Complexity*

Algorithm Complexity: [112] The complexity of an algorithm can be measured indirectly by the ratio of computational time, which is not used for objective function evaluation to the time of objective function evaluation, by:

$$Complexity = (T_2 - T_1)/T_1 \quad \text{Eq. 2.33}$$

in which:

- T_1 = $\sum_{i=1}^{N} t_{1i}/N$, where t_{1i} is the computing time of 10000 objective function evaluations for the problem i. N is the total number of the test functions.
- T_2 = $\sum_{i=1}^{N} t_{2i}/N$, where t_{2i} is the total computing time for the algorithm with 10000 function evaluations for the problem i.

2.6 Statistical Test Methods

Approximations of metaheuristic optimisation algorithms have random characteristics. When two or more sets of solutions are compared, statistical approaches have to be adopted. Frequently used statistical methods are Wilcoxon rank-sum test [136], Student's *t*-test and Z-test.

Wilcoxon rank-sum test [136] is a nonparametric test of the null hypothesis that, for two populations, X and Y, the probability of X being more significant than Y equals the probability of Y being higher than X. The alternative hypothesis H_1 is that the distributions are not equal, and either X being higher than Y or Y being higher than X with a given confidence interval. Two assumptions are made about the population members. First, they are independent of each other. Second, any two observations in the populations can be compared for higher or lower probability than the other (the so-called ordinal property).

The Student's *t*-test is also a statistical hypothesis test. The null hypothesis that the means of two sets of data are not significantly different follows a Student's *t*-distribution. For a sample of normal distributed n observations, the *t*-distribution is the distribution of the location of the sample mean relative to the true mean, divided by the sample standard deviation, and multiplied by the standardising term $\sqrt{n}$. It is why that the *t*-distribution can be used to form a confidence interval for the true mean [137].

Z-test is similar to the Student's *t*-test but is used when the standard deviation is known.

These methods are used to check the outcome of PF approximations: [117]

- Confidence intervals are calculated based on a certain level of the confidence factor, for example, 95%. The results are presented in the range around the mean value.

- The Student's *t*-test is used to check the hypnosis related to comparing mean values of various calculated amounts. It is used for pairwise, parametric testing for whether two data sets are statistically different. The T-test is applied for normally distributed data with a known population standard deviation of the difference.
- Wilcoxon rank-sum test is utilised to check for data set X being higher than data set Y or vice versa or the sets are equal within a specific confidence interval. Wilcoxon rank-sum test is used if the difference is not normally distributed. The distribution of difference of the solution sets obtained by non-deterministic optimization algorithms may not be normal.

The Bonferroni correction is adopted in case of multiple comparisons in hypothesis testing. It tests for the case that the null hypothesis is valid for all comparisons simultaneously or is false for at least one test. The method is stricter than the other methods because it ignores the effects of pdf distribution of all factors in the comparisons. The Bonferroni correction reduces the targeted overall significance level of the test α by testing each individual hypothesis at a significance level of α/k, where k is the number of null hypotheses or the number of test instances involved.

2.7 Visualisation of High Dimensional PF Approximations

Visualisation of the PF approximations may greatly help the decision-makers in their process, and it can also assist their work of interactively searching for optimised solutions. Moreover, efficiencies of optimisation algorithms can be compared and contrasted visually in terms of the dominance relationships, the convergence and diversity of approximations from the algorithms, etc. [2], [138].

Approximated Pareto Front (PF) of many-objective optimisation problems (MaOP) is an $(m-1)$ dimensional surface in m dimensional objective space where m is the number of objective functions involved in the optimisation process. Therefore, it is difficult to visualise it mainly because the number of axes exceeds three, so the human cognitive ability is surpassed. In addition, a large amount of data needs to be displayed simultaneously.

Filipič and Tušar [138] have summarised nine desired properties for an effective high dimensional visualisation method. The method should show dominance relations between PF approximation sets, PF shape, objective range, PF distribution, to maintain robustness, scalability, simplicity, uniqueness, and handle large and multiple data sets. See a more detailed description of these properties and the discussion on previous visualisation methods in Chapter 5 of the thesis. In general, visualisation methods as of today may be effective concerning some of the desired properties but fail in possessing other wanted capabilities [138]–[141]. A new visualisation method covering all the properties above is highly needed.

2.8 Metaheuristic Optimisation Methodology Applied in Advanced Design and Manufacturing

2.8.1 General Remarks

As engineers, we are eager to implement any new theory, methods and algorithms into practical usage. The current section provides an overview of the applications of data-driven evolutionary and swarm optimisation methods in the manufacturing industry, which partially provides the literature review for the application chapter of the thesis, Chapter 6, Minimising Crack Formation in Selective Laser Melting operations.

Design optimisation is finding the proper set of parameters that give the system's best possible performance. It is a process of iterative activities of an analytical stage and a synthesis stage [142]. The system's interrelationships, performance metrics, and design constraints are analysed and established during the analytical phase. Under the system's limitations, the best possible performances are found in the subsequent synthesis stage for specific parameters chosen. Optimisation techniques make it possible to attain the most efficient designs under the circumstances, especially for complex system design and optimal complex systems design under uncertainty. Machine parts are traditionally fabricated by first forming work blank by, for instance, forging or casting and are further machined to their final forms, where excess material is removed. It is, in general, characterised as a subtractive production method. Additive Manufacturing (AM) produces the final product directly by building one layer of time starting from its bottom [143]. AM has distinct advantages in making complex-shaped and customised parts, often in one go. Materials of plastics, as well as metals, can nowadays be used in an AM process. Laser-Based Additive Manufacturing (LBAM) is used to work with metal parts. The

selective laser melting (SLM) technique utilises a high power-density laser to melt and fuse metallic powders.

Achieving good quality, high reliability and good repeatability are significant challenges in using this technology. The process parameters highly influence the final product quality, the production system's consistency, the process's repeatability, and the production setups and procedures [143]. Consequently, the product's final quality, microstructure and mechanical properties are determined mainly by choosing such process parameters [143].

It has also been reported that laser power, layer thickness, and hatch space between adjacent laser paths within the same layer are the most dominating controllable process parameters for the Selective Laser Melting (SLM) process [144]. The most suitable process parameters settings can be found by simultaneously optimising target values: specific qualities, mechanical properties, and geometric characteristics, such as acceptable density level, yield strength, ductility, stiffness, elongation to failure, etc.

Sometimes, these target values are conflicting and cannot be optimised individually in the same production process. For instance, high cooling rates of LBAM may lead to an increase in yield strength of the material and a reduction in ductility or elongation to failure of the final product [143].

A compromise among them must be searched. That's why finding optimised process parameters is a challenging job, and it requires multi-objective process optimisation. [144]

2.8.2 MOO Applications in Product Design

The design process starts with designers' creative ideas, often improved in an iterative process. Optimisation techniques can speed up the process and create new ideas, or inventions designers will otherwise not come over. Controlled by prespecified conditions (constraints), the design is made to the

best ones regarding the crucial parameters determined by the environment in which the model is created. For instance, weight in a machine component design, emissions to air, water, and soil in creating a machining process or workshop, time and cost of production of a machine and its parts, etc., are crucial parameters to be considered.

In Optimal Design of Multilevel Systems [145], analytical target cascading (ATC) is a methodology for optimal system design. The system is subdivided into many hierarchical multilevel systems. Outputs from lower-level subsystems or elements are inputs to higher-level subsystems or the total system. An optimisation problem for each component or subsystem is solved for parameter settings, resulting in the best possible system response. If design parameters are shared among some components or subsystems simultaneously, their final optimal settings are attained through the multi-objective optimisation of subsystems at the level above.

2.8.3 Reliability-Based Design Optimisation

Due to the nature of uncertainty of information and data, a reliability-based approach to design optimisation can be used. In such an analysis, the objective functions are optimised. In contrast, the influence of stochastic variations of some parameters and objective functions are accounted for by using stochastically different variables and objective functions. The robustness of the system solution is tested [146]. When this randomness is introduced in the value of objective functions, it is called a robust design. And when it satisfies the constraints, it is called a reliable design. Probability distributions of Pareto optimal solutions and decision variables can be obtained by using:

- Monte Carlo simulation, but it may be an expensive method [142]

- The mean-value first-order second-moment approach (first-order Taylor expansion about the current design) calculates the mean and standard deviation of the objective functions. [147]

2.8.4 MOO Applications in Machining Operations of Turning, Milling, Drilling, Grinding

MOO methodology is frequently used in determining the parameters of machining operations, where the process parameters are treated as decision variables. Simultaneously, some crucial targets of the production activity are taken as objective functions and are optimised simultaneously concerning these decision variables.

Reducing energy consumption is one of the main tasks in manufacturing industries, which has great significance for ecological, economic, and technical reasons. According to the International Energy Agency, the energy consumption in manufacturing industries is about 30% of the world's total. Most of the energy used today is generated using fossil fuels, and the generation process owes to about 2/3 of the world's greenhouse gas emissions. The energy consumption should be kept to a minimum. It is why the energy consumption in one form or other in simulation and analysis of a machining process is often taken as one of the objective functions to be minimised. Another target for machining operation is the production time which is desirable to be kept to its minimum so that the production throughput is held to its maximum. The third objective often to be minimised is the production cost, for obvious reasons. The fourth objective to be minimised is usually the machining operation's quality, for instance, the surface finish of finished goods. However, in a roughing process, the machining quality, i.e. the surface finish, is of minor importance [148].

In a machining operation, the cutting parameters are decision variables. It is desirable to set these parameters to values so that the energy consumption, the production time spent on the operation, the production cost and the machining quality on the workpiece are simultaneously optimised under the constraints caused by the limitations of equipment capacities and other factors influenced by the circumstances of the operation.

In turning, typical cutting parameters are cutting speed, feed rate and cutting depth. Usual constraints valid in such a machining operation could be [148]:

- The cutting power cannot exceed the maximum power available on the machine's spindle.
- The maximum torque can be applied to the machine spindle: the actual torque exerted on the machine spindle cannot exceed a maximum value.
- The requirement of the tool is obtaining the most fragmented chips.
- The requirement on the workpiece: the boom is limited.
- The requirement on surface finish: specified surface quality is wanted.

In milling operations, depth of cut, feed rate and cutting speed are the main parameters taken as decision variables. The best suitable cutting parameters can be found by simultaneously minimising the machining cost and the machining time [149]. The settings can also be settled by simultaneously minimising the surface roughness and cutting force [150].

Spindle speed, drill diameter, material thickness, and feed rate are process parameters taken as decision variables in a drilling process. These process parameters influence the thrust force and torque generated to the jig on the worktable created during the drilling, which can be considered objective functions. Multiple regression models can find the relationship between power, torque, and the drilling process parameters [151]. The sensitivity of objectives

versus process parameters can be analysed by minor variations of these parameters in optimisation calculations [151].

2.8.5 MOO Application in Additive Manufacturing

Machine parts are traditionally fabricated by first forming work blank by, for instance, forging or casting and are further machined to their final forms, where excess material is removed. It is, in general, characterised as a subtractive production method. Additive Manufacturing (AM) produces the final product directly by building one layer of time starting from its bottom [143]. AM has distinct advantages in making complex-shaped and customised parts, often in one go. Materials of plastics, as well as metals, can nowadays be used in an AM process. Laser-Based Additive Manufacturing (LBAM) is used to work with metal parts. The selective laser melting (SLM) technique utilises a high power-density laser to melt and fuse metallic powders.

Achieving good quality, high reliability and good repeatability are significant challenges in using this technology. The process parameters highly influence the final product quality, the production system’s consistency, the process’s repeatability, and the production setups and procedures [143]. Consequently, the product's final quality, microstructure and mechanical properties are determined mainly by choosing such process parameters [143].

It has also been reported that laser power, layer thickness, and hatch space between adjacent laser paths within the same layer are the most dominating controllable process parameters for the Selective Laser Melting (SLM) process [144]. The most suitable process parameters can be found by simultaneously optimising target values that are specific qualities, mechanical properties, and geometric characteristics, such as acceptable density, yield strength, ductility, stiffness, elongation to failure, etc.

Sometimes, these target values are conflicting and cannot be optimised individually in the same production process. For instance, high cooling rates of LBAM may lead to an increase in yield strength of the material and a reduction in ductility or elongation to failure of the final product [143].

A compromise among them must be searched. That's why finding suitable process parameters is a challenging job, and it requires multi-objective process optimisation [152].

A complete study of analysis on the operative parameters of an SLM manufacturing case can be found in Chapter 6. The edge density, bulk density, and pore number are chosen as objective functions and modelled as functions of four process parameters: laser power, point distance, hatch offset, and exposure time. Three different products are manufactured. The aim is to determine the best combination of the process parameters at which the targets are simultaneously optimised: edge density, bulk density, and the number of pores.

The analytical model is formed using the Radial Basis Function Neural Network (RBFNN).

2.8.6 MOO Application in the Squeeze Casting Process

Squeeze casting is casting with melt metals under pressure. It produces near net-shaped casted products, i.e., no, or minimal further processing is needed before the products can be used. The products often have excellent properties like conventional casting under atmospheric pressure and forgings. These include refined structure, minimum porosity, weldability, heat-treatability, improved mechanical properties, good surface quality, and better dimensional accuracy. No runners and feeders are used in processing, which reduces energy consumption. The post solidification of the products can be monitored, and the data can be used to improve the production process [153].

Properties such as aesthetic appearance, internal soundness of the cast parts, surface roughness, yield strength, and the ultimate tensile strength of finished products are influenced by the process parameter as squeeze pressure, pressure duration, pouring temperature, die temperature, etc. These dependent properties can be formed as objective functions of the process parameters, which are decision variables. The best process parameters can be found by simultaneously optimising the objective functions [153].

2.8.7 MOO Application in Maintenance and Planning

The bottleneck in a production system must be removed to enhance the production throughput. A bottleneck of a production line can be defined as the place where a small change can lead to the most significant improvement of the average performance [154]. A MOP analysis of a problem can adequately identify the production line's gains by formulating the system throughput as the objective function. The total number of changes necessary to improve is expressed as the second objective function [155]. Searching for Pareto Front, the improvement level as a function of several changes is shown, and a decision can be made based on the result and the available resources [155].

A production line can be analysed for multiple resource constraints, and these constraints determine the production capability or the throughput of the line. A job sequencing plan is established, in which individual jobs are elements of it and are used as decision variables. The lead times, throughput and inventory holding costs are influenced by the tasks in the job sequencing plan and are considered objective functions. The best job sequencing plan can be found by simultaneously optimising the objective functions [156].

2.9 Summary and Conclusions

Evolutionary and swarm optimisation methodologies can be used to solve MaOPs. However, the following vital aspects still need to be studied further, and new efficient methods/algorithms are highly desired, which can:

- Ensure that the solutions converge rapidly towards optimality and cover most possibly diversified the whole PF range.
- Effectively measure the diversity of a high dimensional PF approximation set.
- Visually display the pattern and characteristics of PF and the dominance relations among several PF approximations simultaneously.

One of the most efficient solution methods for solving MaOPs is decomposition-based algorithms. The search for optimality is done along with a system of predefined reference vectors or guided by a set of pre-created reference points adapted progressively under the iteration process to cover the PF of arbitrary form, most possibly in uniformity and spread.

The even distribution of these reference vectors or points dramatically influences the resulting diversity of the PF approximations. The clue is to generate these reference vectors so that the points of intersections of the vectors and the true PF or its approximated surface become most possibly equidistant. It then leads to obtaining the most diversified PF approximations. The pre-generated reference vectors are most commonly created by the Das and Dennis method. But it can only make equidistant reference points on a simplex plane, while a real-life PF shape could be arbitrary. There is a strong need to develop a generalised method that can create most possibly equidistant reference points on or in the vicinity of the true PF. It is the first of the major tasks of this thesis work. See Chapter 3.

The diversity of PF approximations determines the completeness of a MaOP solution. But measuring the diversity of a high dimensional PF approximation set is challenging mainly due to the Curse of Dimensionality. Several diversity metrics or indicators have been developed, but all have severe flaws in one way or another. Diversity indicators should be sensitive to the change of diversity and behave monotonically for ever-increasing diversity, which is properties nontrivial to possess. Evaluating diversity by using pre-defined reference vectors is a common technique to formulate a diversity indicator. Unfortunately, the method suffers potential systematic bias in diversity measure, and the bias must be effectively removed. In addition, it is also challenging when different diversity indicators are compared and evaluated for their efficacy and efficiency. An alternative solution to these challenges forms the second task of the thesis work. See Chapter 4.

Visualisation of high dimensional PF is nontrivial, but the desire has always been in MaOP research to develop a more effective visualisation method. It leads to the third task to be carried out in the thesis work. See Chapter 5.

MaOP methodologies are widely used in the analysis of real-life challenges. As engineers, we are eager to implement the new theory, methods and algorithms into practical usage. The theoretical achievements of the thesis work have been utilised to analyse an experimental study in the optimisation of process parameters of a Laser Selective Melting operation. See Chapter 6.

Chapter 3 A New Method for Generating and Indexing Reference Points in Many-Objective Optimisation

Chapter Outline

A new method for creating reference points is proposed, for instance, in the reference point-based Many-objective Optimisation Problem (MaOP). The current standard practice of generating reference points on a unit simplex plane uses the Das and Dennis method [157]. But when the generated reference points are projected onto the actual Pareto Front (PF), it creates uneven distribution. This challenge is particularly prominent in a higher number of objectives when considering solutions' diversity. Via the proposed, the reference points are more evenly generated on an m dimensional B-norm surface in the vicinity of the actual PF and subsequently projected onto it. The B-norm surface is created adaptively by tracking the true PF. The method is thus named as B-norm based PF tracking method (Bn-PFt). A new indexing system of reference points is also proposed to ease the work of algorithmic development. Systematic numerical studies performed on B-norm surfaces of various B values show that reference points created by the proposed Bn-PFt method are more evenly distributed on the surfaces than those projected onto the same surfaces generated using the Das and Dennis method. The method can be readily implemented on a variety of many-objective optimisation algorithms. Using MaOP algorithms on MaF benchmark problems with 3, 5, and 7 objective functions shows that the candidate solution sets obtained have

better diversity by adopting the proposed method's reference points. The above work resulted in the following publication:

K. E. Wu and G. Panoutsos, "A New Method for Generating and Indexing Reference Points in Many-objective Optimisation," 2020 IEEE Congress on Evolutionary Computation (CEC), Glasgow, UK, 2020, pp. 1-8.

3.1 Introduction

The approximated sets to PF of a MOP or a MaOP solution shall ideally be fully converged to a PF, uniformly distributed along the surface of PF, and spread to all peripheries of the front. Uniformity and spread properties of the PF is often referred to as its diversity property. MOP problems have been successfully solved based on Pareto-based or dominance-based strategy, where non-dominated solutions are chosen as parents to generate new offspring candidates in further iterations in evolutionary algorithms. It is often combined with a secondary diversity-related strategy, such as crowding distance-based diversity maintenance, distributing and spreading the solutions to the whole PF. Non-dominated solutions that are more distant from their neighbours are preferred as parent solutions for the following iteration process. This strategy is frequently used in many evolutionary multi-objective optimisation algorithms (EMO), such as NSGA-II [100] and SPEA2 [158]. However, this strategy is less efficient on MaOP problems because the number of non-dominated solutions increases dramatically as the number of objectives increases. Hence the number of non-dominated solutions overflows the pre-set storage space of the archive, which makes the algorithm unable to identify new candidates for further iterations efficiently.

Several other solution strategies have been implemented in the literature to deal with the challenge, often in combinations, in solving MaOP problems, such as dominance enhancement-based, grid-based, knee point-based, DM's preference-based, indicator-based, two archive-based, objective function space reduction-based, decomposition-based, reference vector-based or reference points-based approaches [159].

Algorithms as ε-dominance [160], [161], L-optimality [162], and fuzzy dominance [163] are some representatives of dominance enhancement-based

methods. The Grid-based Evolutionary Algorithm [79] is a typical grid-based one. Knee Point-driven Evolutionary Algorithm [75] is a knee points-based method. Preference-Inspired Coevolutionary Algorithms [164] is the most frequently used algorithm of DM's preference-based approach [159]. When the indicator-based methodology is concerned, the Indicator-Based Evolutionary Algorithm [61], the S-metric selection based evolutionary multi-objective algorithm [165], and the fast hypervolume based evolutionary algorithm [71] can be mentioned. Two-Archive Algorithm [166] and Two-Archive Algorithm II [77] use two separate archives in the MaOP algorithm, one for convergence criterion and one for diversity criterion. In algorithms based on objective function space reduction, the number of objective functions is reduced. Less essential objective functions are removed from the optimisation process, based on eigenvalue analysis or correlation analysis of objective functions [158].

Decomposition-based algorithms transform MaOP into single objective functions by using aggregation function with the help of the weight vectors, optimised simultaneously. Multi-Objective Evolutionary Algorithm based on Decomposition (MOEA/D) [6] is the first algorithm of this kind. Pareto Sampling (MSOPS) [167], later improved version MSOPS-II [168], and MOEA/D-M2M [169], MOEA/DD [170] are some of the representative algorithms of the category. The weight vectors are established with the aid of reference points.

In reference vector-based or reference points-based algorithms, the objective space is covered by a given number of reference vectors or reference points which guide the iteration process towards the final goal, both in terms of diversity and convergence. Non-dominate Sorting Genetic Algorithm III (NSGA-III) [2], Reference Vector-guided Evolutionary Algorithm [7] are typical algorithms of the kind [61], [164]. Reference vectors or points are formed a priori to algorithm start-up.

Li et al. [159] have performed a comprehensive and systematic comparative study among 13 MaOP algorithms, formed based on different strategies of MaOPs, by using them to analyse three main groups of test functions. The conclusion is that none of the algorithms outperforms the others on all types of problems. However, the decomposition-based and reference vector/reference or points-based algorithms are competitive on many test problems. The methodology of generating equidistant reference points is essential in these MaOP algorithms.

Reference vectors are also frequently used as primary tools in forming pure diversity indicators in MaOP research. The included angles between candidate solutions and reference vectors are adopted to measure diversity [61], [100].

Ideally, reference points should be created equidistantly on the searched true PF, but this is impossible since PF is not known a priori. A feasible way out of the dilemma is to adapt reference points as the search for the true PF progresses.

Reference points are most commonly created using Das and Dennis's [157] boundary intersection approach, where uniformly spaced reference points are generated on a unit simplex plane. Since the reference points generated in this way are equidistant on the unit simplex plane only, it is most efficient for searching for PFs with a unit simplex plane as Pareto Front or in its vicinity. It is common to vector-wise project the obtained reference points to PF surfaces of other forms [71]. The major drawback of the practice is that when projected onto the PF surface, the formed reference points are not equidistant. Depending on whether the surface of PF is in convex or concave form, the distributions of the points vary differently. With more considerable distances in mid-area in PF of concave type and decreases towards the peripheral. On the

contrary, for PF of convex shape, the reference points are closer to each other in the mid-area and farther away near the edges.

The proposed research work introduces a new method for creating reference points. The proposed methodology aims to generate more evenly distributed reference points on the surface in the vicinity of the true PF. It is shown that Das and Dennis's reference point creation method is a particular case of the proposed method – hence the proposed is the general case. The main contributions of this chapter to the field of study are:

- Establish an indexing system for reference points so that each reference point can be readily identified in m dimensional space.
- Introduce a new creation method for more equally spaced reference points on curved surfaces based on equidistant points along each two-dimensional edge of the approximated PF. An initial candidate solution set is first obtained by using reference points created using Das and Dennis method. The candidate solutions are then used to determine the parameter B in the B-norm curve. Equidistant reference points are first generated on an edge line of approximated PF. The coordinate values of all intermediate points sat to be equal to their respective amounts on edge based on an equal index.
- Propose an adaptation procedure to create reference points in the MaOP algorithm.

This chapter is organised as follows. Section 4.2 gives an overview of existing methods of creating reference points. Section 4.3 covers the reasoning and formulation of an indexing system for reference points. Section 4.4 provides a detailed description of the formulation of the proposed reference point system. Section 4.5 is devoted to comparative studies of the proposed reference points with the existing ones, where improvements of the introduced new reference

point creation method compared with the others are highlighted. Finally, conclusions are drawn, and future research directions are discussed in Section 4.6.

3.2 Creation Methods of Reference Vectors

The Das and Dennis method is the dominating method for generating reference points [165]. The reference points generated are widely used both as a tool in measuring diversity and as guidance for candidate selection for the next iteration in multi-objective evolutionary algorithms [79], [159].

The method of Das and Dennis creates uniformly spaced reference points on a normalised hyper-plane – an $(m - 1)$-dimensional unit simplex plane to all objective axes, which have an intercept of one on each axis. Reference points are generated as [165]

$$\lambda^i = (\lambda_1^i, \lambda_2^i, \dots, \lambda_m^i) \qquad \text{Eq. 3.1}$$

in which

$$\lambda_j^i \in \left\{\frac{0}{p}, \frac{1}{p}, \dots, \frac{p}{p}\right\} \; and \; \sum_{j=1}^{m} \lambda_j^i = 1$$

where p is the number of divisions along each objective axis and λ_j^i is normalised coordinate value, where i is the i^{th} reference point and j is the j^{th} objective functions.

The number of reference points generated, H, is given by:

$$H = \binom{m + p - 1}{p} \qquad \text{Eq. 3.2}$$

where p is the number of divisions along each axis, and m is the number of axes or objective functions.

The number of reference points to be created may be determined by the resolution requirement on PF, which a DM should decide. Typically, this number is closer to and slightly bigger than the number of candidate solutions [79].

The reference points on the unit simplex are equidistant. But when they are projected to surface an arbitrary form of a true PF, the distances between the points are not equal. See Figure 3.2 for an illustration. As any of the equidistant

points on the simplex plane are projected onto a convex curve along the line linking the point and the origin, the projected points become closer to the centre than at the edge creating unevenly distributed points along the convex curve. It means that the reference points used in a MaOP algorithm to start with are not uniformly distributed. When used to find candidate solutions, the approximation sets cannot be evenly distributed, resulting in a deterioration of uniformity.

The number of reference points increases exponentially with increasing p and m. Already for p=m=8, it generates 6,435 reference points which consume a considerable amount of computational power. To address this challenge, Deb and Jain [79] suggest using two layers of reference points with each of smaller value of p, p_1 for boundary layer and p_2 for inside layer so that the total number of reference lines are dramatically reduced to a manageable level. See an illustrative drawing depicted in Figure 3.1. But the consequence of this is a further reduction of even distribution of reference points on the unit simplex plane, and gaps of non-existing reference points are created between the two layers.

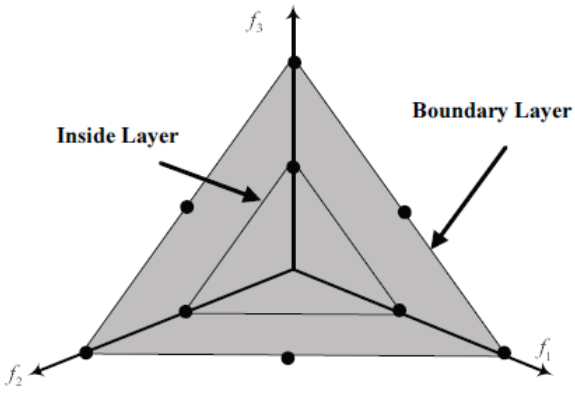

Figure 3.1 - A schematic view on the principle of Deb and Jain's multi-layer method, where p_1=2, p_2=1 [159].

He et al. [171] proposed a novel sampling method of generating reference points by considering PF's actual shape and location, described by the equation

of B-norm. A point $\boldsymbol{F}' = [f_1', f_2', \dots, f_i', \dots, f_m']$ is on a regular surface in m dimensional space if it satisfies Eq. 3.3.

$$\left(\sum_{i=1}^{m} f_i'^B\right)^{1/B} = 1 \qquad \text{Eq. 3.3}$$

in which the value of parameter B determines the shape of the surface:

- $B < 1$, convex surface
- $B = 1$, simplex plane
- $B > 1$, concave surface

Any point $\boldsymbol{F} = [f_1, f_2, \dots, f_i, \dots f_m]$ that is not lying on this surface can be projected onto it by using normalisation strategy with B-norm:

$$\boldsymbol{F}' = \left(\frac{f_1}{\|\boldsymbol{F}\|^B}, \frac{f_2}{\|\boldsymbol{F}\|^B}, \dots, \frac{f_m}{\|\boldsymbol{F}\|^B}\right) \qquad \text{Eq. 3.4}$$

in which

$$\|\boldsymbol{F}\|_B = \left(\sum_{i=1}^{m} |f_i|^B\right)^{1/B} \qquad \text{Eq. 3.5}$$

Figure 3.2 shows the principle of the sampling method. Starting with the centroid of the unit simplex plane, reference points are successively sampled through subdivisions. Reference points are sampled both as vertices of subregions and as the centroid of the subregions.

Using the B-norm of 2.0, the sampling method can generate uniformly distributed reference points on the reference surface of a hypersphere in the 1st octant.

A weakness of the method is that it cannot create equidistant points on surfaces of B-norm except on the surface of B-norm of B=2.0. It fails, especially on creating evenly distributed reference points on surfaces of convex form. See Figure 3.2 for further explanation. Point D is created as the mid-point of B and C'. As it is projected to D' onto the convex curve BD'C' along with OD, the point D' is closer to C' than point B, resulting in unevenly distributed points of B, D'

and C' along the convex curve of BD'C'. When the parameter B of the B-norm surface equals 2.0, the surface becomes a perfect hypercube. The method can create equidistant points on the concave curve of B=2.0.

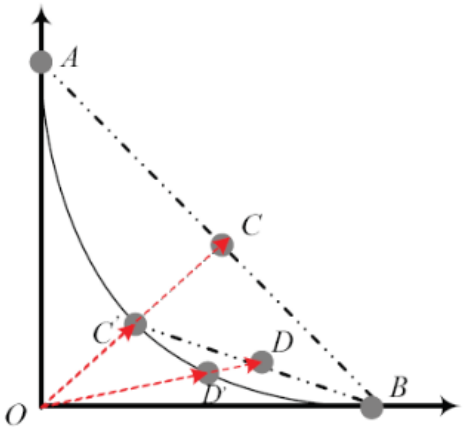

Figure 3.2 - The principle of sampling method [77], where a point C on the unit simplex plane is projected on the surface of B norm C' after the first division and point D' is sampled after further division.

Tian et al. [71] suggest generating reference points on known true PFs starting with the points created by the Das and Dennis method on a unit simplex plane and projecting them to the actual Pareto fronts. Unfortunately, the final distribution of the reference points generated in this way is not uniform. As any of the equidistant points on the unit simplex plane are projected onto a convex curve along the line linking the point and the origin, the projected point becomes closer to the centre than the outskirt resulting in unevenly distributed points along the convex curve. Contrarily, when the point is projected onto a concave curve along the line linking the point and the origin, the projected point turns out to be farther away from the centre than it is to a point on edge, resulting in unevenly distributed points along with the concave curve as well.

PFs of real-world optimisation problems usually have irregular PF, i.e., a PF can be disconnected, degenerated, inverted and badly scaled. Due to the mismatch between the reference vectors' distribution and the PF shape, algorithms using predefined uniformly designed reference vectors fail to obtain sufficiently good diversity solutions. The challenge is dealt with by adopting

adaptively adjusted reference vectors periodically to fit the PF shape as the evolution process undergoes. Ma et al. [172] have recently given a comprehensive review on the reference vector adaptation for handling irregular Pareto fronts.

Reference vectors can be recreated based on the predefined-then-random scheme, where predefined weight vectors in the initialization are utilised in the initiation while further adjustments are made randomly to substitute the obsolete reference vectors as the evolution process continues [7]. The method is straightforward, but the quality of solutions in convergence and uniformity may be limited. In [173], different reference vectors creation strategies are used for exploration and exploitation. In the former, reference vectors linked to most solutions are replaced with randomly generated ones, while in the latter, those with no solutions linked to are replaced by randomly created reference vectors. PICEA-w [174] adopt an adaptation strategy where the population and the weight vectors are co-evolved periodically, and new weight vectors are randomly added.

Reference vectors can be adapted based on fitting-based adjustment. The form of temporarily attained PF is approximated, and new uniform reference vectors are regenerated, matching the actual PF. For example, the reference vector adaptation method used in paλ-MOEA/D [175] is representative. The PF is approximated as $[f_1(x)]^p + \cdots + [f_m(x)]^p = 1$, where p is the model parameter. Reference vectors are regenerated by maximizing the hyper-volume (HV) metric. In DEA-GNG [176], the PF form is learned using a growing neural gas network, and both the reference vectors and the scalarizing functions are adapted neighbour information. DBEA-DS [177] applies two sets of reference vectors to guide the search. The optimal set is chosen in terms of the s-energy metric calculated using the obtained population at each

generation. Fitting-based adjustments can be misguided by attained candidate solution of poor convergence and diversity and may suffer instability problems during estimating parameters of the approximation model for degenerated PFs.

Reference vectors have been adapted using local-population-guided or local-archive guided adjustment principles that exploit local individual density information. SDEA [185] divides the objective space into multiple subregions by the uniform design method. New reference vectors are created in subregions with few nondominated solutions by adding additional ones. MOEA/D-AM2M [178] periodically creates new reference vectors in a subregion by maximising their minimal included angles. VaEA [179] also generates new reference vectors between candidates of the key layer of nondominated sorting based on the principle of maximising the included angles.

OD-RVEA/AR [180] removes reference vector with no candidate linked to them and generate new ones between individuals with the largest included angles. The biggest challenge with angle based adaptation is its difficulty in handling long-tailed/peaked PFs. A-NSGA-III [2] periodically deletes not used reference points, identifies reference points with crowded solutions and adds a simplex with m neighbour reference points to each of them. In PSA [181], each weight vector with an individual solution is adapted slightly to push the candidate away from its nearest nondominated neighbour. The success of local-population-guided adjustment methods in searching for irregular PFs relies on PF approximation realising using the current population. But there is always danger for misguidance to poor convergence and diversity by the current population. In local-archive guided adjustment methods, an external archive is used for weight vector adjustment. MOEA/D-URAW [74] targets many-objective optimization problems (MaOPs) by generating initial reference vectors using a uniformly random method and periodically checking the external archive of

reference vectors and deleting those in the overcrowded area, and adding new ones in the sparse area. Current PF is better approximated when using the external archive than relying merely on the current population, which forms the foundation of reference vector adaption of the methods.

Reference vectors can be recreated based on the neighbour-weight-vector-guided adjustment principle. In EMOSA [182], reference vectors are first generated using a uniform design method and are adapted by keeping them away from their nearest nondominated neighbours. MOEA/D-AWVAM [183] creates extra reference vectors in subregions with few nondominated solutions. In MOEA/HD [184], reference vectors are grouped into different hierarchies and regenerated using the perpendicular bisector between the superior neighbouring individuals. Neighbour-weight-vector-based adjustment is a local improvement procedure and may contribute limitedly to the overall uniformity of PF.

Reference vectors can be created based on preference-based adjustment principles. The methods are particularly beneficial for solving MaOPs since only the region of interest (ROI) is searched with the consequence of reduced requirement on population size. In NUMS-MOEA/DSTM [185], reference vectors are contracted to DM's preference reference vector. In PICEA-g [164], the population and a set of preference points are co-evolved by constantly adding randomly generated preference points. The individual that dominates the largest number of preference points are chosen, and the preference point that is dominated by the largest number of selected individuals is maintained. In a-PICEA-g [186], the diversity maintenance in PICEA-g is further strengthened by introducing the crowding distance concept. In PICEA-w [174], the weights and candidates are co-evolved, and no prior defined weights are needed, making the algorithm robust to the problem geometries. However,

although feasible and practical, the biggest concern with the preference-based adjustment is related to the situations where only local optima are found because the search is guided towards preference directions.

Handling various reference vectors can be challenging. An efficient indexing system to reference points can enhance the clarity of algorithms, save computer power when searching for a specific reference point, and ease algorithmic development of new methods. Finding neighbouring points to a given reference point are made more accessible. A reference point can be easily turned on/off when needed, and new reference points can be generated between existing ones if required. An arbitrary number of reference points can thus be created on the boundary layer and inside layers.

Another feature is that instead of handling the coordinate value of reference points in real numbers, one can identify the reference points with indexes of integers, speeding up computation and saving data storage space.

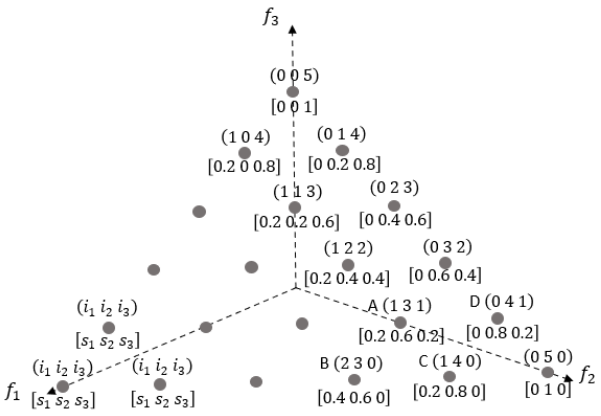

Figure 3.3 - Indexing reference points created using the Das and Dennis method. Numbers in parentheses are indexes, while numbers in brackets are coordinate values of a reference point.

The description of the indexing system is first done with an example in creating reference points on the unit simplex plane. Figure 3.3 displays reference points on the unit simplex plane of 3 objectives and five equal divisions along each objective axis.

All reference points in Figure 3.3 can be created by:

$$[s_1 \;\; s_2 \;\; s_3] = \left[\frac{i_1}{p} \;\; \frac{i_2}{p} \;\; \frac{i_3}{p}\right] \quad \text{Eq. 3.6}$$

where s_1, s_2, and s_3 are coordinate values of a reference point. (i_1, i_2, i_3) are their indexes along f_1, f_2, and f_3 axis, respectively. We have:

$$s_1 + s_2 + s_3 = 1 \quad \text{Eq. 3.7}$$

$$i_1 + i_2 + i_3 = p \quad \text{Eq. 3.8}$$

in which p is the number of divisions on each objective axis.

All reference points are readily found by systematically varying $i_j, j \in \{1, 2, \dots, m\}$ under the assumption that Eq. 3.8 is satisfied. Another exciting feature is that an index and its corresponding coordinate value are causally linked. For two arbitrary reference points, indexes from each are equal, resulting in the same coordinate value. For example, see Figure 3.3, for points A, B, C and D:

$$\begin{gathered} i_1^A = i_1^C = i_3^D = 1 \rightarrow f_1^A = f_1^C = f_3^D = 0.2 \\ i_2^A = i_2^B = 3 \rightarrow f_2^A = f_2^B = 0.6 \\ i_3^A = i_3^D = i_1^C = 1 \rightarrow f_3^A = f_3^D = f_1^C = 0.2 \end{gathered} \quad \text{Eq. 3.9}$$

Eq. 3.9 indicates that coordinates are the same for points with the same index. It can be interpreted as that coordinates of an arbitrary point can be found by comparing its indexes with points along a line of edge (2D hyper-line) and are put equal to the coordinate values of the same index.

In general, the coordinates of a reference point in m objective space are given as:

$$(s_1 \;\; s_2 \;\; \dots \; s_m) = \left(\frac{i_1}{p} \;\; \frac{i_2}{p} \;\; \dots \;\; \frac{i_m}{p}\right) \quad \text{Eq. 3.10}$$

and

$$s_1 + s_2 + \cdots + s_m = 1 \quad \text{Eq. 3.11}$$

$$i_1 + i_2 + \cdots + i_m = p \quad \text{Eq. 3.12}$$

The principle illustrated in Eq. 3.9 can be expanded for the determination of coordinates of an arbitrary reference point in m objective function space by equating the value to the corresponding values to a two-dimensional line with the same index:

$$i_j = i_1^{k,2D} = k \rightarrow f_j = f_1^{k,2D}, j \in (1, 2, \dots, m) \quad \text{Eq. 3.13}$$

where m is the number of objective functions. i_j, $j \in (1, \dots, m)$ is the index of the j^{th} component of the searched reference point. f_j, $j \in (1, \dots, m)$ is the value of the j^{th} component of the searched reference point. $i_1^{k,2D}$ and $f_1^{k,2D}$ are the index and the value of the first coordinate of the reference point with $i_1^{k,2D} = k$ along a two-dimensional edge line on the simplex plane, respectively.

Eq. 3.13 implies that the coordinate values of an arbitrary reference point in m dimensional space can be put equal to corresponding coordinate values of points on a two-dimensional line of edge on the simplex plane by contrasting indexes of them. This property of Eq. 3.13 can be utilised to develop a new system of reference points. See Section 3.4 for details.

3.3 Proposed Method for Generating Reference Points

The proposed method for creating reference points is based on an $(m-1)$ dimensional B-norm surface generated based on the curve fitting of an approximation set of PF. The method turns out to be applicable for generating uniform reference vectors on irregular PFs of discontinuity and inverted types but fails when used on PF of degenerated shape because it suffers instability problem when B-norm surface is adopted to describe such PF patterns. See discussions in Section 3.5.3 for more details. In the start-up phase, an approximation is created using the existing MaOP algorithm and with reference points made by, for instance, Das and Dennis method. The candidate solution set obtained is then used to determine the parameter B in the B-norm curve. A new set of reference points is created, and a new round of approximation is started with refined reference points. Projection of B-norm curve on a 2D plane, for instance $f_1 - f_2$ plane can be attained, which is a 2D edge or boundary of the estimate of PF. Equidistant reference points are first generated on edge. The coordinate values of all internal points are put to be equal to their respective amounts on edge, which have the same index.

Algorithm 1 Procedure for the proposed algorithm **(Bn-PFt)**

Input: X (Solution set)
Output: Z (New refernce line)

1: $X \leftarrow$ Apply non-dominent sorting (X)
2: $X_N \leftarrow$ Normalise the solution (X)
3: $B \leftarrow$ a single optimisation process is carried out to obtain parameter **B** (X_N)
4: $f_N^D \leftarrow$ Division of B-norm edge in plane formed by a pair of objective axis (B)
5: Z $\leftarrow$ Determination of coordinate values of reference points (f_N^D)

The reference point creation method is done on the B-norm surface, which adaptively traces the true PF, named B-norm-based PF tracing (Bn-PFt). The pseudo-code for Bn-PFt is shown in Algorithm 1.

3.3.1 Approximate PF with B-norm Equation

After the first converged solution set has been obtained using Das and Dennis's reference point generating method, the solution set is curve-fitted to take a B-norm equation. The solution set can be used to estimate parameter B as:

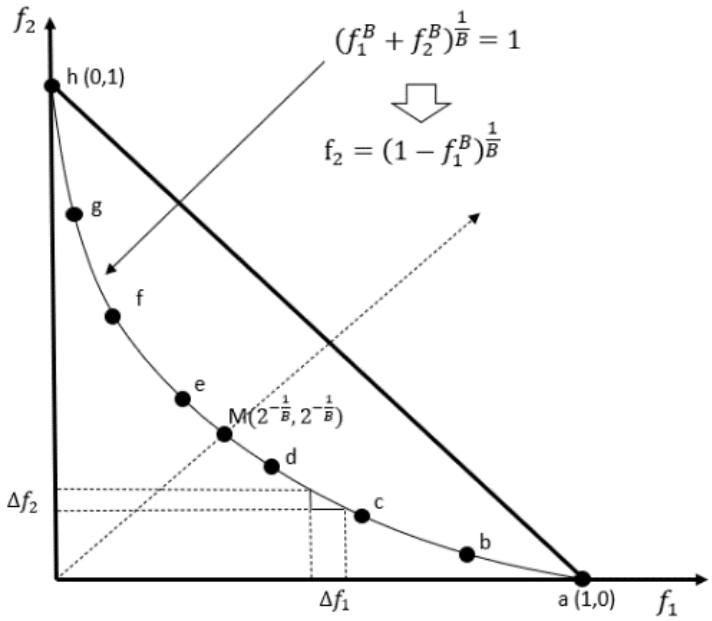

Figure 3.4 - Determination of part's length for p=7

$$F(f_1, f_2, \dots, f_m) = (f_1^B + f_2^B + \cdots + f_m^B)^{\frac{1}{B}} = 1 \quad \text{Eq. 3.14}$$

$$h(B) = 1 - (f_1^B + f_2^B + \cdots + f_m^B)^{\frac{1}{B}} \quad \text{Eq. 3.15}$$

$$B = argmin_B \left(\sum_{k=1}^{N} h_k(B) \right) \quad \text{Eq. 3.16}$$

where N is the number of obtained candidate solutions.

3.3.2 Division of B-norm Edge in a Plane

Due to symmetry, the curve fitted B-norm surface has the same projection on planes formed by any pairwise objective functions. Equidistant reference points need first to be generated on such a projection. See Figure 3.4, illustration of a division of p=7 equal parts.

Due to symmetry, only the locations of reference points on one half of the $f_1 \sim f_2$ curve need to be first determined.

Midpoint M's coordinates:

$$f_1^* = f_2^* \ \ and \ ((f_1^*)^B + (f_2^*)^B)^{\frac{1}{B}} = 1 \qquad \text{Eq. 3.17}$$

which leads to $f_1^* = f_2^* = 2^{-\frac{1}{B}}$

The arc length l_{aM}:

$$l_{aM} = \sum_{j=1}^{n} \sqrt{(\Delta f_1)^2 + (\Delta f_2)^2} \qquad \text{Eq. 3.18}$$

where n is the number of divisions between point f_1^a and that of the midpoint $2^{-\frac{1}{B}}$.

$$\Delta f_1 = \frac{1 - 2^{-\frac{1}{B}}}{n} \qquad \text{Eq. 3.19}$$

$$f_{1,j} = 2^{-\frac{1}{B}} + \Delta f_1 \cdot j \qquad \text{Eq. 3.20}$$

and

$$f_{1,0} = 2^{-\frac{1}{B}}, f_{1,n} = 1, \ j \in (0, 1, 2, \dots, n)$$

By Eq. 3.18:

$$f_{2,j} = \left(1 - \left(f_{1,j}\right)^B\right)^{\frac{1}{B}} \qquad \text{Eq. 3.21}$$

$$f_2 = f_{2,j} - f_{2,j-1}, \qquad where \ j \in (0, 1, 2, \dots, n) \qquad \text{Eq. 3.22}$$

The number of divisions n determines the accuracy of the calculated arc length $\mathrm{l_{aM}}$ and a large number is chosen since the calculation is done only once per tracking operation on the PF (in this work, it is n=1000).

The arch length:

$$l_{ab} = 2l_{aM} \quad \text{Eq. 3.23}$$

The length per division:

$$l_{pd} = \sum_{j=1}^{n_1} \sqrt{(\Delta f_1)^2 + (\Delta f_2)^2} = \frac{l_{ab}}{p} \quad \text{Eq. 3.24}$$

where n_1 is the number of summation points from f_1^b to f_1^a to obtain the length per division l_d. Eq. 3.25 gives n_1.

The coordinate values of point b:

$$f_1^b = f_1^a - n_1 \cdot \Delta f_1 \quad \text{Eq. 3.25}$$

$$f_2^b = \left(1 - \left(f_1^b\right)^B\right)^{\frac{1}{B}} \quad \text{Eq. 3.26}$$

The coordinate of next point c:

$$\sum_{j=1}^{n_2} \sqrt{(\Delta f_1)^2 + (\Delta f_2)^2} = \frac{l_{ab}}{p} \quad \text{Eq. 3.27}$$

where n_2 is the number of summation points from f_1^c to f_1^b.

Eq. 3.26 and Eq. 3.27 are again used to determine (f_1^c, f_2^c):

$$f_1^c = f_1^b - n_2 \cdot \Delta f_1 \quad \text{Eq. 3.28}$$

$$f_2^c = (1 - (f_1^c)^B)^{\frac{1}{B}} \quad \text{Eq. 3.29}$$

The procedure is repeated until coordinates of all points of divisions are obtained.

3.3.3 Determination of Coordinate Values of Reference Points

For an arbitrary reference point, $S[f_1\ f_2\ \ldots\ f_m]$ with indexes $(i_1\ \ i_2\ \ \ldots\ \ i_m)$, its coordinate values can be found directly by picking up corresponding values on the 2D boundary of the attained B-norm curve, where the parameter B is estimated using Eq. 3.18, i.e., through minimising the difference between objective values and their approximated amounts of a B-norm curve.

$$\left[(f_1^1, f_2^1), (f_1^2, f_2^2), \ldots, \left(f_1^k, f_2^k\right), \ldots \left(f_1^{p+1}, f_2^{p+1}\right)\right] \quad \text{Eq. 3.30}$$

$$k \in \{1, 2, \ldots, p+1\}$$

which are organised as given by Eq. 3.13:

$$i_j = i_1^{k,2D} = k \rightarrow f_j = f_1^{k,2D}, j \in \{1, 2, \ldots, m\} \quad \text{Eq. 3.31}$$

The obtained reference point is afterwards projected to the B-norm surface by using Eq. 3.5. See Fig. 3.3 for an illustrative example with three objectives case.

3.4 Numerical Studies

This section deals with discussions on improving the proposed method on the quality of PF approximations in diversity.

The first part of testing is of the visual kind, done in displaying reference points created by Das and Dennis and Bn-PFt methods onto the surface of B-norm with various B values with three objective functions, which differences are revealed visually. Eq. 4 is used to project reference points generated by the Das and Dennis method on the actual B-norm surface as the standard practice. The reference points created in this way are contrasted with those produced by the Bn-PFt method.

In the second part of testing, Reference Vector-guided Evolutionary Algorithm (RVEA) [7] is used to analyse the Benchmark problem of MaF 1-7 and MaF10-13 [112] with 3 and 5 objective functions, with the use of reference point creation of Das and Dennis method and Bn-PFt method. Diversity of approximations is accessed using various quality metrics.

RVEA is chosen in this study because it is a reference vector/point-based evolutionary algorithm. Reference vectors that do not have PF approximations are dropped, unlike other algorithms, e.g., NSGA III, where these reference vectors are regenerated, pointing to different feasible directions. RVEA is more suitable for studying the uniformness of reference points for decomposition-based algorithms.

The bn-PFt method improves the uniformity of distribution of reference points adaptively by tracing the temporarily obtained PF surface. Thus, its usage is based on the current available PF shape and Bn-PFt targets to improve it. MaF Benchmark 8 and 9 are omitted because their PF shapes are readily visualised with chosen two decision variables [79]. MaF 12 and 13 are left out in this study because their PF shapes are identical in 3D, both of perfect

sphere, the same as PF of MaF 5. The benchmarks are designed to consider the effect of non-separable decision variables (MaF 12) and nonlinearly linked with the first and second decision variables (MaF 13) and the impact of high multimodality [79], which are not subject of this work. MaF 14 and 15 are also excluded, mainly because their PF shapes are the same as MaF 1 and 4. Also, the purpose of their primary use is on studying large-scale problems [79], which is not the subject of this study.

The testing is performed on the chosen benchmark problems in 3 and 5 objective functions only because the number of reference points based on the Das and Dennis method increases exponentially with the increasing number of objective functions, resulting in an unpractical number for the MaOP algorithm when handling MaOP with a higher number of objectives. It is also challenging to maintain a precise evaluation when uncertainty is introduced using fewer but incomplete or unsystematic reference points, e.g., those created by the Deb and Jain method [2]. Systematically generating a manageable number of reference points is studied and reported in a separate work.

3.4.1 Parameters and Performance Metrics

A list of parameters used in the study is given in Table 3.1. The outcomes are compared to highlight the efficacy and efficiency of the proposed creation method of reference points. Other algorithmic parameters used in RVEA are based on default values given in [187].

Thirty independent algorithmic executions have been carried out for each test case, and the mean and standard deviation of approximations are determined. The superior ones are identified statistically based on the Wilcoxon Rank Sum Test with a 5% significance level. The Bonferroni correction is also adopted in comparison testing with multiple hypotheses. The method is stricter than the other methods because it ignores the effects of probability density

function distribution of all factors in the comparisons. The Bonferroni correction reduces the desired overall significance level of the test $\alpha = 0.05$ by testing each individual hypothesis at a significance level of α/k, where k is the number of problem instances determined by the number of null hypotheses, disparate algorithms involved and the number of cases in the comparisons, i.e., the total number of problem instances in the comparisons is $2x5 - 1 = 9$. It means that in this case, $k = 9$, and the corrected significance level of the test $\alpha_c = 0.05/9 = 0.0056$.

Table 3.1 - Parameter used in RVEA calculations

Benchmark problem	Number of objectives	Number of decision variables	Number of evaluations
MaF 1-7 and MaF 10-12	3	12	500000
	5	14	1000000

Hypervolume [127], Inverted Generational Distance (IGD) [128], Spread (Δ) [188], Coverage over Pareto Front (CPF) [129], and Spacing metrics [135] are used to check quantitively the evenness of reference points created by Bn-PFt method compared with that of Das and Dennis.

Hypervolume (HV) metric calculates the space enclosed by the candidate solutions and a reference point (Nadir point is often chosen). HV is a Pareto compliant metric which means that as long as a solution set A dominates a solution set B, the HV of A becomes greater than that of B.

IGD is expressed as the averaged distance of nearest Euclidean distances from actual Pareto optimal points to approximated ones calculated by a MaOP algorithm. The smaller the value of IGD is, the more accurate the solution set in terms of convergence and diversity. But IGD is primarily a convergence metric, although a lower value may indicate better diversity simultaneously.

Spread (Δ) measures the distribution and the extent of obtained non-dominated solutions. It is expressed as:

$$\Delta = \frac{d_f + d_l + \sum_{i=1}^{N-1} \left| d_i - \bar{d} \right|}{d_f + d_l + (N-1)\bar{d}} \quad \text{Eq. 3.32}$$

where:

- N: number of non-dominated solutions.
- d_i : Euclidean distances between neighbouring solutions among the obtained non-dominated solutions set, which have a mean value $\bar{d}$.
- $\bar{d}$: mean value of all d_i.
- d_f: Euclidean distances between the extreme solutions of the obtained non-dominated set.
- d_l: Euclidean distances between boundary solutions of the obtained non-dominated set.

A zero Spread value means that the obtained Pareto optimal set is uniformly distributed. Lower Spread (Δ) value is therefore preferred for PF approximation sets.

CPF is formulated first by projecting a solution set to the (m-1)-dimensional unit simplex plane and then to a unit hypercube. Its score for diversity is obtained by calculating the hypervolume of the projected solution set. The higher value of CPF indicates a better diversity score.

The spacing metric is defined as:

$$SP(S) = \sqrt{\frac{1}{|S|-1} \sum_{i=1}^{|S|} \left(d_i - \bar{d}\right)^2} \quad \text{Eq. 3.33}$$

in which $d_i = min_{(s_i, s_j) \in S, s_i \neq s_j} \left\| F(s_i) - F\left(s_j\right) \right\|_1$, which is the $l_1$distance between point $s_i \in S$ and its closest point in S other than s_i, and $\bar{d}$ is the mean value of d_i. The spacing metric is expressed in the averaged distance variance between a point and its closest neighbour. It is improper to evaluate an approximation set with holes or strong local clusters in its domain [167]. The solution sets being studied here do not have holes and regional clusters in their data sets,

so the Spacing metric is used in this study—the lower the value of the Spacing metric, the better the distribution of a solution set.

3.4.2 Reference Points Created on Various B-norm Surfaces

Figure 3.5-3.10 shows comparisons between reference points created by Das and Dennis method and the proposed Bn-PFt method for various B values. As can be observed from the figures, reference points generated by the Bn-PFt method have more even distributions than Das and Dennis's. On surfaces of a convex form, the reference points of the Bn-PFt method spread out and cover the whole surface, while those of the Das and Dennis method gather more in the central areas. On surfaces of concave form, the opposite occurs; the reference points of the Bn-PFt method gather slightly more densely in the central area of the surface while those of Das and Dennis spread more towards peripherals.

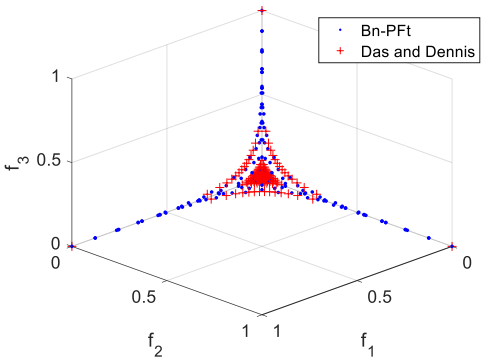

Figure 3.5 - Comparisons between reference points created by Das and Dennis method and the proposed Bn-PFt method for PF of B = 0.3

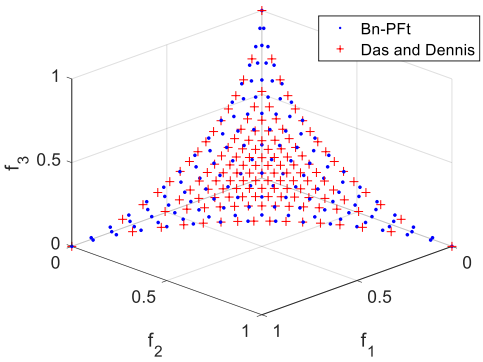

Figure 3.6 - Comparisons between reference points created by Das and Dennis method and the proposed Bn-PFt method for PF of B = 0.6

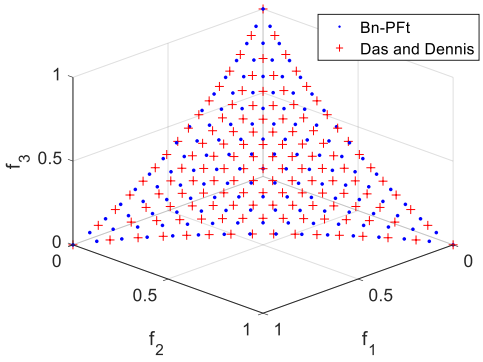

Figure 3.7 - Comparisons between reference points created by Das and Dennis method and the proposed Bn-PFt method for PF of B = 0.8.

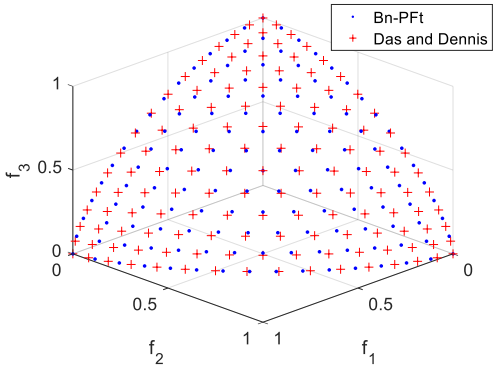

Figure 3.8 - Comparisons between reference points created by Das and Dennis method and the proposed Bn-PFt method for PF of B = 1.5.

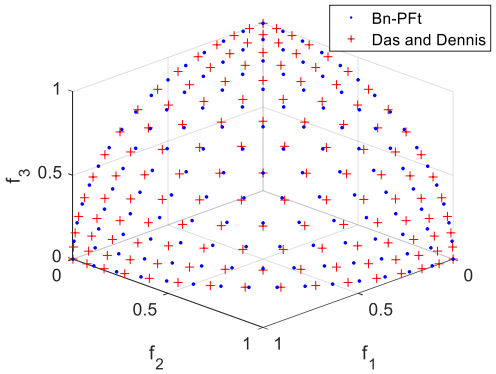

Figure 3.9 - Comparisons between reference points created by Das and Dennis method and the proposed Bn-PFt method for PF of B = 2.0.

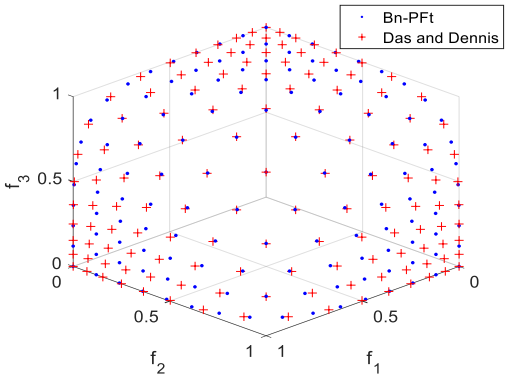

Figure 3.10 - Comparisons between reference points created by Das and Dennis method and the proposed Bn-PFt method for PF of B = 5.0

3.4.3 The Bn-PFt Method Applied in Benchmark Testing

Benchmark problems of MaF 1-7 and 10-11 are analysed using a standard version of the RVEA algorithm [7] with reference points generated by Das and Dennis and Bn-PFt. MaF Benchmark 8 and 9 are omitted because their shapes are readily visualised with the chosen two decision variables [79]. MaF 12 and 13 are excluded because their PF is identical to MaF 5 since the Bn-PFt method is only sensitive to PF shape. MaF 14 and 15 are also left out, mainly because their PF shapes are the same as MaF 1 and 4, respectively. In addition, the primary purpose of their use is on studying large-scale problems [79], which is not the subject of this work.

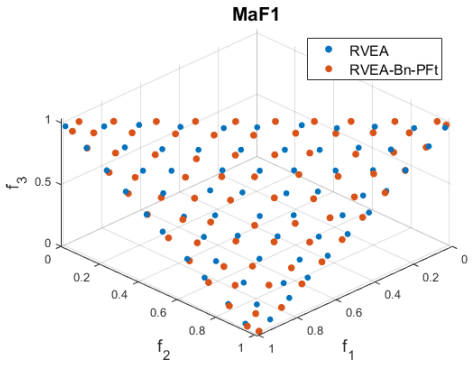

MaF1 M3

Figure 3.11 - Distribution of approximations of MaF1 created using RVEA based on reference points of Das and Dennis method and of Bn-PFt method. m=3 and p=15

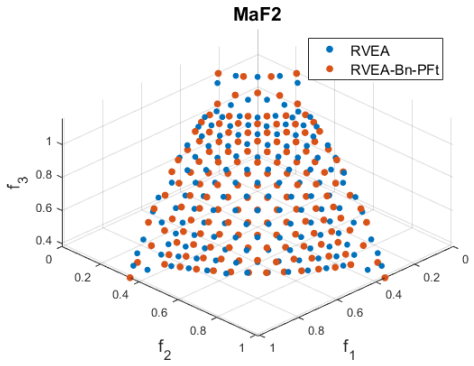

MaF2 M3

Figure 3.12 - Distribution of approximations of MaF2 created using RVEA based on reference points of Das and Dennis method and of Bn-PFt method. m=3 and p=15

3.4.3.1 *Results of Cases with Three Objective Functions*

Figure 3.13-Figure 3.19 visually shows the results of approximations based on the two reference vector generation methods in 3 objective cases with the number of divisions along with each objective, p=15. Table 3.2 - Table 3.6 depicts values of the chosen metrics quantitatively on PF approximations with 3 and 5 objective functions, which are averaged after 30 independent algorithmic executions.

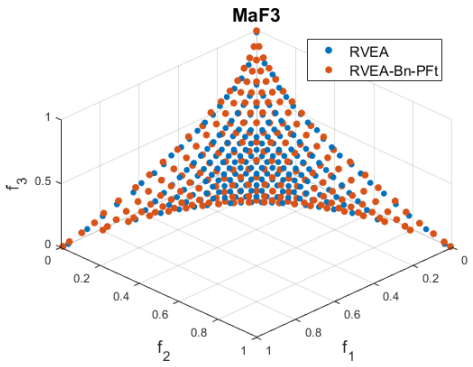

MaF3 M3

Figure 3.13 - Distribution of approximations of MaF3 created using RVEA based on reference points of Das and Dennis method and of Bn-PFt method. m =3 and p =15

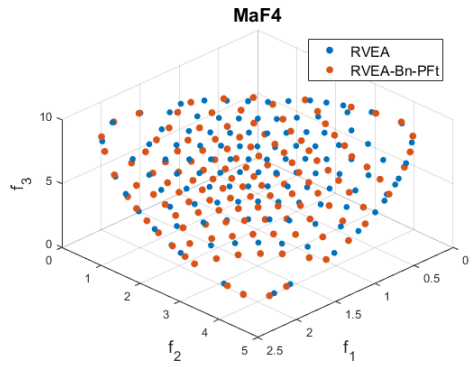

MaF4 M3

Figure 3.14 - Distribution of approximations of MaF4 created using RVEA based on reference points of Das and Dennis method and of Bn-PFt method. m =3 and p =15

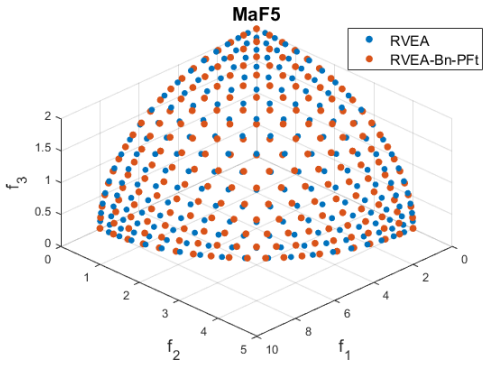

MaF5 M3

Figure 3.15 - Distribution of approximations of MaF5 created using RVEA based on reference points of Das and Dennis method and of Bn-PFt method. m =3 and p =15

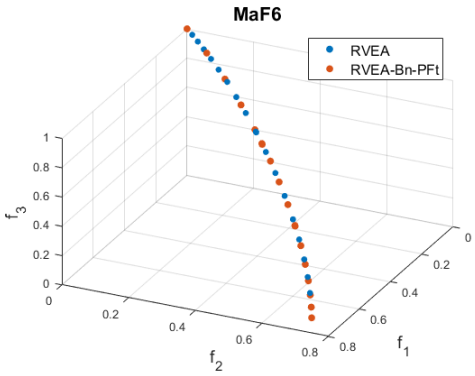

MaF6 M3

Figure 3.16 - Distribution of approximations of MaF6 created using RVEA based on reference points of Das and Dennis method and of Bn-PFt method. m =3 and p =15

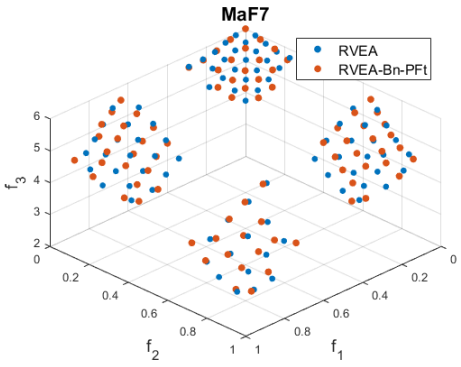

MaF7 M3

Figure 3.17 - Distribution of approximations of MaF7 created using RVEA based on reference points of Das and Dennis method and of Bn-PFt method. m =3 and p =15

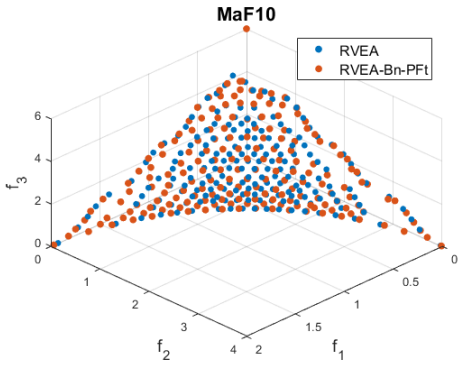

MaF10 M3

Figure 3.18 - Distribution of approximations of MaF10 created using RVEA based on reference points of Das and Dennis method and of Bn-PFt method. m =3 and p =15

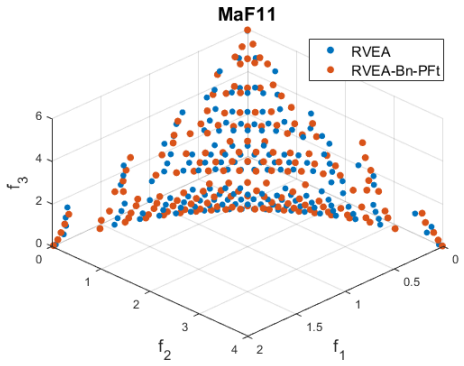

MaF11 M3

Figure 3.19 - Distribution of approximations of MaF11 created using RVEA based on reference points of Das and Dennis method and of Bn-PFt method. m =3 and p =15

As can be seen in Figure 3.13-Figure 3.19, reference points generated by the Bn-PFt method in most of these cases are better distributed and spread out over the whole PF than those created by Das and Dennis. It is self-evident for cases where the PFs are convex and fully cover the entire objective space. See, e.g., Figure 3.13. As stated above in the discussion of PF shape of B-norm kind (Section 4.5.3), the Bn-PFt method gives PF approximations spreading outwards to peripherals from the centre region and distribute more evenly in cases of PF shape of convex type, while creating solutions shrinking towards the centre region in cases of PF shape of concave type. The approximations are also analysed in HV, IGD, Δ, CPF and SP metrics to make the comparisons quantitively. See Table 3.2 - Table 3.6. The exact objective values on PF in IGD calculations are obtained by densely sampling the data on the theoretical PF. The candidate solution sets obtained using reference points of the Bn-PFt method generally have better diversity, as evaluated using HV, IGD, Δ, CPF and SP metrics, than those of adopting reference points of using the standard Das and Dennis. The Bonferroni corrected significance level of the test $\alpha_c = 0.0056$.

Table 3.2 - Approximations of MaF benchmarks in 3D based on the two competing reference point generation methods measured in Hypervolume (HV), $\alpha_c = 0.0056$. (Numbers in bold font show the best metric value)

3D	HV	
	RVEA	RVEA-Bn-PFt
MaF1	2.0261e-01(3.29e-03) -	**2.0984e-01(1.61e-03)**
MaF2	2.4163e-01(1.22e-03) -	**2.4262e-01(8.75e-04)**
MaF3	**9.5440e-01(5.14e-02) =**	**9.6785e-01(5.08e-05)**
MaF4	**5.2167e-01(4.08e-02) =**	**5.0461e-01(5.08e-02)**
MaF5	5.7634e-01(1.49e-05) -	**5.7793e-01(1.24e-05)**
MaF6	**1.8832e-01(7.45e-04) +**	1.8574e-01(2.56e-03)
MaF7	2.6882e-01(2.47e-03) -	**2.7162e-01(1.78e-03)**
MaF10	9.5057e-01(5.93e-04) -	**9.5154e-01(6.85e-04)**
MaF11	9.3617e-01(3.47e-04) -	**9.3816e-01(3.62e-04)**
B or E	**3**	**8**

Note: B or E stand for the number of cases with better or equal performance.
RVEA compared to RVEA-Bn-PFt: "-": worse; "=": equal;"+": better;

When evaluated in HV, the PF approximations show that solutions based on the Bn-PFt method are superior to the Das and Dennis method, with one exception. No statistical evidence differentiates the two methods when used on MaF3 and MaF4. At the same time, the results of MaF6 reveal that the Das and Dennis method performs better than the Bn-PFt method does on average based on 30 independent runs. PF of MaF6 is of degenerate type and consists of a pure arc. The Bn-PFt method, as it is programmed, has challenges in finding a stable parameter B when used with RVEA in this case, as there are about 1/3 of runs that results in better metrics values based on Bn-PFt while the rest are worse. The author has problems understanding why not Bn-PFt as a method should also be superior when analysing benchmark cases like MaF6. In future work shortly, the B-norm parameter estimation's instability problem is further studied when used in analysing degenerate problems.

The more diversified result has been shown in the IGD metric, which is primarily an indicator for measuring convergence. However, to a certain degree, it also reflects the diversity of a PF approximation set. A score of 6:6 is obtained, indicating that the two methods are equal in efficacy. See Table 3.3.

Table 3.3 - Approximations of MaF benchmarks in 3D based on the two competing reference point generation methods valued in IGD, $\alpha_c = 0.0056$. (Numbers in bold font show the best metric value)

3D	IGD	
	RVEA	RVEA-Bn-PFt
MaF1	5.3721e-02(2.12e-03) -	**4.9570e-02(9.31e-04)**
MaF2	2.7947e-02(1.21e-03) -	**2.6299e-02(7.69e-04)**
MaF3	**4.2989e-02(6.13e-02) =**	**2.1217e-02(1.12e-04)**
MaF4	**3.4007e-01(2.66e-01) =**	**3.9989e-01(2.69e-01)**
MaF5	**1.6450e-01(4.86e-06) +**	1.7007e-01(8.59e-05)
MaF6	**2.1611e-02(1.19e-03) +**	2.7126e-02(3.39e-03)
MaF7	7.3631e-02(2.24e-03) -	**7.0967e-02(2.06e-03)**
MaF10	**1.0459e-01(3.42e-03) +**	1.0933e-01(3.44e-03)
MaF11	**1.2086e-01(2.82e-03) =**	**1.2000e-01(3.40e-03)**
B or E	**6**	**6**

Note: B or E stand for the number of cases with better or equal performance RVEA compared to RVEA-Bn-PFt: "-": worse; "=": equal;"+": better;

The results in CPF metric value are also diversified, similar to cases measured in IGD metric values. A score of 6:5 in favour of the Bn-PFt method has been attained. See Table 3.4.

Table 3.4 - Approximations of MaF benchmarks in 3D based on the two competing reference point generation methods valued in CPF, $\alpha_c = 0.0056$. (Numbers in bold font show the best metric value)

3D	CPF	
	RVEA	RVEA-Bn-PFt
MaF1	**7.9030e-01(6.06e-02) =**	**7.8824e-01(2.53e-02)**
MaF2	6.3746e-01(1.25e-02) -	**6.6970e-01(1.00e-02)**
MaF3	7.2046e-01(1.75e-01) -	**8.1642e-01(6.22e-03)**
MaF4	**6.5760e-01(1.62e-01) +**	5.4362e-01(1.56e-01)
MaF5	7.0776e-01(3.07e-04) -	**7.4234e-01(7.31e-04)**
MaF6	**8.0088e-01(7.45e-02) =**	**8.3116e-01(9.27e-02)**
MaF7	7.5820e-01(2.89e-02) -	**7.8916e-01(2.10e-02)**
MaF10	**8.0661e-01(1.49e-02) +**	7.6498e-01(1.70e-02)
MaF11	**8.2809e-01(1.57e-02) +**	7.9161e-01(1.67e-02)
B or E	**5**	**6**

Note: B or E stand for the number of cases with better or equal performance RVEA compared to RVEA-Bn-PFt: "-": worse; "=": equal;"+": better;

In line with HV metric values, Spread (Δ) and Spacing's metric values reveal that better diversity is obtained for PF approximations when using the Bn-PFt method. See Table 3.5 and Table 3.6. Except for the MaF6 benchmark case, better and equal results with the Bn-PFt method have been reached.

Table 3.5 - Approximations of MaF benchmarks in 3D based on the two competing reference point generation methods valued in Spread (Δ), $\alpha_c = 0.0056$. (Numbers in bold font show the best metric value)

3D	Spread (Δ)	
	RVEA	RVEA-Bn-PFt
MaF1	**1.7290e-01(3.89e-02) =**	**1.6305e-01(2.03e-02)**
MaF2	1.2044e-01(4.71e-03) -	**9.5089e-02(2.48e-03)**
MaF3	**2.7442e-01(3.17e-01) =**	**2.5100e-01(5.07e-03)**
MaF4	**3.4309e-01(1.46e-01) =**	**4.0311e-01(1.73e-01)**
MaF5	2.6988e-01(7.44e-05) -	**2.2992e-01(3.45e-04)**
MaF6	**4.1989e-01(1.71e-01) =**	**5.5087e-01(2.56e-01)**
MaF7	3.2933e-01(1.69e-02) -	**2.5017e-01(1.66e-02)**
MaF10	3.4384e-01(1.38e-02) -	**2.7071e-01(1.56e-02)**
MaF11	3.4004e-01(2.01e-02) -	**2.8064e-01(1.41e-02)**
B or E	4	9

Note: B or E stand for the number of cases with better or equal performance RVEA compared to RVEA-Bn-PFt: "-": worse; "=": equal;"+": better;

Table 3.6 - Approximations of MaF benchmarks in 3D based on the two competing reference point generation methods valued in Spacing, $\alpha_c = 0.0056$. (Numbers in bold font show the best metric value)

3D	Spacing	
	RVEA	RVEA-Bn-PFt
MaF1	**3.0012e-02(5.89e-03) =**	**2.9419e-02(2.94e-03)**
MaF2	**1.4623e-02(5.05e-04) =**	**1.4429e-02(4.89e-04)**
MaF3	**4.1829e+02(2.50e+03) =**	**2.1117e-02(3.00e-04)**
MaF4	**2.3932e-01(1.19e-01) =**	**2.9735e-01(1.83e-01)**
MaF5	1.4666e-01(3.97e-05) -	**1.1170e-01(8.51e-05)**
MaF6	**5.0014e-02(9.39e-03) +**	6.8967e-02(2.20e-02)
MaF7	6.7084e-02(5.00e-03) -	**5.6936e-02(4.23e-03)**
MaF10	**1.7064e-01(2.11e-02) -**	**1.5955e-01(2.22e-02)**
MaF11	1.1770e-01(1.39e-02) -	**1.0420e-01(8.04e-03)**
B or E	6	8

Note: B or E stand for the number of cases with better or equal performance RVEA compared to RVEA-Bn-PFt: "-": worse; "=": equal;"+": better;

3.4.3.2 *On Five Objectives*

Generally speaking, a similar conclusion as the case for three objectives can be drawn when analysing the benchmark problems in 5 objectives. Bn-PFt method provides better solutions in diversity than the method of Das and Dennis does.

Higher and better or equal HV metric values are obtained for all cases studied except MaF2, where the Das and Dennis method gives a higher HV value. See Table 3.7.

Table 3.7 - Approximations of MaF benchmarks in 5D based on the two competing reference point generation methods, $\alpha_c = 0.0056$. (Numbers in bold font show the best metric value)

5D	HV	
	RVEA	RVEA-Bn-PFt
MaF1	**1.8769e-03(4.36e-05) =**	**1.8691e-03(4.77e-05)**
MaF2	**1.9033e-01(6.90e-04) +**	1.8932e-01(8.55e-04)
MaF3	**9.8900e-01(4.76e-02) =**	**9.9960e-01(1.38e-04)**
MaF4	**7.0106e-02(1.57e-02) =**	**7.2167e-02(1.14e-02)**
MaF5	8.3463e-01(3.54e-04) -	**8.3713e-01(3.26e-04)**
MaF6	**1.1678e-01(7.38e-04) =**	**1.1653e-01(1.45e-03)**
MaF7	2.5523e-01(9.18e-04) -	**2.5894e-01(3.11e-03)**
MaF10	9.9915e-01(3.78e-05) -	**9.9931e-01(5.00e-05)**
MaF11	9.9853e-01(1.36e-04) -	**9.9871e-01(1.53e-04)**
B or E	**5**	**8**

Note: B or E stand for the number of cases with better or equal performance.
RVEA compared to RVEA-Bn-PFt: "-": worse; "=": equal;"+": better;

IGD values are much diversified and indicate that the Das and Dennis method is better (score 7:5). See Table 3.8.

Table 3.8 - Approximations of MaF benchmarks in 5D based on the two competing reference point generation methods, $\alpha_c = 0.0056$. (Numbers in bold font show the best metric value)

5D	IGD	
	RVEA	RVEA-Bn-PFt
MaF1	**3.1317e-01(2.84e-04) =**	**3.1320e-01(1.16e-04)**
MaF2	1.0054e-01(5.47e-04) -	**9.4594e-02(5.29e-04)**
MaF3	**6.4221e-02(7.05e-02) -**	**4.0738e-02(7.46e-04)**
MaF4	**2.8255e+00(9.14e-01) -**	**2.7412e+00(6.51e-01)**
MaF5	**1.5359e+00(1.25e-04) +**	1.6067e+00(2.33e-04)
MaF6	**5.1344e-02(9.60e-04) +**	5.5338e-02(2.40e-03)
MaF7	3.6793e-01(2.13e-03) -	**3.5607e-01(6.46e-03)**
MaF10	**2.7433e-01(1.98e-03) +**	2.9050e-01(2.58e-03)
MaF11	**2.9557e-01(1.52e-03) +**	3.0426e-01(3.13e-03)
B or E	**7**	**5**

Note: B or E stand for the number of cases with better or equal performance.
RVEA compared to RVEA-Bn-PFt: "-": worse; "=": equal;"+": better;

CPF reveals the superiority of the Bn-PFt method versus that of Das and Dennis, in which the results show better (5 cases) or equal (4 cases) for all cases studied. See Table 3.9.

Table 3.9 - Approximations of MaF benchmarks in 5D based on the two competing reference point generation methods, $\alpha_c = 0.0056$. (Numbers in bold font show the best metric value)

5D	CPF	
	RVEA	RVEA-Bn-PFt
MaF1	**8.3334e-01(0.00e+00) =**	**8.3334e-01(0.00e+00)**
MaF2	**2.0116e-01(1.05e-02) =**	**2.0885e-01(1.41e-02)**
MaF3	**6.5358e-01(1.67e-01) =**	**7.2521e-01(8.82e-02)**
MaF4	**3.9460e-01(9.48e-02) =**	**4.0663e-01(8.62e-02)**
MaF5	5.6506e-01(4.62e-03) -	**5.7348e-01(7.57e-03)**
MaF6	6.4292e-01(4.93e-02) -	**6.9388e-01(6.64e-02)**
MaF7	7.4931e-01(2.02e-02) -	**7.7630e-01(3.04e-02)**
MaF10	6.0953e-01(1.29e-02) -	**6.7182e-01(1.86e-02)**
MaF11	5.8511e-01(1.83e-02) -	**6.6369e-01(2.04e-02)**
B or E	4	**9**

Note: B or E stand for the number of cases with better or equal performance RVEA compared to RVEA-Bn-PFt: "-": worse; "=": equal;"+": better;

When accessed in Spread (Δ), better or equal diversity of approximations adopting the Bn-PFt method than the Das and Dennis is attained for all benchmark cases except for MaF 6. See Table 3.10.

Table 3.10 - Approximations of MaF benchmarks in 5D based on the two competing reference point generation methods, $\alpha_c = 0.0056$. (Numbers in bold font show the best metric value)

5D	Spread (Δ)	
	RVEA	RVEA-Bn-PFt
MaF1	**1.0458e-04(4.05e-04) =**	**9.1685e-05(2.19e-04)**
MaF2	2.1231e-01(4.00e-03) -	**1.9062e-01(5.83e-03)**
MaF3	**3.6841e-01(4.07e-01) =**	**2.5731e-01(5.61e-02)**
MaF4	**4.6857e-01(9.83e-02) =**	**4.2658e-01(9.03e-02)**
MaF5	3.0297e-01(2.54e-04) -	**2.7973e-01(5.35e-04)**
MaF6	**5.3581e-01(3.49e-01) +**	8.5964e-01(1.52e-01)
MaF7	3.9315e-01(8.32e-03) -	**3.1341e-01(1.43e-02)**
MaF10	4.1826e-01(8.41e-03) -	**3.8291e-01(9.12e-03)**
MaF11	3.3814e-01(9.06e-03) -	**2.8579e-01(1.25e-02)**
B or E	**4**	**8**

Note: B or E stand for the number of cases with better or equal performance. RVEA compared to RVEA-Bn-PFt: "-": worse; "=": equal;"+": better;

Table 3.11 - Approximations of MaF benchmarks in 3D based on the two competing reference point generation methods, $\alpha_c = 0.0056$. (Numbers in bold font show the best metric value)

3D	Spacing	
	RVEA	RVEA-Bn-PFt
MaF1	**7.0670e-05(2.85e-04) =**	**5.4685e-05(1.55e-04)**
MaF2	5.7306e-02(1.28e-03) -	**4.9119e-02(1.28e-03)**
MaF3	**2.0926e+07(1.25e+08) =**	**2.7877e-02(2.04e-03)**
MaF4	**1.5158e+00(5.61e-01) =**	**1.3979e+00(2.25e-01)**
MaF5	7.6836e-01(5.37e-04) -	**6.9661e-01(8.49e-04)**
MaF6	**1.7331e+00(9.84e+00) =**	**1.3093e-01(2.19e-02)**
MaF7	3.3936e-01(5.12e-03) -	**3.0522e-01(7.01e-03)**
MaF10	3.6377e-01(7.13e-03) -	**3.3320e-01(1.06e-02)**
MaF11	2.5587e-01(1.23e-02) -	**2.1755e-01(1.87e-02)**
B or E	**4**	**9**

Note: B or E stand for the number of cases with better or equal performance
RVEA compared to RVEA-Bn-PFt: "-": worse; "=": equal;"+": better;

Valued in the Spacing metric, the Bn-PFt method leads to a diversity of approximations either better than or equal to what the Das and Dennis method can generate for all benchmark cases tested. See Table 3.11.

3.5 Discussions

The performance of RVEA-Bn-PFt and RVEA have been tested on nine benchmarks of MaF, in which different PF shapes of regular (MaF3, MaF5 and MaF10), partial coverage (MaF2), discontinuous (MaF7 and maF11), inverted (MaF1 and MaF4) and degenerated (MaF6) are present. Five different diversity indicators are used for evaluations and comparisons, i.e., HV, IGD, CPF, Spread, and Spacing. The effect of the Bn-PFt reference generator on diversity improvement varies depending on the PF shapes of the optimisation problem. First, Bn-PFt improves the diversity for PFs of regular type compared with the uniform design method. Second, Bn-PFt seems to have certain positive but limited effects on PFs of partial, inverted and discontinuous sorts. Third, the effect of Bn-PFt on degenerate type of PFs is questionable, which is due to instability problem when determining the model parameter where the B-norm curve is used to estimate the approximation of PFs. Moreover, the effect of Bn-PFt on asymmetric PFs is not properly evaluated in this thesis, thus needs to be explored in further research work.

Computational complexity and thus the evaluation budget is increased for algorithms with Bn-PFt applied. This is because the reference vectors first need to be created using the uniform design method to identify the basic shape of PFs. Then the Bn-PFt mechanism is needed to regenerate reference points.

3.6 Summary and Conclusions

A new method of generating reference points is proposed, B-norm based PF tracking method (Bn-PFt). The reference points are more evenly created on an m dimensional B-norm surface created adaptively by tracking the actual PF. Numerical studies performed on B-norm surfaces of various B values show that reference points created by the Bn-PFt method are more evenly distributed on PF than those projected onto the same surfaces generated using Das and Dennis method. Simulation results, using RVEA to the Benchmark problems of MaF1-7 and 10-11 with 3 and 5 objective functions, show that measured in HV, IGD, Δ, CPF and SP metrics, the approximation sets obtained using reference points of Bn-PFt method have better diversity than those of using the famous Das and Dennis method. Crucially, the proposed method generates better results in terms of diversity.

Reference points created by the Bn-PFt method with B=1 (unit simplex plane) have the exact location and distribution as those of the Das and Dennis method. In other words, the Das and Dennis method is a particular case of the proposed Bn-PFt method, which is the general case.

A new indexing system of reference points is also proposed to ease algorithmic development in decomposition-based evolutionary computation. The indexing system can enhance the formulation of the Das and Dennis method, save computing resources when searching for a specific reference point, define neighbouring reference points to a particular point in high dimensional objective space, and help facilitate work on algorithmic development of new methods.

The B-norm surface curve used in this study is symmetric in m dimensional objective space, which is most suitable for tracing PF of approximately symmetric forms. For strong non-symmetric or degenerated PFs, the reference

points created by the Bn-PFt method are out of the surface of the true PF. Their projections on the true PF are hampered somewhat when these are projected on the true PF. However, they are still more suitable to guide the search for PF than the Das and Dennis method because they are much nearer to the true PF than the latter.

In the future, more studies can focus upon the following aspects:

- The Bn-PFt method should be expanded to create the most possibly equidistant reference points on non-symmetric PF surfaces.
- Further, formulation using the proposed indexing system to identify neighbouring direct points to a given reference point in high dimensional space shall be studied. The number of neighbours determined by the indexing system can replace the user input parameter – the number of adjacent points in decomposition-based algorithms.

Chapter 4 A New Performance Indicator for Diversity in Many-Objective Optimisation Problems

Chapter Outline

Developing consistent performance indicators for many-objective optimisation algorithms is still challenging, particularly as the number of objectives increases. The challenges are due to the “curse of dimensionality”, such as the formulation complicacy of the problem, its computational complexity and power required, etc. All increase rapidly with the increase of the number of objectives. We introduce a new pure unary diversity indicator, Inverse Ratio of Net Avertence angle (IRNA). A pure diversity indicator is formulated using reference vectors by minimising the sum of the included angles between approximated solution set and reference vectors. It is achieved by rotating the system of reference vectors in all dimensions with an optimised spatial angle. The highest possible diversity score of a solution set is obtained. Performed empirical studies via testing on synthetic solutions on the unit simplex plane as well as on benchmark functions up to 10 objectives show that the proposed performance indicator IRNA is more sensitive to capturing diversity changes compared to other state-of-the-art performance indicators, in particular when the number of objectives increases, thus deeming it highly suitable for many-objective optimisation problems. Resulting publication:

K. E. Wu and G. Panoutsos, "A new Diversity Performance Indicator for Many-objective Optimisation Problems," 2021 IEEE Congress on Evolutionary Computation (CEC), Krakow, Poland, 2021, pp. 144-152.

4.1 Introduction

Various metaheuristic methodologies have been developed to deal with many-objective optimisation problems (MaOP) [159]. There is no single methodology superior to all the rest in solving the plethora of MaOPs [159]. Performance Indicators (PIs) are crucial for assessment on approximations of MaOP algorithms. The mathematical guarantees for diversity and convergence properties and global optima are incredibly challenging to derive [123]. Besides assessing the quality of solutions, PIs may also play a central role in actively guiding the evolution of a solution set toward the best solutions. It is most commonly accepted that the quality of the Pareto Front (PF) approximation is determined by its three major characteristics: convergence, distribution (or evenness) and extent (or spread); the last two jointly describe the diversity property [123], [129], [189]. Convergence indicators are formulated, for instance, by non-dominant sorting of solutions or by measuring and comparing the distance between individuals and the ideal point. However, a diversity indicator is more challenging to develop since a PF's actual shape, and distribution is unknown a priori and challenging to be described due to the limited number of discrete points (e.g., in a high dimensional objective space due to the "curse of dimensionality").

Several design principles are utilised to develop PIs, such as cardinality, distance, hypervolume, dominance, and included angles [189]. PIs based on included angles are formulated by measuring the included angles between the vectors of candidate solutions and the reference vectors adopted as indicative values of diversity [124], [129]. Pure diversity indicators have been developed in this way [124], [129], [190]. Two significant challenges remain to be resolved: One is associated with the distribution of PFs – which can be arbitrary; no existing reference system of vectors can create intersections on PF with

equidistant neighbouring points. Hence uniformity measured by such a system of reference vectors would not be very accurate. The second challenge is that candidate solutions may have a systematic bias in included angles with reference vectors, which may cause inconsistent indicators and hinder the derivation of meaningful metrics for solution sets. A systematic bias often occurs because the reference vector system is created independently to the locations of PF approximations while the latter could locate at different places other than on the reference vectors due to the stochastic nature of metaheuristic optimisation. See Figure 4.1 for details. As the number of objectives increases, a robust calculation of a PI is becoming even more challenging due to the significantly increased formulation complicacy and computational complexity of the problem.

The first challenge (PF distribution) can be relieved by tracing the PF with a B-norm surface and creating more evenly distributed reference points on the B-norm surface [134]. This thesis proposes that the second challenge (systematic bias) can be mitigated by minimising included angles between reference vectors and candidates through rotation of the reference vector system to remove eventual systematic bias in data. The underpinning idea of the proposed PI is to search for an optimised diversity score for each of the individual competing approximation sets by rotating the reference vector system with an optimal angle so that any systematic bias in both data sets is removed. Hence, a new unary diversity indicator is proposed. A reference vector-based pure diversity indicator is expressed with the help of the Inverse Ratio of Net Avertence angles (IRNA) similar to the definitions adopted in [124], [129] but inverted and varies within 0 and 1 where higher values for better diversity scores, as detailed in Section 4.3. Besides, alternative assessment methods for comparing and contrasting efficacy and efficiency among several

performance indicators in terms of monotonicity and sensitivity are suggested and demonstrated numerically through MaF benchmark functions in 3, 5, 7 and 10 objectives.

The rest of the chapter is organised as follows: Section 4.2 gives an overview of state of the art in performance indicators and the creation of reference vectors in MaOP problems, focusing on PIs using reference vectors. Section 4.3 provides a detailed description of the proposed IRNA to evaluate the diversity of MaOP problems. Section 4.4 includes numerical studies, where the effectiveness of IRNA is assessed against two well-established indicators on synthetic and benchmark problems. Finally, Section 4.5 summarises and concludes the chapter.

4.2 Existing Quality Indicators

4.2.1 Quality Indicator In Many-Objective Optimisation

Numerous performance indicators have been designed for the assessment of MaOP approximation sets. Earlier comprehensive surveys on PIs and their properties can be found in the literature [123], [126], [191]. PIs in MaOP have been roughly grouped into three main categories: those which essentially evaluate convergence [132], those mainly assessing diversity [133], and those measuring both convergence and diversity simultaneously [192]. Representative PIs for measurement of convergence only are Generational distance (GD) [193] and GD$^+$ [194], which are distance-based PIs. GD calculates the averaged nearest distance between each candidate of an approximation to the PF. GD$^+$ modifies GD to become Pareto compliant, which means that as long as a solution set A dominates a solution set B, GD$^+$ of A is greater than B.

The diversity of approximations consists of two parts: the candidate solutions' spread and uniformity. When diversity is concerned, PIs are further divided into subgroups for primarily evaluating spread, those for measuring uniformity, and those for assessing both aspects simultaneously. An example of commonly adopted PIs of this kind is Spread (Δ) [188] and Spacing metric (SP) [135]. Some are newly developed, e.g. PD [123] and Coverage over Pareto Front (CPF) [129]. The Spread (Δ) expresses the diversity by using the distribution and the nearest distance between obtained non-dominated solutions. The spacing metric is defined in the averaged sum of the distance variance between a point and its closest neighbour. PD is inspired by biodiversity measurement and puts the diversity score proportional to the number of disparate distances between candidate solutions. CPF measures the diversity first by projecting a solution set to the $(m-1)$-dimensional unit

simplex plane and then to a unit hypercube. Its score for diversity is obtained by calculating the hypervolume of the projected solution set.

PIs for measuring the combined performance of convergence and diversity that are most commonly used in research are Epsilon indicator (ϵ-indicator) [127], Inverted generational distance (IGD) [128], IGD+ [194], Hypervolume (HV) [127], and R-metric [195]. ϵ-indicator is a binary indicator, i.e., two approximation sets A and B are contrasted. It is done by that the indicator value is set to equal the minimum factor such that for any solution in B, there is at least one solution in A that is not worse by the factor. IGD is expressed as the minimum Euclidean distance of nearest Euclidean distances from actual Pareto optimal points to approximated ones. IGD+ is formulated similarly to IGD but is made Pareto compliant. Hypervolume (HV) metric calculates the space enclosed by the candidate solutions and a reference point (Nadir point is often chosen). R-metric consists of three binary indicators and puts scores using a set of utility functions, where the indicator is determined by the expected number of cases the set A are better than the set B. IGD and HV have long been the most popular indicators used in evaluation of approximations of MaOP. IGD differs from GD in three aspects: i) it is based on the minimum Euclidean distance while GD uses the average distance ii) IGD uses the distance calculation starting from the solutions in true PF while GD does it oppositely iii) given sufficient number of well-diversified PF points, IGD would provide a score of combined evaluation of both the diversity and the convergence of a PF approximation set [196].

Deb et al.[100] suggested a Δ metric measuring the extent of spread and distribution achieved by the approximations. The main demerit of the indicator is its difficulty computationally when used in analysing solutions of MaOPs because the indicator is primarily designed for diversity evaluation of bi-

objective problems. Although It can be extended to access approximation of MaOPs using the so-called Voronoi diagram approach, it is difficult to determine the Voronoi diagram for MaOP cases [197].

Mostaghim and Teich [192] propose Sigma Diversity Metric (SDM) to evaluate the diversity of approximations by calculating angular positions of solutions in the objective space. A major demerit of the method is a systematic bias in angular positions of the solution relative to σ reference lines.

Deb and Jain [2] suggest a diversity measure (DM), which measures the diversity against a reference set. Here, solutions are projected on an $(m-1)$ dimensional hyperplane with hyper-boxes. The indicator value is proportional to the number of hyper-boxes containing both a reference solution and a candidate solution. Several challenges exist [198], including its dependence on a reference set, computationally high cost in creating hyper-boxes, and the determination of neighbouring hyper-boxes in high dimensional objective space.

Li et al. [197] propose a pure diversity comparison indicator (DCI) to assess the relative diversity of two or more Pareto front approximations in many-objective optimisation by counting the number of solutions in a grid covering the objective space. No reference set is required for DCI calculation. But the method is sensitive to the number of divisions chosen in the grid. Li et al. [197] suggest a parameter-less performance comparison indicator (PCI) to assess convergence and diversity of approximations using a reference set constructed by dividing the approximation set into clusters and calculating the minimum moves of solutions that weakly dominate these clusters. The merit of PCI is that it does not require any prior reference set. A demerit is that PCI depends on determining the number of clusters utilised in the evaluation, which leads to a variation of indicator value.

The idea of using reference vectors to create a diversity score for contrasting two competing approximation sets has been implemented successfully in the past [124], [129], [191].

Cai et al. [190] define a diversity indicator using reference vectors (DIR) by identifying the systematic deviations of locations of candidate solutions away from the reference vectors and finding the mean values and variances of the so-called coverage vector that stores the number of reference vectors linked to each candidate solution. A major demerit of the method is its inability to deal with local clusters of candidate solutions, which cannot be solved by increasing the number of reference vectors since the regional clusters are not easily detectable in high dimensional space; this largely influences the indicator value. Moreover, the local clusters of data are not easily detected in high dimensional MaOPs a priori.

Tian, Y. et al. [129] proposed most recently a pure diversity PI named CPF by first parallel projecting a solution set to the $(m-1)$-dimensional unit simplex plane and then to a unit hypercube along the reference vectors, and calculating the hypervolume of the projected solution set as the score for its diversity. A significant disadvantage of the method is that the coverage of partially PF is enlarged if it locates higher than the unit simplex plane when parallelly projected onto it because the projection occupies a more significant portion of the unit simplex plane than it should. The enlarged projection is then reprojected to a unit hypercube and creates a too large image of PF approximations. In the opposite case, the coverage is shrunk when projected onto the unit simplex plane. See section 4.4 for details.

4.2.2 Creation of System Reference Vectors

The universally used method for generating a system of reference vectors is the one introduced by Das and Dennis [79], in which a uniformly spaced reference of vectors is created only on a normalised hyper-plane, an $(m-1)$-dimensional unit simplex plane to all objective axes which have an intercept of one on each axis.

Deb and Jain [2] suggest using two layers of reference points, each with a smaller p, p_1 is adopted for the boundary layer and p_2 for the inside layer. The total number of reference lines is significantly reduced to a manageable level.

Tian et al. [187] suggest generating reference points on known true PFs starting with the points created by Das and Dennis method on the unit simplex plane and projecting them to the actual Pareto fronts. Unfortunately, the final distribution of the reference points generated in this way is not uniform.

Wu and Panoutsos [199] propose a B-norm-based Pareto Front tracing method (Bn-PFt) that generates more evenly distributed reference points on the approximated PF. It is done by a B-norm regression based on the approximated PF and creating equally spaced reference points on all of its two-dimensional boundaries; these are used to generate all other internal reference points.

4.3 Formulation of the Proposed Diversity Indicator

In this section, the establishment of the proposed IRNA for evaluating MaOP problems' diversity is described in detail.

4.3.1 Inverted Ratio of Net Avertence Angles (IRNA)

4.3.1.1 *Definition of diversity indicator – IRNA*

Barely using included angles to a predefined set of reference vectors to formulate PI for diversity may fail to account for possible systematic bias in diversity measurement (see Figure 4.1(a)). As can be seen, each candidate solution has a similar angle difference from its closest reference vector. A diversity score based on these angles is inevitably kept incorrectly low (suboptimal). It is even so when assessing approximations of high dimensional MaOPs since the number of solutions is usually very scarce compared to the need to sufficiently cover the high dimensional space. One way to improve the formulation is by introducing a rotating reference vector system to remove eventual systematic bias in avertence angles between approximation sets and reference vectors. By rotating the reference plane with an optimised angle β, the sum of angle difference is decreased, and an optimal diversity score can be obtained. See Figure 4.1(b). The minimised Inverted Ratio of Net Avertence angles (IRNA) is formulated as a pure diversity indicator defined as the sum of unity minus the ratio of the included angle to the maximum possible included angle between individual candidate solutions and the reference vector, See Eq. 4.1.

$$IRNA = \frac{1}{N}\sum_{k=1}^{N}(1 - \frac{1}{\gamma^k}\theta_a^{(k,min)}) \quad \text{Eq. 4.1}$$

in which $\theta_a^{(k,min)}$ is the minimised avertence angle between candidate solution k and its nearest reference vector. It is illustrated in a 3D situation, as shown in

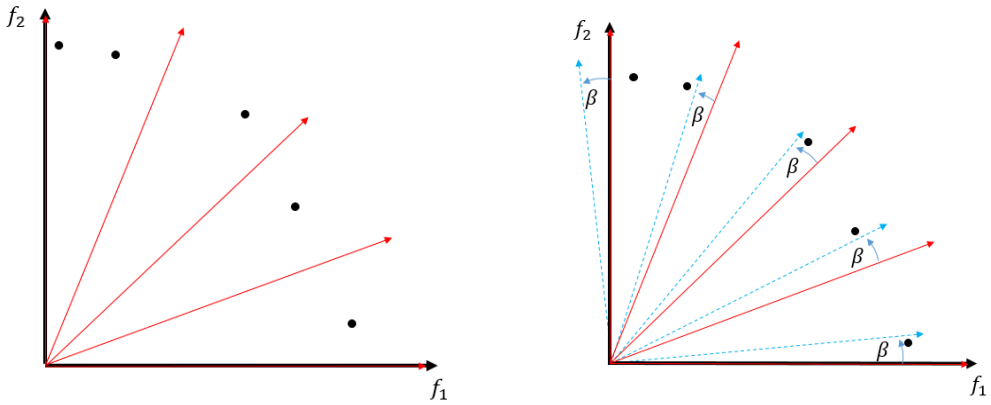

(a) Locations of candidate solutions and reference vectors at the start.

(b) Rotated system of reference vectors with angle β.

Figure 4.1 - A 2D schematic view of the rotation of reference vectors by β, where the sum of included angles is minimised to attain the minimal sum of net avertence angles.

Figure 4.2. γ^k is 1/2 of the included angle between two adjacent reference vectors for candidate k. N is the number of candidate solutions.

IRNA value varies between 0 and 1, and the higher the score of an approximation set indicates better diversity.

4.3.1.2 *Relationship between the Included Angle and Their Projections in m Dimensional Space*

The optimised spatial included angle $\theta_a^{(k,min)}$ is nontrivial to be calculated directly. See Figure 4.2. One way to find the angle is by decomposing all involved angles onto respective 2D planes where arithmetic operations can be done. The resultant angle is found based on the net components.

The included angle formed by two arbitrarily located spatial vectors in high dimensional space can be expressed by their rotational projections on respective 2D planes.

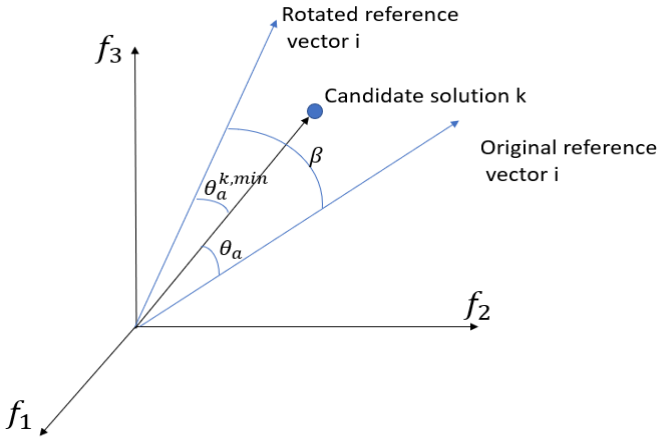

Figure 4.2 - A 2D schematic view of the rotation of reference vectors by β, where the sum of included angles is minimised to attain the minimal sum of net avertence angles.

The included angle can be proven numerically to be given as:

$$\theta_a = \sqrt{(\theta_{12})^2 + (\theta_{23})^2 \ldots + \left(\theta_{ij}\right)^2 \ldots + (\theta_{m1})^2} \qquad \text{Eq. 4.2}$$

in which θ_a is the avertence angle between two spatial vectors in an m dimensional space and can be expressed by θ_{12}, θ_{23}, ..., $\theta_{(m-1)m}$ and θ_{m1}, where θ_{ij}, $i \in \{1, \mathrm{m}\}, j = i + 1 \; and \; j = 1 \; when \; i = m$, are the angles of the rotational projections of the vectors about the axis of *2, 3, …, m* and *1* respectively onto planes formed on *1-2, 2-3, …, m* – 1 axes, and there are m components in total. Figure 4.3(b) illustrates as an example a 3D case of finding θ_{12}, θ_{23} and θ_{31}.

See Figure 4.3 (b). Assuming:

$$\alpha_{\mathrm{R}} \approx \frac{\mathrm{R}_2}{|\mathrm{R}|}, \qquad \alpha_{\mathrm{F}} \approx \frac{\mathrm{F}_2}{|\mathrm{F}|} \qquad \text{Eq. 4.3}$$

$$\theta_{12} = \arccos\left(\frac{[|R| \cdot \cos\alpha_{\mathrm{R}} \quad |R| \cdot \sin\alpha_{\mathrm{R}} \quad 0]\,[|F| \cdot \cos\alpha_F \quad |F| \cdot \sin\alpha_{\mathrm{F}} \quad 0]}{|R||F|}\right) \qquad \text{Eq. 4.4}$$

Eq. 4.3 is only an approximate formulation of α_{R} and α_{F} angles. The exact expressions are $sin\alpha_{\mathrm{R}} = \mathrm{R}_2/|\mathrm{R}|$ and $\sin\alpha_{\mathrm{F}} = \mathrm{F}_2/|\mathrm{F}|$. But when these are inserted into Eq. 4.4 and later in Eq. 4.2, incorrect resultant included angle θ_a is obtained. Only when Eq. 4.3 is used, Eq. 4.2 gives the nearly accurate angle θ_a. This author has not succeeded in explaining this mathematically and

considering Eq. 4.2 as an empirical expression for the resultant included angle between two vectors in m-dimensional space after one of them is rotated with an arbitrary angle β.

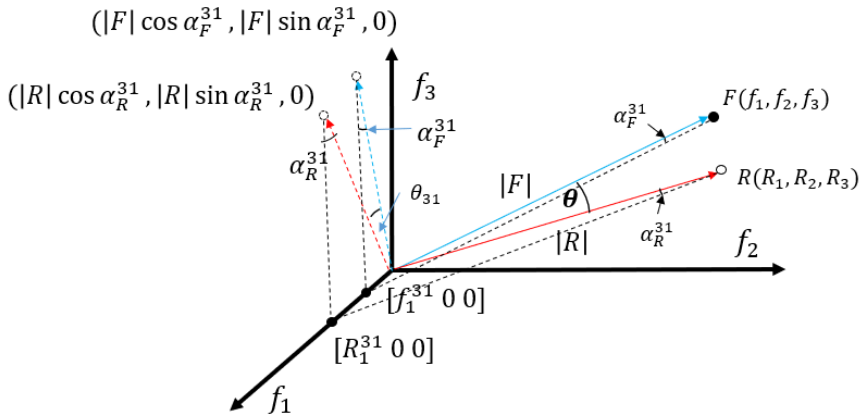

(a) Rotational projection about f_1 axis

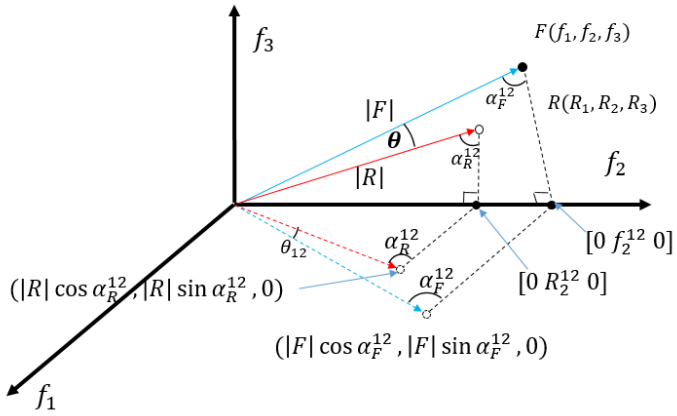

(b) Rotational projection about f_2 axis

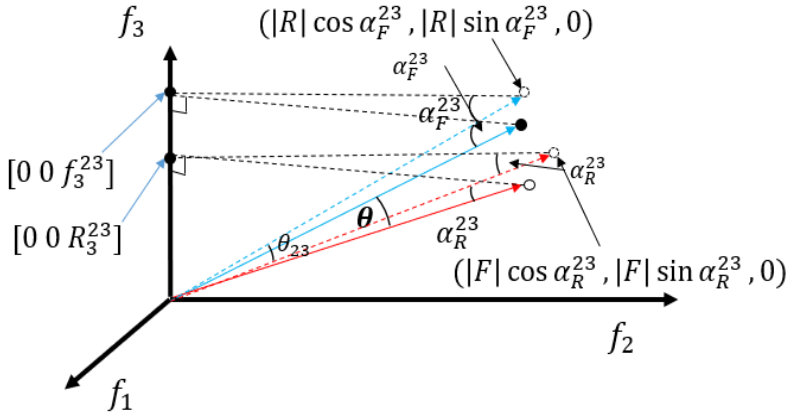

(c) Rotational projection about f_3 axis

Figure 4.3 - Rotational projection of a spatial included angle θ onto the surfaces of pairwise coordinate axes.

Similarly, all other θ_{ij} are found by rotating R and F about f_j axis accordingly. Included angles in high dimensional space can be added or

subtracted by first projecting them onto the same respective planes, and the arithmetic operations are done on the projected components. After component-wise addition or subtraction, the partial results are enumerated back to the resultant spatial angle searched.

Eq. 4.2 is considered an empirical relationship between a spatial angle and its rotational projections in m dimensional space due to the approximation performed as expressed in Eq. 4.3. Its validity is proven numerically in this study, as shown below.

4.3.1.3 *Correction on the Approximated Included Angle θ_{app}*

Expressions of relationships, such as α_R and α_F in Eq. 4.3, are approximate formula, which creates a minor mismatch between the approximated angle θ_{app} and the true θ, as expressed in Eq. 4.2, which is considered an empirical relationship. The deviation is found by randomly generating a large amount of avertence angles (10^5) in any dimensional space. The approximated avertence angles are compared with the exact ones. Eq. 4.4. shows the results.

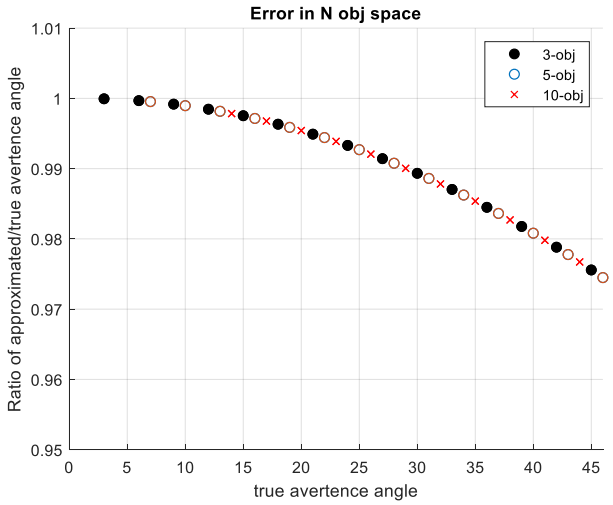

Figure 4.4 - Ratio of the approximated and the actual avertence angle are shown versus the precise avertence angle.

As shown in Figure 4.4, the deviation is not affected by the number of objectives or the dimension of the MaOP problem.

Usually, such a deviation is negligible in 3-objective space since the maximum angle between reference vectors is less than 10 degrees, giving an estimated error of less than 0.13%. However, the number of workable reference vectors in higher-dimensional objective space is limited compared with the space that needs to be covered. The maximum avertence angle could be as high as 45º. (A significantly large number of reference vectors is required to achieve a similar maximum avertence angle as it is the case in a 3D case, which would have required an unpractical amount of reference vectors.). A proposed solution is to utilise a correction function after the approximated avertence angle is obtained to acquire a sufficiently accurate actual avertence angle.

Based on the simulated data, a polynomial correction function can be created to remove the deviation, where the coefficients in the equation are found by using a simple single-objective optimisation:

$$\theta = 7.753 \times 10^{-9} \cdot \theta_{app}^{3} - 1.306 \times 10^{-5} \cdot \theta_{app}^{2} + 5.153 \times 10^{-6} \cdot \theta_{app} + 1.00 \quad \text{Eq. 4.5}$$

It should be noted that Eq. 4.5 is a generic equation for correction on the deviation of approximated avertence angle from the true one. As shown in Figure 4.4, the deviation is the same for cases of any number of objective functions and only depends on the amount of actual avertence angle.

4.3.1.4 *Determination of IRNA*

The proposed IRNA is computed in steps as follows:

Find the components β_{ij} of rotation angle β in the various pairwise coordinate planes by minimisation of the expression:

$$\beta_{ij} = argmin_{\beta_{ij},\ \substack{i=1,\dots,m \\ j=i+1,\dots,m-i+1}} \sum_{k=1}^{N} \sum_{i=1}^{m} \sum_{j=i+1}^{m-i+1} \left| \theta_{ij}^{(k)} - \beta_{ij} \right| \quad \text{Eq. 4.6}$$

in which N is the number of candidate solutions.

Find the components of net avertence angle $\theta_{ij}^{k,net}$

$$\theta_{ij}^{(k,min)} = \theta_{ij}^{(k)} - \beta_{ij}, \quad \text{Eq. 4.7}$$

The vector sum of avertence angle $\theta_a^{(k,min)}$ is given by Eq. 4.2. The diversity indicator IRNA is finally computed using Eq. 4.1.

Algorithm 1 depicts the pseudo-code for the calculation of IRNA. It starts with importing population (X) of n candidate solutions. The algorithm first eliminates dominant solutions (line 1) and then normalises the remaining approximates (line 2). The upper and lower limit of the normalisation range can either be decided by the decision-maker or found using the maximum and the minimum value from the data sets. Systematic reference vectors are created

Algorithm 1 Pseudo Code for IRNA

Input: X (approximation set)
Output: IRNA
1: $X \leftarrow$ Apply non-dominant sorting (X)
2: $X_1 \leftarrow$ Normalise the solution (X)
3: $R \leftarrow$ Build reference plane based on Das and Dennis's approach.
4: $\gamma \leftarrow$ Calculate the minimum angle between each reference line.
5: $X_2 \leftarrow$Assign solutions to the closest reference line (X_1, R)
6: $\theta_{app} \leftarrow$ calculate separate angle value for each solution (X_2)
7: $\theta \leftarrow$ angle correction (θ_{app})
8: $\beta \leftarrow$ a single optimisation process is carried out to obtain optimal angle(θ, γ, R)
9: IRNA $\leftarrow$ calculate diversity value (β)

based on the method of reference point generation proposed by Das and Dennis's (line 3) approach. The minimal angles between the reference vectors are calculated and stored as variables γ (line 4). Each candidate solution is assigned to its closest reference line based on the included angles (Line 5), and IRNA is calculated using the obtained included angles (Line 6).

The reference vectors can also be created using the Bn-PFt method [199] to generate more evenly distributed reference vectors than those based on the Das and Dennis method.

4.4 Numerical Studies on IRNA

Reference vector-based diversity indicators for contrasting two competing approximation sets have also been proposed earlier [133], [138], [201]. But these methods are not considered mainstream in evaluating the diversity of PF approximations of a MaOP [12]. IRNA is therefore compared with the most frequently used one, the hypervolume, and the most recently proposed one, CPF. The comparison methodologies applied in the thesis can be used for contrasting with other reference vector-based diversity indicators, which is part of the future work. The efficacy of IRNA is assessed through four groups of numerical tests where comparisons are performed between IRNA and the most frequently used PI of HV [127] and a recently developed CPF [129]. The reference point for HV evaluation is set to the point 1.1 times of the estimated Nadir point. All objective function values have been normalised before the assessments using the chosen PIs. First, IRNA is applied on a set of synthetic PF of uniformly spaced candidate solutions on a unit simplex plane. The outcome is compared with the HV and the CPF. The comparisons are performed on four different synthetic candidate solution sets. The number of candidate solutions is randomly removed from the complete solution set.

The consistency of the indicators is evaluated as diversity decreases and as the number of objective functions increases. (Section 4.4.1). Second, HV, CPF, and IRNA are tested to assess actual Pareto Front of Benchmarks of MaF [112] in three objective functions. (Section 4.4.2). Third, the comparison is made among HV, CPF and IRNA on PF in 3, 5, 7 and 10 objectives of MaF Benchmark problems with a fixed number of candidate solutions. When the number of candidate solutions is set, the diversity of an approximation is expected to go down as the number of objective functions increases. It tests the sensitivity and monotonicity of the newly proposed diversity measure in

contrast to the existing ones. (Section 4.4.3). Fourth, HV, CPF, and IRNA are used to assess results from the test on convergence process or iteration over MaF Benchmarks. (Section 4.4.4). Finally, IRNA is used in contrasting the performance of PF approximations of MaF benchmarks obtained using three representative and dissimilar MaOP algorithms: NSGA III, GrEA and IBEA (Section 4.4.5).

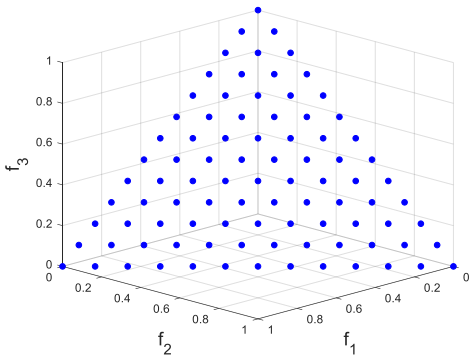

(a) Fully systematically constructed
HV: 0.8417 CPF: 0.7176 IRNA: 1.000

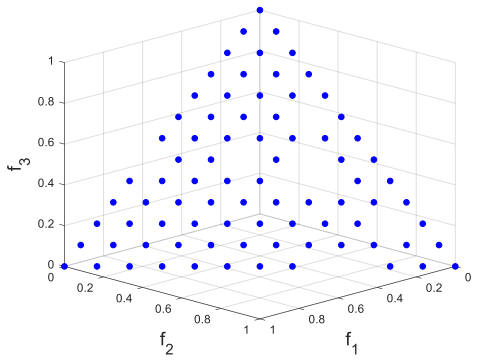

b) 10% randomly chosen and discarded.
HV: 0.8374 CPF: 0.7031 IRNA: 0.9011

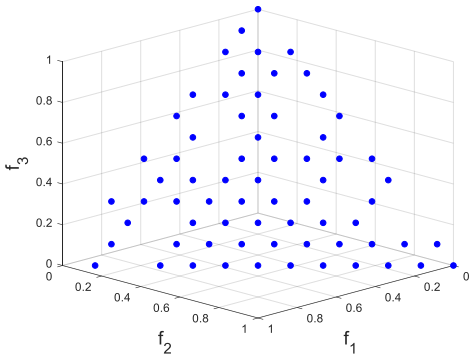

c) 25% randomly chosen and discarded.
HV: 0.8297 CPF: 0.7175 IRNA: 0.7473

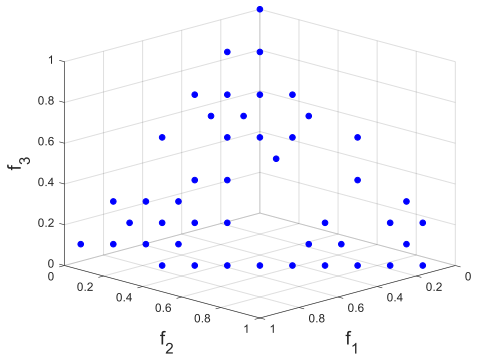

d) 50% randomly chosen and discarded.
HV: 0.8104 CPF: 0.5357 IRNA: 0.5055

Figure 4.5 - A typical set of constructed candidate solutions on the normalised unit simplex plane where a specific portion of randomly chosen solutions is discarded.

The purpose of the tests is to determine the monotonicity and sensitivity of IRNA to known proportional changes of diversity. This test method has been used successfully in earlier studies, e.g. in [123]. Four different cases are studied, a) fully systematically constructed candidate solutions on the unit simplex plane, b) 100% systematically constructed candidate solutions, then 10% of them are randomly discarded, c) 75% systematically constructed and

25% randomly discarded, and d) 50% systematically constructed and 50% randomly discarded. Figure 4.5 displays a typical set of candidate solutions created on the unit simplex plane with 100% systematic creation while 0%, 10%, 25% and 50% are randomly discarded. The competing indicators are calculated and shown in Figure 4.5. The calculation has been repeated up to 20 times to consider the eventual stochastic nature of the problem.

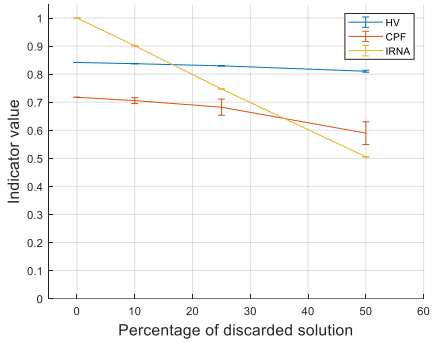

(a) Analysis done on the normalised unit simplex plane of 3 obj.

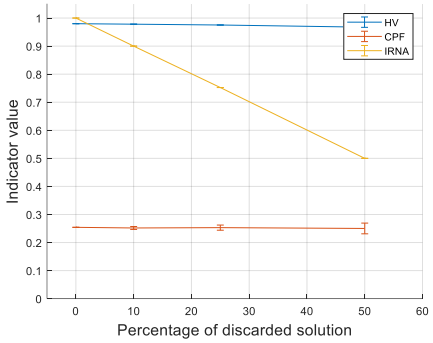

(b) Analysis is done on the normalised unit simplex plane of 5 obj.

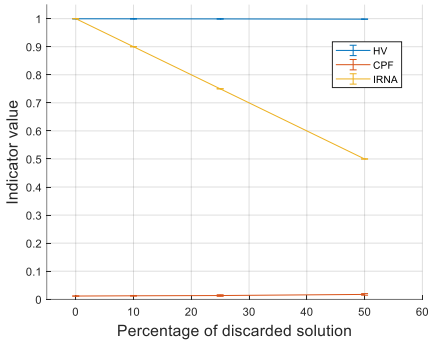

(c) Analysis done on the normalised unit simplex plane of 10 obj.

Figure 4.6 - The values of quality indicator versus percentage of discarded solutions on the normalised unit simplex plane.

As can be seen on values of PIs, HV and CPF start with non-unity value for although 100% perfect diversity and reduces unproportionate with the further reduction of diversity. On the other hand, IRNA begins with unity, reduces proportionately, and effectively captures diversity. The results are also listed in Table 4.1 for 3 objective functions, Table 4.2 for 5 objective functions, and Table 4.3 for 10 objective functions. The indicator values have been depicted versus the percentage of discarded solutions shown in Figure 4.6.

Table 4.1 - Quality indicators of HV, IGD, and IRNA 3 obj. function

	% discarded solution (number of solutions are discarded)			
	0% (0)	10% (9)	25% (22)	50% (45)
HV (↑)	0.8417(±0.00)	0.8374(±0.00)	0.8297(±0.00)	0.8104(±0.00)
CPF (↑)	0.7176(±0.00)	0.7058(±0.01)	0.6823(±0.03)	0.5899(±0.04)
IRNA (↑)	1.0000(±0.00)	0.9011(±0.00)	0.7473(±0.00)	0.5055(±0.00)

Table 4.2 - Quality indicators of HV, CPF, and IRNA 5 obj. function

	% discarded solution (number of solutions are discarded)			
	0% (0)	10% (21)	25% (52)	50% (105)
HV (↑)	0.9799(±0.00)	0.9781(±0.00)	0.9752(±0.00)	0.9675(±0.00)
CPF (↑)	0.2542(±0.00)	0.2519(±0.00)	0.2531(±0.00)	0.2502(±0.01)
IRNA (↑)	1.0000(±0.00)	0.9000(±0.00)	0.7524(±0.00)	0.5000(±0.00)

Table 4.3 - Quality indicators of HV, CPF, and IRNA 10 obj. function

	% discarded solution(number of solutions are discarded)			
	0% (0)	10% (22)	25% (55)	50% (110)
HV (↑)	0.9996(±0.00)	0.9994(±0.00)	0.9991(±0.00)	0.9982(±0.00)
CPF (↑)	0.0115(±0.00)	0.0124(±0.00)	0.0133(±0.00)	0.0173(±0.00)
IRNA (↑)	1.0000(±0.00)	0.9000(±0.00)	0.7500(±0.00)	0.5000(±0.00)

Similar conclusions can be observed from Table 4.1, Table 4.2, and Table 4.3: when the percentage of discarded solutions goes up and the diversity worsens, HV is not sensitive to the change. See Figure 4.6. CPF starts with the value of non-unity and varies nonlinearly. IRNA behaves proportionately with the variation of percentage of randomly discarded approximations. HV values approach one as the dimension of the problem increases. HV measures the hypervolume. The ratio of hypervolume to the volume of whole objective space increases dramatically with the increasing dimension of the MaOP problem, contributing to the non-sensitivity of HV selected candidate solutions' location in many-objective space problems. As the number of objectives increases, IRNA exhibits good sensitivity in capturing the changes in discarded solutions, unlike HV and CPF.

4.4.1 Evaluation on True PF of Benchmark MaF

HV, CPF, and IRNA are tested on actual Pareto Front of Benchmarks of MaF, showing consistency of IRNA in reflecting the diversity of accurate PF

solutions compared with HV and CPF. It is done by that IRNA, HV and CPF are adopted to analyse actual PF solutions of MaF 1-7 and 10-11 to show their capability in measuring the coverage of the PFs in the objective space.

MaF 1-7 and 10-11 are used in the analysis. MaF 8, 9, 12 and 13, 14 and 15 are not taken in this study because MaF 8 and 9 are specially designed to display their PF readily using the two chosen decision variables. MaF 12 and 13 are designed to study nonlinear linkages of decision variables and multi-modality issues that are not subject to this work. Besides, both MaF12 and MaF13 with 3 objectives have the PF shape of a sphere similar to MaF 5. MaF 14 and 15 are designed to study large-scale problems, and their PF shapes are identical to MaF 1 and MaF 4, respectively.

Figure 4.7 depicts the indicator values to various true PF of MaF Benchmarks chosen.

Figure 4.7(a) shows the PF of MaF1, which consists of a partial simplex plane of non-unity. Its coverage on objective space is reflected in HV and IRNA values. CPF is proportional to the coverage of projected PF on a unit simplex plane. The partial PF locates higher up than the unit simplex plane. When projected onto the unit simplex plane, the projection covers a falsely larger portion of the unit simplex plane, resulting in a considerable CPF value.

It should be noted that the maximal achievable value of diversity in IRNA is, in this case, limited to a value much lower than 1.0 no matter how uniform the approximations are distributed within the feasible area of PF because IRNA expresses the coverage of an approximation set in the objective space. The PF only partially covers the space. When several approximation sets obtained using different algorithms are contrasted, the competition targets an IRNA value nearest to this maximum achievable value.

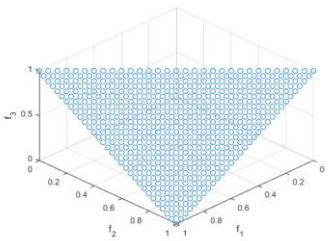

(a) MaF1
HV= 0.24521 CPF= 0.91035
IRNA= 0.27419

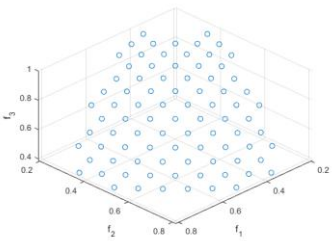

(b) MaF2
HV= 0.21542 CPF= 0.8148
IRNA= 0.3946

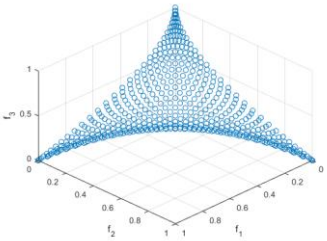

(c) MaF3
HV= 0.97024 CPF= 0.70751
IRNA= 0.41757

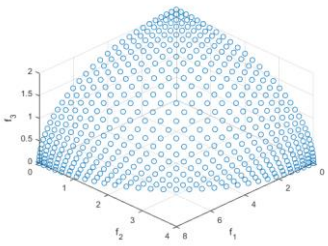

(d) MaF5
HV= 0.58721 CPF= 0.74412
IRNA= 0.99998

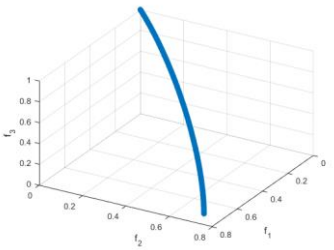

(e) MaF6
HV= 0.20212 CPF= 0.63619
IRNA= 0.050262

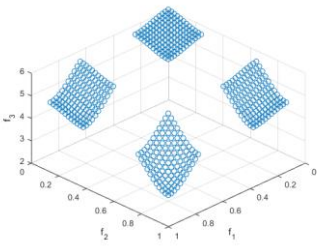

(f) MaF7
HV= 0.28874, CPF= 0.81041
IRNA= 0.26204

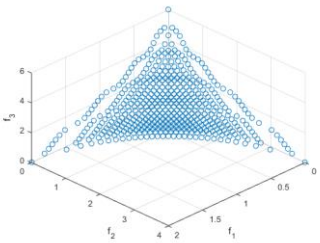

(g) MaF10
HV= 0.95671 CPF= 0.82621
IRNA= 0.9874

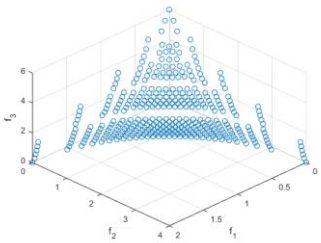

(h) MaF11
HV= 0.94159 CPF= 0.83999
IRNA= 0.50425

Figure 4.7 - True PF of Benchmark of MaF evaluated by HV, CPF and IRNA.

Figure 4.7 (b) displays the PF of MaF2, which is a partial sphere. HV and IRNA have reasonable low values since PF covers only partially the objective space, while the CPF value is too high for the same reason as it is explained for MaF1.

Figure 4.7(c) displays the PF of MaF3, which is in a convex shape. The PF is calculated based on a mathematical formula that creates unevenly distributed candidate solutions. But this gives high HV values since many solutions are concentrated along boundaries favoured by HV [127]. The value of CPF is relatively lower than HV because it fails to cover the simplex plane completely

when it is parallelly projected to the plane. In other words, CPF shows lower diversity estimation on PF of convex shapes, which are located lower than the simplex plane. IRNA accesses the averaged uniformity of an approximation set. The PF solutions shown in Figure 4.7(c) are found using a mathematical expression valid for the benchmark [112], and the result is unevenly distributed although seemingly densely populated. Hence, the sum of inclusion angles in IRNA calculation is averaged over; by dividing with the total number of solutions, IRNA's resulting value is relatively low. Subsequently, the same benchmark is used with NSGA III; the IRNA value is much higher, as in Fig. 4.8 (c). It is because a uniformly distributed set of reference points is utilised in the search for solutions.

Figure 4.7(d) shows the PF of MaF5, which is a sphere. PF covers the objective space fully, reflected in the high IRNA value. When projected on a unit simplex plane, the solutions have uneven distribution, which results in lower CPF values. HV favours candidates located on the boundaries, where such solutions are not overwhelmingly present, as is the case for MaF3. That is why a limited HV value is reached.

Figure 4.7(e) shows PF of MaF6, which consists of a degenerated PF shape of an arc, with low coverage of the objective space, which is in IRNA values since IRNA expresses the coverage and distribution of solutions on the PF in the objective space simultaneously. HV value is also low since only two extremal solutions and otherwise only intermediate solutions of a concave type, resulting in low HV. CPF has too high of a value in this case.

Figure 4.7(f) shows the PF of MaF7 that partially covers the objective space, reflecting HV and IRNA values. For the similar reason stated above, CPF covers a falsely large portion of the unit simplex plane, which results in a considerable CPF value.

Fig. 4.7(g) shows the PF of MaF10 that fully covers the objective space, which is reflected in HV, CPF and IRNA values.

Fig. 4.7(h) shows the PF of MaF11 that covers only partially the objective space, but HV and CPF have relatively high values, while the partial coverage is reflected only on IRNA value. When PF is projected onto the unit simplex plane, it covers falsely a large portion of it, which results in a considerable CPF value. Solutions at knee point and boundary areas contribute more to HV value in the case of a PF of convex shape, and there are plenty of such points in the solution, which lead to high HV value.

4.4.2 HV, CPF and IRNA in Analysing PF Approximations

Comparisons among HV, CPF and IRNA on approximations in 3, 5, 7 and 10 objectives of MaF1-7 and 10-11 applied on PF approximations calculated with NSGA III [2] are performed. See Figure 4.8. The purpose of the tests is to examine the indicators' monotonicity further. With almost the same number of candidate solutions in analysis, it is expected that the diversity of solutions shall go down with the increasing number of objective functions.

Table 4.4 - Number of iterations and candidate solutions

Number of objectives	Number of evaluations	Number of solutions
3	200,000	210
5	500,000	210
7	500,000	210
10	500,000	275

The algorithmic parameters adopted in NSGA III are based on default values acquired from PlatEMO version 2.7 [187]. The number of iterations and number of candidate solutions is listed in Table 4.4. Reference vectors are generated using the Das and Dennis method for the number of objective functions less than or equal to 5, while they are created by the Deb and Jain approach in cases of 7 and 10 objectives. Each Benchmark problem with a

specific number of objectives is calculated 30 times. Approximation sets are evaluated by PIs and shown in their mean values and standard deviations.

Figure 4.8 (a) displays the change of HV, CPF, and IRNA indicator values applied on approximations of MaF1 for the increasing number of objectives. All three indicators behave as expected, i.e., values decrease monotonically with the number of objectives. Still, the values of HV are extremely low on that of 7 and 10 objectives, which is because the volume above PF, which locates higher than unit simplex, decreases drastically with the increasing number of objectives. It can be reasoned as follows. Simplex planes can be in general expressed as:

$$f_1 + f_2 + \cdots + f_m = a_m \quad \text{Eq. 4.8}$$

in which a_m is the value of an objective function at which the simplex plane coincides with f_i axis. ($f_\mathrm{i} = a_m$ while f_j=0, for all $j \neq i$). For midpoint on PF: f_1=f_2=…=f_m, we have:

$$f_1 = f_2 = \ldots = f_m = {a_m}/{m} \quad \text{Eq. 4.9}$$

Its distance to the Ideal point r_m is:

$$r_m = \sqrt{(f_1)^2 + (f_2)^2 + \cdots + (f_m)^2} = {a_m}/{\sqrt{m}} \quad \text{Eq. 4.10}$$

a_m in MaF1 increases more rapidly than $\sqrt{m}$ with increasing m causing r_m increases rapidly, and HV reduces drastically.

In MaF2, HV breaks the trend of monotonicity, which value increases from 5 objectives to 7 and 10 objectives. Hypercube is governed by:

$$(f_1)^2 + (f_2)^2 + \cdots + (f_m)^2 = r^2 \quad \text{Eq. 4.11}$$

in which r is the radius of the hypercube, and in this case, $r < 1.0$. See Figure 4.8(b). The volume of the hypercube is proportional to r^m and HV is proportional to $1/r^m$, and thus increases with the increasing number of objectives.

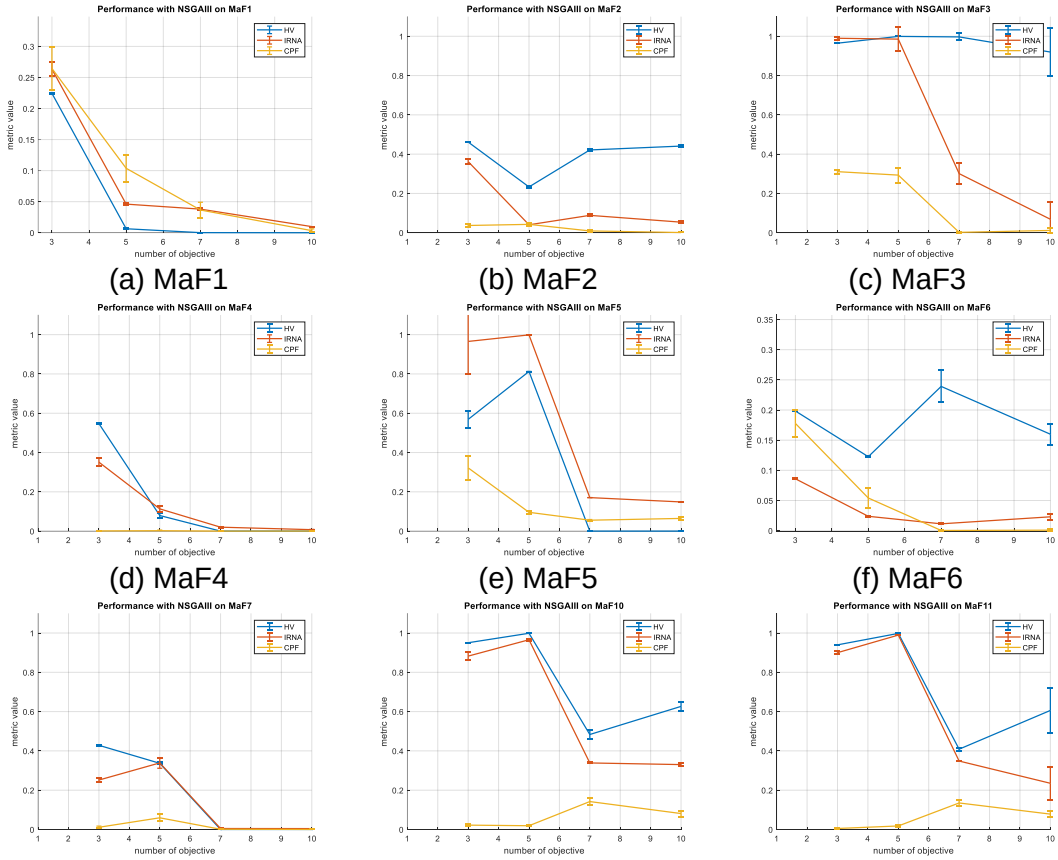

(a) MaF1 (b) MaF2 (c) MaF3

(d) MaF4 (e) MaF5 (f) MaF6

(g) MaF7 (h) MaF10 (i) MaF11

Figure 4.8 - HV, CPF and IRNA evaluate NSGA III analyses benchmark of MaF1-7 and 10-11 with mean value and standard deviation after 30 independent runs and solutions.

When MaF3 is concerned, see Figure 4.8(c), HV value keeps high for all cases of the number of objectives, which is caused by the fact that HV value favours boundary points and knee points on PF of convex shape, which gives high HV in all cases of the number of objectives. CPF has too low a value in 7 and 10 objectives, while IRNA changes monotonically with the number of objectives.

Monotonic change of HV and IRNA with the number of objectives are also observed in results of MaF4, see Figure 4.8(d). It is of partial convex hypercube or partial inverse hypercube. Still, CPF, in this case, has an extremely low level of the reason stated earlier that its projection om simplex plane is shrunk, which covers a falsely small portion of the plane.

In the case of MaF5, see Figure 4.8(e), IRNA has a full score in diversity in 3 and 5 objective cases. Its values decrease as the number of objectives increases because PF is under-represented by the available number of candidate solutions. The values of CPF and HV are too low as a score of such a classical PF.

Non-monotonic behaviour is observed in HV for MaF6, which has a degenerated PF shape, with an increasing number of objectives. See Figure 4.8(f).

PF of MaF7 is of partial type and consists of several flakes in the objective space. Only HV shows a monotonic change from 3 to 5 objectives, while all 3 indicators have near-zero values for 7 and 10 objectives cases. See Figure 4.8(g).

When MaF10 and MaF11 are concerned, only IRNA displays nearly monotonic behaviour. See Figure 4.8 (h) and (i).

Summarised, IRNA shows an overall satisfactory monotonicity feature in all benchmark functions tested. Both HV and CPF may behave either well in some cases or worse in others.

4.4.3 HV, CPF and IRNA in Analysing PF Approximations Over Time

Convergence and diversity of PF approximations are deficient in the early stages of an iteration (low number of iterations) and are gradually improved. Capturing and tracking the improvement accurately is crucial for understanding (and guiding via feedback) the performance of the selected optimisation algorithm. Consistent and sensitive performance indicators should be able to reveal the change.

Benchmarks of MaF 5, 6 and 7 are investigated using NSGA III, where approximations over various iterations are evaluated by the indicators HV, CPF

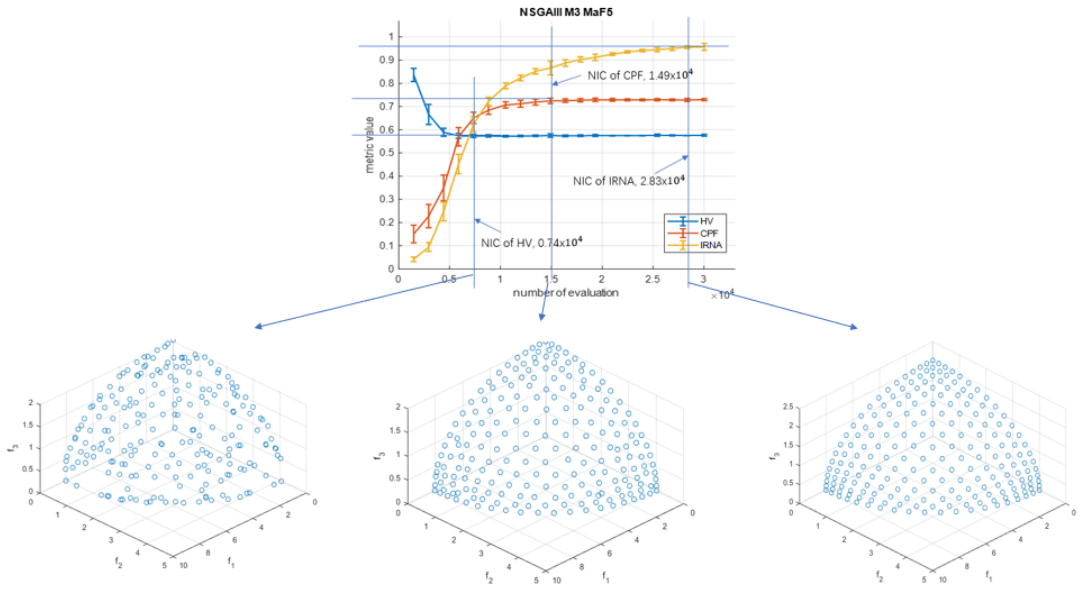

(a) NSGAIII M3 MaF5 converge 25% HV: 0.56478 CPF: 0.60497 IRNA: 0.56138

(b) NSGAIII M3 MaF5 converge 50% HV: 0.57224 CPF: 0.73351 IRNA: 0.88431

(c) NSGAIII M3 MaF5 converge 95% HV: 0.57509 CPF: 0.73410 IRNA: 0.96261

Figure 4.9 - Visually comparing the diversity of solutions at a different nominal number of iterations at convergence (NIC) of the comparing PIs. The result is based on 30 independent runs, and the mean and the standard deviation are shown.

and IRNA so that the performance of each PI is examined. A total of 30 independent runs have been carried out, and the mean value and standard deviation are calculated to take the stochastic effect on the approximations into account. PF of MaF5 consists of a hypercube, i.e., a PF covers the objective space fully. MaF6 comprises a PF of a pure arc, which is of degenerate type. MaF7 is made of several flakes in objective space and is a typical PF of the partial sort. These benchmarks are selected to represent three main PF categories, i.e., full coverage, degenerative, partial. The resulting numerical simulations demonstrate the indicators' consistency, sensitivity, and monotonicity differences.

Each PI gives its nominal number of iterations at convergence (NIC). When analysing approximation sets at various iteration stages using the same algorithm, the diversity indicator that results in the largest NIC (with the best

diversity displayed) is most sensitive to detect diversity changes of solutions. It is explained and demonstrated visually in Figure 4.9 via monitoring the convergence process of MaF5 with 3 objective functions. At the NIC of HV, the diversity is still poor. See Figure 4.9 (a). At NIC of CPF, the diversity is much improved but still can be perfected further. See Figure 4.9 (b). Only when the NIC of IRNA is reached, the diversity becomes superior. See Figure 4.9(c). It is valid for all three cases tested, i.e., MaF5, MaF6 and MaF7. But for keeping clarity of the text, only the result of MaF5 is shown here in the thesis.

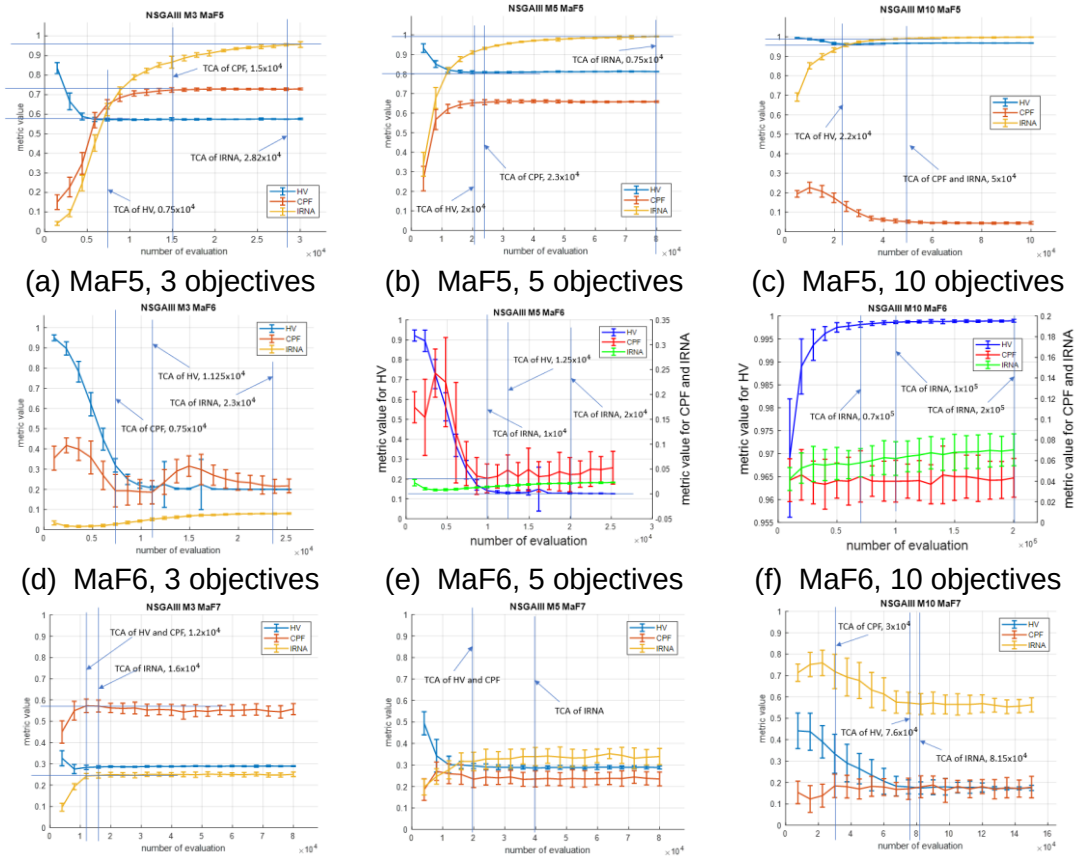

(a) MaF5, 3 objectives (b) MaF5, 5 objectives (c) MaF5, 10 objectives

(d) MaF6, 3 objectives (e) MaF6, 5 objectives (f) MaF6, 10 objectives

(d) MaF7, 3 objectives (e) MaF7, 5 objectives (f) MaF7, 10 objectives

Figure 4.10 - Iterations over time of Benchmark of MaF5-7 analysed by NSGA III after 30 independent runs with mean value and standard deviation and solutions are evaluated by HV, CPF and IRNA in mean value and standard deviation.

Figure 4.10(a) shows the results of approximations of MaF5 in three objectives analysed using NSGA III and evaluated by HV, CPF and IRNA. CPF and IRNA increase gradually and monotonically as the number of evaluations increases, while HV decreases gradually and monotonically to a stable level.

Besides, HV has the lowest NIC followed by CPF while IRNA obtains the highest NIC, which means that IRNA is most sensitive to capture the change of diversity, followed by the CPF indicator. The same trend is observed in approximations of MaF5 of 5 objectives. See Figure 4.10 (b), CPF and IRNA increase gradually and monotonically as the number of evaluations increases. The HV decreases gradually and monotonically to a stable level, and the IRNA value has the largest NIC value. Similar is the case in 10 objectives, except CPF value decreases with the increasing number of iterations and has the same NIC value as IRNA. See Figure 4.10 (c).

IRNA can also describe the diversity of the degenerated type of PF of MaF6. Figure 4.10 (d) depicts the approximation process over time of MaF6 with 3 objective functions. Once again, the IRNA value increases monotonically until a stable level is reached, indicating the end of the approximation process. IRNA has the largest NIC value among the three indicators, and it is also true for MaF6 in 5 and 10 objectives. See Figure 4.10 (e) and 10 (f). The high standard deviation of CPF and IRNA values in these cases should be noted, indicating strong variations in the results.

IRNA's better sensitivity is also demonstrated using approximations of PF of partial types, like MaF7. See Figure 4.10 (g) for 3 objectives, Figure 4.10(h) for 5 objectives and Figure 4.10 (i) for 10 objectives, respectively. In 3 and 5 objective cases, the amount of IRNA displays monotonic increasing behaviour and maintains the largest NIC value among the three indicators. But the situation is changed in the case of 10 objectives; IRNA still varies almost monotonically with the increasing number of iterations but decreasing toward a stable level. It is caused by the more extensive spread of non-converged solutions in the early stage of the approximation process with PF of partial coverage.

We conclude that IRNA exhibits a balanced sensitivity and monotonicity performance and yields arguably a more robust indicator than HV and CPF in all benchmark functions tested.

4.4.4 HV, CPF and IRNA in analysing PF approximations of dissimilar algorithms

This section presents IRNA results in two subsections: Benchmark problems of 3 and 5 objectives, respectively, and are compared against HV and CPF. The adopted algorithms for testing are acquired from PlatEMO [187]. NSGA III is a reference-point based generic algorithm for MaOP. GrEA adopts grids drawn in high dimensional objective space to strengthen the selection pressure towards optimal direction while maintaining an extensive and uniform distribution among solutions. IBEA may adopt several binary performance indicators to select offspring as parents for the next round of iteration. The number of candidate solutions is 210 for all cases.

The number of evaluations used is 2e+5 for 3 objectives cases and 5e+5 for 5 objectives. The parameters adopted in the three algorithms are based on default values acquired from PlatEMO version 2.7 [187]. Thirty algorithmic runs are carried out for each Benchmark problem, and average values and standard deviations of PIs are found. The Wilcoxon rank-sum test with a significance level of 0.05 is also used to analyse the results further and provide each PI's rankings.

4.4.4.1 *Test Results on MaF of three objective functions.*

Figure 4.11 shows 3D scatter plots on one typical approximation set from each algorithm for each benchmark problem. Table 4.5 contains scores of PIs on the approximation sets calculated on 11 commonly used Benchmark problems.

In general, HV reveals a similar ranking in diversity as IRNA does for MaF2, MaF3, MaF4, MaF6, MaF10, MaF11 and MaF13, but with much less proportionate values corresponding to the actual level of diversity. At the same time, CPF often fails in giving consistent values. Take MaF13 as an example. See Table 4.5. HV scores limited value changes when evaluating the approximations from the three different MaOP algorithms, while the variation of CPF is unbefitting.

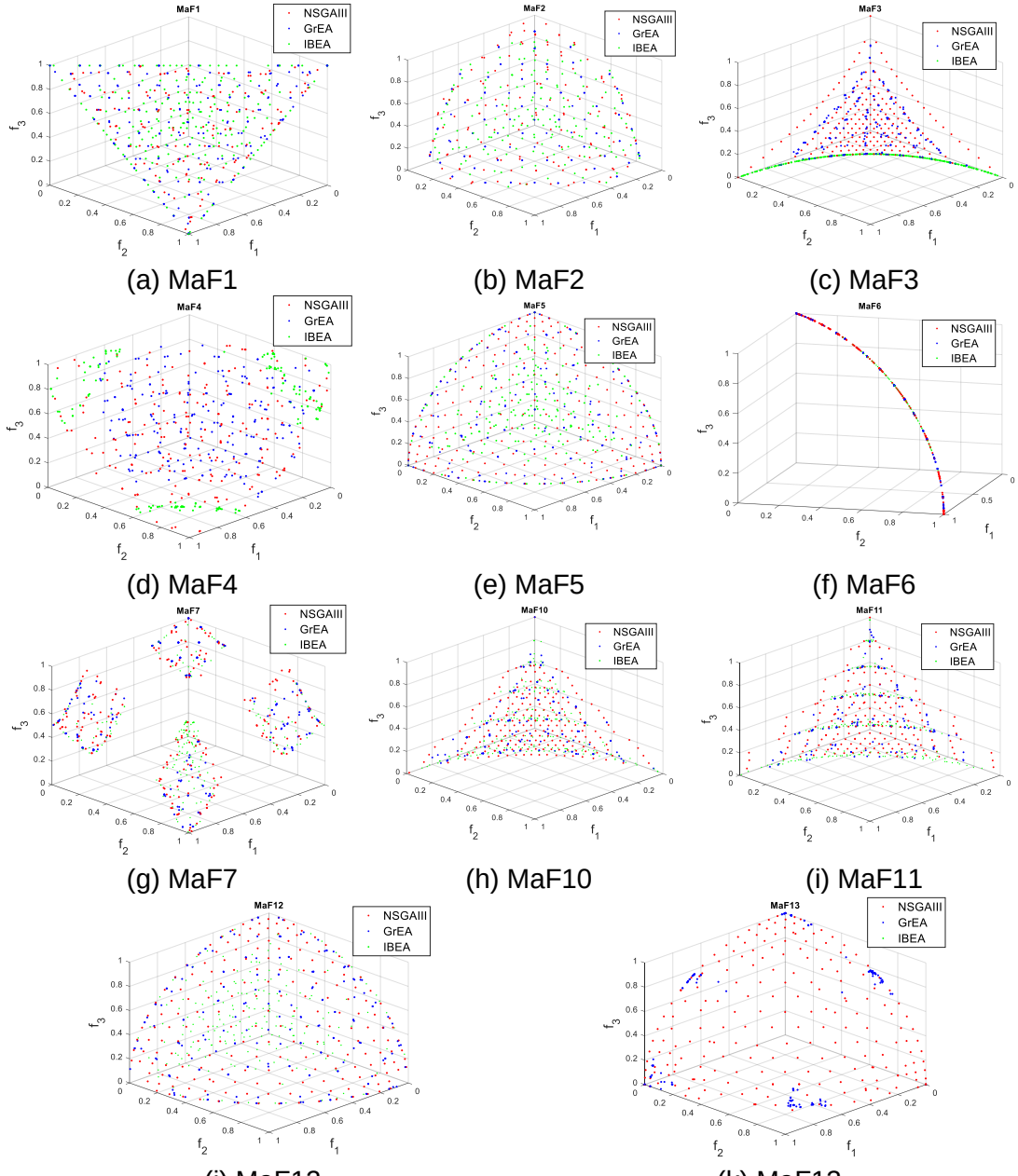

(a) MaF1 (b) MaF2 (c) MaF3

(d) MaF4 (e) MaF5 (f) MaF6

(g) MaF7 (h) MaF10 (i) MaF11

(j) MaF12 (k) MaF13

Figure 4.11 - PF approximation of chosen algorithms for a typical run out of thirty solutions.

Table 4.5 - Values of PIs for specific Benchmark problem, 3 objectives

		NSGAIII	GrEA	IBEA
MaF1	HV	2.245E-01 (7.313E-04) 3	2.277E-01 (6.160E-04) 2	2.314E-01 (3.074E-04) 1
	IRNA	2.633E-01 (1.097E-02) 1	2.155E-01 (5.598E-03) 3	2.260E-01 (3.633E-03) 2
	CPF	2.645E-01 (3.438E-02) 2	2.490E-01 (2.999E-02) 2	4.323E-01 (3.030E-02) 1
MaF2	HV	4.616E-01 (1.607E-03) 2	4.583E-01 (3.598E-04) 3	4.683E-01 (4.989E-04) 1
	IRNA	3.620E-01 (1.239E-02) 1	2.580E-01 (4.452E-03) 3	3.656E-01 (1.339E-02) 1
	CPF	3.692E-02 (7.909E-03) 1	2.879E-02 (5.218E-03) 2	2.228E-02 (9.290E-03) 3
MaF3	HV	9.648E-01 (1.825E-04) 1	9.405E-01 (2.151E-02) 2	8.589E-01 (2.189E-03) 3
	IRNA	9.899E-01 (6.777E-03) 1	2.630E-01 (4.455E-02) 2	8.907E-02 (3.453E-03) 3
	CPF	3.109E-01 (1.088E-02) 1	9.629E-02 (2.612E-02) 2	1.598E-02 (8.960E-03) 3
MaF4	HV	5.472E-01 (1.425E-03) 1	5.297E-01 (2.468E-02) 2	3.599E-01 (1.955E-02) 3
	IRNA	3.509E-01 (2.109E-02) 1	2.597E-01 (3.456E-02) 2	1.009E-01 (8.423E-03) 3
	CPF	1.032E-03 (2.044E-03) 2	5.586E-04 (1.497E-03) 2	2.948E-03 (3.751E-03) 1
MaF5	HV	5.686E-01 (4.198E-02) 2	5.664E-01 (4.825E-04) 3	5.745E-01 (4.004E-04) 1
	IRNA	9.655E-01 (1.645E-01) 1	3.856E-01 (8.078E-03) 2	3.618E-01 (1.074E-02) 3
	CPF	3.219E-01 (6.082E-02) 1	1.101E-01 (1.724E-02) 3	1.324E-01 (1.301E-02) 2
MaF6	HV	1.984E-01 (4.064E-04) 1	1.881E-01 (3.478E-04) 2	1.811E-01 (9.795E-03) 3
	IRNA	8.598E-02 (1.098E-03) 1	5.936E-02 (2.100E-03) 2	3.600E-02 (7.111E-03) 3
	CPF	1.777E-01 (2.269E-02) 2	1.755E-02 (1.013E-02) 3	4.203E-01 (8.516E-02) 1
MaF7	HV	4.284E-01 (9.477E-04) 2	4.198E-01 (3.559E-03) 3	4.326E-01 (8.292E-04) 1
	IRNA	2.516E-01 (9.479E-03) 1	1.623E-01 (8.422E-03) 3	2.186E-01 (6.841E-03) 2
	CPF	1.122E-02 (5.928E-03) 1	1.434E-03 (2.847E-03) 3	1.024E-02 (3.948E-03) 1
MaF10	HV	9.505E-01 (6.533E-04) 1	9.299E-01 (3.548E-03) 3	9.419E-01 (1.969E-03) 2
	IRNA	8.824E-01 (1.859E-02) 1	1.981E-01 (1.353E-02) 3	3.431E-01 (1.302E-02) 2
	CPF	2.211E-02 (4.627E-03) 1	1.836E-02 (5.207E-03) 2	1.393E-02 (5.042E-03) 3
MaF11	HV	9.397E-01 (2.742E-04) 1	9.338E-01 (2.351E-03) 3	9.375E-01 (5.659E-04) 2
	IRNA	8.999E-01 (6.471E-03) 1	2.704E-01 (1.365E-02) 2	2.702E-01 (7.139E-03) 2
	CPF	5.081E-03 (1.739E-03) 2	5.677E-03 (3.761E-03) 1	6.627E-03 (2.967E-03) 1
MaF12	HV	5.578E-01 (1.915E-03) 2	5.570E-01 (1.071E-03) 3	5.661E-01 (1.249E-03) 1
	IRNA	8.993E-01 (2.527E-02) 1	3.760E-01 (7.005E-03) 2	3.546E-01 (1.070E-02) 3
	CPF	4.175E-01 (1.471E-02) 1	1.540E-01 (1.865E-02) 3	1.759E-01 (2.595E-02) 2
MaF13	HV	5.620E-01 (4.105E-03) 1	4.797E-01 (2.739E-02) 2	2.531E-01 (1.063E-02) 3
	IRNA	8.047E-01 (4.961E-02) 1	2.081E-01 (3.834E-02) 2	1.541E-02 (2.402E-03) 3
	CPF	6.090E-01 (4.560E-02) 1	8.697E-02 (2.209E-02) 3	2.543E-01 (2.109E-01) 2

The solutions observed in Figure 4.11 (l) depict that GrEA only gives some local clustered solutions while IBEA does not converge, but their HV amounts are considerable. The CPF values are not consistent with the observations of diversity, and IRNA values are more proportionately and reflect the actual situation. The similar is with the results of MaF3, and significant differences in diversity can be observed. See Figure 4.11 (c). Solutions of NSGA III covers the whole PF. GrEA does not extend to all boundaries and shows a tendency of solutions in local clusters, while those of IBEA are only located at the f1-f2 boundary. While this observation is clear to capture visually, numerically, this is not reflected in HV and CPF (See Table 4.5).

Similar conclusions can be derived from other Benchmarks. For example, for Benchmarks MaF1, MaF5, MaF7 and MaF12, one would expect significant changes captured by a performance indicator (just by visually observing the plots of solutions). However, only IRNA captures such differences in performance reasonably well. In MaF5 in particular, where solutions of NSGA III exhibit (see Figure 4.11 (e)) the best diversity.

4.4.4.2 *Test Results of Five Objective Functions*

Table 4.6 summarises values of PIs on PF approximations of 5 objectives for the chosen Benchmark problems and their rankings. Like the 3 objectives,

Table 4.6 - Values of PIs for specific Benchmark problem, 5 objectives

		NSGAIII	GrEA	IBEA
MaF1	HV	6.408E-03 (5.232E-04) [3]	1.118E-02 (1.860E-04) [2]	1.154E-02 (1.624E-04) [1]
	IRNA	4.608E-02 (1.923E-03) [1]	4.359E-02 (1.328E-03) [2]	3.232E-02 (2.344E-03) [3]
	CPF	1.037E-01 (2.195E-02) [3]	2.601E-01 (2.639E-02) [2]	3.263E-01 (2.542E-02) [1]
MaF2	HV	2.332E-01 (4.950E-03) [3]	2.494E-01 (3.749E-03) [1]	2.438E-01 (3.100E-03) [2]
	IRNA	4.046E-02 (3.960E-03) [3]	4.472E-02 (5.293E-03) [2]	7.655E-02 (9.516E-03) [1]
	CPF	4.262E-02 (7.733E-03) [2]	4.070E-02 (5.396E-03) [2]	5.413E-02 (6.339E-03) [1]
MaF3	HV	9.993E-01 (2.003E-04) [1]	9.157E-01 (1.273E-01) [2]	8.133E-01 (1.927E-01) [3]
	IRNA	9.855E-01 (6.059E-02) [1]	1.248E-01 (6.488E-02) [2]	3.242E-02 (1.165E-02) [3]
	CPF	2.933E-01 (3.848E-02) [1]	3.650E-02 (2.006E-02) [2]	1.034E-03 (2.322E-03) [3]
MaF4	HV	7.943E-02 (1.054E-02) [2]	1.294E-01 (1.547E-03) [1]	7.160E-03 (1.134E-03) [3]
	IRNA	1.133E-01 (1.671E-02) [1]	9.442E-02 (4.086E-03) [2]	4.554E-02 (1.509E-03) [3]
	CPF	2.141E-03 (3.203E-03) [1]	9.524E-04 (1.937E-03) [1]	3.350E-04 (1.275E-03) [2]
MaF5	HV	8.125E-01 (4.466E-04) [1]	8.098E-01 (1.127E-03) [2]	8.100E-01 (9.878E-04) [2]
	IRNA	9.988E-01 (4.720E-04) [1]	4.396E-01 (1.927E-02) [2]	3.180E-01 (1.019E-02) [3]
	CPF	9.576E-02 (6.316E-03) [1]	8.863E-02 (1.630E-02) [2]	6.774E-02 (1.165E-02) [3]
MaF6	HV	1.226E-01 (1.185E-03) [1]	1.185E-01 (3.372E-04) [2]	1.145E-01 (3.773E-03) [3]
	IRNA	2.380E-02 (4.271E-04) [1]	1.198E-02 (2.157E-04) [3]	1.407E-02 (1.310E-03) [2]
	CPF	5.414E-02 (1.612E-02) [2]	1.670E-01 (1.750E-01) [2]	4.265E-01 (1.091E-01) [1]
MaF7	HV	3.369E-01 (4.895E-03) [3]	3.489E-01 (3.051E-03) [1]	3.527E-01 (1.399E-02) [1]
	IRNA	3.388E-01 (2.719E-02) [1]	1.767E-01 (7.233E-03) [2]	1.653E-01 (2.910E-02) [2]
	CPF	5.945E-02 (1.826E-02) [1]	8.017E-03 (7.009E-03) [3]	1.423E-02 (8.415E-03) [2]
MaF10	HV	9.987E-01 (3.773E-05) [1]	9.755E-01 (4.263E-03) [3]	9.876E-01 (1.790E-03) [2]
	IRNA	9.657E-01 (5.639E-03) [1]	1.092E-01 (9.690E-03) [3]	2.121E-01 (1.368E-02) [2]
	CPF	1.911E-02 (3.267E-03) [1]	8.161E-03 (4.771E-03) [2]	1.183E-02 (6.130E-03) [2]
MaF11	HV	9.980E-01 (1.143E-04) [1]	9.719E-01 (4.513E-03) [3]	9.832E-01 (2.685E-03) [2]
	IRNA	9.894E-01 (1.583E-03) [1]	1.617E-01 (1.435E-02) [3]	2.334E-01 (1.312E-02) [2]
	CPF	1.794E-02 (6.213E-03) [1]	7.392E-03 (3.925E-03) [2]	8.472E-03 (4.195E-03) [2]
MaF12	HV	7.770E-01 (2.907E-03) [1]	7.759E-01 (2.763E-03) [1]	7.774E-01 (6.144E-03) [1]
	IRNA	9.228E-01 (1.007E-02) [1]	4.249E-01 (1.145E-02) [2]	2.910E-01 (1.001E-02) [3]
	CPF	2.311E-01 (1.793E-02) [1]	2.183E-01 (2.079E-02) [2]	1.596E-01 (2.039E-02) [3]
MaF13	HV	2.264E-01 (2.213E-02) [1]	1.660E-01 (9.237E-02) [1]	3.649E-03 (4.046E-03) [3]
	IRNA	5.864E-02 (4.769E-03) [1]	3.719E-02 (9.489E-03) [2]	1.434E-02 (3.194E-04) [3]
	CPF	1.174E-01 (2.256E-02) [1]	4.786E-02 (2.335E-02) [3]	1.494E-01 (1.376E-01) [1]

Note - The upper index shows the ranking based on Wilcoxon Rank Sum Test, where 1 represents the highest ranking.

HV, CPF and IRNA yield similar scores in MaF2, MaF3, MaF4, MaF6, MaF10, MaF11 and MaF13, but IRNA is more proportionate relative to different diversity scores. For example, CPF yields, in general, incredibly low values of diversity, which may be caused by increased dimensions (objectives). Low PI values for MaF2 and MaF13 are observed, which indicate nonconvergent solutions of all three algorithms. HV and CPF provide a different ranking than IRNA in the Benchmark of MaF1, MaF5, MaF7 and MaF12. See Table 4.6.

One would expect significant changes captured by a performance indicator for benchmark cases of MaF1, MaF5, MaF7 and MaF12 (just by visually observing the solutions plots). However, only IRNA captures such changes in performance reasonably well. In MaF5 in particular, where solutions of NSGA III exhibit (see Figure 4.11(e)) the best diversity.

Based on the above analysis, we conclude that IRNA exhibits a balanced sensitivity and monotonicity performance and yields arguably a more robust indicator than HV and CPF in all benchmark functions tested.

4.5 Conclusion

A new pure diversity indicator, Inverted Ratio of Net Avertence angles (IRNA), has been introduced. The proposed performance indicator is tested for their efficacy on solutions of known diversity (synthetic data) constructed on the unit simplex plane and approximations of 3, 5, 7 and 10 objectives of Benchmark problems MaF1-7 and 10-13. MOEA algorithm NSGA III is used to reach approximations that the proposed indicator IRNA assessed against the commonly used HV and newly proposed CPF. The novelty of the proposed diversity score is obtained by rotating the reference vector system with an optimal spatial angle. This rotation removes any potential systemic bias in included angles in data of approximations so that impartial scores of a diversity of approximation sets are obtained. Numerical results and analysis show that IRNA yields an overall more balanced performance. IRNA is more sensitive and monotonically proportionate in capturing diversity changes than HV and CPF indicators in the synthetic data problem and in true PF data of MaF benchmark problems and cases when the number of objectives increases above three (for many-objective problems). Moreover, this robust performance is also observed in tracking the convergence process over various iterations, reflecting in maintaining sensitivity and monotonicity as the number of iterations increases before final convergence.

Two methods for assessing sensitivity and monotonicity of performance indicators are proposed; one is studying their variations when evaluating approximations of an increasing number of objectives while keeping the number of candidate solutions constant; the other examines their value changes at various iterations up to final convergence.

The proposed IRNA is assessed against popular performance indicators to provide the first insight. Towards further research, comparisons need to be

made against a broader range of state-of-the-art performance indicators, including additional coverage of types of benchmark problems in terms of dimensionality and complexity.

Chapter 5 Visualisation and Quality Evaluation of Pareto Front Approximations

Chapter Outline

Studying visualisation methods and developing more effective methodologies for MaOP analysis is one of the main objectives of this thesis.

Visualisation of Pareto Front (PF) approximations of MaOP is crucial in understanding and solving a MaOP. Research is ongoing on developing effective visualisation methods with desired properties, such as simultaneously revealing dominance relations, PF shape, objective range, distribution, etc. State-of-the-art visualisation methods in the literature only retain some of the desired properties. A new visualisation method is proposed in this chapter, which possesses the preferred properties of a visualisation method, i.e., display dominance relation, PF shape, objective range, PF distribution, robustness, handling large sets, handling multiple sets, scalability, simplicity and uniqueness. The method named ProD is based on displaying PF approximations via projections (Pro) on the reference vector versus distances (D) to the same reference vector; a vector would link a nominal Ideal point and a nominal Nadir point based on available nondominated PF approximation data. MaF benchmark problems are used to demonstrate the effectiveness of ProD. Results show that ProD exhibits a more balanced performance, compared to the state-of-the-art, in terms of capturing desired visualisation properties. In particular good performance is observed in portraying dominance relations, PF

shape and distribution of non-dominated solutions. Part of the work of this chapter has been published in:

K. E. Wu and G. Panoutsos, "A Visualisation Method for Pareto Front Approximations in Many-objective Optimisation," 2021 IEEE Congress on Evolutionary Computation (CEC), Krakow, Poland, 2021, pp. 1929-1937. (The paper attained The Best Student Paper, Runner up Award).

5.1 Introduction

Approximation sets and approximated Pareto Front (PF) landscape of many-objective optimisation problems (MaOP) consist of vectors in m dimensional objective space where m is the number of objective functions involved in the optimisation process. It is nontrivial to visualise these quantities mainly because the number of axes in such a visualisation exceeds three. A large amount of data is required to be displayed simultaneously on the other. However, visualisation of the approximations is crucial in optimisation research [2]. An effective way of graphically showing the approximations may assist the decision-making process and support interactively searching for optimised solutions. It can also be used to examine and improve the performance of optimisation algorithms as visual comparisons may reveal the dominance relationships to different approximations and display the process of convergence towards PF and diversity of MaOP solutions. Graphical display of approximated PF landscape is also helpful in finding characteristics and challenges of the optimisation problem, such as distance of approximations to the constraint boundaries, local minima embedded in the optimisation problem etc. [2], [138].

Visualisation of high dimensional data sets is usually a process of compressing and mapping data into a two- or three-dimensional space that can be displayed readily with traditional means of figures or charts. Properties of points are easier to analyse and understand. However, although such a mapping aims to maintain the high dimensional properties of the data sets as much as possible, some information is inevitably lost during the mapping process. Therefore, the resulting visualisation process compresses knowledge and extracts fundamental properties from the high-dimensional data set while omitting less essential features [2].

5.1 Introduction

Effective visualisation methods should have the following desired properties, as outlined in [138]:

1) Dominance relation: shall preserve dominance relation between solutions by visualisation,
2) PF shape: should display the PF shape, i.e., its convexity and concavity.
3) Objective range: should reveal the ranges of objectives
4) PF distribution: should exhibit the distribution of solutions
5) Robustness: is a property addressing from the perspective of visualisation only in terms of consistently projecting multiple dimensional solutions in 2D and 3D, i.e., no ambiguity exists. For instance, a method such as RadViz, see Section 5.2 for details, may suffer a robustness challenge since multiple unspecified solutions could be located in the same position after data compression into 2D under visualisation.
6) Handling large sets: it may present large approximation sets
7) Handling multiple sets: it may simultaneously visualise multiple approximation sets
8) Scalability: it should be scalable to any number of objectives
9) Simplicity: it should be simple to construct.

This author proposes an additional desired property:

10) Uniqueness: the visualised image should be unique independent of the sequence of objective functions utilised in the display. For instance, the image of Parallel coordinates changes with the alterations of the objective function sequence.

While effective in their respective targeted desired properties, current visualisation methods possess only some of the above-desired capabilities [138]–[141]. Parallel coordinates, for instance, may identify different types of "patterns", but it has challenges in visualising large and multiple sets of Pareto

fronts. He and Yen [200] sort existing visualisation methodologies into five major groups. Out of each group, one representative method is chosen and tested for representing three commonly accepted PF patterns for visualisation approaches, i.e., simplex plane, sphere, and knee shape. Numerical results reveal that none of the five methods adequately display the basic patterns [200]. Specifically, the major weakness of the current state of the art methods is that they only retain some of the above-mentioned desired properties. Parallel Coordinates [201], for example, fulfils the demands for displaying Dominance Relation, Robustness, Scalability and Simplicity, but is not addressing the rest of the properties. Hence, research is needed to expand the capability of methods that simultaneously possess as many preferred properties as possible.

This chapter proposes a new visualisation method, which exhibits the most desired properties for visualising MaOP approximations. The main unique contribution of this work is the following:

A new visualisation method for high dimensional MaOP approximations is proposed by displaying PF approximations via projections (Pro) on the reference vector versus distances (D) to the same reference vector, ProD. The reference vector is a vector that would link nominal Ideal point and nominal Nadir point calculated based on the available data of PF approximations.

The B-Norm based Pareto Front Tracing method (Bn-PFt) covered in Chapter 3 is utilised to create more evenly spaced reference points in the vicinity of PF and its approximations. It is used to create evenly distributed high dimensional solutions visualised in a two-dimensional space.

The rest of the work is organised as follows. Section 5.2 describes a literature survey on up-to-date visualisation methods in MaOP analysis. Section 5.3 covers the formulation and reasoning of ProD. Section 5.4 includes testing

and simulation results showing the efficacy of ProD. Finally, conclusions are drawn, and future research directions are discussed in section 5.5.

5.2 Existing Visualisation Methods

It is nontrivial to develop a visualisation method for MaOP, which simultaneously satisfies all the requirements listed in Section 5.1. Various visualisation methods in displaying domination relations of approximations of MaOPs exist with varying success and focus on what the methods aim to reveal. A comprehensive review of the topic can be found in [141], [201].

Filipič and Tušar [138] suggest a taxonomy of visualisation methodologies consisting of two major categories: to display simple PF approximation sets and to show repeated approximation sets.

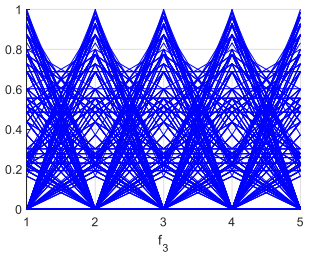

(a) Parallel coordinate

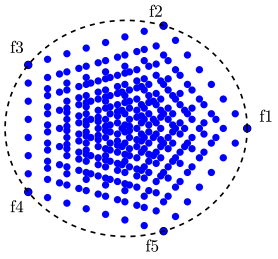

(b) RadViz.

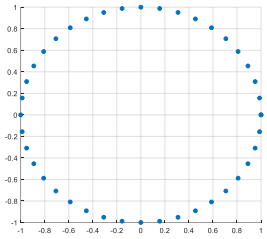

(c) Polar coordinates

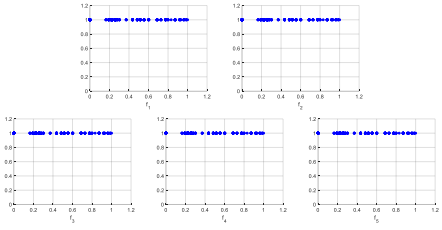

(d) Level diagram

Figure 5.1 - Different visualisation methods used to visualise the actual Pareto front of 5-D DTLZ2. (a) Parallel coordinates. (b) RadViz. (c) Polar coordinates (f) level diagram.

Figure 5.1 shows the results of PF of a unit hypersphere using different visualisation methods. Scatter plot [138] is a straightforward visualisation method frequently adopted. All vectors of approximations of non-dominated data points are projected to a 2D plot by omitting higher dimensions of the vectors other than the two displayed. Similar plots are generated for all combinations of two objective functions, and as a result, a scatter plot matrix is formed. Although the method is simple, robust, and able to reveal the objective

range and handle multiple sets, it is not scalable to high dimensional MaOPs [138]. Neither can it depict dominance relations of approximation sets. PF shape and its distribution are only shown to a limited degree [138].

Parallel coordinates [201]: see Figure 5.1(a). This method maps high dimensional vectors onto a 2D figure using m equally spaced parallel axes. The vectors are drawn as polylines through position on each axis corresponding to each vector component. Parallel coordinates are simple to construct and scalable to any dimensions of MaOP, and no information is lost in the mapping process. The main weaknesses are three-fold: the method fails to display the shape of the PF approximation and possesses limited capability in handling a large amount of approximation data and simultaneous visualisation of several approximations [138]. Radar Chart [202] can be considered a further developed version of parallel coordinates with similar strengths and weaknesses, in which axes are placed radially instead of in parallel.

Radial Coordinate Visualisation (RadViz) [203]: see Figure 5.1(b). The m-dimensional vectors of approximations are mapped onto a two-dimensional plane by uniformly placing the origin of each *m*-dimensional vector along a circle with various anchor points. Each approximation set is expressed by assuming that each anchor i is connected to a spring of force proportional to the objective function f_i. An m-dimensional vector is identified inside the circle. The positions of the vectors are found and displayed on the two-dimensional plot. The method is robust and straightforward, may handle several approximations simultaneously, and can be readily extended to any dimension. However, RadViz fails to reveal the PF front pattern and the dominance relations between solution sets [138]. Multiple disparate vectors may share the same equilibrium position in the plot creating chaotic and unforeseeable patterns or data distribution.

In contrast, the two vectors are neither neighbours nor belonging to any natural groups of vectors. RadViz has been further developed into a 3D version called 3DRadViz [204]. The above-stated shortcoming is also inherited in the 3D version of the method.

PaletteViz: [139] High-dimensional and non-dominated objective vectors are mapped onto multiple two-dimensional Radviz plots. The vectors are sorted after their boundary to the core location in their original high-dimensional space. As is the case for RadViz, the main weakness is that multiple disparate vectors may share the same equilibrium position, causing difficulties in interpreting data distribution.

2D Polar coordinates [122]: see Figure 5.1(c). The objective space is divided into subregions using reference vectors, evenly mapped to a 2D plane following the sequence of generated reference vectors. The best approximation from each subregion is chosen and plotted on the reference vector in a 2D map. The method can reveal the basic patterns of PF of linear and hypercubes while it displays more complex PF shapes with much-reduced success. Moreover, neighbour points on PF are disparately located in the display. In addition, the outcome is nonunique and changes with the sequence of objective functions used. In other words, it violates the desired visualisation property no. 10. See Section 5.1.

Level diagrams [205]: see Figure 5.1(d). Euclidean distance of approximations to the ideal point is displayed as functional values of each objective. The main drawback here is that the method has to utilise an equal number of separate plots like the number of objective functions. The number of plots for visualising MaOP approximations can be overwhelming.

Pryke et al. [206] use a Heatmap visualisation where a tabulation of colour chart is formed. Objectives are taken in columns, and high dimensional vectors

are taken as rows. Although the method is robust and scalable, it fails in showing PF shape, objective range, and distribution. Large or multiple data sets can hardly be displayed, as discussed in [138].

Yamamoto et al. [207] suggest Principal Component Analysis to reduce the number of objectives necessary to be visualised. The challenge is that the number of objectives after reduction may still exceed three, making visualisation difficult.

Other visualisation methods are also available. Freitas et al. [208] propose a method of Aggregation Trees where positively correlated objective functions are merged, and the total number of objective functions is thus reduced. Chiu and Bloebaum [209] introduce the Hyper-radial visualisation (HRV) method in which mapping from high dimensions to 2D is done by expressing 2D vectors in terms of Hyper-radial distance of the original vector to the ideal point. Koochaksaraei et al. [210] suggest a Chord diagram, where objective functions with their respective equal arc length on which scales are indicated and arcs are placed along the peripheral of a circle. Agrawal et al. [211] suggest a Hyperspace Diagonal Counting method to compress and group high dimensional vectors into 3D space mapping. S. Obayashi and D. Sasaki [212] utilise Self-Organised Maps to visualise solutions with many objectives, using trained neural networks to find nearby solutions adopting a unified distance matrix. Yoshimi et al. [213] have further developed the methodology to present the result in a spherical form, improving the display of boundary points. Hence, the above methods target specific desired properties only, therefore not covering all the desired properties described in Section 5.1.

5.3 Proposed Visualisation Method – ProD

In this section, a new visualisation method, ProD, is proposed to identify the pattern of PF and reveal dominance relations among PF approximation sets which can also be utilised to monitor the convergence process and evaluate diversity on approximations from a MaOP algorithm. Its main structure is explained in Section 5.3.1, and its principal characteristics are summarised in Section 5.3.2.

5.3.1 Establishment of ProD

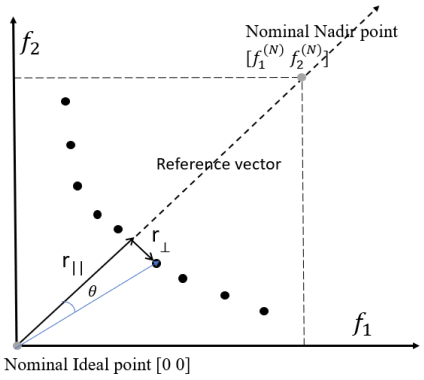

Figure 5.2 - A schematic view: Projection on ($r_{\|}$) and Distance to ($r_{\perp}$) reference vector of a data point in 2D space.

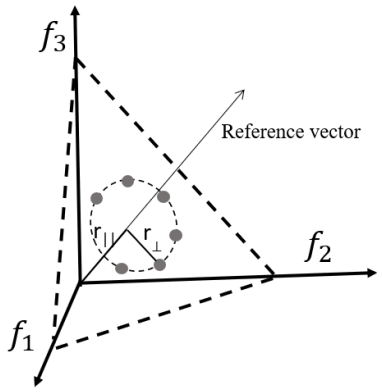

Figure 5.3 - A schematic view: Compression of data in ProD in 3D space.

ProD is proposed to visualise high dimensional vectors of PF approximations of a MaOP in objective function space. It is done with their projections on and distances to a reference vector in the objective space. The reference vector is created by linking nominal Ideal point and Nadir point calculated based on the existing nondominated data set(s) of PF approximations. Figure 5.2 shows a schematic view in 2D space on how projections on and distance to the reference vector of a PF approximation vector are defined.

The projection $r_{\|}$ is given as:

$$r_{\parallel} = [f_1\ f_2\ \ldots\ f_m] * \frac{\boldsymbol{RV}}{|\boldsymbol{RV}|} \quad \text{Eq. 5.1}$$

in which m is the number of objective functions, and $\mathbf{RV}$ is the reference vector that is defined as:

$$\boldsymbol{RV} = \boldsymbol{F}_N - \boldsymbol{F}_I \quad \text{Eq. 5.2}$$

in which $\mathbf{F}_{\mathrm{N}}$ is the vector of Nadir point and $\mathbf{F}_I$ is the vector of the Ideal point. The distance to the reference vector is expressed as:

$$r_{\perp} = sin\ (\theta) * \sqrt{f_1^2 + f_2^2 + \cdots + f_m^2} \quad \text{Eq. 5.3}$$

where angle θ between the vector of candidate solution and reference vector is calculated by

$$\theta = cos^{-1}\left(\frac{[f_1\ f_2\ \ldots\ f_m] * \boldsymbol{RV}}{\sqrt{f_1^2 + f_2^2 + \cdots + f_m^2} * |\boldsymbol{RV}|}\right) \quad \text{Eq. 5.4}$$

The principle of data compression in ProD in 3D space is illustrated in Figure 5.3, in which all data located on the ring (with equal $r_{\parallel}$ and $r_{\perp}$) are compressed to a single data point in ProD. The results are displayed in a two-dimensional plot named ProD (Projection versus Distance to reference vector).

The nominal Ideal point is an auxiliary point with the least values of each objective function as coordinates. In contrast, the nominal Nadir point, on the contrary, consists of coordinates of the largest of each objective. Both points are defined based on current available PF approximation data, so the term "nominal" is used. It is assumed that the origin is moved to the nominal Ideal Point.

ProD may be utilised to display decision variables and their relationships in decision space in a similar manner by defining a reference vector linking the ideal minimum point (the point with components taken from each of the minimal coordinates of all decision variables) and theoretical maximum point (the point

with components equal to each of the maximal coordinates of all decision variables). $r_{\parallel}$ and r $\perp$ are determined using Eqs. 5.1-5.4.

ProD has the capacity for showing points and regions of interest (ROI) for a decision-maker when the Pareto approximations in the ROIs in the objective space are sorted using the surrounding reference points or vectors of the ROIs. The PF of the ROIs can then be visualised in ProD. The corresponding Pareto optimal set in the decision space can also be found, collected, and drawn in ProD using equations like Eqs. 5.1-5.4**.** The reference vectors can be found utilizing the nominal ideal and Nadir points based on the data sets.

As mentioned in the Introduction section, visualisation in high dimensional space is a process of compression of information and extraction on specific fundamental properties out of data set while omitting certain less critical details. The core idea of ProD is to compress all data of the same $r_{\parallel}$ and $r_{\perp}$ values into a single data point. The compressed data point represents all raw data points in the original solution set, which form a ring on the PF surface because all points share the same $r_{\parallel}$ and $r_{\perp}$ values in the 3D case, and it is illustrated in Figure 5.3. In high dimensions, the data points are located on a hyper ring.

5.3.2 Characteristics of ProD

5.3.2.1 *Taxonomy of ProD*

Compared with definitions from the taxonomy of visualisation methodologies [138], ProD is classified into the visualisation method of repeated approximation sets. It is a visualisation method for PF pattern recognition, convergence, and diversity monitoring at a given time and over time under iteration.

5.3.2.2 *Principle of Data Compression in ProD*

It should be noted that the idea of expressing candidate solutions in the form of projections and distances to a reference vector in objective space is

frequently used in the formulation of MaOP algorithms, such as MOEA/D [6]. However, this has never been used for compressing high dimensional data for visualisation purposes.

5.3.2.3 *Convergence and Diversity Evaluation in Light of $r_{\parallel}$ and $r_{\perp}$ Values*

It is well accepted that a point with the best convergence is the one that has the shortest distance to the Ideal point, while a solution set with the best diversity is the one that has candidate solutions of equal distance apart [2]. See Figure 5.4. Point A is a point on PF with the closest distance among all points on line A to B to the Ideal point. Similarly, point A has the shortest distance to the Ideal point among the points from A to C. Point A is thus a measure of the convergence with the smallest distance to Ideal Plane, a term proposed by this author, which is expressed as $r_{\parallel}$. The diversity may be expressed as candidate solutions of equal distance to the reference vector, which is related to $r_{\perp}$, i.e. good diversity can be approximated by points with equal distance in $r_{\perp}$. The above means that $r_{\parallel}$ and $r_{\perp}$ values of candidate solutions can reflect the convergence and diversity of an approximation set and thus the dominance relations between individual approximations.

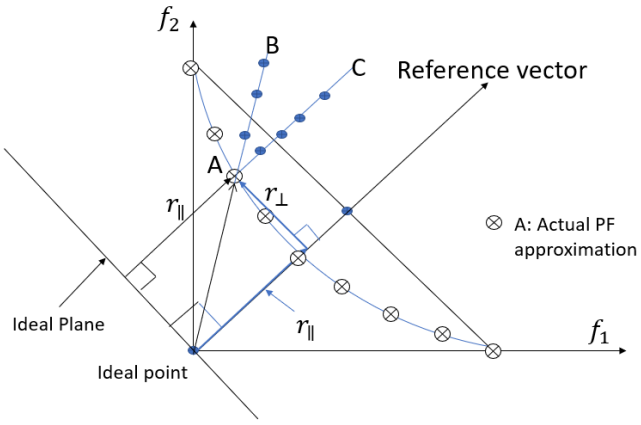

Figure 5.4 - Convergence and diversity evaluation in light of $r_{\parallel}$ and $r_{\perp}$ values

5.3.2.4 *Normalisation Versus Non-Normalisation in ProD*

Objective functions are commonly normalised under the execution of MaOP algorithms employing the coordinate values of nominal Nadir and nominal Ideal points to avoid impacts from poorly scaled optimisation problems on the solution process. Normalisation on objective functions has also been performed when making ProD plots so that the scale of each objective's same order is guaranteed. But normalisation can also change the final PF shape patterns, and it sometimes creates more complicated ProD images. See more detailed discussions in Section 5.4. In practice, ProD should be prepared based on both normalised and unnormalised data, and the one with the most straightforward PF shape or most minor "clouds" in ProD should be chosen.

5.3.2.5 *Data Compression and Organization in ProD*

Since discrete data points represent PF, the whole PF in the objective space can be considered as consisting of a finite number of regions of candidate solutions of different distances $r_{\perp}$ to Reference Vector. See schematic view displayed in Figure 5.5, where different grouped regions are displayed in distinctive colours. And approximations in each region form a subgroup. Each subgroup can be analysed by quality metrics, which measure convergence and diversity based on data in that region. Data points from all regions form pseudo-PF, which can be utilised in contrasts and comparisons between two competing approximations. The optimal number of regions would be linked to the resolution of PF approximations, which is proportional to the number of divisions along with each objective function, p. Therefore, it is suggested that the number of regions is set to be equal to number p. The maximal extent of $r_{\perp,max}$ is obtained through sorting all $r_{\perp}$ values. This will be studied further as future work.

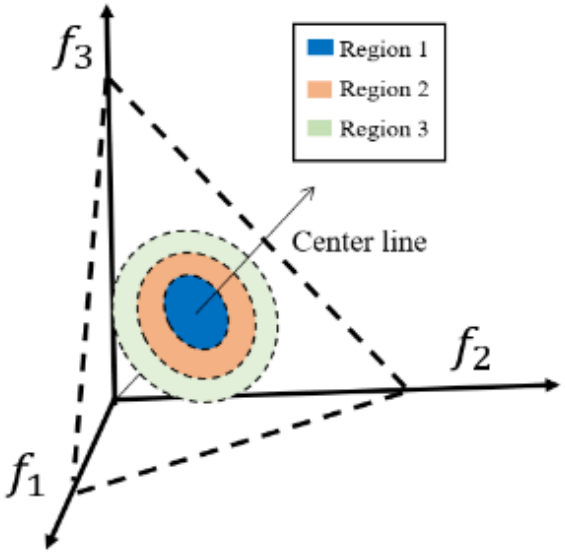

Figure 5.5 - Regions of PF and its approximation.

5.3.2.6 *ProD Provides a Necessary but Insufficient Condition in Diversity Evaluation*

In ProD, a necessary condition for an approximation set with the best convergence and diversity must simultaneously possess properties of that it has the lowest $r_{\parallel}$ values (the best convergence) while it has $r_{\perp}$ values starting from zero and spread out to the most extensive possible range (the best diversity). But this is, unfortunately, an insufficient condition for good diversity. Although $r_{\perp}$ values cover the complete range, each of them may have different coverage of candidate solutions, see Figure 5.4, and ProD cannot differentiate the number of data, nor can it determine the diversity of data in each and same region. Multiple solutions may occur for given $r_{\parallel}$ or $r_{\perp}$ values in ProD, resulting in "cloud" like shapes on PF images are formed. These occur when PFs are asymmetric about the reference vector and data with the same $r_{\perp}$ may have different projections on the reference vector resulting in several data points lying vertically at the same $r_{\perp}$. The folded shape of PF in ProD makes it challenging to determine dominance relations of two approximation sets having approximately equal performances. In addition, as is discussed further in Section 5.4, most real-life MaOP has PFs with highly irregular patterns. It forms

"clouds" in PROD, which cause a 'folded' PF front that again creates uncertainty when used to assess dominance relations between approximations.

Performance metrics can evaluate the diversity of candidate solutions in each region that provide regional diversity information. The distribution of diversity of PF may also be revealed in this way, a topic that is studied further.

5.3.2.7 *ProD Reveals an Objective Range*

Range of an individual objective function f_i can be displayed via marked $r_{\parallel}(f_{i,max})$ and $r_{\perp}(f_{i,max})$ indicating $f_{i,max}$ value in ProD if it is needed. The objective range is proportional to $r_{\parallel}$ and $r_{\perp}$values through relation: $\sqrt{r_{\parallel}^2 + r_{\perp}^2}$.

5.3.2.8 *The Major Benefits of ProD*

The primary benefit of the new visualisation approach is that it possesses in a balanced manner all the desired properties of a visualisation method highlighted in Chapter 5.1. These are, among other properties, visualisation of PF shape and distribution, dominance relations among multiple approximation sets. The results section shows these properties qualitatively and quantitatively

5.4 Numerical testing

This section is organised as follows. The first subsection provides information about selected algorithms adopted in the testing and the related parameters and MaF Benchmarks (Subsection 5.4.1). Then it follows with the presentation of results of testing on properties and performance of ProD as a visualisation tool in revealing PF shape and its distributions (Subsection 5.4.2). Further, in the subsection that follows, the ability of ProD in displaying Dominance Relations among multiple approximation sets is demonstrated (Subsection 5.4.3). In the last subsection, properties of ProD in the content of satisfying other requirements as a visualisation tool are highlighted and discussed (Subsection 5.4.4).

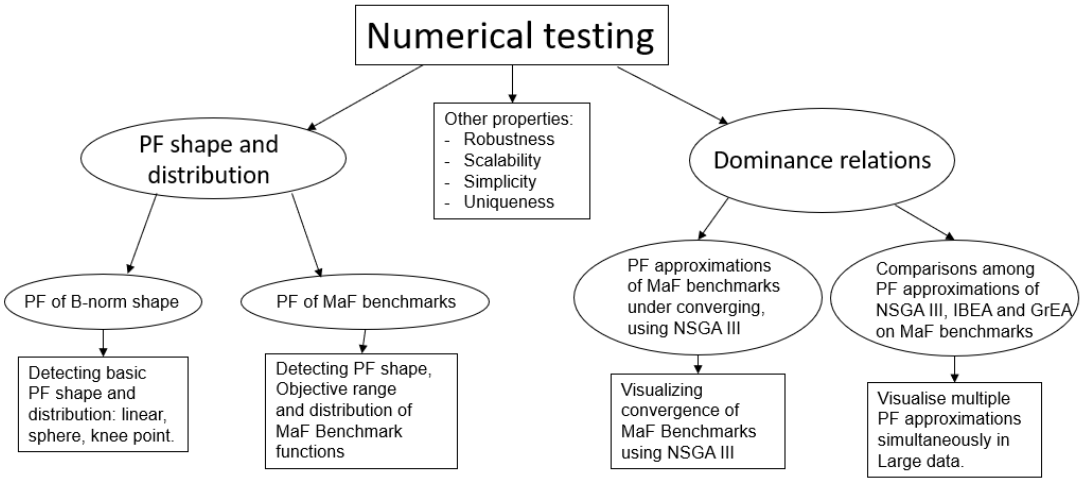

Figure 5.6 - Numerical testing main structure

Three commonly used MaOP algorithms, NSGA III [2], GrEA [79] and IBEA [61], are adopted in this testing section. MaF benchmarks are analysed under various given amounts of iterations. Solutions are displayed in ProD for comparisons. 3D scatter plots are also drawn to assist in the understanding of the basic PF pattern in the actual benchmark problem.

5.4.1 Optimisation Algorithms and Benchmark Problems

The adopted algorithms are acquired from PlatEMO [187]. NSGA III is a reference-point and nondominated sorting based genetic algorithm for MaOP. GrEA adopts grids drawn in high dimensional objective space to strengthen the selection pressure towards optimality while maintaining an extensive and uniform distribution among solutions. IBEA may adopt several binary performance indicators to select offspring as parents for the next round of iteration.

Table 5.1 - Number of solutions generated

Number of objectives	Number of solutions for algorithms	Number of solutions used to generate actual Pareto Front
3	210	496
5	210	10626
10	220	92376

Eleven scalable MaF Benchmarks used for CEC'2017 Competition on Evolutionary many-objective optimisation [112] are selected to demonstrate the properties of PROD and evaluate the performance of the algorithms. Tested Benchmarks are MaF 1-7 and MaF 10-13 [187]. MaF 8 and 9, 14 and 15 are not taken in this study. MaF 8 and 9 are specially designed to display their PF readily. In contrast, MaF 14 and 15 are designed to study large-scale problems that are difficult to handle by the chosen MaOPs, and the PF shape of MaF 14 is similar to MaF 1, and MaF 15 is identical to MaF 4.

All the results shown in this section are obtained using MATLAB 2017b. The numbers of candidate solutions used are listed in Table 5.1. The parameters adopted in the three algorithms are based on default values acquired from PlatEMO version 2.7 [187].

5.4.2 ProD Revealing PF Shape and its Distributions

In this subsection, properties and performance of ProD as a visualisation tool in uncovering PF shape and its distributions in high dimensional objective

space are presented. Here, the functioning of ProD is shown in two parts. First, ProD is used to visualise and recognise PF shapes of B-norm type in 3, 5 and 10 dimensions corresponding to the plane, sphere and imitated knee point shapes, which is a fundamental capability of a visualisation method. Second, the accurate PF surfaces of MaF Benchmarks are presented in ProD, showing the visualisation method can convert authentic Benchmark PFs in high dimensional objective spaces to simple shapes in two-dimensional space, where basic shapes of PFs are preserved and visualised.

5.4.2.1 *Visualising PF Shapes and Their Distribution of B-norm Type*

A prerequisite to the capability of a visualisation method is that it can display PF of 3 basic surfaces of any dimensions, i.e., plane, sphere and knee [138], [139], which in current work are expressed as B-norm surfaces with different B parameter values. B-norm functions usually are named F-norm functions in mathematics. The functions are termed as B-norm functions in this thesis to avoid confusion with the objective function vector F in the objective space. B-norm type of surfaces is a family of symmetric surfaces in high dimensional space. The B-norm surface of unity with a small B value (0.3 or 0.5) is used to imitate a PF shape of knee point. In general, B-norm surfaces are governed by Eq. 5.5, where B is the parameter determining the curvature.

$$(f_1^B + f_2^B + \cdots + f_m^B)^{1/B} = 1 \qquad \text{Eq. 5.5}$$

In Chapter 3, Bn-PFt applied to generate more equally spaced reference points on B-norm surfaces in high dimensions is introduced. See Figure 5.7(a), (b), (c), (g), (h), and (i).

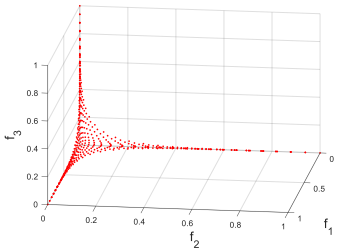

a) 3D Scatter plot, B = 0.3

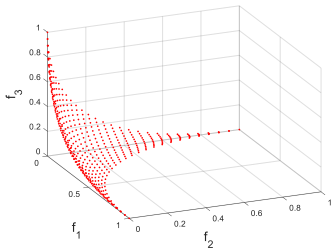

b) 3D Scatter plot, B = 0.5

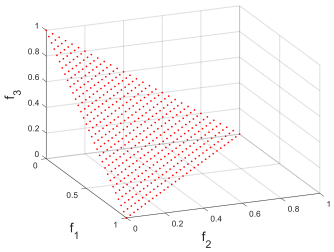

c) 3D Scatter plot, B = 1.0

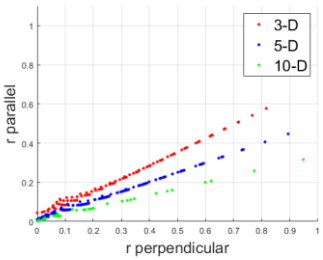

d) ProD plot, B = 0.3

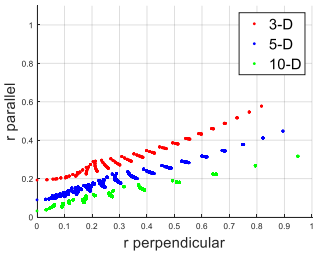

e) ProD plot, B = 0.5

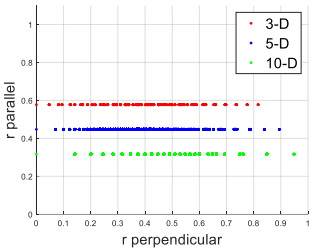

f) ProD plot, B = 1.0

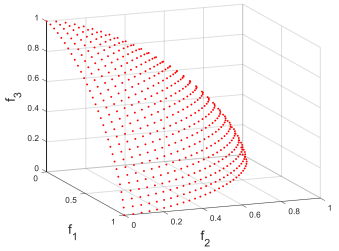

g) 3D Scatter plot, B = 1.5

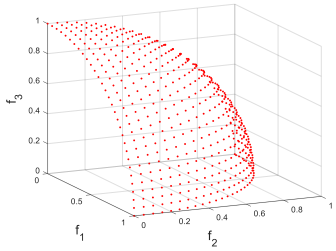

h) 3D Scatter plot, B = 2.0

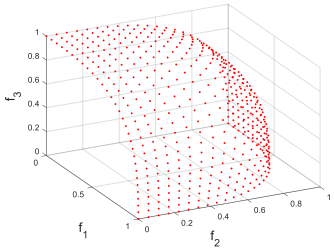

i) 3D Scatter lot, B = 3.0

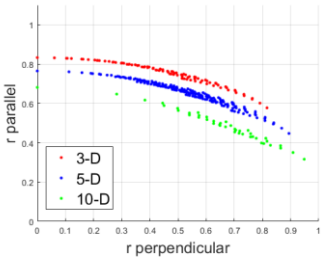

j) ProD plot, B = 1.5

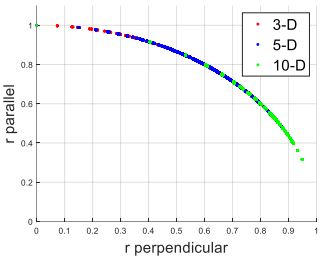

k) ProD plot, B = 2.0

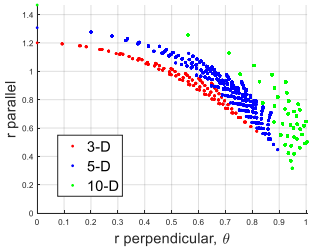

m) ProD plot, B = 3.0

Figure 5.7 - ProD plots of B-norm surfaces with B values of 0.3, 0.5, 1.0, 1.5, 2.0, and 3.0 in 3D, 5D and 10D. The three basic surfaces: 1) linear (B = 1.0), and 2) sphere (B = 2.0) and 3) knee point surface represented by B = 0.3.

Figure 5.7(d), (e), (f), (j), (k), and (m) display visually these basic types of PF surfaces of various B parameter values in 3D, 5D and 10D problems, which demonstrate the capability and consistency of ProD in presenting three basic shapes: linear, sphere and knee point. Parameters used to generate Figure 5.7 are listed in Table 5.1.

In ProD, unit simplex planes in objective space in any dimensional problems appear as distinct horizontal line segments with distances to $r_{\perp}$ axis decreasing as the number of objective functions increases. See Figure 5.7(c), (g).

Hyper spheres appear in ProD as distinct circular arc segments falling together in all dimensions and bending downwards. See Figure 5.7 (h), (k).

PF of knee point shape is imitated by B-norm surface with $B < 1.0$. See Figure 5.7(a) and (b). Their images in ProD with some folded patterns bend upward, indicating the shapes are in convex form. See Figure 5.7(d) and (e).

Results of PFs in 10D show a limited number of data points for low $r_{\perp}$ values, due to the limited number of available reference points adopted in these areas (intermediate area) [2]. Moreover, many of the data have the same $r_{\parallel}$ or $r_{\perp}$ values and thus fall onto a single data point in ProD.

A comparable visualisation method to ProD is the 2D Polar coordinates method which displays PF shape of convex type as a rhombus with bent edges inward and concave type as ellipses [200]. Since real-life PF may have several primary forms, e.g., PF of MaF7, Polar coordinates may visually create an unclear and indistinct pattern.

ProD shows that the curve starts with some folded area near the origin at a low B value for surfaces of other B values. The "clouded" area gradually moves up along the curve as the B value increases until it disappears at B value reaching 1.0, at which a distinct horizontal line segment forms. Then, it bends downward with a further increase of B as thicker or indistinct line segments until B at 2.0, when all lines of any dimensional problem fall together and form circular arc segments. See Figure 5.7. With a further increase in B value, the curves depart with the phenomenon that the higher dimension, the more volume is encircled by the curves. The curves also bend more strongly downward as the B value increases further.

The above implies that ProD is efficient in indicating basic PF shape of convexity, plane and concavity, and their degree of crook.

5.4.2.2 *Visualising PF Shape and Distribution of MaF Benchmark Functions*

Accurate PF surfaces of MaF Benchmarks are presented in ProD, showing that the visualisation method can identify the shapes and distribution of true PF of Benchmark functions in high dimensional objective spaces. Only results of the most representative benchmarks are displayed here for enhanced readability. See Table 5.2.

Table 5.2 - Results of benchmarks presented in this chapter

Benchmark	MaF1	MaF3	MaF5	MaF6	MaF7
PF Characteristic	Plane	Convex	Concave	Degenerated	Discontinuous

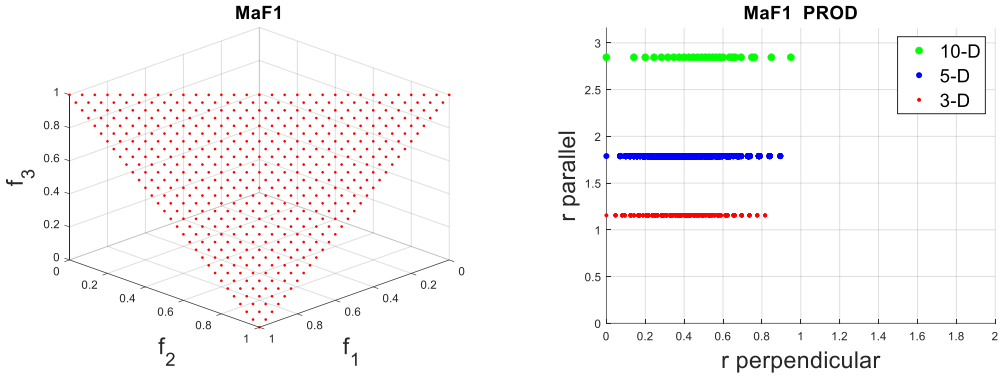

(a) MaF1 in 3D (b) ProD for 3D, 5D and 10D

Figure 5.8 - Scatter plot for PF of 3D and ProD for PF of MaF1 in 3D, 5D and 10D are displayed in the same plot, showing the differences and minimising the number of plots.

Figure 5.8 shows scatter plot for PF of 3D MaF1 (Figure 5.8 (a)) and the results of ProD of true PF of 3D (red), 5D (blue) and 10D (green) (see Figure 5.8 (b)). (The 3D, 5D and 10D results are plotted in the same figure to save space in the presentation. But they actually represent solutions from different dimensional space projected to 2D.). Here, four major issues are worth notifying. First, all three PFs consist of distinct horizontal lines, indicating that MaF1 has PF patterns of simplex planes in all dimensions studied and has data

symmetrically distributed about the reference vector. Second, all three PF solutions cover only partially the objective space. Third, as the number of objectives increases, maximum $r_{\perp}$ for each PF solution case increases, indicating objective space enclosed by PF in higher dimensional problem increases. It implies that via ProD, it is possible to reveal the range of objectives. Fourth, curves locate higher up as the number of objective functions increases, indicating distances of solutions to ideal points increase in higher dimensions for this benchmark problem.

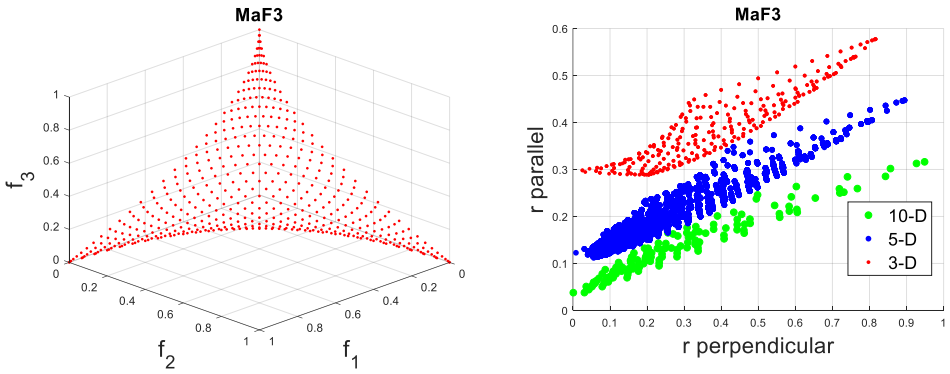

(a) 3D scatter plot, MaF3 (b) ProD, MaF3

Figure 5.9 - Scatter plot for PF of 3D and ProD for PF of MaF3 in 3D, 5D and 10D.

Accurate PF solutions of MaF3 in 3D, 5D and 10D are unsymmetrical about reference vector, although they are symmetric about f_3 axis, see Figure 5.9(a), but all three solutions cover their respective whole objective space. Folded images of PF occur in ProD due to this asymmetry. The images in ProD implies that a good approximation set of convergence and diversity must cover the whole shaded areas, as shown in the figure.

As shown in Figure 5.10 (a), PF of MaF5 in 3D has a sphere that transformed into ProD, a distinct arc is exhibited and is stretched to the maximal extent, indicating that PF covers the whole objective space. The diameter or curvature of the arcs corresponds to the sphere's diameter. PF of MaF5 in 5D and 10D are of hyperspheres which are also revealed in ProD. See Figure 5.10.

Pure arcs in ProD mean that all the PF solutions are equidistant to the nominal Ideal Point.

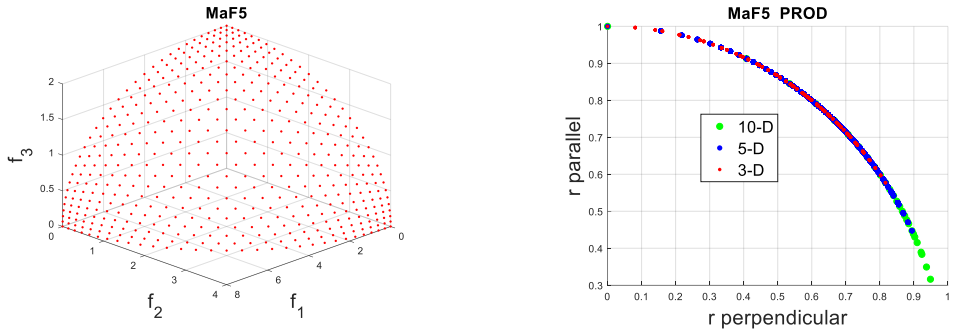

(a) 3D scatter plot, MaF5 (b) ProD, MaF5

Figure 5.10 - Scatter plot for PF of 3D and ProD for PF of MaF5 in 3D, 5D and 10D.

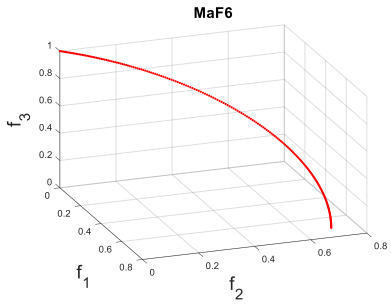

(a) 3D scatter plot, MaF6

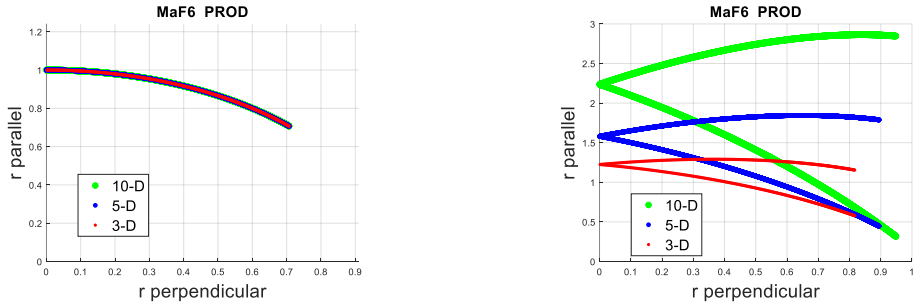

b) PROD without normalisation (c) PROD with normalisation

Figure 5.11 - Scatter plot for PF of 3D and ProD for PF of MaF6 in 3D, 5D and 10D

PF of MaF 6 is a degenerated type (a single curve in objective space) and consists of a circular arc that can be considered part of a cube or a hypercube. See Figure 5.11(a). When unnormalised, its shapes of 3D, 5D and 10D in ProD exbibit as pure circular arcs indicating PF shapes of sphere or hypersphere, but there are only two PF solutions per ProD point, belonging to PF solutions on each side of reference vector only. See Figure 5.11(a) and Figure 5.11(b).

When MaF6 is normalised, the circular arcs are split, and patterns of swallows appear in the ProD plot, see Figure 5.11(c). It is caused by the fact that normalisation has stretched patterns at diverse places differently, resulting in the original pairs of points which had the same $r_{\parallel}$ and $r_{\perp}$ values now depart. Based on the above analysis, one can come to conclusion that ProD alone will have challenges in detecting PFs of degenerated type with certainty. ProD should be performed both on PF solutions with and without normalisation to reveal different features of PFs. By normalisation, in this case, the PF shape of hyperarc is detected, while without normalisation, the PF shape can form either a circular arc or hypersphere. An alternative and more reliable method in detecting PF of degenerated type is using a proper diversity metric, e.g., IRNA covered in Chapter 4. Due to the scarcity of PF solutions in objective space, degenerated PFs have extremely low IRNA values. (IRNA$\cong 0.05$, see Chapter 4, Section 4.4).

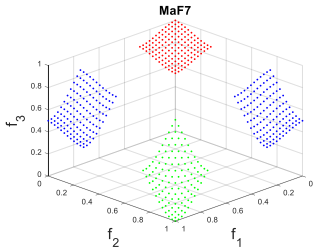

(a) Scatter plot of PF solution of MaF7

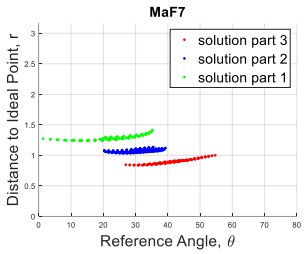

(b) ProD for 3D case only

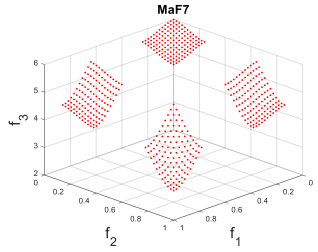

(c) 3D scatter plot, MaF7

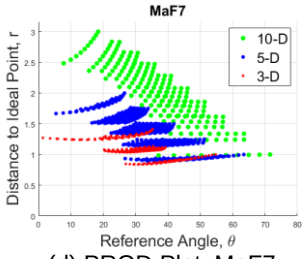

(d) PROD Plot, MaF7

Figure 5.12 - Scatter plot for PF of 3D and ProD for PF of MaF7 in 3D, 5D and 10D

PF of MaF7 is discontinuous and has four flakes in 3D scatter plot, but its image in ProD reveals three groups of piecewise surfaces. See Figure 5.12(a)(b). The first piece locates closest to $f_1 - f_2$ plane, the third one with the highest f_3 values while the second one has two flakes situated between the

lower and the upper. ProD of Figure 5.12(b) also discloses that each data group appears as a thicker line indicating near symmetry about the reference vector, but not perfect. It is worth noticing that ProD of 5 and 10 objectives unveil 5 and 10 clusters of solutions, respectively, which means that PF patterns in higher objective space might have more clusters than what is observed in 3D space.

Based on the above discussions, ProD can reveal the basic PF shape of benchmark problems of MaFs of any dimensions, i.e., whether it is in convex, planar, concave, degenerated, or discontinuous form. But ProD cannot distinguish degenerated PF of pure arc from a sphere, see Figure 5.11 and Figure 5.12, except that sphere shows a more significant extent in $r_{\perp}$ values. The two highly dissimilar cases may further be distinguished by using some proper diversity metrics, e.g., IRNA. Discontinuous PF may be treated as consisting of several individual PFs, which can be analysed separately. In all cases shown above, PF distributions are displayed in ProD, another critical property.

5.4.3 ProD in Displaying Dominance Relations

This section focuses on the capability of ProD in visualising dominance relations between approximation sets. The results are also presented in two parts. In the first part, using the MaOP algorithm, NSGA III, approximations on chosen Benchmark problems at several time intervals (at several given iteration numbers) are visualised. The solutions are compared and contrasted in convergence and diversity and displayed in ProD. In the other part, ProD is utilised to compare approximations of different MaOP algorithms at equal numbers of iterations, in which convergence and diversity are contrasted, where the capability of ProD in revealing dominance relations are further documented. Only the benchmark cases listed in Table 5.2 are shown and discussed here for better readability reasons.

5.4.3.1 *ProD in Visualising Dominance Relations*

In this section, the ability of ProD to visualise dominance relations among PF approximation sets is demonstrated by displaying the convergence process of a MaOP algorithm at a given time and over time. NSGA III is used to obtain approximations of ongoing convergence as the evaluation progresses. Other MaOP algorithms could be chosen as well.

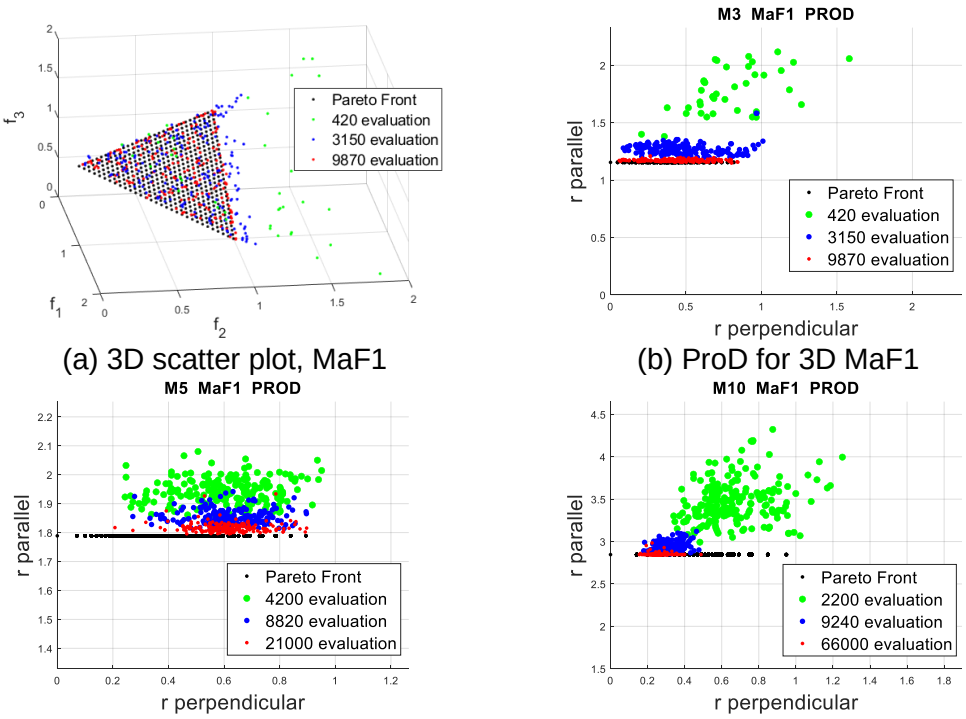

(a) 3D scatter plot, MaF1

(b) ProD for 3D MaF1

(c) ProD for 5D MaF1

(d) ProD for 10D MaF1

Figure 5.13 - Capability of ProD in showing dominance relations between PF approximation sets and revealing convergence process of Benchmark MaF1. The exact PF is shown in black dots. The figures reveal the converging process of the optimisation towards the final PF and the quality of approximations in diversity, the better spread along $r_{\perp}$ axis, the better the diversity. The approximations in 3 objectives are satisfactory in convergence and diversity (red dots), while the diversity is poor for 5 and 10 objective cases.

Figure 5.13 displays PF approximations on MaF1 after various iterations, which are displayed in different colours. The black dots represent the actual PF. It clearly shows the convergence process during the algorithm execution. In Figure 5.13(c), a notable feature is the absence of data points at small $r_{\perp}$ values, a common phenomenon occurred more or less in most test cases,

which is due to the limited amount of reference points created in these areas and are used in NSGA III. In Figure 5.13(d), the absence of data points in the 10D case is observed both for small and large $r_{\perp}$ values, which indicates that NSGA-III based on small number of reference points is only capable of finding solutions in part of PF in high dimensions.

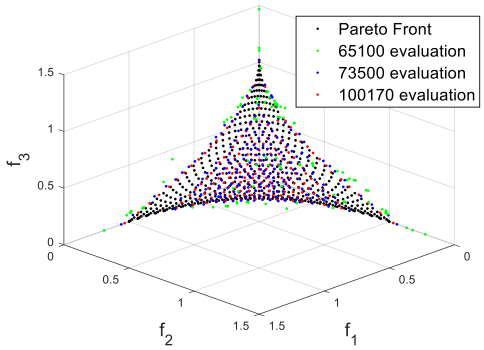

(a) 3D scatter plot, MaF3

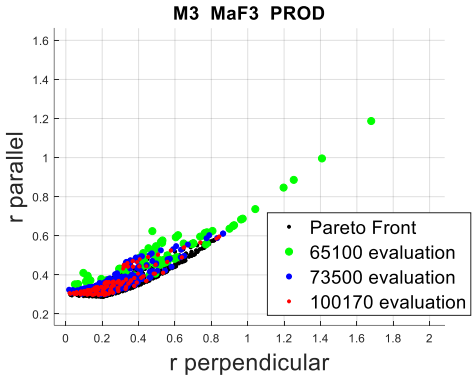

(b) ProD for 3D MaF3, data with normalisation

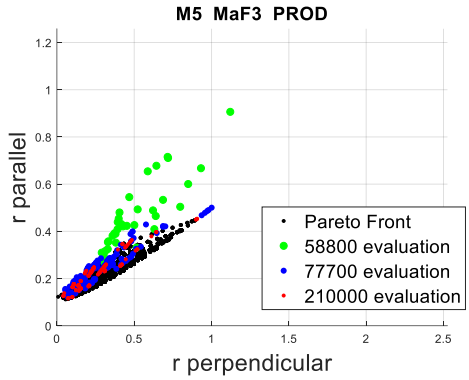

(c) ProD for 5D MaF3, data with normalisation

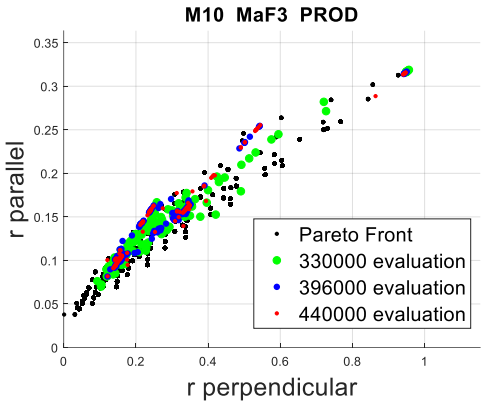

(d) ProD for 10D MaF3, data with normalisation

Figure 5.14 - Capability of ProD in showing dominance relations between PF approximation sets and revealing convergence process of Benchmark MaF3, data with normalisation.

PF of MaF 3 is of convex type covering the whole objective space. Its convexity is revealed by ProD since all curves of various dimensional problems bend upwards. See Figure 5.14. That reveals that the solutions' convergence process is being improved (lowered) with the increasing number of iterations. The best convergence and diversity of solutions are reached when solutions are achieved with approximations that cover the whole PF areas (black dots).

But 10D solutions have limited diversity due to the insufficient number of candidate solutions used in the algorithm's execution. See Figure 5.14(d).

The PF shape of MaF 5 is in concave form as a symmetrical sphere about the reference vector (see Figure 5.15(a)). It can be observed that solutions of NSGA III starting from areas of large$r$ $r_{\parallel}$ and $r_{\perp}$ values and converges and spreads out to the whole PF as iterations continue. But this spread-out process is reduced in 5D cases and ceased entirely in 10D cases. See Figure 5.15(c) and (d).

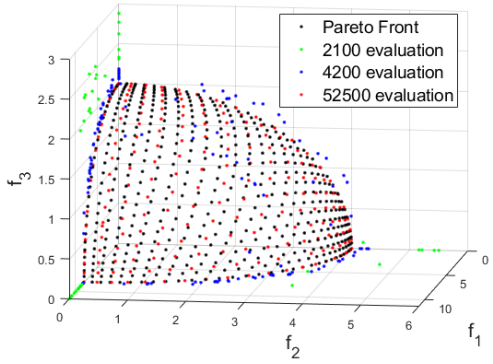

(a) 3D scatter plot, MaF5

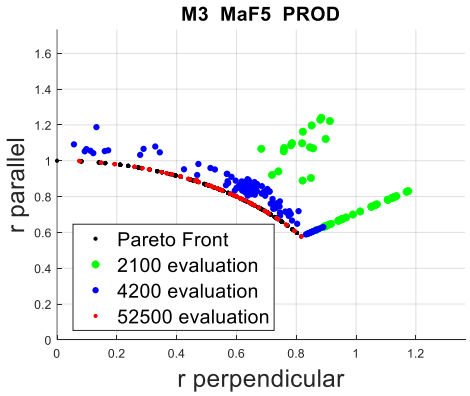

(b) ProD for 3D MaF5, data with normalisation

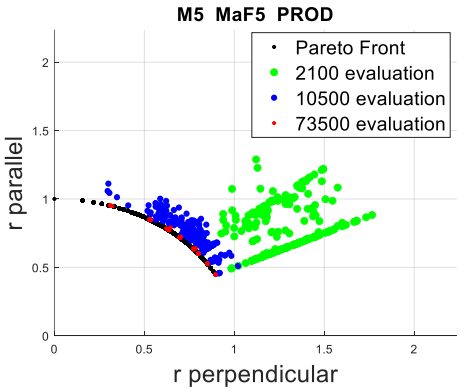

(c) ProD for 5D MaF5, data with normalisation

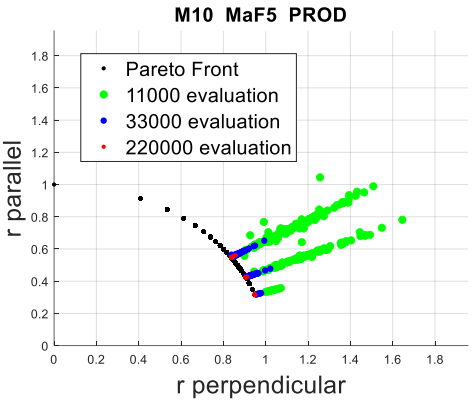

(d) ProD for 10D MaF5, data with normalisation

Figure 5.15 - Capability of ProD in showing dominance relations between PF approximation sets and revealing convergence process of Benchmark MaF5, data with normalisation.

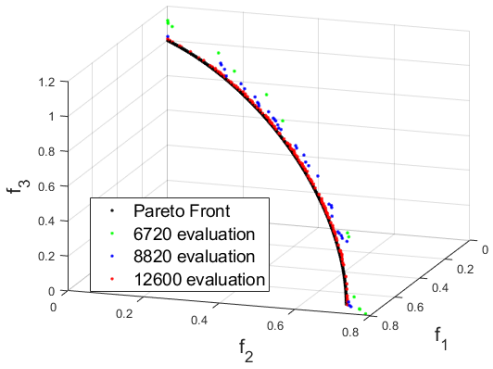

(a) 3D scatter plot, MaF6

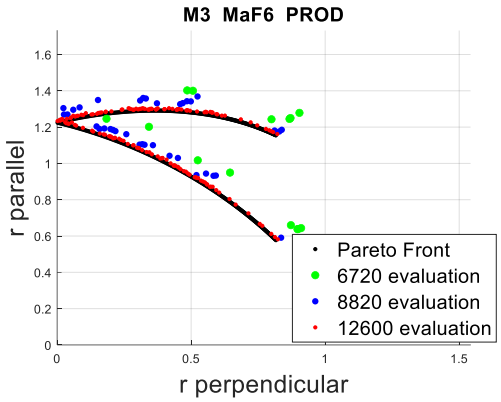

(b) ProD for 3D MaF6, data with normalisation

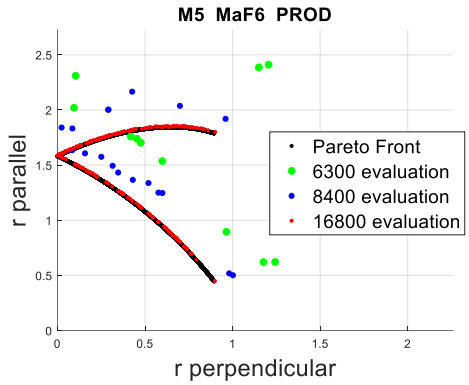

(c) ProD for 5D MaF6, data with normalisation

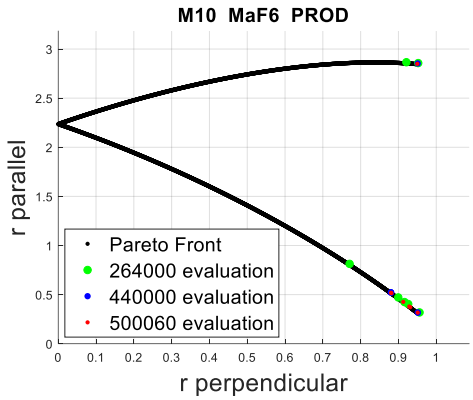

(d) ProD for 10D MaF6, data with normalisation

Figure 5.16 - Capability of ProD in showing dominance relations between PF approximation sets and revealing convergence process of Benchmark MaF6, data with normalisation.

PF of MaF 6 is an arc in 3D, and data in Figure 5.16 have been normalised while those in Figure 5.17 are unnormalized. ProD shows satisfactory convergence and diversity properties of solutions in 3D and 5D cases. Still, NGSA III fails to iterate toward true PF in 10D (see Figure 5.16(d) and Figure 5.17(d)) for the majority of candidate solutions. The results may indicate that NSGA III has challenges to solve degraded cases as the type of MaF6 in high dimensions.

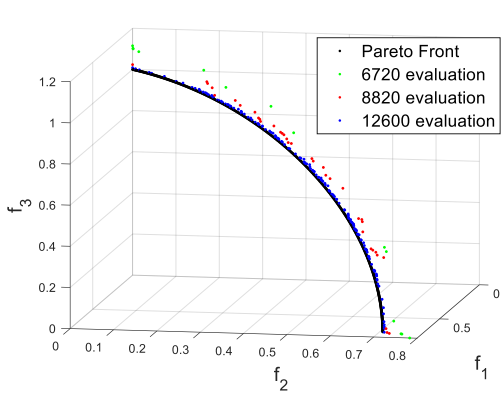

(a) 3D scatter plot, MaF6

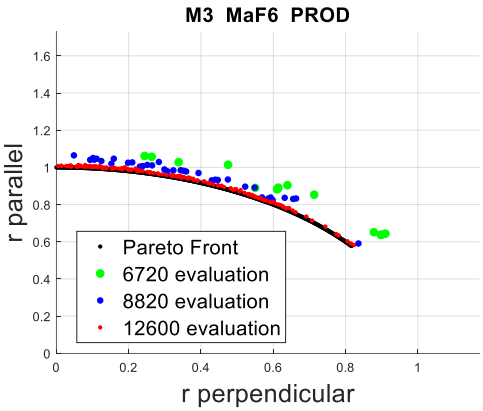

(b) ProD for 3D MaF6, data with normalisation

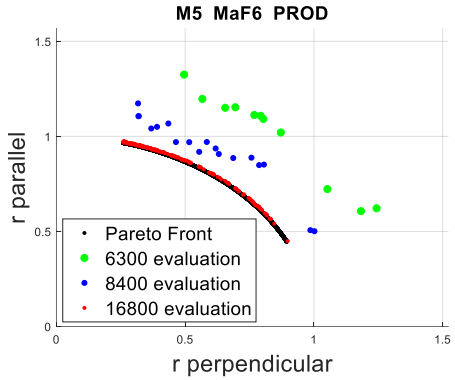

(c) ProD for 5D MaF6, data with normalisation

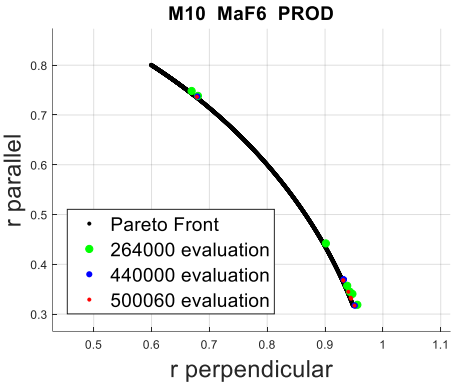

(d) ProD for 10D MaF6, data without normalisation

Figure 5.17 - Capability of ProD in showing dominance relations between PF approximation sets and revealing convergence process of Benchmark MaF6, data with normalisation.

Figure 5.18 shows roughly the convergence process of approximations of MaF7. Again, the most striking thing observed here is the limited diversity of solutions in cases of high dimensionality. See Figure 5.18(d).

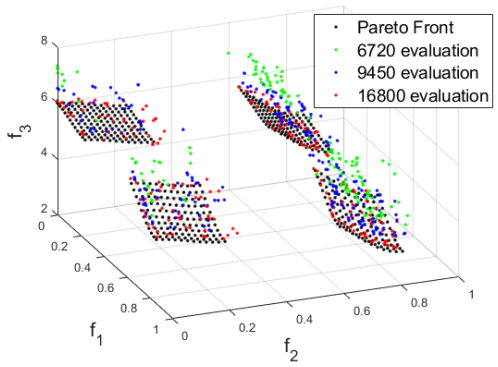

(a) 3D scatter plot, MaF7

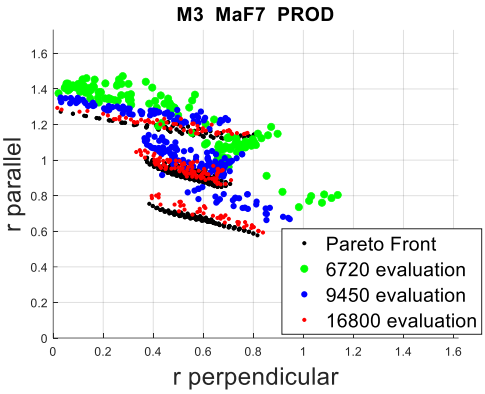

(b) ProD for 3D MaF7, data without normalisation

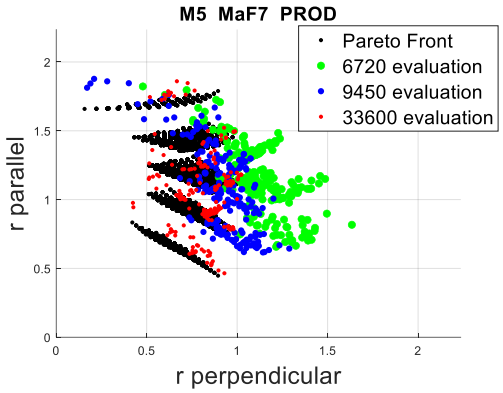

(c) ProD for 5D MaF7, data without normalisation

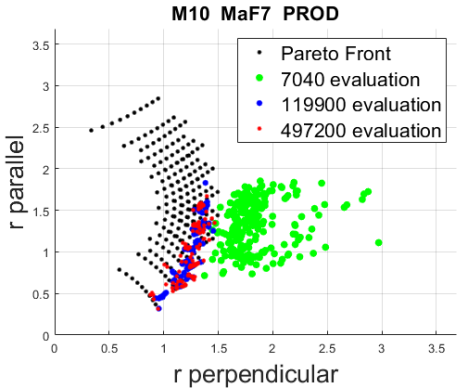

(d) ProD for 10D MaF7, data without normalisation

Figure 5.18 - Capability of ProD in showing dominance relations between PF approximation sets and revealing convergence process of Benchmark MaF6, data without normalisation.

As can be concluded, based on the above discussions, ProD can visualise Dominance Relations among multiple PF approximation sets, thus can display a converging process of optimisation. Domination Relations are harder to be detected in ProD when the contrasting approximation sets are close in performance. A performance metric can be used in such cases, e.g., Hypervolume or IRNA.

5.4.3.2 *ProD in visualising dominance relations*

In this section, the ability of ProD in revealing dominance relations is further demonstrated by visualising approximation sets of three algorithms: NSGA III, IBEA and GrEA, after the same and the large number of iterations corresponding to the final stage of completed approximation. Solution sets from the chosen algorithms after a various specific number of iterations are displayed

in ProD. A necessary requirement on good diversity performance of an approximation set is that it has $r_{\perp}$ values distribute uniformly and from the lowest possible value spreads out to the most extensive possible range. When its convergence property is concerned, it has the best convergence when the value of $r_{\parallel}$ is the lowest, covering the whole shaded area of true PF in ProD. As stated in Section 5.3, the diversity requirement stated above is necessary but insufficient. No guarantee for satisfactory diversity of an approximation set is assured, although candidate solutions are uniformly distributed within the whole range of $r_{\perp}$ because each data point in ProD may have better or worse diversity within the region it represents. But, on the other hand, an approximation set with data distribution without having full coverage of $r_{\perp}$ axis in ProD is weak in diversity. An evaluation metric must check the diversity of an approximation set before a conclusion is made, e.g., Hypervolume metric or IRNA.

Figure 5.19 displays PF approximations from the three chosen algorithms on MaF1 after various iterations. Figure 5.19(b) shows the diversity and convergence of 3D MaF1 after 2520 functional evaluations. Visually, the approximation set from IBEA has the best convergence and diversity for this 3D case after this number of evaluations. GrEA ranks second-best, while NSGA III suffers relatively slower convergence speed. Still, the quality in diversity is roughly the same as those obtained using the other two algorithms. That is also the case for 5D after 6720 function evaluations. But for the 10D case, after 154000 evaluations, the situation is much changed. Many approximations of NSGA III are nearly converged to PF, but solutions concentrate in a narrower region, meaning some reduced or weakened diversity. See Figure 5.19(d). For IBEA, most solutions are converged, but there are some outliers of not fully converged candidates, while its diversity is better than is the case for NSGA III. For GrEA, many candidates are not converged to PF, but those already

converged show better spread stretching far to areas away from the reference line or central region. But solutions are scarce in the central region near the reference vector.

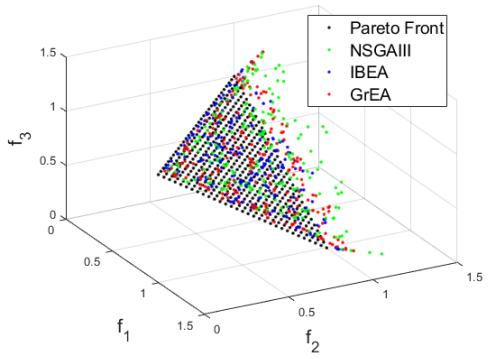

(a) Approximations in 3D scatter plot, MaF1

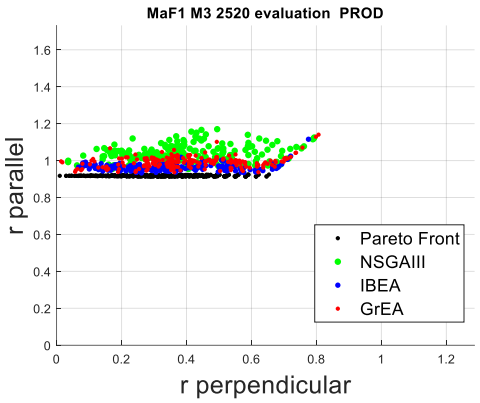

(b) Approximations in ProD after 31500 iterations, 3D MaF1

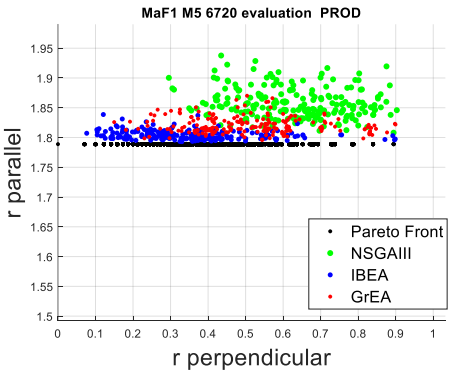

(c) Approximations in ProD after 6720 iterations, 5D MaF1

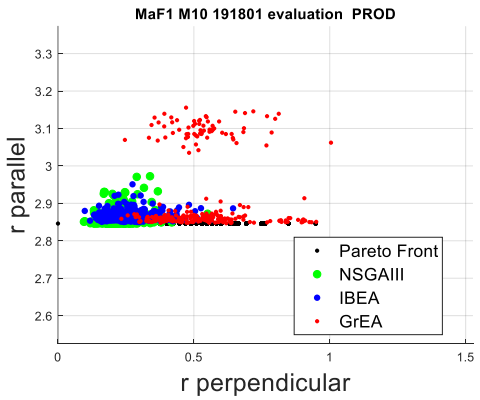

(d) Approximations in ProD after 42000 iterations, 10D MaF1

Figure 5.19 - ProD, showing comparisons on the convergence and diversity of Benchmark MaF1 among three chosen algorithms.

5.4 Numerical testing

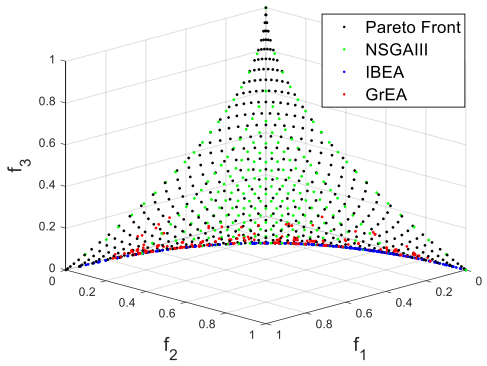

(a) Approximations in 3D scatter plot, MaF3

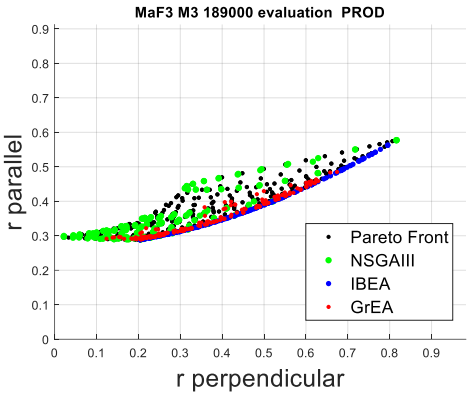

(b) Approximations in ProD, 3D MaF3

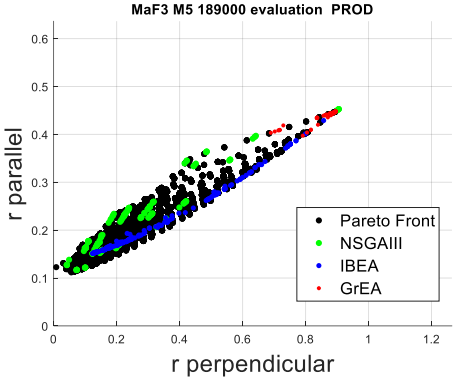

(c) Approximations in ProD, 5D MaF3

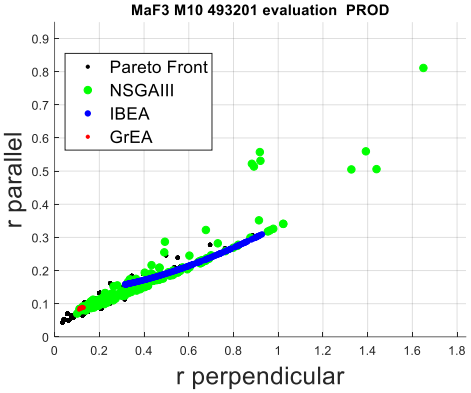

(d) Approximations in ProD, 10D MaF3

Figure 5.20 - ProD, showing comparisons on the convergence and diversity of Benchmark MaF3 among three chosen algorithms.

Figure 5.20 shows 3D scatter plot and the convergence in ProD of MaF3 for 3D, 5D and 10D cases. It is interesting to note that PF approximations of IBEA and GrEA, although converged, almost all solutions located only in f_1-f_2 plane, indicating insufficient diversity. In ProD, both approximations are in the bottom of clouded areas instead of covering the whole range of true PF (black dots). Solutions from NSGA III have the best diversity and cover almost all of the true PF. Similar is the case with instances of 5D as well as 10D. IBEA finds PF solutions along with a narrow band only, while GrEA considers only a small PF area and almost fails in finding converged solutions.

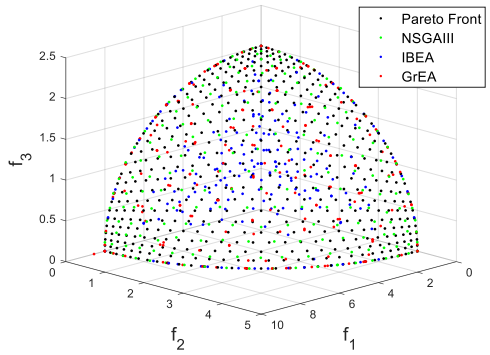

(a) Approximations in 3D scatter plot, MaF5

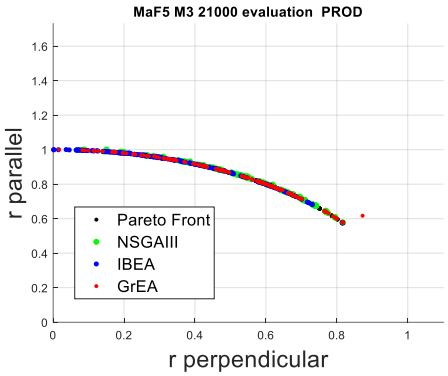

(b) Approximations in ProD, 3D MaF5

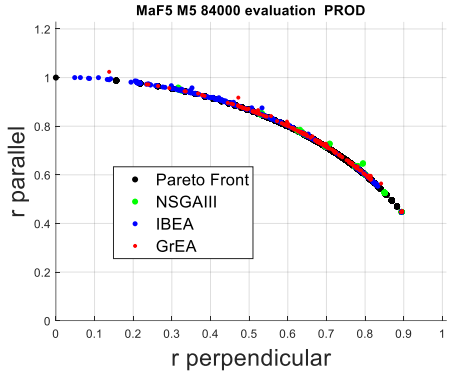

(c) Approximations in ProD, 5D MaF5

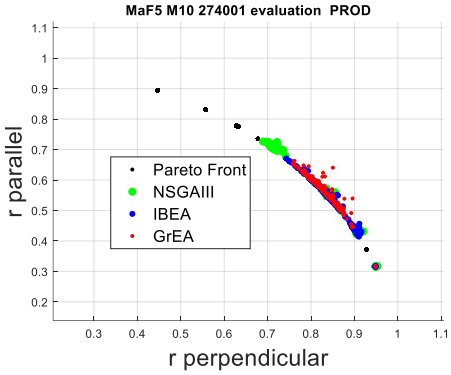

(d) Approximations in ProD, 10D MaF5

Figure 5.21 - ProD, showing comparisons on the convergence and diversity of Benchmark MaF5 among three chosen algorithms.

PF of MaF 5 consists of a sphere. See Figure 5.21(a). Roughly speaking, all three algorithms give satisfactory results in convergence and diversity in 3D cases. See Figure 5.21(b). But the diversity property is weaker for GrEA and NSGA III solutions than IBEA in the 5D case. See Figure 5.21(c). All three algorithms give unsatisfactory results in diversity in 10D instances due to the insufficient number of candidate solutions used.

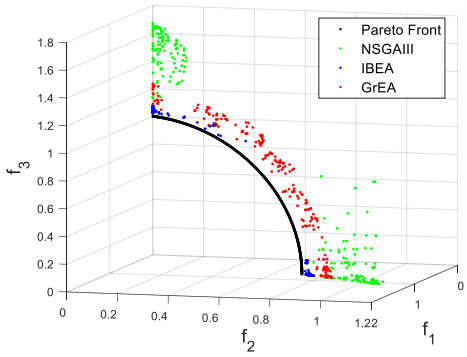

(a) Approximations in 3D scatter plot, MaF6

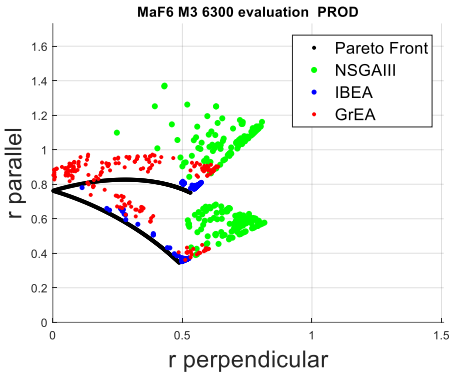

(b) Approximations in ProD, 3D MaF6

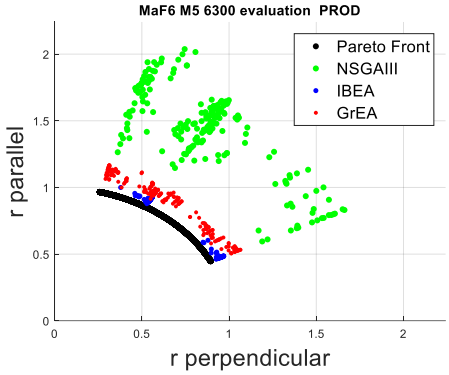

(c) Approximations in ProD, 5D MaF6

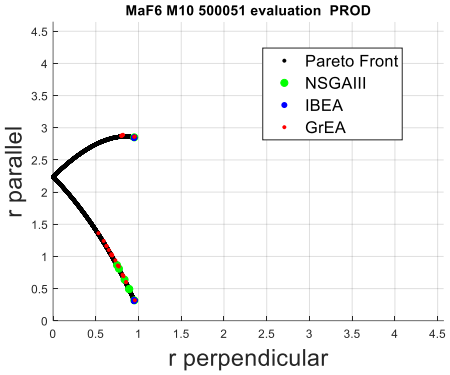

(d) Approximations in ProD, 10D MaF6

Figure 5.22 - ProD, showing comparisons on the convergence and diversity of Benchmark MaF6 among three chosen algorithms.

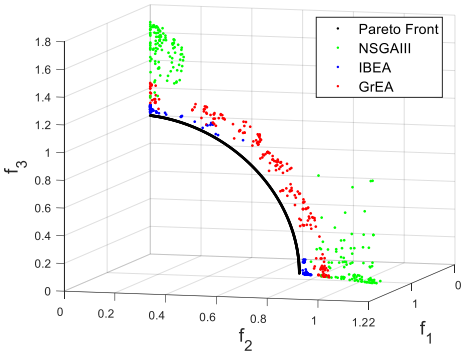

(a) Approximations in 3D scatter plot, MaF6

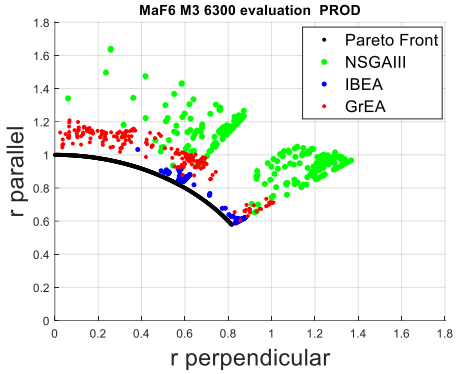

(b) Approximations in ProD, 3D MaF6, without normalisation.

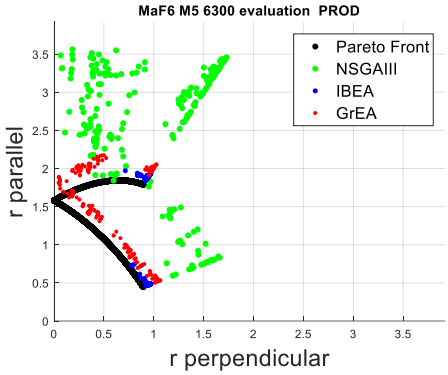

(c) Approximations in ProD, 5D MaF6, without normalisation.

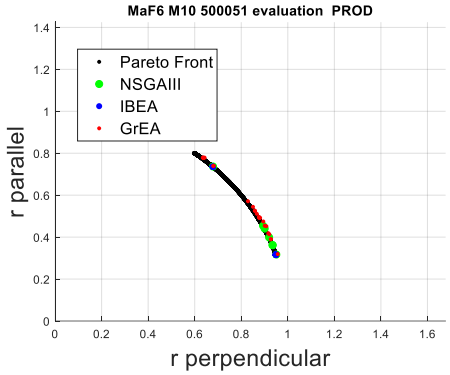

(d) Approximations in ProD, 10D MaF6, without normalisation.

Figure 5.23 - ProD, showing comparisons on the convergence and diversity of Benchmark MaF6 among three chosen algorithms. No data normalisation.

PF of MaF 6 is an arc in 3D, which shape is degenerated. See Figure 5.22(a). ProD shows satisfactory convergence and diversity properties of solutions in 3D and 5D cases for all three algorithms. Still, all three algorithms reveal their inability to iterate toward true PF (see the large scale of the vertical axis in Figure 5.22(d) and Figure 5.23(d)). The results indicate that the three chosen algorithms have difficulties solving degraded cases as the type of MaF6 in high dimensions.

5.4 Numerical testing

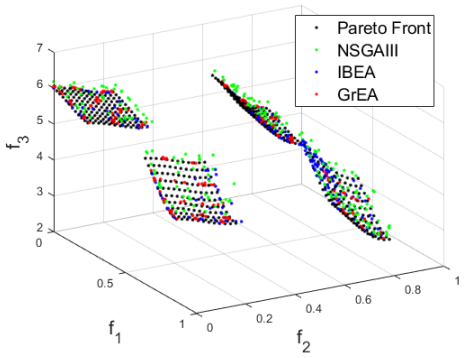

(a) Approximations in 3D scatter plot, MaF7

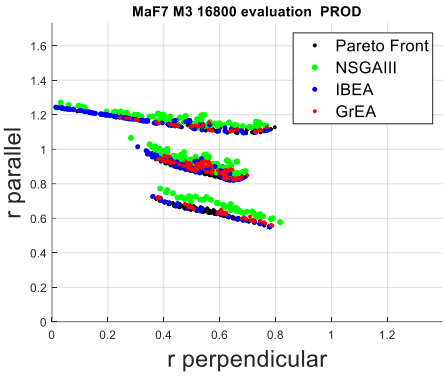

(b) Approximations in ProD, 3D MaF7

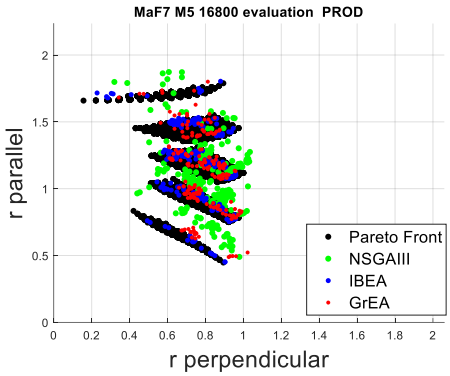

(c) Approximations in ProD, 5D MaF7

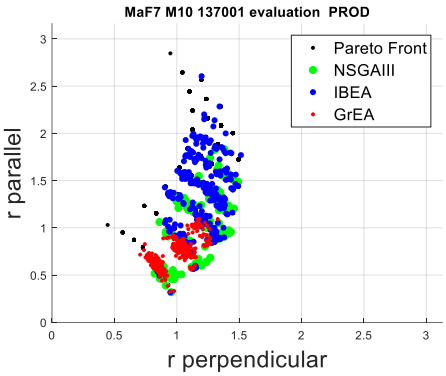

(d) Approximations in ProD, 10D MaF7

Figure 5.24 - ProD, showing comparisons on the convergence and diversity of Benchmark MaF7 among three chosen algorithms.

Approximations from the 3D case of MaF7 after 16800 functional evaluations show almost equally good results from all three chosen algorithms (see Figure) (b). However, the convergence of NSGA III results is somewhat weaker than for the other two algorithms. See Figure 5.24(b). For the 5D case, after 16,800 evaluations, the situation becomes unclear. But one can still see that IBEA gives the best results in convergence and diversity while NSGA III generates the least converged approximations. See Figure 5.24(c). For the 10D case, uncertainty dominates the picture. See Figure 5.24(d). IBEA seems to give the best results in diversity compared to the other two algorithms. But none of the three algorithms generates satisfactory approximations in diversity because only a limited number of intermediate points exist in the solutions.

Results and discussions provided above further confirm the ability of ProD in visualising Dominance Relations among multiple PF approximation sets,

where it is used to contrast approximation sets from different MaOP algorithms in optimisation analysis. Dominance relations may be harder to be detected in ProD when the contrasting approximation sets are close in performance. A performance metric can be used in such cases, e.g., Hypervolume or IRNA.

5.4.4 ProD as a Visualisation Tool in Satisfying Other Requirements

Properties of ProD in meeting other requirements as a visualisation tool, described in Chapter 1, are highlighted and discussed.

- Distribution of PF of candidate solutions is depicted in ProD as functions of their projections ($r_{\parallel}$) on and distance ($r_{\perp}$) to reference vector.
- Display in ProD remains robust and meaningful when data of high dimensions are mapped to 2D. The robustness of a visualisation method means that the addition or removal of data should not significantly impact the visualisation image. The robustness of visualised image of approximated PF is essential for our perception of the searched PF. ProD satisfies the requirement because that $r_{\parallel}$ and $r_{\perp}$ of data are well defined and remain so with the increase or decrease of data visualised.
- ProD is capable of visualising large data sets and multiple sets simultaneously. Large data sets are often created for approximated PF, especially for high dimensional MaOPs, and a visualisation method must handle them. In addition, concurrent visualisation of several data sets is needed when multiple PF data sets are contrasted. There is, in principle, no limit for ProD in this aspect in contrast to the method of Parallel Coordinates, which lead to the unrecognisable image when a large number of data have to be displayed.
- ProD is scalable to any number of objectives and is simple to construct.

- Pareto front representations in ProD are unique, independent of the sequence of existing objective functions. $r_{\parallel}$ and $r_{\perp}$ values are invariant to the change of order of objective functions.

5.5 Conclusion and Future Research Directions

In ProD, better convergence of an approximation set is indicated by its shorter projection on the reference vector ($r_{\parallel}$), while better diversity of it is revealed by its more extensive spread and more uniform distributed solutions along the axis of distance $r_{\perp}$ to reference vector. The latter is a necessary but insufficient requirement on diversity; hence, the diversity performance of approximation sets should be judged using appropriate diversity metrics.

ProD exhibits a more balanced performance than the state-of-the-art in capturing desired visualisation properties. In particular good performance is observed in portraying dominance relations, PF shape and distribution. The main properties of ProD are reflected upon the desired properties of visualisation methods described in Introduction section 5.1.1, which are achieved in a more balanced manner than existing visualisation methods can fulfil.

- ProD may visually depict the distribution of high dimensional PF approximations as functions of their projections ($r_{\parallel}$) on and distance ($r_{\perp}$) to reference vector.
- ProD may roughly reveal the overall dominance relationships between two approximation sets in convergence and diversity but not sufficiently precisely between two individual approximations.
- ProD remains robust and meaningful when data of high dimensions are mapped to 2D.
- ProD is capable of visualising large data sets and multiple sets simultaneously.
- ProD is scalable to any number of objectives and is simple to construct.
- ProD creates a unique image of high dimensional PF approximations, independent of the sequence of existing objective functions.

As future research directions, several topics deserve further study:

- First, using performance metrics on regional data in ProD would be an exciting topic to explore further, as well as researching the optimal definition and allocation of the data regions, which should be able to be related to the resolution of PF surface in general and the number of divisions along with each objective function, for decomposition-based algorithms in particular.
- Second, the ProD visualisation mechanism could also potentially be used as a binary performance indicator, where the distribution of two approximation sets in metric value of some kind along $r_{\perp}$ axis of approximations of different iteration numbers or dissimilar algorithms can be compared and contrasted. The sum of regional metric values can be used as a final quality indicator.

Chapter 6 Minimising Crack Formation in Selective Laser Melting operations

Chapter Outline

While accounting for different part designs, optimising multiple process parameters is a common but nontrivial task in additive manufacturing. Process expertise and knowledge are often used in the manufacturing industry and prototyping laboratory settings, combined with available numerical and analytical models to set process parameters for a given part design. It usually involves experimental trials before settling for a final set of parameters that satisfy some performance metrics, generally relevant to the part quality. This chapter demonstrates a systematic Machine Learning framework for optimising process conditions in Laser-Powder Bed Fusion or Selective Laser Melting (SLM) while accounting for part design for the first time, using a conservative amount of experimental data. We exploit the capability of a class of universal approximation data-driven models to capture the process-part behaviour, and we then optimise `concurrently process parameters for various part designs. The proposed framework is demonstrated and experimentally validated on a Selective Laser Melting process for material CM247L. It's a nickel super alloyed compound commonly used in critical aerospace applications due to its mechanical properties. Being able to 3D print this material would be of enormous importance to the aerospace industry. The obtained PF approximations are made most evenly distributed in the objective space adopting the B-norm based Pareto Front tracking method (Bn-PFt) developed

in this thesis work. The final approximations have been checked for the diversity property utilising the performance indicator, the Inverse Ratio of Net Avertence angles (IRNA) also proposed in this thesis. The outcomes have been effectively visualised in the high dimensional space of both objective and decision one, applying the technique of Projection on and Distance to a centre vector (ProD) elaborated in this study. Results show that the proposed framework can be utilised to achieve improved performance in minimising part micro-cracking, and crucially this is achieved with ranges of discovered process parameter set that yields the best results in all part designs. Due to the data-driven nature of the proposed framework, this work can be extended to other material/process combinations and expand the number of optimisation objectives, for example, to address part density, build time, or mechanical performance of resulting parts.

6.1 Introduction

Machine parts are traditionally fabricated by first forming work blank or ingots through, for instance, forging or casting and are further machined to their final forms, where excess material is removed. It is, in general, characterised as a subtractive production method. Additive Manufacturing (AM) is a group of production methods that makes the final product directly by building one layer of time starting from its bottom [214]. The manufacturing process is also referred to as 3D printing. Materials of plastics, as well as metals, can nowadays be used in an AM process. AM revolutionises the world of manufacturing. It has distinct advantages in making complex-shaped and customised parts, often in one go. Prototypes of specialised components can be produced quickly and at a relatively low cost. Production is speeded up, and downtime is much reduced when replacement parts are manufactured on-site if components break down.

Moreover, AM can manufacture a final product as a whole or a few parts, rather than producing many individual components and assembling them. Thus, products can be designed more optimised and compact; without excess arrangements for assembling, such as welds and spaces for fasteners, are removed. In addition, AM manufactured objects often elude the need for post-production treatment, such as heat treatments and specialised machining for metal products.

Laser-Based Additive Manufacturing (LBAM) is a popular area of AM technology and is dedicated to working with metal parts. LBAM techniques are categorised into two major subgroups, Direct Metal Laser Sintering (DMLS) and Selective Laser Melting (SLM). DMLS can build objects out of almost any metal alloy because the coherence of the metal powder mixture is based on sintering, where hard and high melting temperature metal is sintered with other metals

with lower melting temperatures. SLM technique utilises a high power-density laser to melt and fuse metallic powders. A skinny layer of metal powder covers across the work surface is slowly and steadily heated up by a laser beam moving across the surface being manufactured in both processes. New layers of powder are then rolled on in place and fused on the object one cross-section at a time.

A significant additional advantage of LBAM, beyond the benefits of an AM method in general, is that metal products can be manufactured with less residual stresses and internal defects than traditionally produced ones using subtractive production methods. DMLS can be utilised to build products with internal channels and detailed shapes that could not be cast or subsequently machined. SLM utilises a high-powered laser to melt each layer of metal powder fully. The objects created are denser and more robust than those using DMLS based on sintering, where metal powders are only partially melted. SLM is beneficial when producing metal components of high melting point and high ductile-brittle transition temperature, like tungsten.

Traditional subtractive production methods have a relatively high setup cost since many auxiliary equipment and tools might be needed, for instance, moulds for generating raw castings or ingots. These different arrangements are spared when using SLM. But, in general, SLM has a high cost per part, and it is most feasible when used in situations where only very few pieces are needed to be made. For instance, spare parts of machines, implants, and components for the aerospace industry. SLM is nowadays frequently used to make orthopaedic implants in medical science and manufacture complicated and lightweight parts for aerospace. The products are nontrivial to be made by traditional manufacturing due to their compact design and no physical access of tooling to surfaces for machining.

Today, one major demerit of SLM is that the method can only be used on metals that have suitable flow characteristics when melted, such as stainless steel, tool steel, titanium, cobalt chrome, and aluminium parts. Expansion toward the usage of most metals is still an ongoing research subject. Moreover, SLM uses a high-energy laser and hits up a layer of metal powder locally to surpass the melting point of the metals. It creates high-temperature gradients locally around the working spot, which leads to stress concentrations and dislocations in the material structure inside the final product. It has considerable impacts on the resulting mechanical properties of the object due to the formation of cracks and pores. Several process parameters exist that determine the quality of an SLM operation in terms of production time, surface roughness, crack, and pore formulation internally and along with the edges, such as laser power, point distance, hatch offset and exposure time, etc. [215]. The most suitable process parameters can be found by simultaneously optimising target values that are specific qualities, mechanical properties, and geometric characteristics, such as acceptable density, yield strength, ductility, stiffness, elongation to failure, etc. But in most cases, these target values are conflicting and cannot be optimised individually in the same production process. For instance, high cooling rates of SLM may lead to an increase in yield strength of the material and a reduction in ductility or elongation to failure of the final product [214]. A compromise among them must be searched. That's why finding suitable process parameters is a challenging job, and it requires multi-objective process optimisation. The most desired properties can be attained by optimising these outcomes or objectives to the dominating process parameters. The operation analysis requires that the mathematical relationships between the objectives and the process parameters or decision variables are established, i.e., the manufacturing process is modelled. Next, well-planned

experiments and simulations are performed, and the obtained data are subsequently analysed so that the process model is established and verified. Further, the well tested mathematical model is optimised to the targeted process parameters or design variables so that decision-makers can utilise the results to improve their operations.

The main focus of this study is to identify the optimal process parameters in an SLM process subject to minimising Crack Formation using evolutionary many-objective optimisation (MaOP) methodologies. In this author's knowledge, such a work is still essential to be carried out in the field of research, possibly due to the complexity and high uncertainty in measuring, modelling, and analysing cracking from an SLM manufacturing process.

A method for finding the ranges of optimised process parameters is proposed using the ProD visualisation method covered in Chapter 5 and Parallel Coordinates (see Chapter 5). The decision-makers can choose the optimal process parameters or decision variables to guide their SLM operations.

Due to significant variations in the validation data, i.e., high uncertainties when analysed with the developed surrogate models, the procedure of a robust optimisation analysis is presented and recommended to be done as part of the future work of this study.

The chapter is organised as follows. Section 6.2 describes the principles of the working process of SLM and the primary defect formations. Section 6.3 summarises some previous major studies in analysing AM/SLM process using ML and EMO methodologies. Modelling the Selective Laser Melting process is covered in Section 6.4. Section 6.5 explains the experimental setup and the related process modelling. The modelling results are summarised and discussed in Section 6.6. The optimisation analysis and the results are

presented and discussed in Section 6.7. Section 6.8 discusses the necessity of robust optimisation in the study and the data required accordingly. Discussions on various issues are taken in Section 6.9. Finally, a summary and the future work discussions are taken in Section 6.10.

6.2 Principles of the Working Process of SLM and Main Defect Formations

A significant challenge in achieving good quality in the Selective Laser Melting (SLM) process is achieving high reliability and good repeatability on the manufactured product. It has been reported that the quality of the final product, the consistency of the production system, the repeatability of the process and the production setups and procedures are highly influenced by the process parameters [214]. Consequently, the product's final quality, microstructure and mechanical properties are determined by selecting such process parameters [214]. This chapter provides a short overview of the working principle of an SLM process and how the various defects are formed.

6.2.1 The Working Process and the Main Components

An SLM operation starts by slicing the data from a 3D CAD file into layers to a 20 to 100 micrometres thickness. The making of a product undergoes inside a chamber containing either argon or nitrogen at oxygen levels below 500 parts per million [216]. Thin layers of fine metal powder are first evenly spread out using a coater blade or a roller onto a metal substrate plate placed on the top of an indexing table that may move vertically in a tightly controlled manner. These metal powders are spherical and produced by gas atomisation using pre-alloys. The metal particles in such a shape ensure a high flowability and packing density, which help spread and homogenise the powder layers. A low percentage of much finer metal particles (15 - 63 µm) are added to the powder to enhance the flowability further. The thin layer of metal powder is then fused by a high-power laser beam, usually a ytterbium fibre, with an effect of typically about 200 watts. The laser beam scans the product layer, controlled by two high-frequency scanning mirrors. The operation is repeated layer after

layer until the object is constructed [216]. The process is illustrated in Figure 6.1. Before the laser irradiates, the metal powder is preheated to a temperature right below the melting temperature of the metal.

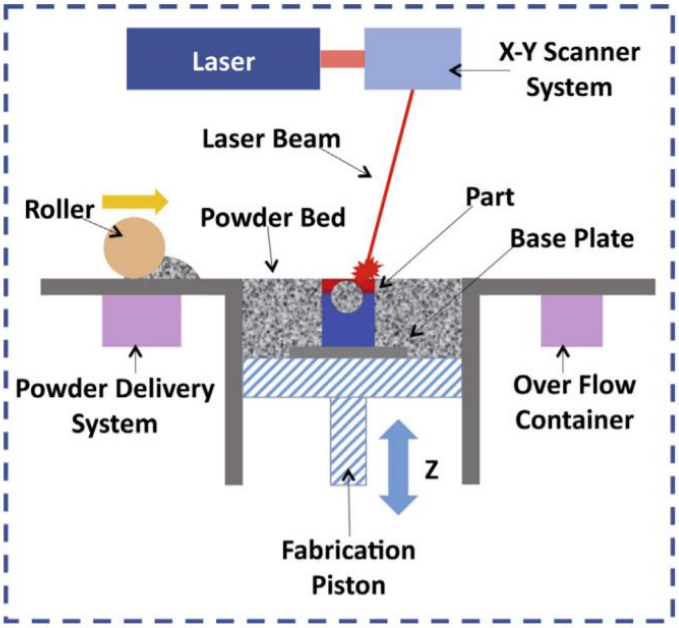

Figure 6.1 - The process is shown by the principle sketch of an SLM process (Taken from [216]).

The process parameters are often categorised into three main groups: pre-process, in-process, and post-process parameters. The pre-process parameters include preheating temperature of the metal powder, etc. The in-process parameters include laser power, point distance, hatch offset, exposure time, etc. In contrast, the post-process parameters encompass stress relief measures through heat or thermomechanical treatments that reduce residual stresses, close pores and transform the hard and brittle microstructures to softer ones to improve the mechanical properties. The choice of process parameters leads to a big difference in the final quality of the SLM built. This study focuses on the effects of the in-process parameters on the cracking formation and its length density in the created objects. Specifically, these parameters are laser power, point distance, hatch offset, exposure time, and volume energy density. These parameters are illustrated in Figure 6.2. The point distance is the focal offset distance between the focus of the F- theta lens

and the surface of the metal powder. The hatch offset or hatch spacing is the distance between the centre lines of two adjacent paths of the laser within the same layer and is a factor that impacts the results on the overlapped areas [215]. The exposure time is causally related to the scan velocity of the laser beam. The volume energy density is defined as:

$$E_v = {}^{P}/_{(v \cdot h \cdot t)} \qquad \text{Eq. 6.1}$$

where

- P is the laser power
- v is the scanning velocity
- h is the hatch distance
- t is the powder layer thickness.

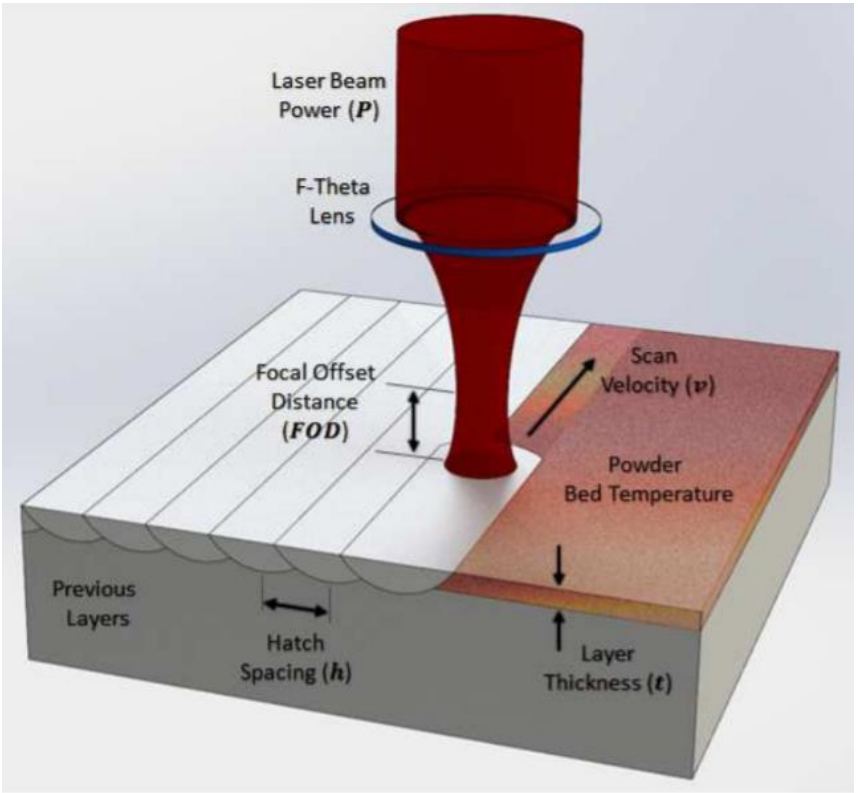

Figure 6.2 - Illustration of operating parameters studied for SLM processing (taken from [215]).

6.2.2 Defect Formation

The concentrated laser power results in a high-temperature gradient in and around the building area. It generates several types of defects, which directly impacts the mechanical properties of the manufactured part. Combined with the scanning movement of the laser beam, a complicated picture of solid-state transformations, thermal fluid dynamics, particle dynamics, etc., are created locally. A schematic display of the circumstances is shown in Figure 6.3.

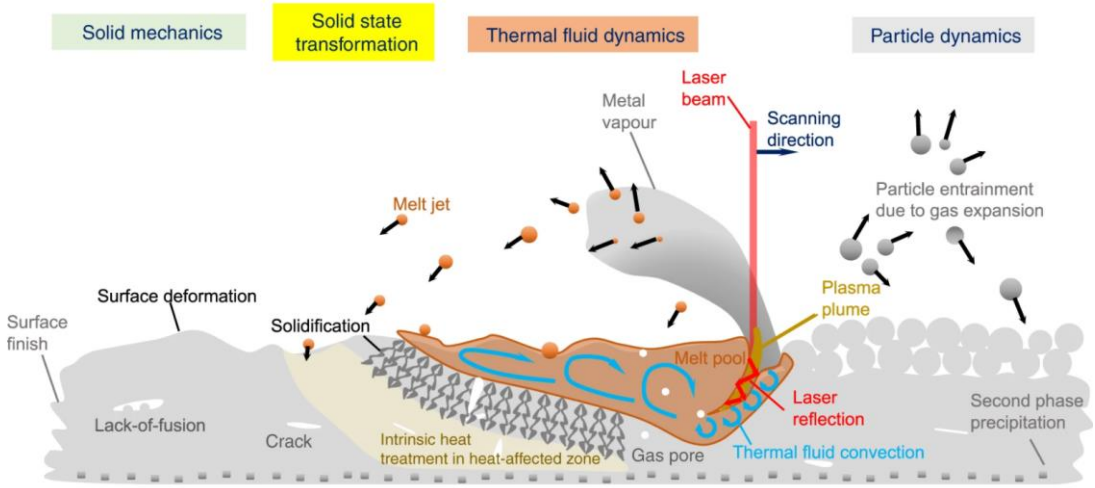

Figure 6.3 - Schematic display on local conditions around the building spot in an SLM operation (taken from [217]).

Two significant defects commonly occur. One is the lack of fusion (LOF) that results in the formation of pores in the solidified regions. The other is cracking that forms during the solidification of the built material.

LOF is caused by gases dissolved first in the melt and entrapped in the object after the melt is solidified. Inadequate powered laser source or too high of a scanning speed of the laser source across the built area may lead to the lack of fusion. The metal particles' strong thermal fluid dynamical movement causes the metal grains to melt incompletely, resulting in incoherent solidification. In addition, the flow of melt under thermal tension makes inhomogeneous compositions gather at certain areas forming pores. The convection currents induced by the laser beam can be the driving force for

irregular melt flow. The overall composition of the semi-molten metal is changed, and weaker or porous regions may occur [218].

Moreover, weaker material microstructures like dendrites may occur and progress along temperature gradients at different speeds. The built material in such areas has weakened mechanical properties in strength and fatigue life. Further, pores may also form when the laser scan velocity changes when the formed holes close, and gases are trapped in the solidifying metal [219].

Cracking occurs inevitably when the built metal alloys have low thermal conductivity and high thermal expansion coefficients, causing high-level internal stresses and stress concentrations, leading to material fractures [218]. Another reason for crack formation is the microstructure wise precipitates within the bulk structure caused by the repetitive heating on solidified lower layers under the laser beam scanning. Moreover, the convection currents cast oxides in the melt to different locations. These oxides are non-wetting to the base material and function as local cracks [217], [218].

Specifically, the material quality used in this study is a nickel superalloy - CM247L. It is an alloy with good mechanical strength in high temperature working environments characterised by excellent mechanical strength, resistance to thermal creep, good surface stability, and corrosion resistance. Its basic structure is face-centred cubic (FCC) austenitic. The material's mechanical strength is enhanced by solid solution strengthening and precipitation strengthening. The Solid solution strengthening is done by adding alloys to the crystalline lattice of the base metal and forming a solid solution, which hinders the plastic deformation in the material. In the precipitation strengthening, alloying beyond the solubility limit makes a second phase precipitates such as gamma prime and carbides along grain boundaries, inhibiting grain boundary motion and thus further

strengthening the material against yielding [220]. Additionally, the material's corrosion resistance is made possible using alloys such as chromium. But carbide formation could be harmful because microcracks are often formed around them under repeated local melting and solidification process in an SLM process, leading to stress concentrations when the material is loaded and causing the reduction of yield strength and fatigue strength of the alloy [221].

6.3 Previous Studies in Analysing AM/SLM Process using ML and EMO Methodologies

Evolutionary Multi-objective Optimisation (EMO) methodology is frequently applied to analyse an optimised AM process. The first group where such optimisation targets are called topology optimisation, where stress distributions, concentrations and material deformations are analysed using Finite Element Analysis (FEA). A surrogate model is established describing the relationship between the product's topology and its design objectives as stress distributions, stress concentrations and material deformations, etc., subject to various loading conditions. EMO is applied to obtain optimal topology parameters under the assumption that the product would ideally and optimally have the same performance after the material is removed [222]–[225]. The second group optimises machining tool paths using neural networks [226]. Using an evolutionary algorithm, Xiang Lu has applied Particle Swarm Optimisation (PSO) and tried to improve and optimise the melt-decomposition moulding (FDM/MDM) process by optimising its controlling parameters. Bingbing Hu [227] use Simulated Annealing (SA) based algorithm to optimise parameters in an adaptive slicing approach. In Laser Powder Bed Fusion (L-PBF/SLM), the parameter setting is an operation of vital importance, affecting the final product's performance, quality, and cost.

Conventionally, the setting is based upon the intuition and experience of the operators, which usually are not the optimal choices. Several studies have been carried out to alleviate this problem. Byun and Lee (2006) [228] created an algorithm based on the weighted sum approach to determine the optimal build direction for many AM processes [228]. Brika et al. (2017) [229] applied a weighted-sum method for laser powder bed fusion to attain balanced and optimal manufacturing parameters by optimising the objectives for reaching the

best possible mechanical properties in the roughness of supporting structures and time cost. Padhye and Deb [230] applied an Evolutionary algorithm of Multi-objective PSO (MOPSO) and Non-dominated Sorting Genetic Algorithm II (NSGA-II) to minimise surface roughness and build time in a Selective Laser Sintering (SLS) process. Mezzetta et al. [231] analysed the relationship between static mechanical properties and heat treatment as a post-processing measure and established an optimal setting for SLM using EMO [231]. In this author's knowledge, none of the previous work targets optimising process parameters subject to microcracking in the field of research, possibly due to the complexity and high uncertainty in measuring, modelling, and analysing microcracking in an SLM manufacturing process.

6.4 Modelling the Selective Laser Melting Process

The exact physical functional relationship governing the objective function and the design variables is often unknown. A surrogate model or an approximation model is usually developed to replace the physical functional relationship and mimic the behaviour of the physical model as closely as possible while being computationally cheap(er) to evaluate. (These are also called response surface models, metamodels or emulators.) The elaboration of surrogate models for design objective and constraint functions requires experiments and simulations to evaluate as a function of design variables. Such a model's development is based on a data-driven, bottom-up approach, where the functional relationship is found solely based on the input-output behaviour.

6.4.1 Data-Driven Surrogate Model

Several approaches can be used to develop a surrogate model. Each is suitable for the characteristics of data available, such as polynomial regression, kriging, support vector machines, space mapping, artificial neural networks and Bayesian networks, Fourier surrogate modelling, random forests [232] and radial basis function.

This study's modelling of the Selective Laser Melting process uses data-driven modelling - Radial Basis Function Neural Network (RBFNN) [233], [234]. It has been proven that the basic RBFNN formulation can be viewed as a Type-1 Fuzzy Logic System (FLS) of either Mamdani or Takagi-Sugeno-Kang type (TSK) [235], [236]. This functional equivalence has been further extended in [237], [238] to design high-order fuzzy systems that can better deal with noisy signals and improve the trade-off between accuracy, model transparency, and model simplicity. As pointed out in [235], [236], an RBFNN can be viewed as a FLS whose main inference engine is interpreted as an adaptive filter [237]. It

resembles an additive weighted combination of the Membership Functions (MFs) of the fired-rule output sets in the hidden layer of the RBFNN (See Figure 6.4). Thereby, every hidden receptive unit in the RBFNN is functionally equivalent to a fuzzy rule R^i described by a multi-variable Gaussian MF,

$$\mu_{R^i}(\vec{x}_p, y) = \mu_{R^i}[x_1, \dots, x_n, y] \quad \text{Eq. 6.2}$$

where the input vector $\vec{x}_p \in \{X_1, X_2, \dots, X_n\}$ and the implication engine is defined as [239]:

$$\mu_{R^i}(\vec{x}_p, y) = \mu_{A^i \to G^i}[T_{k_1}^n \mu_{F_k^i}(x_k) * \mu_{G^i(y)}] \quad \text{Eq. 6.3}$$

where * is the minimum t-norm (triangular norm) that represents the shortest Euclidean distance to the input vector $\vec{x}_p$. And each receptive unit is the i^{th} fuzzy rule: R^i, where $i = 1, \dots, M$, and M is the number of MFs. T-norm fuzzy logics are based on membership functions that take the actual unit interval [0, 1] for the system of truth values and use functions called t-norms for permissible interpretations of approximate reasoning. Therefore, the firing strength of each receptive unit is as follows:

$$\mu_{A^i \to G^i}(\vec{x}_p, y) = \prod_{k=1}^{n} \mu_{F_k^i}(x_k) = f_i\left(exp\left[-\frac{\sum_{k=1}^{n}(x_k - m_{ki})^2}{\sigma_i^2}\right]\right) \quad \text{Eq. 6.4}$$

where $A^i = F_1^i \text{x} F_2^i \text{x} \dots \text{x} F_n^i$, $G^i = G_1^i \text{x} G_2^i \text{x} \dots \text{x} G_n^i$ and m_{ki} and σ_i are the centre and width of a multi-variable Gaussian MF, respectively. n is the number of input parameters or decision variables. By combining all the rules in the output layer, the output y_p is given as: see Figure 6.4

$$y_p = \frac{\sum_{i=1}^{M} \mu_{A^i \to G^i}(\vec{x}_p, y)\omega_i}{\sum_{i=1}^{M} \mu_{A^i \to G^i}(\vec{x}_p, y)} \quad \text{Eq. 6.5}$$

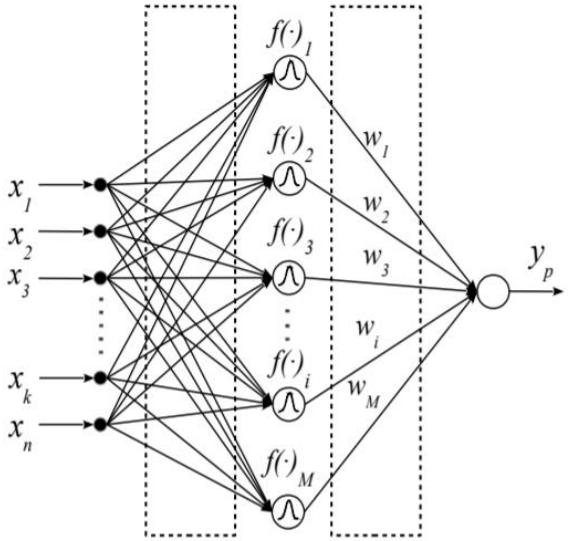

Figure 6.4 - Parameter identification applied to the GT2 RBFNN ((RBFNN, Taken from [235]).

6.4.2 Determination of Model Parameters

The centre m_{ki} and the width σ_i of the multi-variable Gaussian MF_i in Eq. 6.5 must be determined using experimental or simulated data before the weights ω_i are trained in the RBF Neural Network. It is done first by grouping the input data or decision variable data into clusters, and from which the centre m_{ki} and the width σ_i are found for the cluster i:

$i \in \{1, \ldots,$ the number of clusters$\}$. The number of clusters is put equal to the number of membership functions M or the number of radial base functions, $f_i, i \in \{1, \ldots, M\}$.

The data set is analysed by a cluster analysis and arranged in groups (clusters), where more similar data are organised in the same assembly. It can be achieved in many different ways with dissimilar outcomes depending on the definition of data similarity, such as distances between cluster members, density, particular statistical distributions, etc. In this study, clustering is done by granular computing, and their compatibility defines the data similarity.

The surrogate model has been parametrically optimised as [233], [234].

6.5 Experimental Setup and the Process Modelling

This section provides an overview of the CM245L data set and the determination of model parameters required to develop the numerical model. CM245 Data Set is an Additive Manufacturing Data Set. The data set in this study has been obtained with the help of HiETA technologies, UK.

6.5.1 Experimental Setup

As shown in Figure 6.5, CM245L trials involved building simultaneously a batch of three different Nickel superalloy builds, 30 pieces of each type, using Selective Laser Melting (SLM), i.e., a solid cube (sample 1), a slotted box with thin flaps (sample 2) and 5 millimetres (sample 3) thick flaps, respectively.

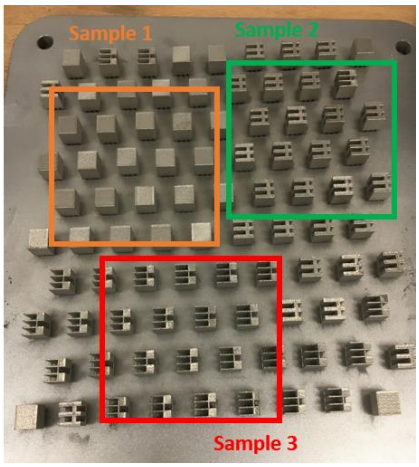

Figure 6.5 - Three different types of products, 30 pieces each, are manufactured simultaneously by SLM technology.

As detailed in Table 6.1, the experimental setup involves four input parameters and two different sets of outputs. The microcracking for each sample was measured at each experiment, and the associated density average was also calculated. The edge and bulk crack length densities are used to study the build quality of each sample. Three objective functions are modelled in each output set, which describe the functional relationship valid for each build. In general, in metal-based additive manufacturing, some process parameters

such as built orientation, laser power, hatch spacing, point distance, and volume energy density are sensitive to environmental variations and influence each other, regardless of the powder bed quality. These parameters affect especially the fabrication quality, including residual porosity and edge density. Table 6.1 lists the attribute information of the SLM data set.

Table 6.1 - Attribute information of the SLM data set

Input/output	Unit	Minimum	Maximum
Laser power	Watts	80	200
Point distance	µm	50	130
Hatch offset	µm	10	50
Exposure time	µs	20	80
Bulk Crack length Density (Output)	mm/mm²		
Edge Crack Length Density (Output)	mm/mm²		

There are in total 28 data samples (decision variables and objective function values) that have been collected from the experiment.

6.5.2 Model management

This study aims to determine under which operational conditions defined by the four decision variables or the process parameters like laser power, point distance, hatch offset, and exposure time, the outcome in terms of the edge crack length density, the bulk crack length density on the three disparate products manufactured are at their minimum. Specifically, the study investigates the best combination of the process parameters at which the targets: the edge crack length density and the bulk crack length density on each of the three built are either per crack type or simultaneously optimised [240]. The definition of the decision variables and the objective functions are listed in Tables 6.2 and 6.3.

Table 6.2 - Definition of the decision variables

Process parameter	Laser power	Point distance	Hatch offset	Exposure time
Decision variable	x_1	x_2	x_3	x_4

Table 6.3 - Definition of the objective functions

Output	The bulk crack length density, sample 1	The bulk crack length density, sample 2	The bulk crack length density, sample 3	The edge crack length density, sample 1	The edge crack length density, sample 2	The edge crack length density, sample 3
Objective function	f_1	f_2	f_3	f_4	f_5	f_6

The decision variables and the objective functions are subject to the box constraints defined in Table 6.1.

The decision variable and the values of the objective function are normalised prior to the modelling work so that both types of variables vary within the range of [0.0, 1.0]. The maximal and minimal values of decision variables are listed in Table 6.1, while those amounts of objective functions are obtained by sorting based on experimental data. The extremal data of bulk crack lengths and edge crack lengths are listed in Table 6.4.

Table 6.4 - The ranges of objective function values

Objective	f_1	f_2	f_3	f_4	f_5	f_6
Maximum	1.9380	4.5950	3.9300	8.3750	7.3500	5.2850
Minimum	0.2170	0.7740	0.3670	0.7920	0.7480	0.5820

The uncertainty comes from the numerical simulations. The total number of data samples (objective function and decision variables) is 26. 70% of the total, i.e., 18 are randomly selected and used in model creation, while the rest are used in error estimation. The selection is made ten times for each surrogate model construction to attain statistical information. The final surrogate model of each objective function is based on the average one of all ten surrogate models. The separation of data for modelling and testing is made as a trade-off in balancing estimation on model variance and the number of surrogate models handled. An alternative is to use Leave-One Out (LOO) selection technique. Still, it would lead to too many surrogate models. The function values must be repeatedly found in the latter optimisation process since the averaged surrogate model is used as each objective function.

A surrogate model is formed using the Generalised type 2 Radial Basis Neural Network (GT2 RBFNN) based on 18 data samples each time. Figure 6.6 shows the main procedure applied in creating a GT2 RBFNN model.

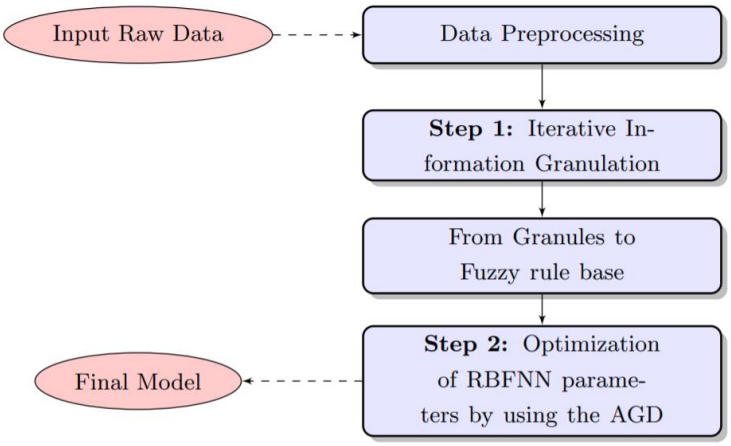

Figure 6.6 - The main procedures of modelling - GT2 RBFNN.

The Adaptive Gradient Descent (AGD) approach is utilised to optimise the parameters σ_i^2 and m_{ik} and to determine the optimal number of fuzzy rules according to cross-validation results [239].

For each objective function, min surface, average surface and maximum surface models are estimated by contrasting and averaging these ten individual surrogate models. See the results section, Section 6.6. The average surface models of all the objective functions are used in the optimisation analysis.

6.6 The Surrogate Models

6.6.1 Various surrogate models

Some typical scatter plots of the model outputs in the three levels as functions of the laser power, the point distance, the hatch offset, and the exposure time are shown in Figure 6.7-Figure 6.12.

Modelling the crack length density is a nontrivial task, as indicated in Figure 6.7-Figure 6.12, where the predicted and the laboratory tested amounts differ considerably in many cases studied.

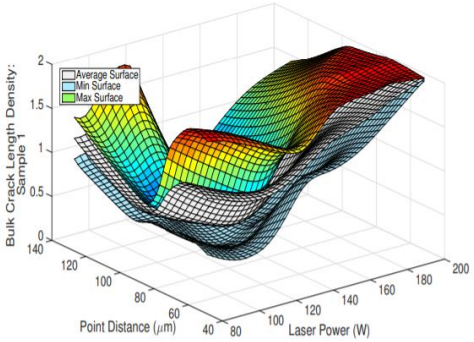

(a) Scatter plot as the functions of Laser power and Point distance.

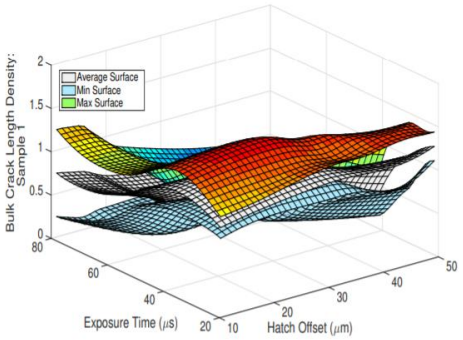

(b) Scatter plot as the functions of Hatch offset and Exposure time.

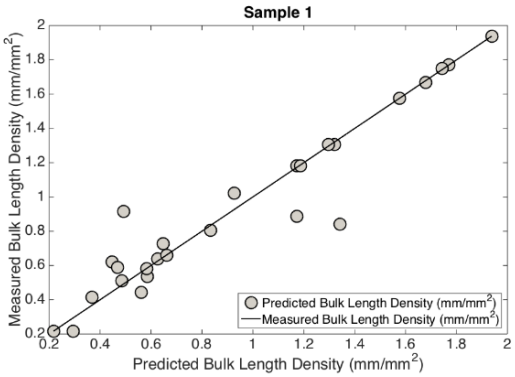

(c) Comparison between the predicted and measured quantity.

Figure 6.7 - Modelling Bulk Crack Length Density, sample 1.

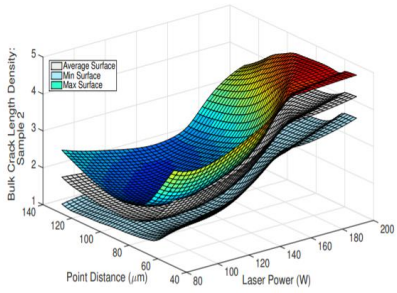

(a) Scatter plot as the functions of Laser power and Point distance.

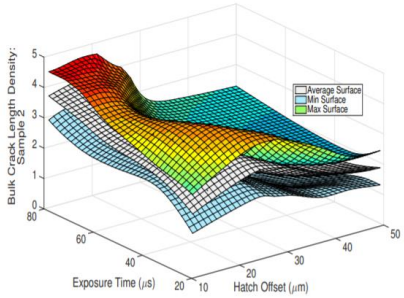

(b) Scatter plot as the functions of Hatch offset and Exposure time.

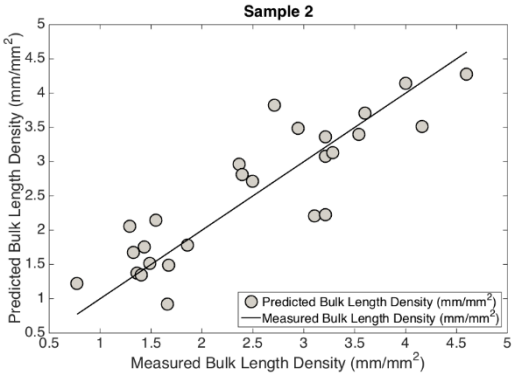

(c) Comparison between the predicted and measured quantity.

Figure 6.8 - Modelling Bulk Crack Length Density, sample 2.

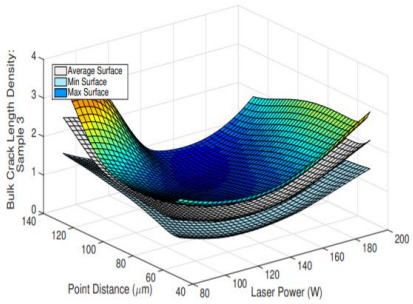

(a) Scatter plot as the functions of Laser power and Point distance.

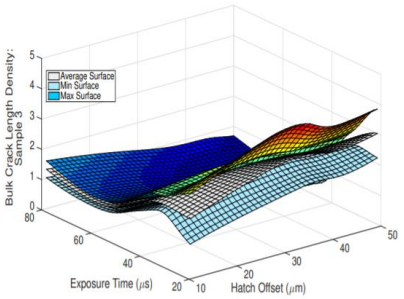

(b) Scatter plot as the functions of Hatch offset and Exposure time.

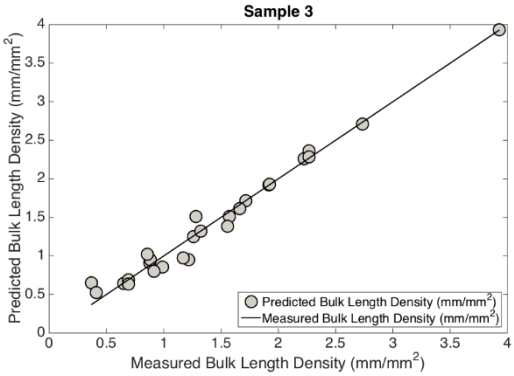

(c) Comparison between the predicted and measured quantity.

Figure 6.9 - Modelling Bulk Crack Length Density, sample 3.

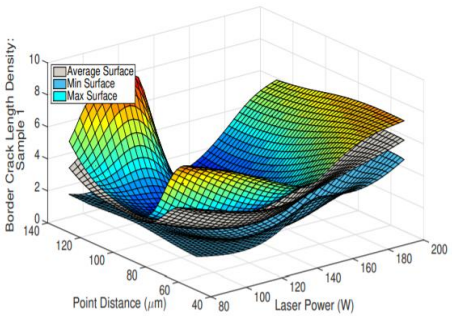

(a) Scatter plot as the functions of Laser power and Point distance.

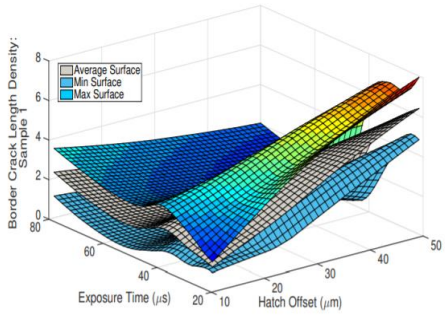

(b) Scatter plot as the functions of Hatch offset and Exposure time.

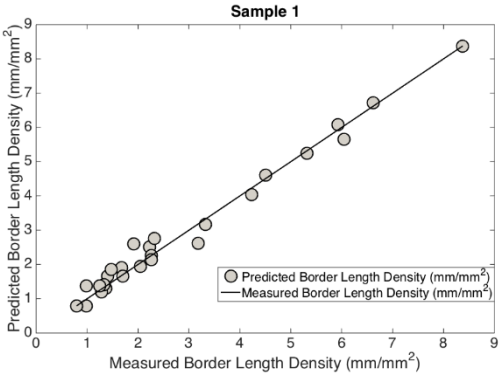

(c) Comparison between the predicted and measured quantity.

Figure 6.10 - Modelling Edge Crack Length Density, sample 1.

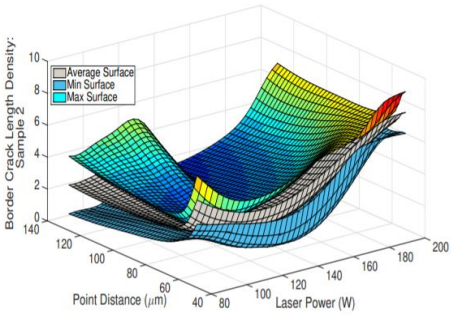

(a) Scatter plot as the functions of Laser power and Point distance.

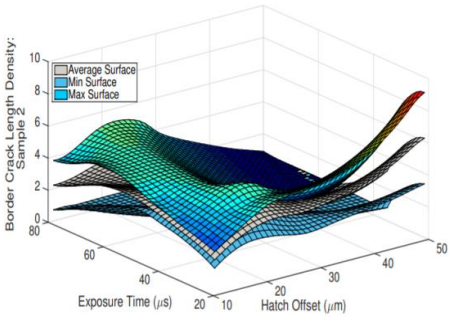

(b) Scatter plot as the functions of Hatch offset and Exposure time.

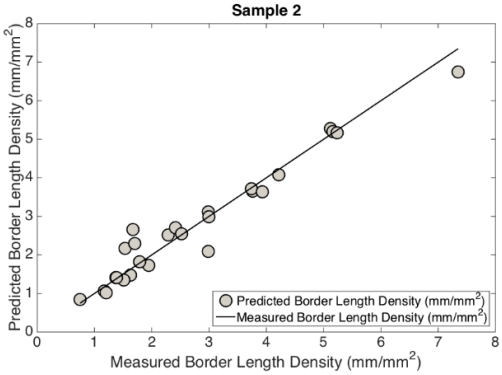

(c) Comparison between the predicted and measured quantity.

Figure 6.11 - Modelling Edge Crack Length Density, sample 2.

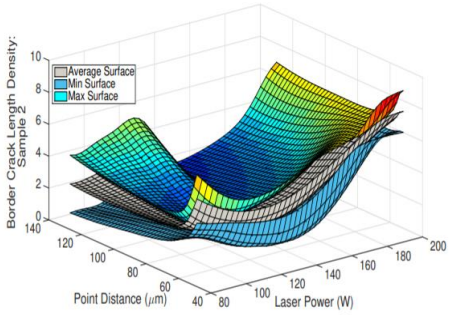

(a) Scatter plot as the functions of Laser power and Point distance.

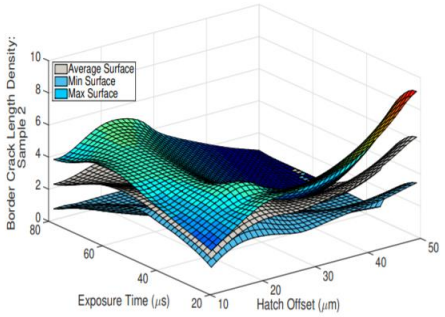

(b) Scatter plot as the functions of Hatch offset and Exposure time.

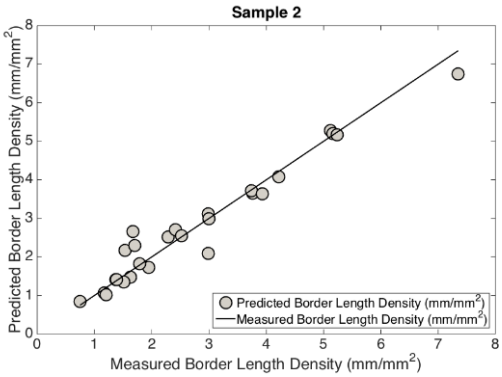

(c) Comparison between the predicted and measured quantity.

Figure 6.12 - Modelling Edge Crack Length Density, sample 3.

The figures reveal in a general manner that the minimised crack density varies over the ranges of process variables, which is indicated by the cavities in the figures. Interestingly, there are seemingly two such cavities for the edge crack length density. See Figure 6.12. It is verified in the optimisation analysis using metaheuristic methods shown in the latter sections.

6.6.2 The error estimates of surrogate models

The modelling errors of the surrogate models are measured using the frequently used error metrics: the root mean square error ($RMSE$), the maximum absolute error (*MaxAE*) and the coefficient of determination (R^2). $RMSE$ provides a global error estimation, while *MaxAE* is a local error metric that measures the maximum approximation error of the surrogate model. R^2 indicates a quantity for variance present in the experimental data [28].

Root Mean square error is defined as:

$$RMSE = \sqrt{\frac{1}{N_{test}}\sum_{i=1}^{N_{test}}(y_i(\boldsymbol{x}_i) - \hat{y}_i(\boldsymbol{x}_i))^2} \quad \text{Eq. 6.6}$$

where $y_i(x_i)$ is the actual response, $\hat{y}_i(x_i)$ is the prediction for $y_i(x_i)$ obtained with the constructed surrogate models. N_{test} is the number of collected samples.

The maximum absolute error is expressed as:

$$\text{MaxAE} = max|y_i(\boldsymbol{x}_i) - \hat{y}_i(\boldsymbol{x}_i)|, \quad i = 1, \dots, N_{test} \quad \text{Eq. 6.7}$$

The coefficient of determination

$$R^2 = 1 - \frac{\sum_{i=1}^{N_{test}}(y_i(\boldsymbol{x}_i) - \hat{y}_i(\boldsymbol{x}_i))^2}{\sum_{i=1}^{N_{test}}(y_i(\boldsymbol{x}_i) - \bar{y}_i(\boldsymbol{x}_i))^2} \quad \text{Eq. 6.8}$$

where $\bar{y}_i(x_i)$ is the mean of the actual responses and N_{test} is the total number of verification samples. When this metric is used as an indicator of the goodness-of-fit of a surrogate model, its values are distributed in the interval [0, 1]. In general, $R^2 < 0.5$ suggests that the relation between the predicted and actual values is weak; $0.5 < R^2 < 0.8$ indicates that substantial error variation exists in the surrogate, possibly due to a large measurement spread [28]. The error metric values of various objective functions are listed in Table 6.5.

Table 6.5 The error metric values for the various surrogates

metric	f_1	f_2	f_3	f_4	f_5	f_6
$RMSE$	0.0809	0.4661	0.1169	0.1643	0.2566	0.1519
MaxAE	0.2609	1.0597	0.2857	0.4154	0.4953	0.2892
R^2	0.9746	0.7957	0.9779	0.9934	0.9739	0.9837

As shown in Table 6.5, $RMSE$ metric varies between about 15% to 25% of a maximum of around 1.0 for the objectives, while MaxAE value shows individual spikes of 29% to 100%, especially uncertain test data are obtained with the bulk crack length density of the built 2, where $RMSE$ is as high as 0.4661, and MaxAE value exceeds 100% while R^2 turns out to be less than 0.8, indicating large errors in the data. High R^2 metric values have been obtained for all the other objective functions, which indicates a strong relationship

between the predictions and the observations, i.e., satisfactory quality surrogates are created.

6.7 Optimisation Analysis and the Results

6.7.1 The Chosen MaOP Methodology and Parameter Settings

Three commonly used but dissimilar MaOP algorithms, NSGA III [2], GrEA [79] and IBEA [61], are adopted in this analysis section to examine the final approximated PF. It is done to strengthen the reliability of the analysis since no guarantee can be given for correct answers when using evolutionary algorithms since the methodologies are heuristic and stochastic. And no free lunch theorem tells us that no single algorithm is superior to others for all situations. The adopted algorithms are acquired from PlatEMO [187]. These algorithms utilise disparate solution principles. NSGA III is a reference-point and nondominated sorting based genetic algorithm for MaOP. GrEA adopts grids drawn in high dimensional objective space to strengthen the selection pressure towards optimality while maintaining an extensive and uniform distribution among solutions. IBEA may adopt several binary performance indicators to select offspring as parents for the next round of iteration. The above three dissimilar algorithms are chosen for comparing and contrasting the efficacy of the three disparate methods in solving the specific optimisation problem. The newly proposed methods described in Chapters 3, 4 and 5 are utilised in the comparisons.

All the results shown in this section are obtained using MATLAB 2018a. The number of candidate solutions adopted in the analysis is listed in Table 6.5. The parameters applied in the three algorithms are based on default values acquired from PlatEMO version 2.7 [187].

Table 6.5 - Number of solutions generated

Number of objectives	Number of solutions for algorithms	Max. number of iterations used to generate authentic Pareto Front
3	210	300,000
6	210	3,000,000

The three objective optimisation analyses cover the cases where the three bulk crack density objectives and the three edge crack density objectives are studied separately, while the optimisation case with 6 objectives investigates the optimal operating conditions when all the six objective functions are optimised simultaneously.

The B-norm based Pareto Front tracing method (Bn-PFt) discussed in Chapter 3 has been implemented into NSGA III to enhance the diversity of the final PF. The performance indicator IRNA described in Chapter 4 has been utilised to assess the quality of the PFs obtained using the three MaOP algorithms. Further, the newly proposed high dimensional visualisation method ProD covered in Chapter 5 is applied to visualise the high dimensional PF data in the objective and decision spaces.

6.7.2 The Cases Studied

The analysis on three SLM manufactured products of different designs have been performed. The crack length densities at both the bulk and edges regions are measured and modelled, i.e., six objective functions in total are obtained. MOP and MaOP are performed on diverse combinations of the objective functions, resulting in the cases analysed as listed in Table 6.6.

Table 6.6 - The cases analysed by MOP/MaOP

Objective function	Sample	MOP analysis	MaOP analysis
The bulk crack length densities, f_1	1	MOP- Bulk crack analysis (MOP-EC), dimension: 3 objectives (f_1, f_2, f_3) x 4 decision variables: x_1, x_2, x_3 and x_4	MaOP-BEC: Combined Bulk crack and edge crack analysis. Dimension: 6 objectives $(f_1, f_2, \dots, f_6)$ x 4 decision variables: Laser power, Point distance, Hatch offset and Exposure time. $(x_1, x_2, x_3$ and $x_4)$
The bulk crack length densities, f_2	2		
The bulk crack length densities, f_3	3		
The edge crack length densities, f_4	1	MOP- edge cracks analysis (MOP-BC), dimension: 3 objectives (f_4, f_5, f_6) x 4 decision variables: Laser power, Point distance, Hatch offset and Exposure time $(x_1, x_2, x_3$ and $x_4)$	
The edge crack length densities, f_5	2		
The edge crack length densities, f_6	3		

6.7.3 The Analysis Results

The presentation of the results of optimisation analysis is divided into three major parts, MOP-Bulk Crack Length analysis (MOP-BC), MOP-Edge Crack Length analysis (MOP-EC), and Bulk Crack and Edge Crack Length combined analysis (MaOP-BEC). See Table 6.3 for details.

6.7.3.1 *MOP-Bulk Crack Length Analysis (MOP-BC)*

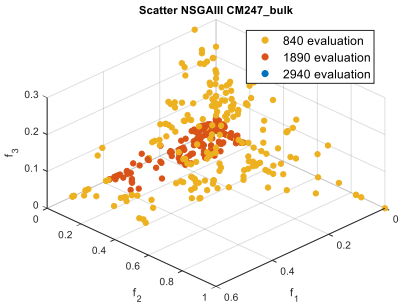

(a) The convergence process, NSGA III

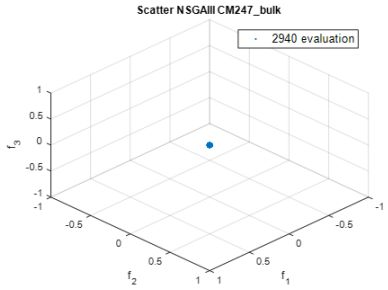

(b) The final PF approximation, NSGA III

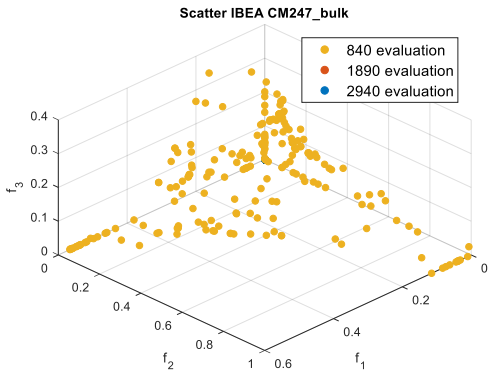

(c) The convergence process, IBEA.

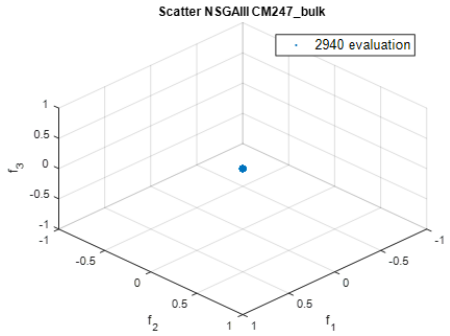

(d) The final PF approximation, IBEA.

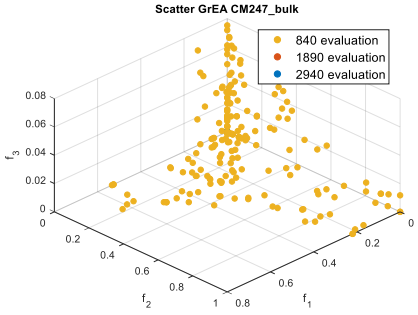

(e) The convergence process, GrEA

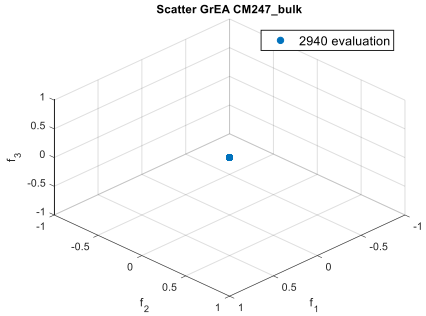

(f) The final PF approximation, GrEA

Figure 6.13 - The iteration process and the final PF approximation of MOP-BC, based on NSGA III ((a) and (b)), IBEA ((c) and (d)) and GrEA ((e) and (f)).

Figure 6.13 shows the iteration process (visualised in different colours) of optimising the three objective functions of Bulk Crack Length Density for the three different SLM built, using the three different evolutionary algorithms, NSGA III, IBEA, GrEA, where a convergence process is revealed. The other two algorithms, IBEA and GrEA, give much faster convergence than NSGA III so that the convergence process is less easily seen (see Figure 6.13(c) and (e), no data points in red emerged). What is remarkable in all cases is that the final PF converges to a single point. It means that the objective functions (f_1, f_2, f_3) of Bulk Crack Length density of the three different products are not conflicting, and the optimised solution of the three functions is reached simultaneously. The final Pareto Front consists of one single value. See Figure 6.13(b), (d) and (f). Please note that there are around 210 non-dominated solutions in the decision space. See Section 6.7.4.1 for details. The indicator value Inverted Ratio of Net Avertence angle (IRNA) covered in Chapter 4 becomes 1.0 since only one data point of PF approximation exists.

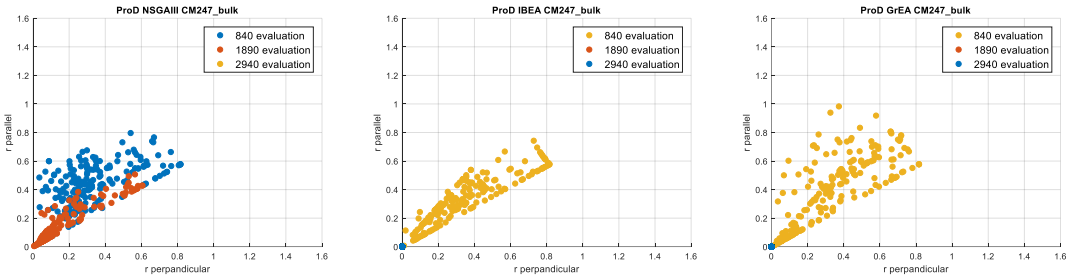

NSGA III IBEA GrEA

Figure 6.14 - The convergence process of multi-objective optimisation of Bulk Crack Length Densities of the three manufactured products is shown in ProD. NSGA III, IBEA and GrEA are used in the analysis.

1) Pareto front in ProD

As displayed in Figure 6.14, the final PF in ProD also shows the convergence to a single point. But the Pareto optimal solution set is spread to a larger area in decision space.

2) Decision Variables in ProD

The corresponding Pareto optimal solution set can also be rearranged in amounts of $r_{\perp}$ and $r_{\parallel}$ as similarly as it is done with objective functions in Chapter 5 and visualised in ProD:

$$r_{\parallel} = \boldsymbol{x}_i * \frac{\boldsymbol{RF}}{|\boldsymbol{RF}|} \quad \text{Eq. 6.9}$$

in which $\boldsymbol{x}_i$ is the Pareto optimal solution number i and $i = 1, 2, \dots, N$, and N is the number of data in the Pareto optimal set. $\boldsymbol{RF}$ is the reference vector which is defined as:

$$\boldsymbol{RF} = \boldsymbol{x}_{nom,max} - \boldsymbol{x}_{nom,min} \quad \text{Eq. 6.10}$$

where $\boldsymbol{x}_{nom,max}$ is the nominal maximum decision vector, a fictive vector consisting of the maximal components of all data in the Pareto optimal set and $\boldsymbol{x}_{nom,min}$ is a similar fictive vector, the nominal minimum decision vector, comprising the minimal components of the whole Pareto optimal set, respectively. The distance of a solution to the reference vector is expressed as:

$$r_{\perp} = |\boldsymbol{x}_i| \cdot sin\left(cos^{-1}\left(\frac{\boldsymbol{x}_i * \boldsymbol{RF}}{|\boldsymbol{x}_i| * |\boldsymbol{RF}|}\right)\right) \quad \text{Eq. 6.11}$$

The ProD visualising the decision variables is displayed in Figure 6.15. As can be seen, although the optimised PF solution is a single point, its corresponding decision variable values spread to a larger area, which is illustrated in blue colour. It means that many different combinations of the decision variable values can lead to the minimised Bulk Crack Length Density. The Pareto optimal solutions found using the three disparate algorithms are the same in the objective space. Suppose only the range of Pareto optimal solutions in decision space is considered. In that case, the algorithm that gives the broadest range of Pareto optimal set in the decision space is the best one, which shows a broader range of solutions. As shown in Fig. 6.15, IBEA provides more optimal solutions because they cover a larger area in the decision space.

A conclusion is made that it is relatively easy to obtain the optimised decision variable values for attaining Bulk Crack Length Density optimality, and the solution becomes stable and robust. The experimental data from the laboratory have confirmed the conclusion.

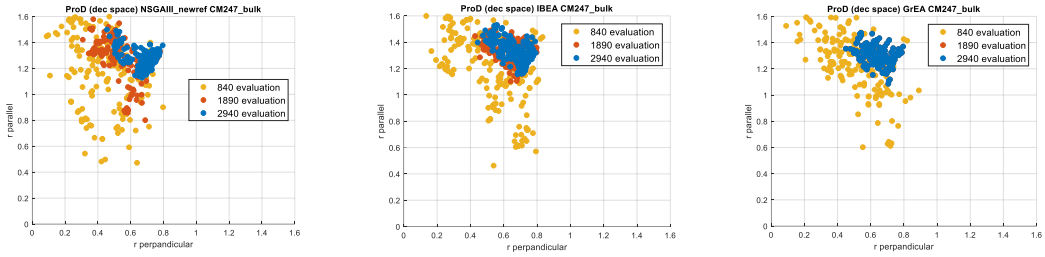

NSGA III IBEA GrEA

Figure 6.15 - The optimised decision variables are shown in Prod from the approximations using NSGA III, IBEA and GrEA for the MOP-BC case.

6.7.3.2 *MOP-Edge Crack Length Density Analysis (MOP-EC)*

1) Check on the effect of using the Bn-PFt method in diversity enhancement

The Bn-PFt method proposed in Chapter 3 is utilised to enhance the diversity of PF approximations found in NSGA III, a reference point based algorithm. Fig. 6.16 shows the PF approximation sets found by NSGA III with and without using the Bn-PFt method.

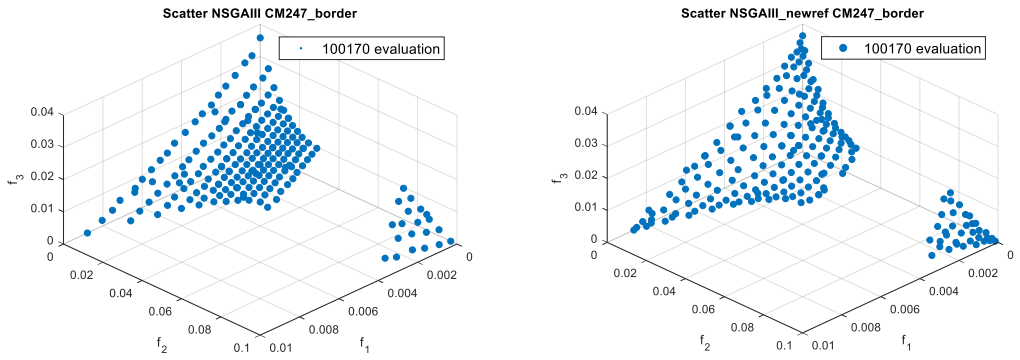

(a) NSGA III without Bn-PFt HV=0.9421 (b) NSGA III with Bn-PFt HV=0.9437

Figure 6.16 - The diversity of PF approximation sets found by NSGA III with/without Bn-PFt method implemented evaluated with HV metric.

As shown in Fig. 6.16, the PF approximation set with Bn-PFt implemented has a somewhat more uniform distribution based on visual observations.

Measured in hypervolume metric, the PF approximation set with Bn-PFt implemented is slightly better than its counterpart.

2) Pareto Front Approximation

The outcome of MOP analysis of the three edge crack length objectives from each of the three products is displayed in Figure 6.17. The result shows clearly the convergence process and a final PF that indicates the three objective functions are conflicting.

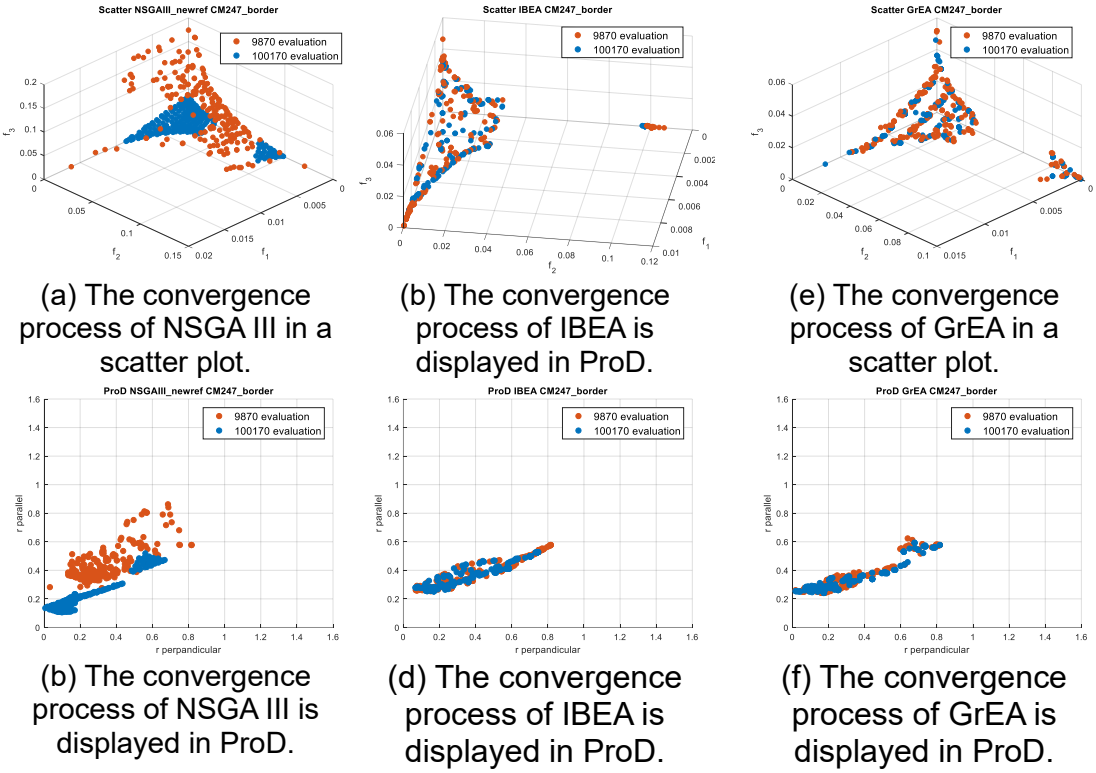

(a) The convergence process of NSGA III in a scatter plot.

(b) The convergence process of IBEA is displayed in ProD.

(e) The convergence process of GrEA in a scatter plot.

(b) The convergence process of NSGA III is displayed in ProD.

(d) The convergence process of IBEA is displayed in ProD.

(f) The convergence process of GrEA is displayed in ProD.

Figure 6.17 - The iteration process and the final PF approximation of MOP-EC are displayed based on NSGA III, IBEA and GrEA.

Each of all three algorithms reveals a PF in two clusters. Hence, a discontinuous PF is formed. NSGA III has shown a slower convergence speed because the approximations after 9670 iterations are far from the final PF (the brown dots in Fig. 6.17) compared with IBEA and GrEA. But NSGA III provides an approximation result with the best diversity, where the candidate solutions are spread more evenly over the entire PF. It is hard to judge which solution

diversity is better between IBEA and GrEA, but it can be done utilising IRNA and HV. See Table 6.7.

3) The Diversity Measurement

The diversity of PF approximations from the three MaOP algorithms is measured by the diversity indicator IRNA and HV. The result is listed in Table 6.7.

Table 6.7 - The IRNA scores on the PF approximations of NSGA III, IBEA and GrEA (MOP-EC)

Analysis case	Algorithm	IRNA	HV
The Edge Crack Length (MOP-EC) optimisation	NSGAIII	0.8290	0.9421
	IBEA	0.1929	0.9238
	GrEA	0.1841	0.9568

As revealed in Table 6.7, the approximation set attained in diversity using NSGA III is far superior to the other two algorithms in diversity in IRNA values. At the same time, HV favours too much the extremal solutions and provides the metric values that rank the PF of GrEA as the best algorithm delivering the PF in the best diversity. This conclusion is not in line with the visual observations. Hence, the results obtained by adopting NSGA III are studied in more detail. Figure 6.18 shows the final converged PF from NSGA III calculation, consisting of two clusters. A larger one at the higher f_1 and the lower f_2 function ranges (f_1 is the test piece no. 1, a solid cube and f_2 is the test piece no. 2, a slotted box with thin flaps of 2 mm thickness), and a smaller one at a higher f_2 function values and lower f_1 and f_3 function values (f_3 is the objective function of sample 3 - thick flaps in 5 millimetres thickness). It is also reflected on the ProD figure, see Figure 6.18 (b).

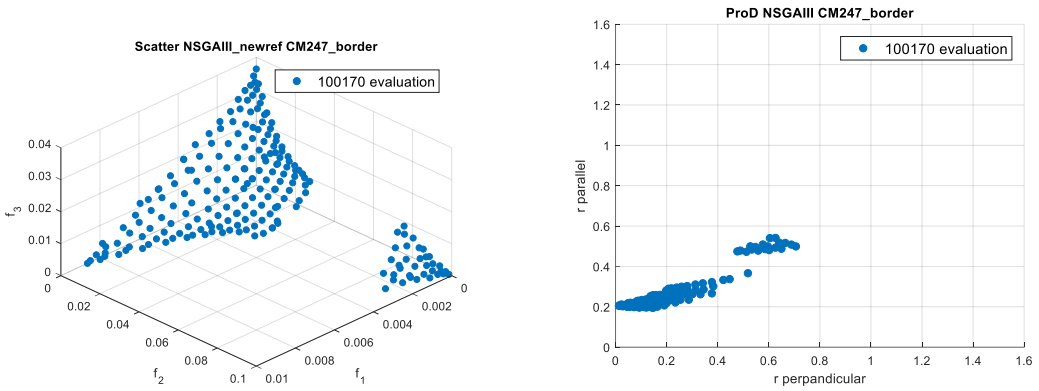

(a) The final PF approximation (b) The corresponding PF in ProD

Figure 6.18 - The final PF displayed in NSGA III

4) The results for decision variables

Figure 6.19 reveals the pairwise scatter plots of the decision variables at optimality. Two small regions of the optimised solutions in decision variables are evident. The same conclusion can be made when observing the results of decision variables in ProD, see Figure 6.19. Two small regions also emerge, representing the optimised operational conditions of the process parameters. It coincides with what is observed in the scatter plots of the objective functions shown in Figure 6.12 for objective 3, in which two pits appear in the landscape of the function and the scatter plots in Figure 6.18. It is interesting to note the narrow regions of optimal solutions.

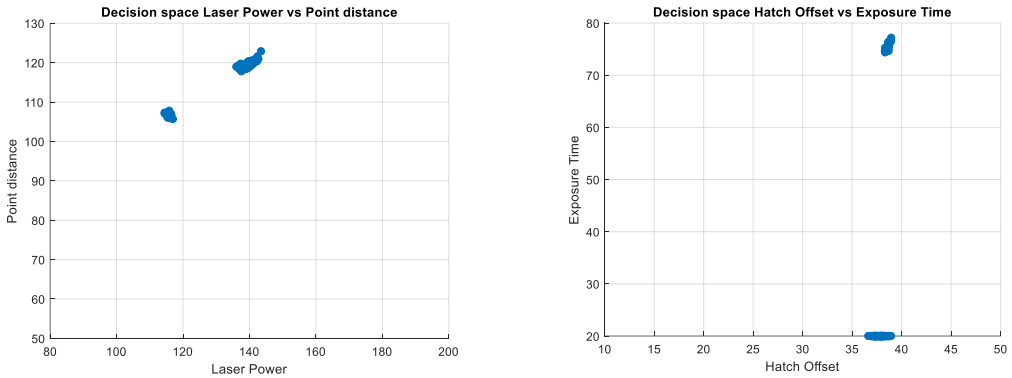

(a) Laser power and point distance at the optimum. (b) Hatch offset and exposure time at the optimum.

Figure 6.19 – The scatter plots showing the values of process parameters/decision variables at the optimum after 10,0170 iterations.

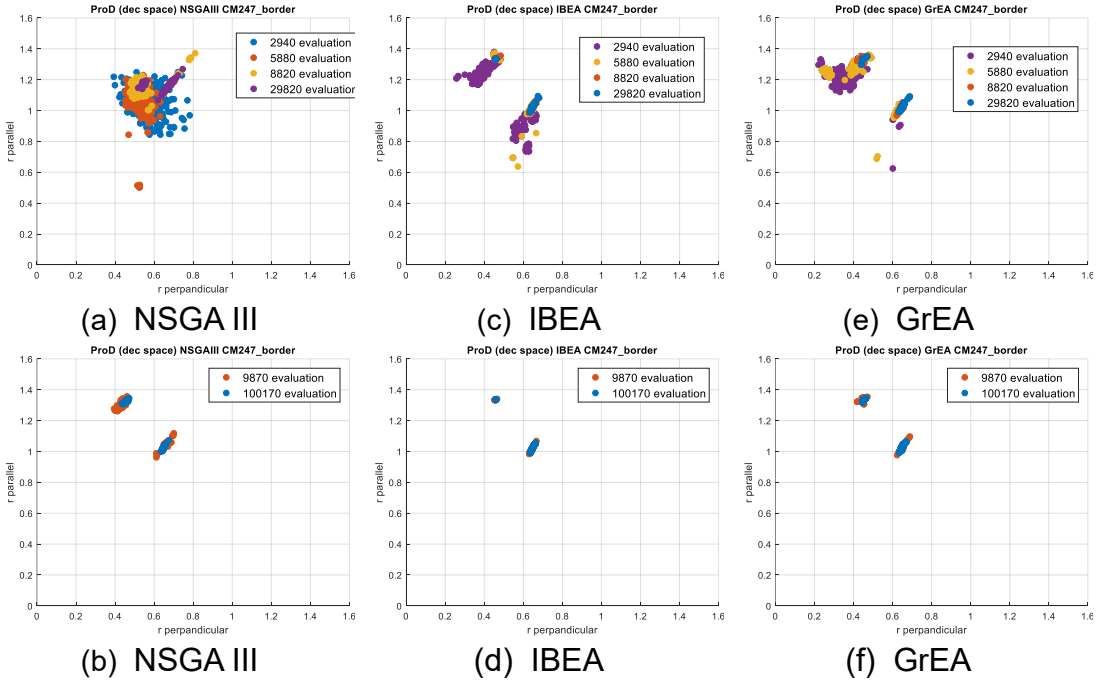

Figure 6.20 - The contraction of the area of optimality in decision space as convergence progresses. Figure 6.19 (a),(c),(e) show the contraction of the area of optimality in decision space as the convergence undergoes. Figures (b),(d),(f) show the area of optimality in decision space after 100170 iterations.

Figure 6.20 shows the contraction of the areas representing the optimised conditions for decision variables as the iteration number increases. It reveals that the area is conjoint in the early stages of the approximations. It contracts further as the number of iterations increases, and then the solution separates, and the previously joined area is split into two distinct regions, see Figure 6.20(a). The two regions further contract as the number of iterations go up. See Figure 6.20(b). All three applied algorithms lead to the same conclusion. The good news is that the location of the contracting area of optimality in decision space is in the same area, not spreading out to a large part of decision space, indicating qualitatively better robustness of the solution, i.e., the reduction in optimality is limited when deviations occur on the decision variables.

6.7.3.3 *Bulk Crack and Edge Crack Length Density in the combined analysis (MaOP-BEC)*

We now combine the six objective functions and optimise them simultaneously. These are Bulk Crack Length density (f_1, f_2, f_3) and Edge Crack Length density (f_4, f_5, f_6) valid for the three products constructed, respectively, forming a total of six objectives to be optimised subject to the four decision variables: the laser power (x_1), the point distance (x_2), the hatch offset (x_3), and the exposure time (x_4).

1) Pareto front approximation and corresponding decision space solutions

No significant change in convergence or diversity of the approximations is observed from an iteration number of 270,000 to 2,700,000, indicating the convergence process is completed, see Figure 6.21, where small changes take place from the yellow to purple dots.

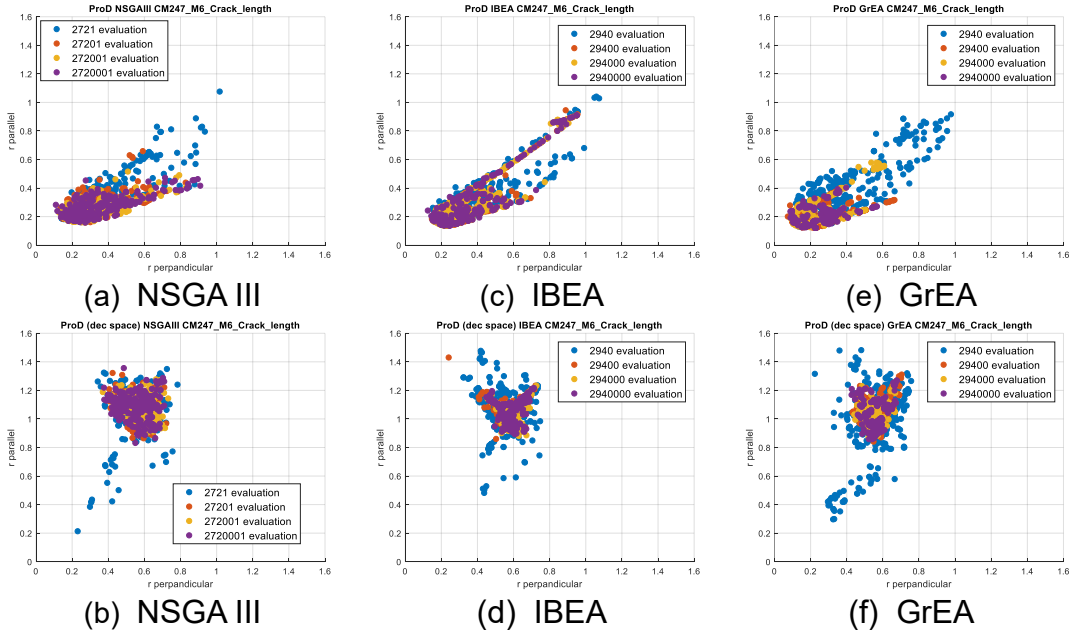

(a) NSGA III (c) IBEA (e) GrEA

(b) NSGA III (d) IBEA (f) GrEA

Figure 6.21 - The convergence process of 6 objective MaOP-BEC, where objectives of bulk crack length and edge crack length are combined. Figure (a),(c),(e) show the convergence process of MaOP-BEC. Figure (b),(d),(f) show the decision variables in ProD.

The Pareto optimal set from NSGA III is more densely populated and concentrated in a small area than the case of the other two algorithms. See Figure 6.21(b), (d) and (f). Hence, it is proposed to choose a set of decision variables originating from the central and most densely populated areas in ProD of decision variables if the optimised operating conditions are to be found. The reasoning for this choice is that the values of the decision variables are still inside the areas of near-optimal and is more stable subject to eventual uncertainty that would occur on these decision variables.

2) Diversity Assessment

The diversities of PF approximations are measured by the IRNA and HV indicators. See Table 6.8.

Table 6.8 - The IRNA and HV scores on the PF approximations of NSGA III, IBEA and GrEA (MOP-BEC)

Analysis case	Algorithm	IRNA	HV
The Edge Crack Length (MaOP-BEC) optimisation (6 objective functions.)	NSGAIII	0.1765	0.9307
	IBEA	0.0733	0.9186
	GrEA	0.0669	0.8941

As shown in Table 6.8, the PF approximation set of NSGA III has the best diversity in IRNA and HV. Still, the IRNA value is more distinct than the HV metric quantity in judging the diversity property. Therefore further analysis of the optimisation problem is based on the results from NSGA III.

6.7.4 The Choice of Optimised Decision Variables

It is nontrivial to give the optimised value ranges of the decision variables, especially for high dimensional cases. In the current study, the number of decision variables is four, and the optimised combination of the decision variables is difficult to be displayed in a scatter plot. One mitigation could be that the optimised decision variable sets are plotted in Parallel Coordinates. The range of each decision variable and its combinations can be revealed.

6.7.4.1 *The Bulk Crack Length Optimisation Case (MOP-BC)*

Figure 6.22 shows the optimised process parameters when the objective functions of the Bulk Crack Length of the three products are optimised. As can be seen, the upper limit of the range of laser power is somewhat uncertain. More candidate solutions are needed in this area before a firm conclusion can be made.

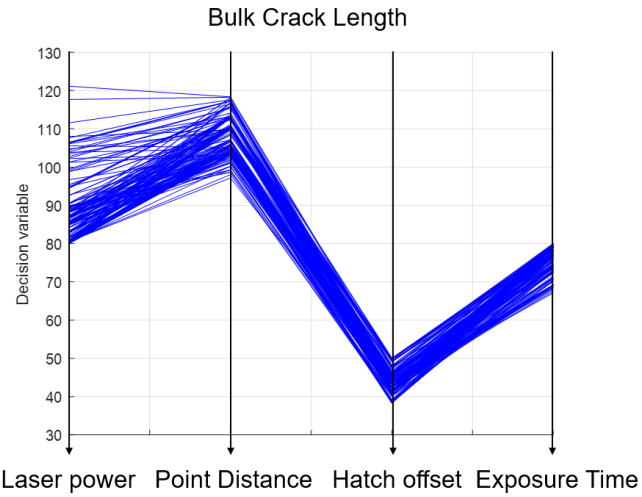

Figure 6.22 - The decision variables displayed in Parallel Coordinates show their ranges of optimised values, MOP-BC case based on NSGA III results.

Table 6.9 - The range of optimised process parameters, MOP-BC

	Laser power	Point Distance	Hatch offset	Exposure Time
max	122	118.4	50	80
min	80	97.2	38.3	67.1

6.7.4.2 *The Edge Crack Length Optimisation Case (MOP-EC)*

The optimised process parameters in the MOP-EC case consist of two ranges except for the range of Hatch Offset, which emerges as one range. See Figure 6.23.

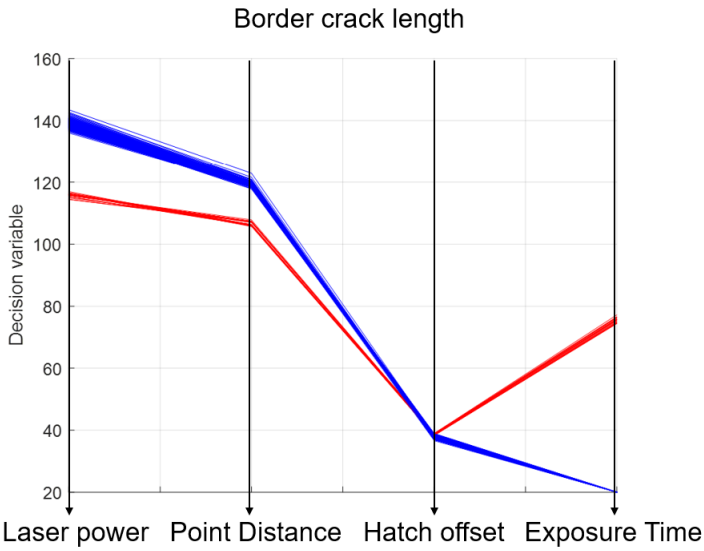

Figure 6.23 - The decision variables displayed in Parallel Coordinates show their ranges of optimised values, MOP-EC case based on NSGA III results. The areas in blue and red colours: Pareto optimal solutions corresponding to the larger and the smaller clusters of PF, respectively.

The figure also reveals that the combinations of values of process parameters are essential to ensure the trade-off optimality of the objective functions. The two ranges of Pareto optimal solution, indicated by the red and blue colours, corresponding to the larger and the smaller clusters of PF, respectively, are listed in Table 6.10 and Table 6.11. As a verification, the mid-level process parameter values of range 1 (blue line in Figure 6.24) are chosen. The values of the corresponding objective functions are found and plotted in the PF. It shows that the candidate solution is located on the PF (the red spot shown in Figure 6.24(b)).

Table 6.10 - The range of optimised process parameters, MOP-EC,

Redline	Laser power	Point Distance	Hatch offset	Exposure Time
max	116.9	107.8	38.9	77.2
min	114.5	105.7	38.4	74.3

Table 6.11 - The range of optimised process parameters, MOP-BC

Blueline	Laser power	Point Distance	Hatch offset	Exposure Time
max	143.5	122.8	38.9	20.03
min	136	117.8	36.6	20

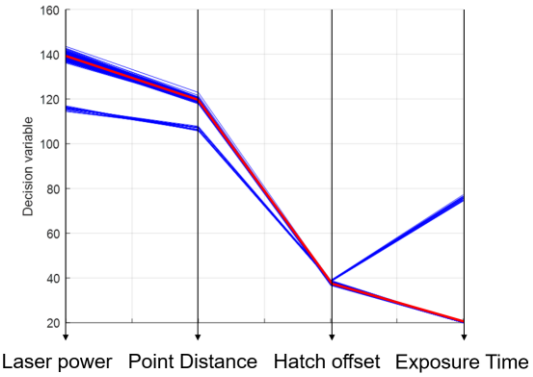

(a) The mid-level process parameters in the first range are chosen.

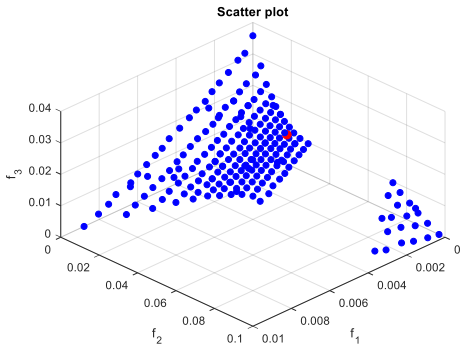

(b) The red spot represents the constructed solution

Figure 6.24 - The decision variables displayed in Parallel Coordinates show their ranges of optimised values, MOP-EC case.

6.7.4.3 *The Bulk and the Edge Crack Length Optimisation Case (MaOP-BEC)*

Figure 6.25 shows the process parameters of the combined Bulk and Edge Crack Length optimisation case.

As can be observed, the upper limit of the laser power range is somewhat uncertain. More solutions on the optimised objective functions are needed, and also the related decision variables. The ranges of process parameters are listed in Table 6.12.

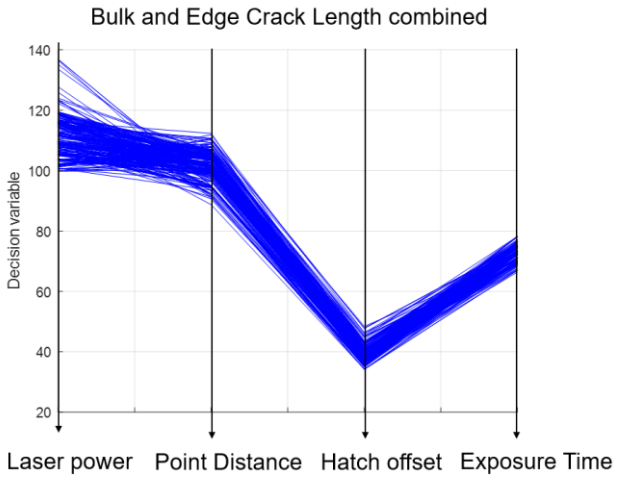

Figure 6.25 - The decision variables displayed in Parallel Coordinates show their ranges of optimised values, MaOP-BEC case.

Table 6.12 - The range of optimised process parameters, MaOP-BEC

	Laser power	Point Distance	Hatch offset	Exposure Time
max	136.8	112.3	48.4	78.2
min	99.7	88.7	34.1	66.3

6.8 Validation Tests and Veracity of the MOP Analysis

New tests are conducted to examine the variances in the edge crack length density measurements. Validation tests have been performed using the same experimental layout as previously but achieved in a separate round. Two additional test groups have been conducted. One test set resulting in 6 data samples is executed employing the same process parameters as some of those chosen previously to identify the amount of the deviations in the results. It is done because the crack formation mechanism is highly complicated, especially on the edges of objects where large temperature gradients occur and the cyclic thermal stresses reach their maximum. The outcomes of the experiments are thus complicated to be modelled with high certainty. The other set of tests, also providing 6 data samples, are carried out to verify the efficacy of the MOP analysis. These tests are accomplished using optimised machine settings identified using the PF solutions of the MOP analysis in the decision space (parameter space). Despite the significant variances in the test data, the MOP analysis may still help the decision-makers choose optimised machine settings (process parameters).

6.8.1 Results of Duplicated Tests for Edge Crack Length Density

Six new data samples of edge crack length density are obtained using the same machine settings as those of the corresponding previous tests. The chosen machine settings are listed in Table 6.13, and the corresponding measured objective function values (the edge crack length densities) are shown in Table 6.14.

Table 6.13 - The chosen machine settings (decision variables) for tests of edge crack length density

Sample ID	Laser Power, x_1	Point Distance, x_2	Hatch Offset, x_3	Exposure Time, x_4
30	110	70	40	35
37	170	110	20	65
42	80	90	30	50
44	140	50	30	50
46	140	90	10	50
50	140	90	30	50

Table 6.14 - Comparisons of edge crack lengths from the previous and duplicated experiment tests

	Measured Border Length Density (mm/mm²) (Data set 1)						Difference between the two experiment		
	Previous Test			Duplicated Test					
Sample ID	Objective No.			Objective No.			Objective No.		
	1	2	3	1	2	3	1	2	3
50	1.332	1.37	1.719	0.646	1.328	1.214	0.686	0.042	0.505
37	4.502	3.737	3.782	1.524	2.899	3.018	2.978	0.838	0.764
44	1.469	1.675	1.636	0.729	1.114	1.515	0.740	0.561	0.121
42	2.322	3.927	2.519	1.443	2.45	1.894	0.879	1.477	0.625
46	1.702	1.949	1.542	0.422	0.778	0.752	1.280	1.171	0.790
30	3.181	2.416	1.598	2.216	2.78	2.653	0.965	0.364	1.055

As can be observed from Table 6.11, large deviations in the edge crack length density data between the two rounds of tests exist, confirming the complexity of the problem studied. It is visually displayed in Fig. 6.25.

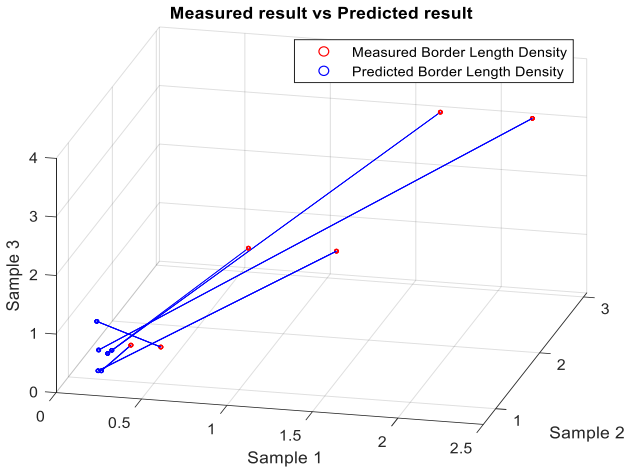

Fig. 6.25 Comparisons between the original test data (blue dots) and the validation data (red dots), where the comparable data points are linked with straight lines.

Interestingly, the duplicated test of No. 46 gives extremely low edge crack length densities (marked in yellow).

Table 6.15 lists a set of six machine parameter settings selected based on the Pareto optimal solutions from the MOP analysis, which are collected based on six chosen points on the approximated PF and the corresponding Pareto optimal solutions in the decision space are identified. A comparison between the experimentally achieved and the predicted edge crack length densities are shown in Table 6.16.

Table 6.15 - Data of decision variables chosen based on the suggestion from MOP analysis

Sample ID	Laser Power	Point Distance	Hatch Offset	Exposure Time
108	135.8	117	36	20
109	122.7	93	35	70
110	118.3	106	39	70
111	127.9	113	35	20
112	152.9	106	14	20
113	116.5	107	39	80

Table 6.16 - Comparisons of data between the predicted and the experiment results

Sample ID	Predicted border crack length (mm/mm²)			Measured border length (mm/mm²)			Difference between the two experiments		
	Objective No.			Objective No.			Objective No.		
	1	2	3	1	2	3	1	2	3
108	0.232	0.774	0.371	1.251	2.234	1.242	1.019	1.46	0.871
109	0.218	0.841	0.659	2.182	3.071	2.913	1.964	2.23	2.254
110	0.218	1.044	0.405	1.77	2.58	3.398	1.552	1.536	2.993
111	0.249	0.781	0.367	0.438	0.719	0.906	0.189	0.062	0.539
112	0.217	0.802	1.185	0.58	0.848	0.781	0.363	0.046	0.404
113	0.219	1.137	0.371	0.814	1.93	1.488	0.595	0.793	1.117

Extreme variations in the experimental data and large deviations exist between the predicted values and the experimental data. Remarkably, the test sets of No. 111 and 112 provide the results (marked in yellow) that surpass all other values on the three manufactured objects. It is verified by applying a non-dominated sorting operation on these data, and most of the solutions are inferior to the two data sets.

6.8.2 The error estimates of surrogate models using the validation data

The modelling errors are analysed using the validation data and expressed in error metrics: the root mean square error ($RMSE$), the maximum absolute error (*MaxAE*) and the coefficient of determination (R^2), which are formulated in Eqs. 6.6 – 6.8. The results are listed in Table 6.16.

Table 6.17 The error metric values for the various surrogates based on the validation data

Error metric	f_1	f_2	f_3	f_4	f_5	f_6
$RMSE$	0.5060	1.0251	0.9941	1.2065	1.1829	1.0991
MaxAE	1.1241	1.9416	1.8083	1.3533	2.2131	2.5573
R^2	-1.4191	-0.2238	-1.4997	-2.6981	-0.9244	-0.4824

As the error metric values reveal, extreme variations exist in the validation data. $RMSE$ values show more than 100% deviation, while *MaxAE* quantities

display values from more than 100% to more than 250%. The worst of all, the R^2 results turn to be negative for all objectives. All these imply no functional relationship between these data and the surrogate models. A conclusion is thus made that it is not viable to compare the test results from disparate rounds of the experiment. And there might be other governing process parameters that are not fully understood and influence the SLM operations.

6.9 Discussions

As discussed in Section 6.6, the surrogate models created based on the primary experimental data work satisfactorily, although considerable uncertainty exists. But the validation test reveals that the existing surrogate models cannot describe the new results accurately. See section 6.8. Data from different trials of experiments are inconsistent, and the experiment is difficult to be repeated. Other factors may influence the outcome, such as ambient temperature, humidity, under what testing instants the data are gathered, uncertainty in the measurements, raw material quality variations, etc. Further studies should be conducted to identify these unknown conditions by conducting various test runs under the same experimental setting. The optimisation analysis on the SLM process is still practical when the outcome guides the parameter selection online within the same experimental setting and operation.

The optimisation analysis should be conducted multiple times to assess the uncertainties related to the optimisation operation since the methodologies adopted are stochastic. This could be done in future work so that the conclusions of this thesis can be confirmed further. On the other hand, the uncertainty in the actual process may be too large for conclusive analysis on the performance of the optimisation; one can therefore look into estimating and using uncertainty to enhance the optimisation performance. Moreover, the lack of sufficiently large experimental data makes developing better surrogate models difficult. More experimental testing should therefore be needed in the future. Further, the surrogate model management should be enhanced using techniques discussed in Section 2.2.2.5.

The surrogate model may result in non-optimal operational conditions without considering the prediction uncertainty. Hence, a necessary analytical

step is quantifying the combined effect of uncertainties in the design variables, model parameters, and surrogate models on optimality. The uncertainties in the surrogate model could be handled by the optimization process using robust optimization (RO) methods, where the Pareto optimal solutions are obtained that are both optimal and relatively insensitive to input, parametric and model uncertainties [29]. This is beyond the scope of the thesis, hence not addressed.

Two types of RO methods are available: deterministic approaches and probabilistic approaches. In deterministic approaches, the robustness of the optimality is analysed by inserting the prescribed non-statistical variation ranges of various variables and gradient information into the original optimization problem. The analysis is done based on extreme variations of all variables, which might be improper when finding the true robust optimality. In probabilistic approaches, RO is performed based on optimisations such as the expectations and the variances of the original objective functions expressed utilising the probability distributions of the variations of the decision variables, process parameters and variance of the surrogate model itself. The main procedure of a representative probabilistic approach is discussed as follows.

1) The optimisation problem formulation:

$$\begin{aligned} &Min\ \boldsymbol{F}(\boldsymbol{X}) = \left\{\mu_i\left(f_i(\boldsymbol{X},\boldsymbol{V})\right) + c\sigma_i\left(f_i(\boldsymbol{X},\boldsymbol{V})\right)\right\},\ \ i = 1,2,\dots,m \\ &\text{Subject to } G_j(\boldsymbol{X},\boldsymbol{V}) = \mu_j\left(g_j(\boldsymbol{X},\boldsymbol{V})\right) + c\sigma_j\left(g_j(\boldsymbol{X},\boldsymbol{V})\right) \le 0, \\ &\qquad j = 1,2,\dots,j \quad \boldsymbol{x} \in (\Omega,T,P) \subset R^n \end{aligned} \qquad \text{Eq. 6.12}$$

where $\boldsymbol{F}(\boldsymbol{x})$ is the objective function vector; $\boldsymbol{X}$ is the stochastic decision variable vector (plus eventual stochastic model parameter vector which can be treated similarly as it is done with the stochastic decision variables, if it needs to be taken into consideration); $\boldsymbol{V}$ represents the uncertainty of the MF surrogate

model itself; $\mu_i\left(f_i(\boldsymbol{X},\boldsymbol{V})\right)$ is the expectation and $\sigma_i\left(f_i(\boldsymbol{X},\boldsymbol{V})\right)$ is the deviation of the objective function i, respectively; the parameter c is a customer chosen constant that relates to the significance level of the analysis (for instance, $c=3$ corresponds to a significance level of 0.9987); (Ω,T,P) is the probability space, described with such as expected value, deviation and probability density, etc.; $\mu_j\left(g_j(\boldsymbol{X},\boldsymbol{V})\right)$ is the expectation and $\sigma_j\left(g_j(\boldsymbol{X},\boldsymbol{V})\right)$ is the deviation of j^{th} constraint, respectively; $k,m,n\ and\ J$ are the number of model parameters, objective functions, decision variables and constraints, respectively.

2) Random analysis of the design variables:

X_i is expressed as:

$$X_i = x_i + W_i,\ i=1,2,\dots,n \qquad \text{Eq. 6.13}$$

where x_i is the deterministic part of X_i and W_i is the stochastic part. It assumes the stochastic independence of the decision variables and W is normally distributed $N(0,\sigma_{x_i})$, which means:

$$E(W_i)=0,\ Var(W_i)=\sigma_{x_i},\ and\ Cov\left(W_i,W_j\right)=0,\ \text{for}\ j\neq i \qquad \text{Eq. 6.14}$$

X_i follows a multivariate normal distribution $N(x_i,\sigma_{x_i})$.

Based on the three-sigma quality principle,

$$\sigma_{x_i}=\frac{\overline{x_i}+\Delta x_i-(\overline{x_i}-\Delta x_i)}{6}=\frac{\Delta x_i}{3} \qquad \text{Eq. 6.15}$$

in which Δx_i is the tolerance of decision variable X_i, which is determined experimentally.

3) Random analysis of the uncertainty process parameters

The randomness of process parameters such as the physical and mechanical properties of materials is described by the parameters' probability density functions, based on which a simulated sample of the corresponding random

process parameter can be estimated. The randomness of process parameters can be treated similarly to the random decision variables.

4) Generation a random decision variable

The random values of a decision variable x_i can be found by the acceptance-rejection sampling method; randomly chosen two numbers r_{i1} and r_{i2} from a uniform distribution on the interval [0, 1]:

$$x_i = r_{i1}\left(x_{i,max} - x_{i,min}\right) + x_{i,min} \quad \text{Eq. 6.16}$$

If $r_{i2} \leq \frac{p(x_i)}{p_{x_i,max}}$, then x_i is accepted as the chosen random decision variable. If not, reselect r_{i1} and r_{i2}, and repeat the random selection of r_{i1} and r_{i2}.

5) Expectation and deviation of objective functions

The expectation $\mu_i\left(f_i(\boldsymbol{X},\boldsymbol{V})\right)$ and the standard deviation $\sigma_i\left(f_i(\boldsymbol{X},\boldsymbol{V})\right)$ of the objective function $f_i(\boldsymbol{X},\boldsymbol{V})$ are given as [7]:

$$\mu_i\left(f_i(\boldsymbol{X},\boldsymbol{V})\right) = E[Y_i(\boldsymbol{X},\boldsymbol{V})] = \int_w \hat{y}_i(\boldsymbol{x}+\boldsymbol{w}) \cdot p(\boldsymbol{w}) d\boldsymbol{w} \quad \text{Eq. 6.17}$$

where $Y_i(\boldsymbol{X},\boldsymbol{V})$ is the stochastic response function i; $\hat{y}_i(x+w)$ is the surrogate model i; $p(\boldsymbol{w})$ is the cumulative probability density function. When the random parameters $w_i, i = 1, 2, \ldots, n$ are independent:

$$p(\boldsymbol{w}) = \prod_{i=1}^{n} p(w_i) \quad \text{Eq. 6.18}$$

in which $p(w_i)$ is the marginal probability density function of w_i.

$$
\begin{aligned}
&\sigma_i^2\big(f_i(\boldsymbol{X},\boldsymbol{V})\big)\\
&= Var[Y_i(\boldsymbol{X},\boldsymbol{V})]\\
&= E\big[Var[Y_i(\boldsymbol{x}+\boldsymbol{w},\boldsymbol{V})|\boldsymbol{V}]\big] + E[E[Y_i(\boldsymbol{x}+\boldsymbol{w},\boldsymbol{V})|\boldsymbol{V}]^2] - E\big[E[Y_i(\boldsymbol{x}+\boldsymbol{w},\boldsymbol{V})|\boldsymbol{V}]\big]^2\\
&= \int_w s^2(\hat{y}_i(\boldsymbol{x}+\boldsymbol{w}))\cdot p(\boldsymbol{w})d\boldsymbol{w} + \int_w \hat{y}_i{}^2(x+\boldsymbol{w})\cdot p(\boldsymbol{w})d\boldsymbol{w}
\end{aligned}
\qquad \text{Eq. 6.19}
$$

$$
-[\int_w \big(\hat{y}_i(\boldsymbol{x}+\boldsymbol{w})\big)\cdot p(\boldsymbol{w})d\boldsymbol{w}]^2
$$

where $s^2(\hat{y}_i(\boldsymbol{x}+\boldsymbol{w}))$ is the mean square error (MSE_i) of the surrogate model i.

Eqs. 6.17 and 6.19 can be solved numerically using the Monte Carlo integration method.

6.10 Summary and Conclusions

The modelling and analysis of crack formation in the SLM process on those formed along or around edges of objects made of the nickel superalloy CM247L are intricate. CM247L is a material with high strength, thermal stability, good corrosion resistance, etc., and is commonly used in critical aerospace applications. The material is sensitive for microcrack formation in manufacturing using the SLM process, although it possesses exceptional properties. Mastered the behaviour of this material after 3D printing would be essential to the aerospace industry. The analysis has been done in this chapter using multi- and many-objective optimisations on data-driven crack formation models to the four chosen main process parameters: laser power, point distance, hatch offset, and exposure time, targeting on finding the optimal process condition. The analysis results reveal that it is relatively easy to achieve optimised operational conditions with minimised bulk crack formation because the range of the optimal process parameters is extensive. But it is much harder to identify such optimised operational parameters for minimising the edge cracks since their corresponding ranges are narrow.

The obtained Pareto Front approximations have been enhanced in diversity by adopting the newly developed methodology, Bn-PFt (see Chapter 3 of the thesis). Analysed by IRNA (see Chapter 4), the algorithm NSGA III turns out to provide the best quality of solution set in diversity among the three chosen algorithms: NSGA III, IBEA and GrEA in handling the current optimisation problems.

ProD has been used to visualise PF approximations in objective space and reveal clusters of the optimised solutions of the process variables in the decision space.

The PF of MOP bulk crack length density optimisation consists of a single point, which means the objective functions are not conflicting. Interestingly, the optimised range in decision space covers a wide area, indicating many combinations of process parameters may result in optimality – the minimised bulk crack length density. It also means that finding proper process parameters by which the minimised formation of bulk cracks is a relatively easy task.

The PF of MOP edge crack length density optimisation forms a convex front and indicates conflicting objective functions. The corresponding optimised process parameters are located in two narrow regions, visualised in 2D scatter plots and ProD. It is more challenging to find optimised process parameters than minimising bulk cracks. A choice might be less reliable due to the narrow range for optimality and the current uncertainty in the process parameters. On the other hand, the optimal and less optimal Pareto solutions are clustered in and around a similar location in the decision space, indicating a limited reduction in optimality when decision variables deviate from their optimal values. It means that the solutions can be robust in a qualitative sense.

The ProD reveals that the PF from the simultaneous optimisation of all three bulk crack and edge crack objective functions has an unsymmetric convex type in the objective space. The corresponding area of optimised process parameters in decision space is clustered but spread to a larger region than the separate MOP crack cases analysed, indicating a compromise in minimising crack length in bulk and at edges simultaneously.

By plotting the optimised process parameters in Parallel coordinates, the estimates of ranges of optimised process parameters have been attained.

The results from validation tests are disappointing. The values of error metrics confirm no functional relationship between the surrogate models and the data from the validation test. It means that the experiments are hard to be

repeated in disparate rounds of tests, although the settings are seemingly the same. Other governing parameters regulate the relationship.

The application chapter, Chapter 6, has demonstrated an optimisation study on real case problems targeting finding the optimised process parameters of an operation, from experimental testing, modelling to process optimisation, and identifying the optimised governing process parameters.

As future work, some more experimental work should be performed to identify and clarify additional governing process parameters which may explain the extreme variation of test data from disparate rounds of experiments. Moreover, a stochastic robust optimisation analysis is performed to verify the influence of uncertainty on the setting of the optimal operational conditions.

Chapter 7 Conclusion and Future Work

The difficulty of solving MaOP increases drastically with the rise of the number of objectives to be optimised beyond three, where several challenges emerge affecting the design of optimisation algorithms:

1) The number of Pareto optimal solutions needed to describe the PF grows nearly exponentially.
2) The dominance relation used in environmental selection becomes less discriminative, i.e., two arbitrary solutions are more likely to be mutually non-dominated.
3) The possible search directions to obtain an approximation of the Pareto front increase, complicating the search towards the optimality.
4) The visualisation of an optimiser's search performance becomes difficult and inevitably leads to a loss of Pareto dominance relation information between solutions since mapping a higher-dimensional space to a 2, or 3-dimensional space takes place.
5) The number of preference parameters grows quadratically when expressed to each pair of objectives in preference-based algorithms.
6) Evaluation of the performance of PF solutions becomes more challenging. Some often used indicators are also costly to calculate computationally, such as the hypervolume, and it complies with comparing sets of points based on the dominance relation.

7) Distances between weight vectors in decomposition-based MOEAs increase so that the assumption that the neighbouring sub-problems share similar information becomes less prominent, which reduces the performance of decomposition-based MOEAs for many-objective problems.

8) The distance between neighbouring solutions on PF turns out to be so large that it becomes more challenging to identify high-quality Pareto optimal solutions.

Uncertainty analysis in applications of many-objective optimization is an important issue and is handled by robust optimization (RO) methods. The surrogate model may result in non-optimal operational conditions without considering the prediction uncertainty. Hence, a necessary analytical step is quantifying the combined effect of uncertainties in the design variables, model parameters, and the surrogate models on optimality. The Pareto optimal solutions obtained should be both optimal and relatively insensitive to input, parametric and model uncertainties. Two types of RO methods are available: deterministic approaches and probabilistic approaches. In deterministic approaches, the robustness of the optimality is analysed by inserting the prescribed non-statistical variation ranges of various variables and gradient information into the original optimization problem. The analysis is done based on extreme variations of all variables, which might be improper when finding the true robust optimality. In probabilistic approaches, RO is performed based on optimisations such as the expectations and the variances of the original objective functions expressed utilising the probability distributions of the variations of the decision variables, process parameters and variance of the surrogate model itself.

The current thesis deals with three significant challenges in a MaOP analysis. First, equidistant reference points on the searched Pareto Front of arbitrary form are required but nontrivial to be created as the number of objectives rises. Second, evaluation of the quality of Pareto front approximations in a high number of objectives is nontrivial. Third, visualisation of the high dimensional solutions is problematic. Mitigation of the above difficulties is part of the main tasks of the thesis work. Three new methods are proposed. Comprehensive numerical studies have been performed to validate the new methodologies. In addition, all new methods and their related algorithms have been used in a real-life application: optimisation analysis on a selective laser melting operation. The outcomes show that the proposed methods can enhance MaOP study in diversity, solution evaluation and visualisation.

7.1 Generating and Indexing Reference Points in MaOP Analysis

The decomposition-based MaOP algorithms belong to an influential group of solution techniques in optimisation problems of a high number of objective functions. The convergence toward Pareto Front occurs along with a set of systematically generated and most possibly evenly distributed reference vectors or reference points in the feasible high dimensional objective space. The evenness of the reference vectors created is vital for achieving PF approximations in superior diversity. As it is of the current version, the method is restricted to fully covered PF shapes in objective space, although it improves the diversity of discontinuous PFs. Its effect is questionable when used to handle degenerated PF types.

A new method of generating reference points is proposed, B-norm based PF tracking method (Bn-PFt). The reference points are more evenly created on an m dimensional B-norm surface created adaptively by tracking the actual PF. Numerical studies performed on B-norm surfaces of various B values show that reference points created by the Bn-PFt method are more evenly distributed on PF than those projected onto the same surfaces generated using Das and Dennis method. Simulation results, using RVEA to the Benchmark problems of MaF1-7 and 10-11 with 3 and 5 objective functions, show that measured in HV, IGD, Δ, CPF and SP metrics, the approximation sets obtained using reference points of Bn-PFt method have better diversity than those of using the famous Das and Dennis method. Crucially, the proposed method generates better results in terms of diversity. Reference points created by the Bn-PFt method with B=1 (unit simplex plane) have the exact location and distribution as those

of the Das and Dennis method. In other words, the Das and Dennis method is a particular case of the proposed Bn-PFt method, which is the general case.

A new indexing system of reference points is also proposed to ease algorithmic development in decomposition-based evolutionary computation. The indexing system can enhance the formulation of the Das and Dennis method, save computing resources when searching for a specific reference point, define neighbouring reference points to a particular point in high dimensional objective space, and help facilitate the work on algorithmic development of new methods.

The B-norm surface curve used in this study is symmetric in m dimensional objective space, which is most suitable for tracing PF of approximately symmetric forms. For strong non-symmetric or degenerated PFs, the reference points created by the Bn-PFt method are out of the surface of the true PF. Their projections on the true PF are hampered somewhat when these are projected on the true PF. However, they are still more suitable to guide the search for PF than the Das and Dennis method because they locate much nearer to the true PF than the latter.

In the future, more studies can focus upon the following aspects:

- The bn-PFt method should be expanded to create the most possibly equidistant reference points on non-symmetric PF surfaces.
- Further, formulation using the proposed indexing system to identify neighbouring direct points to a given reference point in high dimensional space shall be studied. It can replace the user input parameter – the number of adjacent points in the MOEA/D algorithm.

7.2 A New Pure Diversity Indicator-IRNA

Well converged and evenly distributed Pareto Front approximations provide the utmost information to decision-makers in the decision-making process. PF solutions in high dimensions (more than three objective functions involved in the optimisation process) are often intricate to be accessed quality-wise in forms of their convergence and diversity properties. It is because of the limited cognitive capability of humans for the recognition of features visually in high dimensional space. A new diversity indicator is proposed in this work, the Inverse Ratio of Normalised Avertence angles (IRNA). It is a pure diversity indicator for evaluating high dimensional PF approximations and is formulated using reference vectors by minimising the sum of the included angles between approximated solution set and reference vectors. It is achieved by rotating the system of reference vectors in all dimensions with an optimised spatial angle. The highest possible diversity score of a solution set is obtained. Any potential systematic bias in the avertence angles is thus removed. Through various numerical testing, it is proven that IRNA is more sensitive to capturing diversity changes than other state-of-the-art performance indicators, also as the number of objectives increases, thus deeming it particularly suitable for many-objective optimisation problems. In addition, as suggested in this work, is two new methods in contrasting the efficacy and efficiency of diversity indicators in general. One is to test the indicators by analysing the PF approximations when increasing the number of objectives of the benchmark problem while keeping the number of candidate solutions constant. It is then expected that the diversity indicator value declines monotonically, and the indicators, which behave more accordingly, are better. The other is to test the indicators on measuring the diversity change during the convergence process. It is known that the diversity is lacking in the early iterations and is continuously being improved as the

iterations endure. The histogram of the diversity indicators should display a monotonic and, typically, an ever-increasing characteristic. The ever-increasing trends are often altered when the PF of the solutions degenerate. The values of diversity indicators may oscillate and show decreasing trend as the iteration continues. Both differentiation methods have been utilised to test the feasibility of IRNA versus other frequently used or newly proposed diversity indicators. The methodology of Bn-PFt can be incorporated into the concept of IRNA, making the reference vectors most evenly distributed in the objective space after considering the actual shape of the PF approximation. The accuracy of the IRNA score is thus considerably enhanced. A major weakness is that the method relies heavily on the evenness of intersections between reference vectors and the actual Pareto front. These intersections usually are not precisely uniformly distributed on the true PF, which reduces the veracity of the method.

As future work, more existing diversity indicators shall be analysed, compared, and contrasted using the methodologies proposed in this work.

7.3 Visualisation and Evaluation of Pareto Front Approximations

Visualisation of high dimensional data is arduous due to the limitation of our cognitive capability. PF data attained using MaOP are high dimensional. It is hard to know the pattern of such a PF approximation, such as convex, plane, or concave form, or a combination of several primary forms distributed spatially. PF shapes often cover the objective space partially or turn out to have degenerated as a line segment in the objective space. In addition, no single MaOP algorithm is superior to all others in various categories of optimisation problems. Commonly, several algorithms are adopted in the optimisation analysis. There is a need to find the domination relations between PF approximations sets and identify the PF solution of the highest quality. All the detailed knowledge of the above may assist decision-makers in choosing the most suitable decision variables to control better the process studied. The proposed visualisation methodology, ProD, attempts to deal with the challenge. High dimensional data are rearranged into two amounts: the projection and the distance to a reference vector. Various numerical testing reveals that ProD possesses the properties a suitable visualisation method should have balanced, which means the desired properties are mainly satisfied.

As significant future work, dominance relations among nearly equally good approximations must be found, and the performances are differentiated. The current version of ProD has difficulties doing so in a reliable manner. Using good quality indicators locally at various distance values to the reference vector might be an appropriate way to go. But organising and regional clustering data that can be analysed by the indicators utilised is an unsolved issue and further studied.

7.4 Minimising Crack Formation in Selective Laser Melting

The data from comprehensive experiments on the edge and bulk crack length density formed in Selective Laser Melting manufacturing of three different products performed using a nickel superalloy - CM247L by HiETA were studied. The material CM247L is a nickel super alloyed compound commonly used in critical aerospace applications due to its mechanical properties. Being able to 3D print this material would be of enormous importance to the aerospace industry. The modelled objective functions combine, and two MOP cases and one MaOP case are created, subsequently optimised. The first MOP case optimises the bulk crack length density on the three products subject to the process parameters: the laser power, the point distance, the hatch offset and the exposure time. The other MOP case studied minimises the edge crack length density on the three artefacts. Both cases have a dimension of 3 objective functions and 4 decision variables. Then, the 6 objective functions are optimised simultaneously in the last case, forming a MaOP analysis.

Three well-known and dissimilar MaOP algorithms are adopted to perform the optimisation analysis, NSGA III, IBEA and GrEA. The Bn-PFt methodology has been incorporated in NSGA III to enhance the diversity of the PF approximations. The IRNA diversity indicator has been used to check the diversity properties of the three sets of PF approximations from each of the chosen MaOP algorithms. The results are visualised using ProD. It was found that NSGA III provided the best PF approximations in diversity. The solutions from NSGA III are taken for further analysis – finding the optimised process/decision variables.

The main conclusions are as follows.

The error of the developed surrogate models is analysed by adopting error metrics of the root mean square error ($RMSE$), the maximum absolute error (*MaxAE*) and the coefficient of determination (R^2). The results indicate that the accuracy of the surrogate models is acceptable, although considerable significant variations between the test data and modelled data exist.

The PF of MOP bulk crack length density optimisation consists of a single point, which means the objective functions are not conflicting. Interestingly, the optimised range in decision space covers a wide area, indicating many combinations of process parameters resulting in optimality – the minimised bulk crack length density. It also means that finding proper process parameters by which the minimised formation of bulk cracks is a relatively easy task. The observation from the experimental testing has confirmed the conclusion.

The PF of edge crack length density forms a convex front, meaning that the objective functions are conflicting. The corresponding optimised process parameters are located in two narrow regions, visualised in 2D scatter plots and ProD. It is more challenging to find optimised process parameters than minimising bulk cracks. A choice might be less reliable due to the narrow range for optimality and the current uncertainty in the process parameters. The conclusion has also been verified from the observations made during the experimental testing.

The ProD reveals that the PF from the simultaneous optimisation of all three bulk crack and edge crack objective functions has an unsymmetric convex type in the objective space. The corresponding area of optimised process parameters in decision space is clustered but spread to a larger region than the separate MOP crack cases analysed, indicating a compromise in minimising crack length in bulk and at edges simultaneously.

By plotting the optimised process parameters in Parallel coordinates, the estimates of ranges of optimised process parameters have been attained.

Validation tests have been carried out later. The results are disappointing, and the error metric values reveal no functional relations between the validation test data and the surrogate models. It implies that the experiment is nontrivial to be repeated since other unknown influencing factors must be considered when we go from one actual experimental setting to another, despite the same test procedures being followed.

The application chapter, Chapter 6, has demonstrated the effectiveness of Bn-PFt, IRNA, and ProD to enhance an optimisation study on a real case problem targeting finding the optimised process parameters of an SLM operation.

Two major future works are suggested. One is to perform several more disparate tests, where possible influencing factors, such as ambient temperature, moisture, the temperature at various experimental equipment and parts, etc., are monitored so that the hidden causes can be identified, which contribute to the deviations between different experimental runs. The other is executing a robust optimisation analysis to detect the robust PF of the study.

Reference

[1] A. E. Eiben and J. E. Smith, *Introduction to Evolutionary Computing*. Berlin, Heidelberg: Springer Berlin Heidelberg, 2003. doi: 10.1007/978-3-662-05094-1.

[2] K. Deb and H. Jain, 'An Evolutionary Many-Objective Optimization Algorithm Using Reference-Point-Based Nondominated Sorting Approach, Part I: Solving Problems With Box Constraints', *IEEE Trans. Evol. Comput.*, vol. 18, no. 4, pp. 577–601, Aug. 2014, doi: 10.1109/TEVC.2013.2281535.

[3] Y. Cui, Z. Geng, Q. Zhu, and Y. Han, 'Review: Multi-objective optimization methods and application in energy saving', *Energy*, vol. 125, pp. 681–704, 2017, doi: 10.1016/j.energy.2017.02.174.

[4] D. H. Wolpert and W. G. Macready, 'No free lunch theorems for optimization', *IEEE Trans. Evol. Comput.*, vol. 1, no. 1, pp. 67–82, Apr. 1997, doi: 10.1109/4235.585893.

[5] R. Allmendinger, A. Jaszkiewicz, A. Liefooghe, and C. Tammer, 'What if we Increase the Number of Objectives? Theoretical and Empirical Implications for Many-objective Optimization', *ArXiv Prepr. ArXiv210603275*, 2021.

[6] Qingfu Zhang and Hui Li, 'MOEA/D: A Multiobjective Evolutionary Algorithm Based on Decomposition', *IEEE Trans. Evol. Comput.*, vol. 11, no. 6, pp. 712–731, Dec. 2007, doi: 10.1109/TEVC.2007.892759.

[7] R. Cheng, Y. Jin, M. Olhofer, and B. Sendhoff, 'A Reference Vector Guided Evolutionary Algorithm for Many-Objective Optimization', *IEEE Trans. Evol. Comput.*, vol. 20, no. 5, pp. 773–791, Oct. 2016, doi: 10.1109/TEVC.2016.2519378.

[8] Y. Jin, H. Wang, T. Chugh, D. Guo, and K. Miettinen, 'Data-Driven Evolutionary Optimization: An Overview and Case Studies', *IEEE Trans. Evol. Comput.*, vol. 23, no. 3, pp. 442–458, Jun. 2019, doi: 10.1109/TEVC.2018.2869001.

[9] K. Miettinen, *Nonlinear Multiobjective Optimization*, vol. 12. Boston, MA: Springer US, 1998. doi: 10.1007/978-1-4615-5563-6.

[10] J. Nocedal and S. J. Wright, *Numerical optimization*. New York: Springer, 1999.

[11] A. Ruszczynski, *Nonlinear optimization*. Princeton university press, 2011.

[12] R. T. Mohammed, R. Yaakob, A. A. Zaidan, N. M. Sharef, R. H. Abdullah, B. B. Zaidan, K. A. Dawood, 'Review of the Research Landscape of Multi-Criteria Evaluation and Benchmarking Processes for Many-Objective Optimization Methods: Coherent Taxonomy, Challenges and Recommended Solution', *Int. J. Inf. Technol. Decis. Mak.*, vol. 19, no. 06, pp. 1619–1693, Nov. 2020, doi: 10.1142/S0219622020300049.

[13] D. P. Kroese, Z. Botev, T. Taimre, and R. Vaisman, *Data science and machine learning: Mathematical and statistical methods*. CRC Press, 2019.

[14] A. B. Owen, ‘Controlling Correlations in Latin Hypercube Samples’, *J. Am. Stat. Assoc.*, vol. 89, no. 428, pp. 1517–1522, Dec. 1994, doi: 10.1080/01621459.1994.10476891.

[15] N. V. Queipo, R. T. Haftka, W. Shyy, T. Goel, R. Vaidyanathan, and P. Kevin Tucker, ‘Surrogate-based analysis and optimization’, *Prog. Aerosp. Sci.*, vol. 41, no. 1, pp. 1–28, Jan. 2005, doi: 10.1016/j.paerosci.2005.02.001.

[16] A. S. Hedayat, N. J. A. Sloane, and J. Stufken, *Orthogonal arrays: theory and applications*. Springer Science & Business Media, 2012.

[17] B. Tang, ‘Orthogonal Array-Based Latin Hypercubes’, *J. Am. Stat. Assoc.*, vol. 88, no. 424, pp. 1392–1397, Dec. 1993, doi: 10.1080/01621459.1993.10476423.

[18] M. W. Gardner and S. Dorling, ‘Artificial neural networks (the multilayer perceptron)—a review of applications in the atmospheric sciences’, *Atmos. Environ.*, vol. 32, no. 14–15, pp. 2627–2636, 1998.

[19] S. Koziel and X.-S. Yang, Eds., *Computational Optimization, Methods and Algorithms*, vol. 356. Berlin, Heidelberg: Springer Berlin Heidelberg, 2011. doi: 10.1007/978-3-642-20859-1.

[20] I. Steinwart and A. Christmann, *Support vector machines*. Springer Science & Business Media, 2008.

[21] C. Jin and L. Wang, ‘Dimensionality Dependent PAC-Bayes Margin Bound.’, 2012, vol. 12, pp. 1034–1042.

[22] M. Emmerich, ‘Single-and multi-objective evolutionary design optimization assisted by gaussian random field metamodels’, *Diss. Univ. Dortm.*, 2005.

[23] L. Rokach and O. Z. Maimon, *Data mining with decision trees: theory and applications*, vol. 69. World scientific, 2007.

[24] Y. Jin, ‘Fuzzy modeling of high-dimensional systems: complexity reduction and interpretability improvement’, *IEEE Trans. Fuzzy Syst.*, vol. 8, no. 2, pp. 212–221, Apr. 2000, doi: 10.1109/91.842154.

[25] Z.-H. Zhou, ‘Ensemble learning, Encyclopedia of Biometrics’, 2009.

[26] B. Efron, ‘Estimating the Error Rate of a Prediction Rule: Improvement on Cross-Validation’, *J. Am. Stat. Assoc.*, vol. 78, no. 382, pp. 316–331, Jun. 1983, doi: 10.1080/01621459.1983.10477973.

[27] A. Saltelli and I. M. Sobol’, ‘Sensitivity analysis for nonlinear mathematical models: Numerical experience’, *Mat. Model.*, vol. 7, Jan. 1995.

[28] P. Jiang, Q. Zhou, and X. Shao, *Surrogate model-based engineering design and optimization*. Springer, 2020.

[29] M. Janga Reddy and D. Nagesh Kumar, ‘Evolutionary algorithms, swarm intelligence methods, and their applications in water resources engineering: a state-of-the-art review’, *H2Open J.*, vol. 3, no. 1, pp. 135–188, Jan. 2020, doi: 10.2166/h2oj.2020.128.

[30] Y. Shi and R. Eberhart, ‘A modified particle swarm optimizer’, in *1998 IEEE International Conference on Evolutionary Computation Proceedings. IEEE World Congress on Computational Intelligence (Cat. No.98TH8360)*, Anchorage, AK, USA, 1998, pp. 69–73. doi: 10.1109/ICEC.1998.699146.

[31] M. R. Bonyadi and Z. Michalewicz, ‘Particle Swarm Optimization for Single Objective Continuous Space Problems: A Review’, *Evol. Comput.*, vol. 25, no. 1, pp. 1–54, Mar. 2017, doi: 10.1162/EVCO_r_00180.

[32] J. Saveca, Z. Wang, and Y. Sun, ‘Improved Differential Evolution Based on Mutation Strategies’, in *Advances in Swarm Intelligence*, Cham, 2018, pp. 233–242.

[33] D. Whitley, ‘A genetic algorithm tutorial’, *Stat. Comput.*, vol. 4, no. 2, Jun. 1994, doi: 10.1007/BF00175354.

[34] J. H. Holland, ‘Adaptation in Natural and Artificial Systems: An Introductory Analysis with Applications to Biology, Control, and Artificial Intelligence’, p. 245.

[35] J. H. Holland, ‘Genetic Algorithms Computer programs that “evolve” in ways that resemble natural selection can solve complex problems even their creators do not fully understand’, p. 5.

[36] M. Taherdangkoo, M. Paziresh, M. Yazdi, and M. Bagheri, ‘An efficient algorithm for function optimization: modified stem cells algorithm’, *Open Eng.*, vol. 3, no. 1, Jan. 2013, doi: 10.2478/s13531-012-0047-8.

[37] O. M. Shir and A. Yehudayoff, ‘On the covariance-Hessian relation in evolution strategies’, *Theor. Comput. Sci.*, vol. 801, pp. 157–174, 2020.

[38] N. Hansen, ‘The CMA Evolution Strategy: A Comparing Review’, in *Towards a New Evolutionary Computation*, vol. 192, J. A. Lozano, P. Larrañaga, I. Inza, and E. Bengoetxea, Eds. Berlin, Heidelberg: Springer Berlin Heidelberg, 2006, pp. 75–102. doi: 10.1007/3-540-32494-1_4.

[39] C. Igel, T. Suttorp, and N. Hansen, ‘A computational efficient covariance matrix update and a (1+1)-CMA for evolution strategies’, in *Proceedings of the 8th annual conference on Genetic and evolutionary computation - GECCO ’06*, Seattle, Washington, USA, 2006, p. 453. doi: 10.1145/1143997.1144082.

[40] A. Auger and N. Hansen, ‘A Restart CMA Evolution Strategy With Increasing Population Size’, in *2005 IEEE Congress on Evolutionary Computation*, Edinburgh, Scotland, UK, 2005, vol. 2, pp. 1769–1776. doi: 10.1109/CEC.2005.1554902.

[41] R. Poli, W. B. Langdon, N. F. McPhee, and J. R. Koza, ‘A Field Guide to Genetic Programming. lulu. com’, *Contrib. JR Koza*, 2008.

[42] M. Dorigo, V. Maniezzo, and A. Colorni, ‘Ant system: optimization by a colony of cooperating agents’, *IEEE Trans. Syst. Man Cybern. Part B Cybern.*, vol. 26, no. 1, pp. 29–41, 1996.

[43] R. Storn and K. Price, ‘Differential Evolution - A Simple and Efficient Heuristic for Global Optimization over Continuous Spaces’, *J. Glob. Optim.*, vol. 11, no. 4, pp. 341–359, 1997, doi: 10.1023/A:1008202821328.

[44] R. Storn, ‘On the usage of differential evolution for function optimization’, in *Proceedings of North American Fuzzy Information Processing*, Berkeley, CA, USA, 1996, pp. 519–523. doi: 10.1109/NAFIPS.1996.534789.

[45] S. Das, S. S. Mullick, and P. N. Suganthan, ‘Recent advances in differential evolution – An updated survey’, *Swarm Evol. Comput.*, vol. 27, pp. 1–30, Apr. 2016, doi: 10.1016/j.swevo.2016.01.004.

[46] J. Liu and J. Lampinen, ‘A Fuzzy Adaptive Differential Evolution Algorithm’, *Soft Comput.*, vol. 9, no. 6, pp. 448–462, Jun. 2005, doi: 10.1007/s00500-004-0363-x.

[47] A. K. Qin and P. N. Suganthan, ‘Self-adaptive Differential Evolution Algorithm for Numerical Optimization’, in *2005 IEEE Congress on Evolutionary Computation*, Edinburgh, Scotland, UK, 2005, vol. 2, pp. 1785–1791. doi: 10.1109/CEC.2005.1554904.

[48] J. Brest, S. Greiner, B. Boskovic, M. Mernik, and V. Zumer, ‘Self-Adapting Control Parameters in Differential Evolution: A Comparative Study on Numerical Benchmark Problems’, *IEEE Trans. Evol. Comput.*, vol. 10, no. 6, pp. 646–657, Dec. 2006, doi: 10.1109/TEVC.2006.872133.

[49] Wen-Jun Zhang and Xiao-Feng Xie, ‘DEPSO: hybrid particle swarm with differential evolution operator’, in *SMC’03 Conference Proceedings. 2003 IEEE International Conference on Systems, Man and Cybernetics. Conference Theme - System Security and Assurance (Cat. No.03CH37483)*, Washington, DC, USA, 2003, vol. 4, pp. 3816–3821. doi: 10.1109/ICSMC.2003.1244483.

[50] L. Zuo, L. Liu, H. Wang, and L. Tan, ‘A Hybrid Differential Evolution Algorithm and Particle Swarm Optimization with Alternative Replication Strategy’, in *Advances in Swarm Intelligence*, Cham, 2018, pp. 487–497.

[51] H. Wang, Z. Wu, and S. Rahnamayan, ‘Enhanced opposition-based differential evolution for solving high-dimensional continuous optimization problems’, *Soft Comput.*, vol. 15, no. 11, pp. 2127–2140, Nov. 2011, doi: 10.1007/s00500-010-0642-7.

[52] J. Kennedy’ and R. Eberhart, ‘Particle Swarm Optimization’, *IEEE*, p. 7, 1995.

[53] J. Kennedy and R. Mendes, ‘Population structure and particle swarm performance’, in *Proceedings of the 2002 Congress on Evolutionary Computation. CEC’02 (Cat. No.02TH8600)*, Honolulu, HI, USA, 2002, vol. 2, pp. 1671–1676. doi: 10.1109/CEC.2002.1004493.

[54] P. Garg, ‘A Comparison between Memetic algorithm and Genetic algorithm for the cryptanalysis of Simplified Data Encryption Standard algorithm’, *ArXiv Prepr. ArXiv10040574*, 2010.

[55] M. Pelikan, ‘Probabilistic model-building genetic algorithms’, 2011, pp. 913–940.

[56] O. Grodzevich and O. Romanko, ‘Normalization and other topics in multi-objective optimization’, 2006.

[57] K. Miettinen, F. Ruiz, and A. P. Wierzbicki, ‘Introduction to Multiobjective Optimization: Interactive Approaches’, in *Multiobjective Optimization*, vol. 5252, J. Branke, K. Deb, K. Miettinen, and R. Słowiński, Eds. Berlin, Heidelberg: Springer Berlin Heidelberg, 2008, pp. 27–57. doi: 10.1007/978-3-540-88908-3_2.

[58] M. Gong, S. Wang, W. Liu, J. Yan, and L. Jiao, ‘Evolutionary computation in China: A literature survey’, *CAAI Trans. Intell. Technol.*, vol. 1, no. 4, pp. 334–354, Oct. 2016, doi: 10.1016/j.trit.2016.11.002.

[59] Y. Tian, H. Wang, X. Zhang, and Y. Jin, ‘Effectiveness and efficiency of non-dominated sorting for evolutionary multi-and many-objective optimization’, *Complex Intell. Syst.*, vol. 3, no. 4, pp. 247–263, 2017.

[60] D. Mueller-Gritschneder, H. Graeb, and U. Schlichtmann, ‘A Successive Approach to Compute the Bounded Pareto Front of Practical Multiobjective Optimization Problems’, *SIAM J. Optim.*, vol. 20, no. 2, pp. 915–934, Jan. 2009, doi: 10.1137/080729013.

[61] E. Zitzler and S. Künzli, ‘Indicator-Based Selection in Multiobjective Search’, in *Parallel Problem Solving from Nature - PPSN VIII*, Berlin, Heidelberg, 2004, vol. 3242, pp. 832–842. doi: 10.1007/978-3-540-30217-9_84.

[62] V. Miranda, H. Hrvoje, and Á. Jaramillo Duque, ‘Stochastic Star Communication Topology in Evolutionary Particle Swarms (EPSO)’, *Int. J. Comput. Intell. Res.*, vol. 4, no. 2, 2008, doi: 10.5019/j.ijcir.2008.130.

[63] P.-Y. Yin, F. Glover, M. Laguna, and J.-X. Zhu, ‘A Complementary Cyber Swarm Algorithm’:, *Int. J. Swarm Intell. Res.*, vol. 2, no. 2, pp. 22–41, Apr. 2011, doi: 10.4018/jsir.2011040102.

[64] G. Yu, Y. Jin, and M. Olhofer, ‘Benchmark problems and performance indicators for search of knee points in multiobjective optimization’, *IEEE Trans. Cybern.*, vol. 50, no. 8, pp. 3531–3544, 2019.

[65] M. Bhattacharya, R. Islam, and J. Abawajy, ‘Evolutionary optimization: A big data perspective’, *J. Netw. Comput. Appl.*, vol. 59, pp. 416–426, Jan. 2016, doi: 10.1016/j.jnca.2014.07.032.

[66] J. Ryu, S. Kim, and H. Wan, ‘Pareto front approximation with adaptive weighted sum method in multiobjective simulation optimization’, in *Proceedings of the 2009 Winter Simulation Conference (WSC)*, Austin, TX, USA, Dec. 2009, pp. 623–633. doi: 10.1109/WSC.2009.5429562.

[67] A. Masood, G. Chen, Y. Mei, and M. Zhang, ‘Reference Point Adaption Method for Genetic Programming Hyper-Heuristic in Many-Objective Job Shop Scheduling’, in *Evolutionary Computation in Combinatorial Optimization*, vol. 10782, A. Liefooghe and M. López-Ibáñez, Eds. Cham: Springer International Publishing, 2018, pp. 116–131. doi: 10.1007/978-3-319-77449-7_8.

[68] I. Y. Kim and O. de Weck, ‘Adaptive Weighted Sum Method for Multiobjective Optimization’, presented at the 10th AIAA/ISSMO Multidisciplinary Analysis and Optimization Conference, Albany, New York, Aug. 2004. doi: 10.2514/6.2004-4322.

[69] Z. Li, K. Lin, M. Nouioua, and S. Jiang, ‘A Decomposition Based Evolutionary Algorithm with Angle Penalty Selection Strategy for Many-Objective Optimization’, in *Advances in Swarm Intelligence*, vol. 10941, Y. Tan, Y. Shi, and Q. Tang, Eds. Cham: Springer International Publishing, 2018, pp. 561–571. doi: 10.1007/978-3-319-93815-8_53.

[70] L. Zhen, M. Li, D. Peng, and X. Yao, ‘Objective reduction for visualising many-objective solution sets’, *Inf. Sci.*, vol. 512, pp. 278–294, 2020.

[71] J. Bader and E. Zitzler, ‘HypE: An Algorithm for Fast Hypervolume-Based Many-Objective Optimization’, *Evol. Comput.*, vol. 19, no. 1, pp. 45–76, Mar. 2011, doi: 10.1162/EVCO_a_00009.

[72] G. Dhiman, M. Soni, H. M. Pandey, A. Slowik, and H. Kaur, ‘A novel hybrid hypervolume indicator and reference vector adaptation strategies based evolutionary algorithm for many-objective optimization’, *Eng. Comput.*, vol. 37, no. 4, pp. 3017–3035, Oct. 2021, doi: 10.1007/s00366-020-00986-0.

[73] J. W. Gorman and J. E. Hinman, ‘Simplex Lattice Designs for Multicomponent Systems’, *Technometrics*, vol. 4, no. 4, pp. 463–487, Nov. 1962, doi: 10.1080/00401706.1962.10490034.

[74] L. R. de Farias, P. H. Braga, H. F. Bassani, and A. F. Araújo, ‘MOEA/D with uniformly randomly adaptive weights’, 2018, pp. 641–648.

[75] X. Zhang, Y. Tian, and Y. Jin, ‘A Knee Point-Driven Evolutionary Algorithm for Many-Objective Optimization’, *IEEE Trans. Evol. Comput.*, vol. 19, no. 6, pp. 761–776, Dec. 2015, doi: 10.1109/TEVC.2014.2378512.

[76] W. Elshamy, H. M. Emara, and A. Bahgat, ‘Clubs-based Particle Swarm Optimization’, in *2007 IEEE Swarm Intelligence Symposium*, Honolulu, HI, USA, Apr. 2007, pp. 289–296. doi: 10.1109/SIS.2007.367950.

[77] Handing Wang, Licheng Jiao, and Xin Yao, ‘Two_Arch2: An Improved Two-Archive Algorithm for Many-Objective Optimization’, *IEEE Trans. Evol. Comput.*, vol. 19, no. 4, pp. 524–541, Aug. 2015, doi: 10.1109/TEVC.2014.2350987.

[78] V. K. Reddy and L. S. S. Reddy, ‘Performance Evaluation of Particle Swarm Optimization Algorithms on GPU using CUDA’, p. 17.

[79] S. Yang, M. Li, X. Liu, and J. Zheng, ‘A Grid-Based Evolutionary Algorithm for Many-Objective Optimization’, *IEEE Trans. Evol. Comput.*, vol. 17, no. 5, pp. 721–736, Oct. 2013, doi: 10.1109/TEVC.2012.2227145.

[80] H. Wang and X. Yao, ‘Corner sort for Pareto-based many-objective optimization’, *IEEE Trans. Cybern.*, vol. 44, no. 1, pp. 92–102, 2013.

[81] X. Cai, Z. Mei, and Z. Fan, ‘A decomposition-based many-objective evolutionary algorithm with two types of adjustments for direction vectors’, *IEEE Trans. Cybern.*, vol. 48, no. 8, pp. 2335–2348, 2017.

[82] Y.-H. Zhang *et al.*, ‘DECAL: Decomposition-based coevolutionary algorithm for many-objective optimization’, *IEEE Trans. Cybern.*, vol. 49, no. 1, pp. 27–41, 2017.

[83] Y. Xiang, Y. Zhou, L. Tang, and Z. Chen, ‘A Decomposition-Based Many-Objective Artificial Bee Colony Algorithm’, *IEEE Trans. Cybern.*, vol. 49, no. 1, pp. 287–300, Jan. 2019, doi: 10.1109/TCYB.2017.2772250.

[84] T. Chugh, ‘Scalarizing Functions in Bayesian Multiobjective Optimization’, 2020, pp. 1–8.

[85] A. Trivedi, D. Srinivasan, K. Sanyal, and A. Ghosh, ‘A Survey of Multiobjective Evolutionary Algorithms Based on Decomposition’, *IEEE Trans. Evol. Comput.*, vol. 21, no. 3, pp. 440–462, Jun. 2017, doi: 10.1109/TEVC.2016.2608507.

[86] M. Grabisch, J.-L. Marichal, R. Mesiar, and E. Pap, ‘Aggregation functions: means’, *Inf. Sci.*, vol. 181, no. 1, pp. 1–22, 2011.

[87] A. Santiago *et al.*, ‘A survey of decomposition methods for multi-objective optimization’, in *Recent Advances on Hybrid Approaches for Designing Intelligent Systems*, Springer, 2014, pp. 453–465.

[88] K. Miettinen and M. M. Mäkelä, ‘On scalarizing functions in multiobjective optimization’, *Spectr.*, vol. 24, no. 2, pp. 193–213, 2002.

[89] S. Jiang, S. Yang, Y. Wang, and X. Liu, ‘Scalarizing Functions in Decomposition-Based Multiobjective Evolutionary Algorithms’, *IEEE Trans. Evol. Comput.*, vol. 22, no. 2, pp. 296–313, Apr. 2018, doi: 10.1109/TEVC.2017.2707980.

[90] R. Wang, Z. Zhou, H. Ishibuchi, T. Liao, and T. Zhang, ‘Localized Weighted Sum Method for Many-Objective Optimization’, *IEEE Trans. Evol. Comput.*, vol. 22, no. 1, pp. 3–18, Feb. 2018, doi: 10.1109/TEVC.2016.2611642.

[91] Y. Hua, Q. Liu, K. Hao, and Y. Jin, ‘A Survey of Evolutionary Algorithms for Multi-Objective Optimization Problems With Irregular Pareto Fronts’, *IEEECAA J. Autom. Sin.*, vol. 8, no. 2, pp. 303–318, 2021.

[92] Y. Hua, Y. Jin, and K. Hao, ‘A clustering-based adaptive evolutionary algorithm for multiobjective optimization with irregular Pareto fronts’, *IEEE Trans. Cybern.*, vol. 49, no. 7, pp. 2758–2770, 2018.

[93] H. Yicun, J. Yaochu, H. Kuangrong, and Y. Cao, ‘Generating multiple reference vectors for a class of many-objective optimization problems with degenerate Pareto fronts’, *Complex Intell. Syst.*, vol. 6, no. 2, pp. 275–285, 2020.

[94] Q. Liu, Y. Jin, M. Heiderich, T. Rodemann, and G. Yu, ‘An adaptive reference vector-guided evolutionary algorithm using growing neural gas for many-objective optimization of irregular problems’, *IEEE Trans. Cybern.*, 2020.

[95] C. Si, J. Shen, W. Guo, and L. Wang, ‘On the Cooperation Between Evolutionary Algorithms and Constraint Handling Techniques’, in *Advances in Swarm Intelligence*, Cham, 2018, pp. 42–50.

[96] K. A. Abul and M. G. P. F. Edite, ‘GLOBAL COMPETITIVE RANKING FOR CONSTRAINTS HANDLING WITH MODIFIED DIFFERENTIAL EVOLUTION’:, in *Proceedings of the International Conference on Evolutionary Computation Theory and Applications*, Paris, France, 2011, pp. 42–51. doi: 10.5220/0003672200420051.

[97] M. Garza-Fabre, E. Rodriguez-Tello, and G. Toscano-Pulido, ‘Constraint-handling through multi-objective optimization: The hydrophobic-polar model for protein structure prediction’, *Comput. Oper. Res.*, vol. 53, pp. 128–153, Jan. 2015, doi: 10.1016/j.cor.2014.07.010.

[98] K. Li, R. Chen, G. Fu, and X. Yao, ‘Two-Archive Evolutionary Algorithm for Constrained Multiobjective Optimization’, *IEEE Trans. Evol. Comput.*, vol. 23, no. 2, pp. 303–315, Apr. 2019, doi: 10.1109/TEVC.2018.2855411.

[99] C. A. Coello Coello and A. D. Christiansen, ‘MOSES: A MULTIOBJECTIVE OPTIMIZATION TOOL FOR ENGINEERING DESIGN’, *Eng. Optim.*, vol. 31, no. 3, pp. 337–368, Feb. 1999, doi: 10.1080/03052159908941377.

[100] K. Deb, A. Pratap, S. Agarwal, and T. Meyarivan, ‘A fast and elitist multiobjective genetic algorithm: NSGA-II’, *IEEE Trans. Evol. Comput.*, vol. 6, no. 2, pp. 182–197, Apr. 2002, doi: 10.1109/4235.996017.

[101] E. Mezura-Montes and C. A. C. Coello, ‘Constraint-handling in nature-inspired numerical optimization: past, present and future’, *Swarm Evol. Comput.*, vol. 1, no. 4, pp. 173–194, 2011.
[102] Y. Jin and J. Branke, ‘Evolutionary Optimization in Uncertain Environments—A Survey’, *IEEE Trans. Evol. Comput.*, vol. 9, no. 3, pp. 303–317, Jun. 2005, doi: 10.1109/TEVC.2005.846356.
[103] Y. Jin, H. Wang, and C. Sun, ‘Data-driven evolutionary optimization’, 2021.
[104] H.-G. Beyer and B. Sendhoff, ‘Robust optimization–a comprehensive survey’, *Comput. Methods Appl. Mech. Eng.*, vol. 196, no. 33–34, pp. 3190–3218, 2007.
[105] Y. Jin and B. Sendhoff, ‘Trade-off between performance and robustness: An evolutionary multiobjective approach’, 2003, pp. 237–251.
[106] S. Huband, P. Hingston, L. Barone, and L. While, ‘A review of multiobjective test problems and a scalable test problem toolkit’, *IEEE Trans. Evol. Comput.*, vol. 10, no. 5, pp. 477–506, Oct. 2006, doi: 10.1109/TEVC.2005.861417.
[107] K. Deb, ‘Multi-objective Genetic Algorithms: Problem Difficulties and Construction of Test Problems’, *Evol. Comput.*, vol. 7, no. 3, pp. 205–230, Sep. 1999, doi: 10.1162/evco.1999.7.3.205.
[108] E. Zitzler, K. Deb, and L. Thiele, ‘Comparison of Multiobjective Evolutionary Algorithms: Empirical Results’, *Evol. Comput.*, vol. 8, no. 2, pp. 173–195, Jun. 2000, doi: 10.1162/106365600568202.
[109] K. Deb, L. Thiele, M. Laumanns, and E. Zitzler, ‘Scalable Test Problems for Evolutionary Multiobjective Optimization’, in *Evolutionary Multiobjective Optimization*, A. Abraham, L. Jain, and R. Goldberg, Eds. London: Springer-Verlag, 2005, pp. 105–145. doi: 10.1007/1-84628-137-7_6.
[110] D. A. V. Veldhuizen, ‘Multiobjective Evolutionary Algorithms: Classifications, Analyses, and New Innovations’, p. 270.
[111] R. Cheng *et al.*, ‘A benchmark test suite for evolutionary many-objective optimization’, *Complex Intell. Syst.*, vol. 3, no. 1, pp. 67–81, Mar. 2017, doi: 10.1007/s40747-017-0039-7.
[112] R. Cheng *et al.*, ‘Benchmark Functions for CEC’2018 Competition on Many-Objective Optimization’, p. 22.
[113] B. Da *et al.*, ‘Evolutionary Multitasking for Single-objective Continuous Optimization: Benchmark Problems, Performance Metric, and Baseline Results’, *ArXiv170603470 Cs*, Jun. 2017, Accessed: Jul. 11, 2021. [Online]. Available: http://arxiv.org/abs/1706.03470
[114] B. Zhang, K. Shafi, and H. Abbass, ‘On Benchmark Problems and Metrics for Decision Space Performance Analysis in Multi-Objective Optimization’, *Int. J. Comput. Intell. Appl.*, vol. 16, no. 01, p. 1750006, Mar. 2017, doi: 10.1142/S1469026817500067.
[115] C.-L. Yu, Y.-Z. Lu, and J. Chu, ‘Multi-objective Optimization with Combination of Particle Swarm and Extremal Optimization for Constrained Engineering Design’, vol. 7, no. 4, p. 10, 2012.
[116] N. Chase, M. Rademacher, E. Goodman, R. Averill, and R. Sidhu, ‘A Benchmark Study of Multi-Objective Optimization Methods’, p. 24.

[117] J. B. Kollat and P. M. Reed, ‘Comparing state-of-the-art evolutionary multi-objective algorithms for long-term groundwater monitoring design’, *Adv. Water Resour.*, vol. 29, no. 6, pp. 792–807, Jun. 2006, doi: 10.1016/j.advwatres.2005.07.010.

[118] K. Deb, A. Sinha, and S. Kukkonen, ‘Multi-objective test problems, linkages, and evolutionary methodologies’, in *Proceedings of the 8th annual conference on Genetic and evolutionary computation - GECCO ’06*, Seattle, Washington, USA, 2006, p. 1141. doi: 10.1145/1143997.1144179.

[119] V. L. Huang *et al.*, ‘Problem Definitions for Performance Assessment on Multi-objective Optimization Algorithms’, 2007, p. 20.

[120] T. N. Huu and H. T. Van, ‘A PROBABILITY-DRIVEN SEARCH ALGORITHM FOR SOLVING MULTI-OBJECTIVE OPTIMIZATION PROBLEMS’, p. 12, 2012.

[121] V. Lattarulo and G. T. Parks, ‘Testing of the multi-objective alliance algorithm on benchmark functions’, in *Proceeding of the fifteenth annual conference companion on Genetic and evolutionary computation conference companion - GECCO ’13 Companion*, Amsterdam, The Netherlands, 2013, p. 1679. doi: 10.1145/2464576.2482751.

[122] Z. He and G. G. Yen, ‘Visualization and Performance Metric in Many-Objective Optimization’, *IEEE Trans. Evol. Comput.*, vol. 20, no. 3, pp. 386–402, Jun. 2016, doi: 10.1109/TEVC.2015.2472283.

[123] H. Wang, Y. Jin, and X. Yao, ‘Diversity Assessment in Many-Objective Optimization’, *IEEE Trans. Cybern.*, vol. 47, no. 6, pp. 1510–1522, Jun. 2017, doi: 10.1109/TCYB.2016.2550502.

[124] E. Zitzler, J. Knowles, and L. Thiele, ‘Quality Assessment of Pareto Set Approximations’, in *Multiobjective Optimization*, vol. 5252, J. Branke, K. Deb, K. Miettinen, and R. Słowiński, Eds. Berlin, Heidelberg: Springer Berlin Heidelberg, 2008, pp. 373–404. doi: 10.1007/978-3-540-88908-3_14.

[125] E. Zitzler, L. Thiele, M. Laumanns, C. M. Fonseca, and V. G. da Fonseca, ‘Performance assessment of multiobjective optimizers: an analysis and review’, *IEEE Trans. Evol. Comput.*, vol. 7, no. 2, pp. 117–132, Apr. 2003, doi: 10.1109/TEVC.2003.810758.

[126] D. A. Van Veldhuizen and G. B. Lamont, ‘On measuring multiobjective evolutionary algorithm performance’, in *Proceedings of the 2000 Congress on Evolutionary Computation. CEC00 (Cat. No.00TH8512)*, La Jolla, CA, USA, 2000, vol. 1, pp. 204–211. doi: 10.1109/CEC.2000.870296.

[127] E. Zitzler and L. Thiele, ‘Multiobjective evolutionary algorithms: a comparative case study and the strength Pareto approach’, *IEEE Trans. Evol. Comput.*, vol. 3, no. 4, pp. 257–271, Nov. 1999, doi: 10.1109/4235.797969.

[128] C. A. C. Coello and N. C. Cort&#xfffd;s, ‘Solving Multiobjective Optimization Problems Using an Artificial Immune System’, *Genet. Program. Evolvable Mach.*, vol. 6, no. 2, pp. 163–190, Jun. 2005, doi: 10.1007/s10710-005-6164-x.

[129] Y. Tian, R. Cheng, X. Zhang, M. Li, and Y. Jin, ‘Diversity Assessment of Multi-Objective Evolutionary Algorithms: Performance Metric and Benchmark

Problems [Research Frontier]', *IEEE Comput. Intell. Mag.*, vol. 14, no. 3, pp. 61–74, Aug. 2019, doi: 10.1109/MCI.2019.2919398.
[130] E. Zitzler, 'Evolutionary Algorithms for Multiobjective Optimization: Methods and Applications', p. 134.
[131] M. P. Hansen and A. Jaszkiewicz, 'Evaluating the quality of approximations to the non-dominated set', p. 31.
[132] L. While, P. Hingston, L. Barone, and S. Huband, 'A faster algorithm for calculating hypervolume', *IEEE Trans. Evol. Comput.*, vol. 10, no. 1, pp. 29–38, Feb. 2006, doi: 10.1109/TEVC.2005.851275.
[133] S. Mostaghim and J. Teich, 'A New Approach on Many Objective Diversity Measurement', p. 15.
[134] C. Audet, J. Bigeon, D. Cartier, S. Le Digabel, and L. Salomon, 'Performance indicators in multiobjective optimization', *Eur. J. Oper. Res.*, vol. 292, no. 2, pp. 397–422, 2018, doi: 10.1016/j.ejor.2020.11.016.
[135] J. R. Schott, 'Fault tolerant design using single and multicriteria genetic algorithm optimization', 1995.
[136] M. P. Fay and M. A. Proschan, 'Wilcoxon-Mann-Whitney or t-test? On assumptions for hypothesis tests and multiple interpretations of decision rules', *Stat. Surv.*, vol. 4, no. none, Jan. 2010, doi: 10.1214/09-SS051.
[137] Z. Chen, B. Wang, and A. N. Gorban, 'Multivariate Gaussian and Student-t process regression for multi-output prediction', *Neural Comput. Appl.*, vol. 32, no. 8, pp. 3005–3028, Apr. 2020, doi: 10.1007/s00521-019-04687-8.
[138] B. Filipic and T. Tusar, 'Visualization in Multiobjective Optimization', in *Proceedings of the 2016 on Genetic and Evolutionary Computation Conference Companion*, Denver Colorado USA, Jul. 2016, pp. 735–751. doi: 10.1145/2908961.2926994.
[139] A. K. A. Talukder and K. Deb, 'PaletteViz: A Visualization Method for Functional Understanding of High-Dimensional Pareto-Optimal Data-Sets to Aid Multi-Criteria Decision Making', *IEEE Comput. Intell. Mag.*, vol. 15, no. 2, pp. 36–48, May 2020, doi: 10.1109/MCI.2020.2976184.
[140] S. Greco, K. Klamroth, J. D. Knowles, and G. Rudolph, 'Understanding Complexity in Multiobjective Optimization (Dagstuhl Seminar 15031)', p. 68 pages, 2015, doi: 10.4230/DAGREP.5.1.96.
[141] T. Tusar and B. Filipic, 'Visualization of Pareto Front Approximations in Evolutionary Multiobjective Optimization: A Critical Review and the Prosection Method', *IEEE Trans. Evol. Comput.*, vol. 19, no. 2, pp. 225–245, Apr. 2015, doi: 10.1109/TEVC.2014.2313407.
[142] M. Gobbi, I. Haque, P. Papalambros, and G. Mastinu, 'A Critical Review of Optimization Methods for Road Vehicles Design', presented at the 11th AIAA/ISSMO Multidisciplinary Analysis and Optimization Conference, Portsmouth, Virginia, Sep. 2006. doi: 10.2514/6.2006-6998.
[143] N. Shamsaei, A. Yadollahi, L. Bian, and S. M. Thompson, 'An overview of Direct Laser Deposition for additive manufacturing; Part II: Mechanical behavior,

process parameter optimization and control', *Addit. Manuf.*, vol. 8, pp. 12–35, Oct. 2015, doi: 10.1016/j.addma.2015.07.002.

[144] M. Van Elsen, 'Complexity of Selective Laser Melting: a new optimisation approach', 2007.

[145] H. M. Kim, D. G. Rideout, P. Y. Papalambros, and J. L. Stein, 'Analytical Target Cascading in Automotive Vehicle Design', *J. Mech. Des.*, vol. 125, no. 3, pp. 481–489, Sep. 2003, doi: 10.1115/1.1586308.

[146] M. Gobbi, G. Mastinu, and M. Caudano, 'Stochastic Multi-Objective Optimisation of a Gearbox Synchroniser and Selector Mechanism', in *Design Engineering, Volumes 1 and 2*, Washington, DC, USA, Jan. 2003, pp. 113–124. doi: 10.1115/IMECE2003-43005.

[147] M. Gobbi, 'Optimal and Robust Design of Ground Vehicle Systems', in *Volume 2: Automotive Systems, Bioengineering and Biomedical Technology, Fluids Engineering, Maintenance Engineering and Non-Destructive Evaluation, and Nanotechnology*, Torino, Italy, Jan. 2006, pp. 225–234. doi: 10.1115/ESDA2006-95471.

[148] H. Hassine, M. Barkallah, and A. Bellacicco, 'Multi Objective Optimization for Sustainable Manufacturing, Application in Turning', *Int. J. Simul. Model.*, pp. 98–109, Mar. 2015, doi: 10.2507/IJSIMM14(1)9.292.

[149] K. Bouzakis, R. Paraskevopoulou, and G. Giannopoulos, 'Multi-objective optimization of cutting conditions in milling using genetic algorithms', 2008, pp. 763–773.

[150] Abraham Gilbert, Shamnadh. M, and TKM College of Engineering / Kerala University, 'Multi - Objective Optimization of Milling Parameters in HCHCr (D3) Steel by Genetic Algorithm', *Int. J. Eng. Res.*, vol. V4, no. 08, p. IJERTV4IS080511, Aug. 2015, doi: 10.17577/IJERTV4IS080511.

[151] R. K. Tiwari, 'Multi Objective Optimization of Drilling Process Variables Using Genetic Algorithm for Precision Drilling Operation', p. 17.

[152] G. Strano, 'Multi-objective Optimisation in Additive Manufacturing', p. 289.

[153] G. C. M. Patel, P. Krishna, P. R. Vundavilli, and M. B. Parappagoudar, 'Multi-Objective Optimization of Squeeze Casting Process using Genetic Algorithm and Particle Swarm Optimization', *Arch. Foundry Eng.*, vol. 16, no. 3, pp. 172–186, Sep. 2016, doi: 10.1515/afe-2016-0073.

[154] J. Li and S. M. Meerkov, *Production systems engineering*. Springer Science & Business Media, 2008.

[155] A. H. C. Ng, J. Bernedixen, and L. Pehrsson, 'WHAT DOES MULTI-OBJECTIVE OPTIMIZATION HAVE TO DO WITH BOTTLENECK IMPROVEMENT OF PRODUCTION SYSTEMS?', p. 10.

[156] R. Khalil, D. Stockton, P. Singh, and L. Manyonge, 'A Multi-Objective Optimization Approach Using Genetic Algorithms for Quick Response to Effects of Variability in Flow Manufacturing', *Int. J. Adv. Comput. Sci. Appl.*, vol. 3, no. 9, 2012, doi: 10.14569/IJACSA.2012.030902.

[157] I. Das and J. E. Dennis, 'Normal-Boundary Intersection: A New Method for Generating the Pareto Surface in Nonlinear Multicriteria Optimization Problems',

SIAM J. Optim., vol. 8, no. 3, pp. 631–657, Aug. 1998, doi: 10.1137/S1052623496307510.

[158] E. Zitzler, M. Laumanns, and L. Thiele, 'SPEA2: Improving the Strength Pareto Evolutionary Algorithm', *Eidgenöss. Tech. Hochsch. Zür. ETH Inst. Für Tech. Inform. Kommun. TIK*, p. 21, 2001, doi: 10.3929/ETHZ-A-004284029.

[159] K. Li, R. Wang, T. Zhang, and H. Ishibuchi, 'Evolutionary Many-Objective Optimization: A Comparative Study of the State-of-the-Art', *IEEE Access*, vol. 6, pp. 26194–26214, 2018, doi: 10.1109/ACCESS.2018.2832181.

[160] M. Laumanns, L. Thiele, K. Deb, and E. Zitzler, 'Combining Convergence and Diversity in Evolutionary Multiobjective Optimization', *Evol. Comput.*, vol. 10, no. 3, pp. 263–282, Sep. 2002, doi: 10.1162/106365602760234108.

[161] D. Hadka and P. Reed, 'Borg: An Auto-Adaptive Many-Objective Evolutionary Computing Framework', *Evol. Comput.*, vol. 21, no. 2, pp. 231–259, May 2013, doi: 10.1162/EVCO_a_00075.

[162] Xiufen Zou, Yu Chen, Minzhong Liu, and Lishan Kang, 'A New Evolutionary Algorithm for Solving Many-Objective Optimization Problems', *IEEE Trans. Syst. Man Cybern. Part B Cybern.*, vol. 38, no. 5, pp. 1402–1412, Oct. 2008, doi: 10.1109/TSMCB.2008.926329.

[163] G. Wang and H. Jiang, 'Fuzzy-Dominance and Its Application in Evolutionary Many Objective Optimization', in *2007 International Conference on Computational Intelligence and Security Workshops (CISW 2007)*, Harbin, Heilongjiang, China, Dec. 2007, pp. 195–198. doi: 10.1109/CISW.2007.4425478.

[164] R. Wang, R. C. Purshouse, and P. J. Fleming, 'Preference-Inspired Coevolutionary Algorithms for Many-Objective Optimization', *IEEE Trans. Evol. Comput.*, vol. 17, no. 4, pp. 474–494, Aug. 2013, doi: 10.1109/TEVC.2012.2204264.

[165] N. Beume, B. Naujoks, and M. Emmerich, 'SMS-EMOA: Multiobjective selection based on dominated hypervolume', *Eur. J. Oper. Res.*, vol. 181, no. 3, pp. 1653–1669, Sep. 2007, doi: 10.1016/j.ejor.2006.08.008.

[166] A. Zhou, B.-Y. Qu, H. Li, S.-Z. Zhao, P. N. Suganthan, and Q. Zhang, 'Multiobjective evolutionary algorithms: A survey of the state of the art', *Swarm Evol. Comput.*, vol. 1, no. 1, pp. 32–49, Mar. 2011, doi: 10.1016/j.swevo.2011.03.001.

[167] E. J. Hughes, 'Multiple single objective pareto sampling', in *The 2003 Congress on Evolutionary Computation, 2003. CEC '03.*, Canberra, Australia, 2003, vol. 4, pp. 2678–2684. doi: 10.1109/CEC.2003.1299427.

[168] E. J. Hughes, 'MSOPS-II: A general-purpose Many-Objective optimiser', in *2007 IEEE Congress on Evolutionary Computation*, Singapore, Sep. 2007, pp. 3944–3951. doi: 10.1109/CEC.2007.4424985.

[169] H.-L. Liu, F. Gu, and Q. Zhang, 'Decomposition of a Multiobjective Optimization Problem Into a Number of Simple Multiobjective Subproblems', *IEEE Trans. Evol. Comput.*, vol. 18, no. 3, pp. 450–455, Jun. 2014, doi: 10.1109/TEVC.2013.2281533.

[170] K. Li, K. Deb, Q. Zhang, and S. Kwong, ‘An Evolutionary Many-Objective Optimization Algorithm Based on Dominance and Decomposition’, *IEEE Trans. Evol. Comput.*, vol. 19, no. 5, pp. 694–716, Oct. 2015, doi: 10.1109/TEVC.2014.2373386.

[171] C. He, L. Pan, H. Xu, Y. Tian, and X. Zhang, ‘An improved reference point sampling method on Pareto optimal front’, in *2016 IEEE Congress on Evolutionary Computation (CEC)*, Vancouver, BC, Jul. 2016, pp. 5230–5237. doi: 10.1109/CEC.2016.7748353.

[172] X. Ma, Y. Yu, X. Li, Y. Qi, and Z. Zhu, ‘A Survey of Weight Vector Adjustment Methods for Decomposition-Based Multiobjective Evolutionary Algorithms’, *IEEE Trans. Evol. Comput.*, vol. 24, no. 4, pp. 634–649, Aug. 2020, doi: 10.1109/TEVC.2020.2978158.

[173] R. Cheng, Y. Jin, and K. Narukawa, ‘Adaptive reference vector generation for inverse model based evolutionary multiobjective optimization with degenerate and disconnected Pareto fronts’, 2015, pp. 127–140.

[174] R. Wang, R. C. Purshouse, and P. J. Fleming, ‘Preference-inspired co-evolutionary algorithms using weight vectors’, *Eur. J. Oper. Res.*, vol. 243, no. 2, pp. 423–441, Jun. 2015, doi: 10.1016/j.ejor.2014.05.019.

[175] J. Siwei, C. Zhihua, Z. Jie, and O. Yew-Soon, ‘Multiobjective optimization by decomposition with Pareto-adaptive weight vectors’, 2011, vol. 3, pp. 1260–1264.

[176] Y. Liu, H. Ishibuchi, N. Masuyama, and Y. Nojima, ‘Adapting Reference Vectors and Scalarizing Functions by Growing Neural Gas to Handle Irregular Pareto Fronts’, *IEEE Trans. Evol. Comput.*, pp. 1–1, 2020, doi: 10.1109/TEVC.2019.2926151.

[177] K. S. Bhattacharjee, H. K. Singh, T. Ray, and Q. Zhang, ‘Decomposition based evolutionary algorithm with a dual set of reference vectors’, 2017, pp. 105–112.

[178] H.-L. Liu, L. Chen, Q. Zhang, and K. Deb, ‘Adaptively Allocating Search Effort in Challenging Many-Objective Optimization Problems’, *IEEE Trans. Evol. Comput.*, vol. 22, no. 3, pp. 433–448, Jun. 2018, doi: 10.1109/TEVC.2017.2725902.

[179] Y. Xiang, Y. Zhou, M. Li, and Z. Chen, ‘A vector angle-based evolutionary algorithm for unconstrained many-objective optimization’, *IEEE Trans. Evol. Comput.*, vol. 21, no. 1, pp. 131–152, 2016.

[180] H. Zhao, C. Zhang, B. Zhang, P. Duan, and Y. Yang, ‘Decomposition-based sub-problem optimal solution updating direction-guided evolutionary many-objective algorithm’, *Inf. Sci.*, vol. 448, pp. 91–111, 2018.

[181] P. Czyżżak and A. Jaszkiewicz, ‘Pareto simulated annealing—a metaheuristic technique for multiple-objective combinatorial optimization’, *J. Multi-Criteria Decis. Anal.*, vol. 7, no. 1, pp. 34–47, 1998.

[182] H. Li and D. Landa-Silva, ‘Evolutionary multi-objective simulated annealing with adaptive and competitive search direction’, 2008, pp. 3311–3318.

[183] K. Harada, S. Hiwa, and T. Hiroyasu, ‘Adaptive weight vector assignment method for MOEA/D’, 2017, pp. 1–9.

[184] H. Xu, W. Zeng, D. Zhang, and X. Zeng, 'MOEA/HD: a multiobjective evolutionary algorithm based on hierarchical decomposition', *IEEE Trans. Cybern.*, vol. 49, no. 2, pp. 517–526, 2017.

[185] K. Li, R. Chen, G. Min, and X. Yao, 'Integration of preferences in decomposition multiobjective optimization', *IEEE Trans. Cybern.*, vol. 48, no. 12, pp. 3359–3370, 2018.

[186] R. Wang, R. C. Purshouse, and P. J. Fleming, 'On finding well-spread Pareto optimal solutions by preference-inspired co-evolutionary algorithm', 2013, pp. 695–702.

[187] Y. Tian, R. Cheng, X. Zhang, and Y. Jin, 'PlatEMO: A MATLAB Platform for Evolutionary Multi-Objective Optimization [Educational Forum]', *IEEE Comput. Intell. Mag.*, vol. 12, no. 4, pp. 73–87, Nov. 2017, doi: 10.1109/MCI.2017.2742868.

[188] Y.-N. Wang, L.-H. Wu, and X.-F. Yuan, 'Multi-objective self-adaptive differential evolution with elitist archive and crowding entropy-based diversity measure', *Soft Comput.*, vol. 14, no. 3, pp. 193–209, Feb. 2010, doi: 10.1007/s00500-008-0394-9.

[189] N. Riquelme, C. Von Lucken, and B. Baran, 'Performance metrics in multi-objective optimization', in *2015 Latin American Computing Conference (CLEI)*, Arequipa, Peru, Oct. 2015, pp. 1–11. doi: 10.1109/CLEI.2015.7360024.

[190] X. Cai, H. Sun, and Z. Fan, 'A diversity indicator based on reference vectors for many-objective optimization', *Inf. Sci.*, vol. 430–431, pp. 467–486, Mar. 2018, doi: 10.1016/j.ins.2017.11.051.

[191] M. Li and X. Yao, 'Quality evaluation of solution sets in multiobjective optimisation: A survey', *ACM Comput. Surv. CSUR*, vol. 52, no. 2, pp. 1–38, 2019.

[192] D. A. Van Veldhuizen and G. B. Lamont, 'Evolutionary computation and convergence to a pareto front', 1998, pp. 221–228.

[193] H. Ishibuchi, H. Masuda, Y. Tanigaki, and Y. Nojima, 'Modified Distance Calculation in Generational Distance and Inverted Generational Distance', in *Evolutionary Multi-Criterion Optimization*, vol. 9019, A. Gaspar-Cunha, C. Henggeler Antunes, and C. C. Coello, Eds. Cham: Springer International Publishing, 2015, pp. 110–125. doi: 10.1007/978-3-319-15892-1_8.

[194] O. Schutze, X. Esquivel, A. Lara, and C. A. C. Coello, 'Using the averaged Hausdorff distance as a performance measure in evolutionary multiobjective optimization', *IEEE Trans. Evol. Comput.*, vol. 16, no. 4, pp. 504–522, 2012.

[195] K. Li, K. Deb, and X. Yao, 'R-Metric: Evaluating the Performance of Preference-Based Evolutionary Multiobjective Optimization Using Reference Points', *IEEE Trans. Evol. Comput.*, vol. 22, no. 6, pp. 821–835, Dec. 2018, doi: 10.1109/TEVC.2017.2737781.

[196] Qingfu Zhang, Aimin Zhou, and Yaochu Jin, 'RM-MEDA: A Regularity Model-Based Multiobjective Estimation of Distribution Algorithm', *IEEE Trans. Evol. Comput.*, vol. 12, no. 1, pp. 41–63, Feb. 2008, doi: 10.1109/TEVC.2007.894202.

[197] M. Li, S. Yang, and X. Liu, ‘Diversity Comparison of Pareto Front Approximations in Many-Objective Optimization’, *IEEE Trans. Cybern.*, vol. 44, no. 12, pp. 2568–2584, Dec. 2014, doi: 10.1109/TCYB.2014.2310651.

[198] Y. Tian, X. Xiang, X. Zhang, R. Cheng, and Y. Jin, ‘Sampling Reference Points on the Pareto Fronts of Benchmark Multi-Objective Optimization Problems’, in *2018 IEEE Congress on Evolutionary Computation (CEC)*, Rio de Janeiro, Jul. 2018, pp. 1–6. doi: 10.1109/CEC.2018.8477730.

[199] K. E. Wu and G. Panoutsos, ‘A New Method for Generating and Indexing Reference Points in Many Objective Optimisation’, in *2020 IEEE Congress on Evolutionary Computation (CEC)*, Glasgow, United Kingdom, Jul. 2020, pp. 1–8. doi: 10.1109/CEC48606.2020.9185793.

[200] Z. He and G. G. Yen, ‘Comparison of visualization approaches in many-objective optimization’, in *2017 IEEE Congress on Evolutionary Computation (CEC)*, Donostia, San Sebastián, Spain, Jun. 2017, pp. 357–363. doi: 10.1109/CEC.2017.7969334.

[201] A. Inselberg, *Parallel Coordinates*. New York, NY: Springer New York, 2009. doi: 10.1007/978-0-387-68628-8.

[202] F. Kudo and T. Yoshikawa, ‘Knowledge extraction in multi-objective optimization problem based on visualization of Pareto solutions’, in *2012 IEEE Congress on Evolutionary Computation*, Brisbane, Australia, Jun. 2012, pp. 1–6. doi: 10.1109/CEC.2012.6256449.

[203] D. J. Walker, RichardM. Everson, and J. E. Fieldsend, ‘Visualizing Mutually Nondominating Solution Sets in Many-Objective Optimization’, *IEEE Trans. Evol. Comput.*, vol. 17, no. 2, pp. 165–184, Apr. 2013, doi: 10.1109/TEVC.2012.2225064.

[204] A. Ibrahim, S. Rahnamayan, M. V. Martin, and K. Deb, ‘3D-RadVis: Visualization of Pareto front in many-objective optimization’, in *2016 IEEE Congress on Evolutionary Computation (CEC)*, Jul. 2016, pp. 736–745. doi: 10.1109/CEC.2016.7743865.

[205] X. Blasco, J. M. Herrero, J. Sanchis, and M. Martínez, ‘A new graphical visualization of n-dimensional Pareto front for decision-making in multiobjective optimization’, *Inf. Sci.*, vol. 178, no. 20, pp. 3908–3924, Oct. 2008, doi: 10.1016/j.ins.2008.06.010.

[206] A. Pryke, S. Mostaghim, and A. Nazemi, ‘Heatmap Visualization of Population Based Multi Objective Algorithms’, in *Evolutionary Multi-Criterion Optimization*, vol. 4403, S. Obayashi, K. Deb, C. Poloni, T. Hiroyasu, and T. Murata, Eds. Berlin, Heidelberg: Springer Berlin Heidelberg, 2007, pp. 361–375. doi: 10.1007/978-3-540-70928-2_29.

[207] Y. Masafumi, Y. Tomohiro, and F. Takeshi, ‘Study on effect of MOGA with interactive island model using visualization’, 2010, pp. 1–6.

[208] A. R. R. de Freitas, P. J. Fleming, and F. G. Guimarães, ‘Aggregation Trees for visualization and dimension reduction in many-objective optimization’, *Inf. Sci.*, vol. 298, pp. 288–314, Mar. 2015, doi: 10.1016/j.ins.2014.11.044.

[209] P.-W. Chiu and C. L. Bloebaum, ‘Hyper-Radial Visualization (HRV) method with range-based preferences for multi-objective decision making’, *Struct. Multidiscip. Optim.*, vol. 40, no. 1–6, pp. 97–115, Jan. 2010, doi: 10.1007/s00158-009-0361-9.

[210] R. Haghnazar Koochaksaraei, R. Enayatifar, and F. G. Guimarães, ‘A New Visualization Tool in Many-Objective Optimization Problems’, in *Hybrid Artificial Intelligent Systems*, vol. 9648, F. Martínez-Álvarez, A. Troncoso, H. Quintián, and E. Corchado, Eds. Cham: Springer International Publishing, 2016, pp. 213–224. doi: 10.1007/978-3-319-32034-2_18.

[211] G. Agrawal, C. Bloebaum, and K. Lewis, ‘Intuitive Design Selection using Visualized n-Dimensional Pareto Frontier’, in *46th AIAA/ASME/ASCE/AHS/ASC Structures, Structural Dynamics and Materials Conference*, Austin, Texas, Apr. 2005, pp. 1–14. doi: 10.2514/6.2005-1813.

[212] S. Obayashi and D. Sasaki, ‘Visualization and Data Mining of Pareto Solutions Using Self-Organizing Map’, in *Evolutionary Multi-Criterion Optimization*, vol. 2632, C. M. Fonseca, P. J. Fleming, E. Zitzler, L. Thiele, and K. Deb, Eds. Berlin, Heidelberg: Springer Berlin Heidelberg, 2003, pp. 796–809. doi: 10.1007/3-540-36970-8_56.

[213] M. Yoshimi, ‘Visualization of Pareto Solutions by Spherical Self-Organizing Map and It’s acceleration on a GPU’, *J. Softw. Eng. Appl.*, vol. 05, no. 03, pp. 129–137, 2012, doi: 10.4236/jsea.2012.53020.

[214] N. T. Aboulkhair, M. Simonelli, L. Parry, I. Ashcroft, C. Tuck, and R. Hague, ‘3D printing of Aluminium alloys: Additive Manufacturing of Aluminium alloys using selective laser melting’, *Prog. Mater. Sci.*, vol. 106, p. 100578, Dec. 2019, doi: 10.1016/j.pmatsci.2019.100578.

[215] H. Shipley *et al.*, ‘Optimisation of process parameters to address fundamental challenges during selective laser melting of Ti-6Al-4V: A review’, *Int. J. Mach. Tools Manuf.*, vol. 128, pp. 1–20, May 2018, doi: 10.1016/j.ijmachtools.2018.01.003.

[216] S. M. Thompson, L. Bian, N. Shamsaei, and A. Yadollahi, ‘An overview of Direct Laser Deposition for additive manufacturing; Part I: Transport phenomena, modeling and diagnostics’, *Addit. Manuf.*, vol. 8, pp. 36–62, Oct. 2015, doi: 10.1016/j.addma.2015.07.001.

[217] C. Panwisawas, Y. T. Tang, and R. C. Reed, ‘Metal 3D printing as a disruptive technology for superalloys’, *Nat. Commun.*, vol. 11, no. 1, p. 2327, Dec. 2020, doi: 10.1038/s41467-020-16188-7.

[218] B. Zhang, Y. Li, and Q. Bai, ‘Defect Formation Mechanisms in Selective Laser Melting: A Review’, *Chin. J. Mech. Eng.*, vol. 30, no. 3, pp. 515–527, May 2017, doi: 10.1007/s10033-017-0121-5.

[219] A. A. Martin *et al.*, ‘Dynamics of pore formation during laser powder bed fusion additive manufacturing’, *Nat. Commun.*, vol. 10, no. 1, p. 1987, Dec. 2019, doi: 10.1038/s41467-019-10009-2.

[220] C. T. Sims, ‘A History of Superalloy Metallurgy for Superalloy Metallurgists’, in *Superalloys 1984 (Fifth International Symposium)*, 1984, pp. 399–419. doi: 10.7449/1984/Superalloys_1984_399_419.

[221] T. J. Carter, ‘Common failures in gas turbine blades’, *Eng. Fail. Anal.*, vol. 12, no. 2, pp. 237–247, Apr. 2005, doi: 10.1016/j.engfailanal.2004.07.004.

[222] J. Fu, J. Huang, and J. Liu, ‘Topology Optimization With Selective Problem Setups’, *IEEE Access*, vol. 7, pp. 180846–180855, 2019, doi: 10.1109/ACCESS.2019.2958645.

[223] J. Hub, ‘A Study on Topology Optimization of Airplane Air Brake Bracing Beam’, in *2019 International Conference on Military Technologies (ICMT)*, Brno, Czech Republic, May 2019, pp. 1–4. doi: 10.1109/MILTECHS.2019.8870028.

[224] G. Yongxin, Z. Lihua, L. Zhijia, G. Yimin, and M. Lingxi, ‘Optimization Design of Star Tracker Bracket of Small Satellite for 3D Printing’, in *2019 5th International Conference on Control, Automation and Robotics (ICCAR)*, Beijing, China, Apr. 2019, pp. 808–811. doi: 10.1109/ICCAR.2019.8813432.

[225] G. D’Emilia, A. Di Ilio, A. Gaspari, E. Natale, R. Perilli, and A. G. Stamopoulos, ‘The role of measurement and simulation in additive manufacturing within the frame of Industry 4.0’, in *2019 II Workshop on Metrology for Industry 4.0 and IoT (MetroInd4.0&IoT)*, Naples, Italy, Jun. 2019, pp. 382–387. doi: 10.1109/METROI4.2019.8792876.

[226] K.-Y. Fok, N. Ganganath, C.-T. Cheng, H. H.-C. Iu, and C. K. Tse, ‘Tool-Path Optimization using Neural Networks’, in *2019 IEEE International Symposium on Circuits and Systems (ISCAS)*, Sapporo, Japan, May 2019, pp. 1–5. doi: 10.1109/ISCAS.2019.8702473.

[227] B. Hu, G. Jin, and L. Sun, ‘A Novel Adaptive Slicing Method for Additive Manufacturing’, in *2018 IEEE 22nd International Conference on Computer Supported Cooperative Work in Design ((CSCWD))*, Nanjing, China, May 2018, pp. 218–223. doi: 10.1109/CSCWD.2018.8465247.

[228] H.-S. Byun and K. H. Lee, ‘Determination of the optimal build direction for different rapid prototyping processes using multi-criterion decision making’, *Robot. Comput.-Integr. Manuf.*, vol. 22, no. 1, pp. 69–80, Feb. 2006, doi: 10.1016/j.rcim.2005.03.001.

[229] S. Brika, Z. Yf, B. M, and M. J, ‘Multi-Objective Build Orientation Optimization for Powder Bed Fusion by Laser’, *Ind. Eng. Manag.*, vol. 06, no. 04, 2017, doi: 10.4172/2169-0316.1000236.

[230] N. Padhye and K. Deb, ‘Multi-objective optimisation and multi-criteria decision making in SLS using evolutionary approaches’, *Rapid Prototyp. J.*, vol. 17, no. 6, pp. 458–478, Oct. 2011, doi: 10.1108/13552541111184198.

[231] J. Mezzetta *et al.*, ‘Microstructure-Properties Relationships of Ti-6Al-4V Parts Fabricated by Selective Laser Melting’, *Int. J. Precis. Eng. Manuf.-Green Technol.*, vol. 5, no. 5, pp. 605–612, Oct. 2018, doi: 10.1007/s40684-018-0062-1.

[232] S. K. Dasari, A. Cheddad, and P. Andersson, ‘Random Forest Surrogate Models to Support Design Space Exploration in Aerospace Use-Case’, in *Artificial*

Intelligence Applications and Innovations, vol. 559, J. MacIntyre, I. Maglogiannis, L. Iliadis, and E. Pimenidis, Eds. Cham: Springer International Publishing, 2019, pp. 532–544. doi: 10.1007/978-3-030-19823-7_45.

[233] A. Rubio-Solis and G. Panoutsos, 'Iterative information granulation for novelty detection in complex datasets', in *2016 IEEE International Conference on Fuzzy Systems (FUZZ-IEEE)*, Vancouver, BC, Canada, Jul. 2016, pp. 953–960. doi: 10.1109/FUZZ-IEEE.2016.7737791.

[234] A. Rubio-Solis, A. Baraka, G. Panoutsos, and S. Thornton, 'Data-driven interval type-2 fuzzy modelling for the classification of imbalanced data', in *Practical Issues of Intelligent Innovations*, Springer, 2018, pp. 37–51.

[235] J.-S. R. Jang and C.-T. Sun, 'Functional equivalence between radial basis function networks and fuzzy inference systems', *IEEE Trans. Neural Netw.*, vol. 4, no. 1, pp. 156–159, Jan. 1993, doi: 10.1109/72.182710.

[236] A. Rubio-Solis and G. Panoutsos, 'Interval Type-2 Radial Basis Function Neural Network: A Modeling Framework', *IEEE Trans. Fuzzy Syst.*, vol. 23, no. 2, pp. 457–473, Apr. 2015, doi: 10.1109/TFUZZ.2014.2315656.

[237] A. Rubio-Solis, U. Martinez-Hernandez, and G. Panoutsos, 'Evolutionary Extreme Learning Machine for the Interval Type-2 Radial Basis Function Neural Network: A Fuzzy Modelling Approach', in *2018 IEEE International Conference on Fuzzy Systems (FUZZ-IEEE)*, Rio de Janeiro, Jul. 2018, pp. 1–8. doi: 10.1109/FUZZ-IEEE.2018.8491583.

[238] A. Rubio-Solis, P. Melin, U. Martinez-Hernandez, and G. Panoutsos, 'General Type-2 Radial Basis Function Neural Network: A Data-Driven Fuzzy Model', *IEEE Trans. Fuzzy Syst.*, vol. 27, no. 2, pp. 333–347, Feb. 2019, doi: 10.1109/TFUZZ.2018.2858740.

[239] A. Rubio-Solis and G. Panoutsos, 'An ensemble data-driven fuzzy network for laser welding quality prediction', in *2017 IEEE International Conference on Fuzzy Systems (FUZZ-IEEE)*, Naples, Italy, Jul. 2017, pp. 1–6. doi: 10.1109/FUZZ-IEEE.2017.8015496.

[240] A.Rubio Solis and G. Panoutsos, 'REPORT : NEURAL FUZZY MODELLING OF POROSITY , AND BULK AND EDGE DENSITY .', 2018.